Loughborough University

This item was submitted to Loughborough's Institutional Repository (https://dspace.lboro.ac.uk/) by the author and is made available under the following Creative Commons Licence conditions.

creative commons

COMMONS DEED

Attribution-NonCommercial-NoDerivs 2.5

You are free:

- to copy, distribute, display, and perform the work

Under the following conditions:

Attribution. You must attribute the work in the manner specified by the author or licensor.

Noncommercial. You may not use this work for commercial purposes.

No Derivative Works. You may not alter, transform, or build upon this work.

- For any reuse or distribution, you must make clear to others the license terms of this work.
- Any of these conditions can be waived if you get permission from the copyright holder.

Your fair use and other rights are in no way affected by the above.

This is a human-readable summary of the Legal Code (the full license).

Disclaimer

For the full text of this licence, please go to:
http://creativecommons.org/licenses/by-nc-nd/2.5/

DEVELOPMENT OF PARAMETRIC FINITE ELEMENT MODELLING METHODS FOR NONWOVEN MATERIALS INCLUDING RATE DEPENDENT MATERIAL BEHAVIOUR

by

Baris SABUNCUOGLU

A Doctor of Philosophy Thesis

Submitted in partial fulfilment of the requirements for the award of

Doctor of Philosophy of Loughborough University

April 2012

© by Baris SABUNCUOGLU, 2012

CERTIFICATE OF ORIGINALITY

This is to certify that I am responsible for the work submitted in this thesis, that the original work is my own except as specified in acknowledgments or in footnotes, and that neither the thesis nor the original work contained therein has been submitted to this or any other institution for a degree.

…… (Signed)

…… (Date)

ABSTRACT

Thermally bonded nonwovens are low-price substitutes for traditional textiles. They are used in many areas including filtration, automotive and aerospace industries. Hence, understanding deformation behaviours of these materials is required to design new products tailored for specific applications in different areas. Because of their complex and random structure, numerical simulations of nonwoven materials have been a challenging task for many years. The main aim of the thesis is to develop a computational modelling tool to simulate the effect of design parameters on structural behaviour of low-density nonwoven materials by using a finite element method. The modelling procedure is carried out with a parametric modelling technique, which allows a designer to run a series of analyses with different design parameters and observe the effects of these parameters on the mechanical behaviour of nonwoven materials.

The thesis also presents the study of rate–dependent behaviour of nonwoven fibres. Novel test and data-interpretation procedures are proposed to determine the creep behaviour of fibres in the nonwoven structure. Some case studies are presented to demonstrate the effectiveness of the model.

The developed computational tool allows macro and micro-scale structural investigation of nonwoven materials. Two additional studies are presented, performed with the developed tool. In the first study, the effect of design parameters on tensile stiffness of nonwovens was determined by performing numerical analyses with various nonwoven models. In the second one, strain distribution in fibres is studied thoroughly together with factors affecting the distribution. The models, developed in the thesis can also be employed in further studies of nonwovens, such as investigation of their damage and fracture behaviour.

Keywords: Thermally bonded nonwoven; Finite element analysis; Orientation distribution; Creep; Viscoelasticity; Strain distribution

to my family

ACKNOWLEDGEMENTS

I would like to express my gratitude to my supervisors Prof. Vadim V. Silberschmidt and Prof. Memis Acar for their help and guidance throughout the course of this study. Their positive outlook and confidence in my research inspired me and encouraged me for the accomplishment this thesis.

I would also like to thank to my parents Saadet and Tezer Sabuncuoglu and my sister Dr. Deniz Sabuncuoglu Tezcan for all their love, patience and encouragement throughout this study.

Many thanks to my colleagues in Mechanics of Advanced Materials Research Group at Loughborough University. I am especially grateful for the support of Dr. Emrah Demirci, Farukh Farukh and Andy Sandaver for their continuous help throughout my research.

Finally, very special thanks to my wife Dr. Suna Sabuncuoglu for all her encouragement and precious support during the study.

PUBLICATIONS

Journal Papers

Sabuncuoglu, B., Acar, M., Silberschmidt, V.V., 2011. Analysis of Creep Behavior of Polypropylene Fibers, *Applied Mechanics and Materials*, 66, 410-415.

Farukh, F., Demirci, E., **Sabuncuoglu, B.,** Acar, M., Pourdeyhimi, B., Silberschmidt, V.V., 2011. Numerical Modelling of Damage Initiation in Low-Density Thermally Bonded Nonwovens, *Computational Materials Science*, (accepted).

Sabuncuoglu, B., Acar, M., Silberschmidt, V.V., 2012. A Parametric Finite Element Analysis Method for Low-Density Thermally Bonded Nonwovens, *Computational Materials Science*, 52, 164-170.

Sabuncuoglu, B., Acar, M., Silberschmidt, V.V., 2012. Finite Element Modelling of Thermally Bonded Nonwovens: Effect of Manufacturing Parameters on Tensile Stiffness, *Computational Materials Science,* (accepted).

Conferences

Sabuncuoglu, B., Acar M., Silberschmidt, V.V., 2010. Finite Element Analysis of Thermally Bonded Nonwovens under Large Deformation: A Discontinuous Model with a Large Number of Fibres, *20th International Workshop on Computational Mechanics of Materials (IWCMM 20),* Loughborough, UK.

Sabuncuoglu, B., Acar, M., Silberschmidt, V.V., 2011. Analysis of Creep Behavior of Polypropylene Fibers, *International Conference on Advances in Experimental Mechanics: Integrating Simulation and Experimentation (ISEV 2011).* Edinburgh, UK.

Sabuncuoglu, B., Demirci, E., Acar, M., Silberschmidt, V.V., 2011. Finite Element Modelling of Thermally Bonded Nonwoven Materials; a Parametric Model with Orientation Based Distribution of Fibres, *21st International Workshop on Computational Mechanics of Materials (IWCMM 21),* Limerick, Ireland.

Farukh, F., **Sabuncuoglu, B**., Demirci, E., Acar, M., Pourdeyhimi, B., Silberschmidt, V.V., 2011. Numerical Modelling of Damage Initiation in Low-Density Thermally Bonded Nonwovens, *21st International Workshop on Computational Mechanics of Materials (IWCMM 21),* Limerick, Ireland.

CONTENTS

CHAPTER 1

DEFINITION OF THE STUDY

Nonwoven materials have been used in many areas of industry mainly as filtration materials. Due to new technological developments during the past few years, understanding of the mechanical behaviour of nonwovens is demanded more and more by manufacturing companies. Deformation and failure behaviours of nonwovens under various loading and environmental conditions are strongly related to their mechanical properties. There are two main factors that determine their mechanical properties. The first one is the raw material of the structure, from which the fibres were made of. The second one is the manufacturing method utilized to obtain the fibrous network of nonwovens. For the first factor, since their raw material is generally polymers, the final materials obtained can be optimized for specific purposes by varying the molecular structure. For the second one, parameters such as bond-point shape, density and orientation of fibres can be modified to obtain the desired mechanical properties of the final product. In order to determine the effect of these parameters, there should be a suitable tool to predict their effect on the mechanical behaviour of nonwoven materials. This will allow companies to manufacture novel materials with reduced efforts and costs thanks to the benefits of simulation-based predictions and manufacturing according to specific needs. With fewer trials and better predictions, the production of nonwovens will gain speed and the costs will be reduced since fewer trial products will be manufactured.

1.1 Aims and Objectives of the Study

The main aim of this study is to develop a computational modelling method in order to predict the effect of various issues related to the material used and the manufacturing method utilized for the production of nonwoven materials. The computational modelling for nonwovens is accomplished by using a finite element

approach with a more comprehensive structure. The study differs from the previous ones in many ways. The first, and the most important one, is that the model is parametric to be modified easily. In the early finite element studies of nonwovens, generally only a particular type of nonwoven was investigated without model parameterization. Hence, in order to change some modelling details, respective modifications should be implemented by hand in those studies. As an example, to change the dimensions of a bond point, all the mesh should be deleted, geometry should be modified, meshed again and other adjustments should be performed again such as changing the line numbers of applied boundary conditions, changing the points of load application and the parameters defined according to coordinate systems. In the current parametric approach, the model is generated by a code written in a programming language so that the program can be run by reading a specific code that the software can understand. Hence, it is possible to build the structure with changing some parameters in the algorithm and running the software again. In this way, the effects of modelling parameters can be altered easily to understand their effect on the mechanical behaviour.

The second benefit is that parametric models allow building the features of a finite element model with more details that cannot be modelled by using the software's graphical user interference or, at least, take much time. The new approach can enhance modelling of large number of fibres using an automated task and permit the investigation of micro-structural behaviour. The features of the model make it open to many further studies such as damage, fracture, fatigue etc.

Following are the additional objectives of the research:

1. Determination of the rate-dependent mechanical behaviour of fibres in the nonwoven structure;

2. Developing a novel method to determine the rate-dependent behaviour of fibres and implementing it into the finite element model of nonwovens;

3. By using the developed tool, the analysis of the effect of various parameters related to production and loading conditions of nonwovens on their deformation behaviour;

4. Understanding the mechanism of non-homogeneous distribution of strains of the fibres and the effect of parameters on this distribution.

The parametric finite-element modelling procedure, presented in the thesis, was developed mainly for the structural analysis of low-density nonwovens. However, an additional study was performed in order to demonstrate the effectiveness of the modelling method for high-density nonwovens.

The thesis does not cover damage, fracture or fatigue behaviours of nonwoven materials; the effect of environmental conditions such as temperature or humidity on the structural behaviour was not studied as well. However, the approach, developed in the thesis can be extended to these areas.

1.2 Research Methodology

The methodology utilized in this research is summarized schematically in Figure 1.1. The study starts with the introduction to nonwoven materials and brief explanation of the underlying mechanisms related to the mechanics of nonwovens. These sections also include the previous studies related with the research. After that, the material tests and data analyses are performed to understand tensile and creep nature of fibres under various loading rates. Then a novel parametric modelling method with a patterned fibrous structure is utilized. Some case studies are performed to see the effect of material properties on the structural behaviour. Due to the conclusions obtained from this method, a different modelling method with a random fibrous structure is utilized. The effect of manufacturing parameters on the tensile stiffness and the analysis of strain distributions are studied with this new developed model. Finally, the conclusions obtained from the entire study are presented and further recommendations are given.

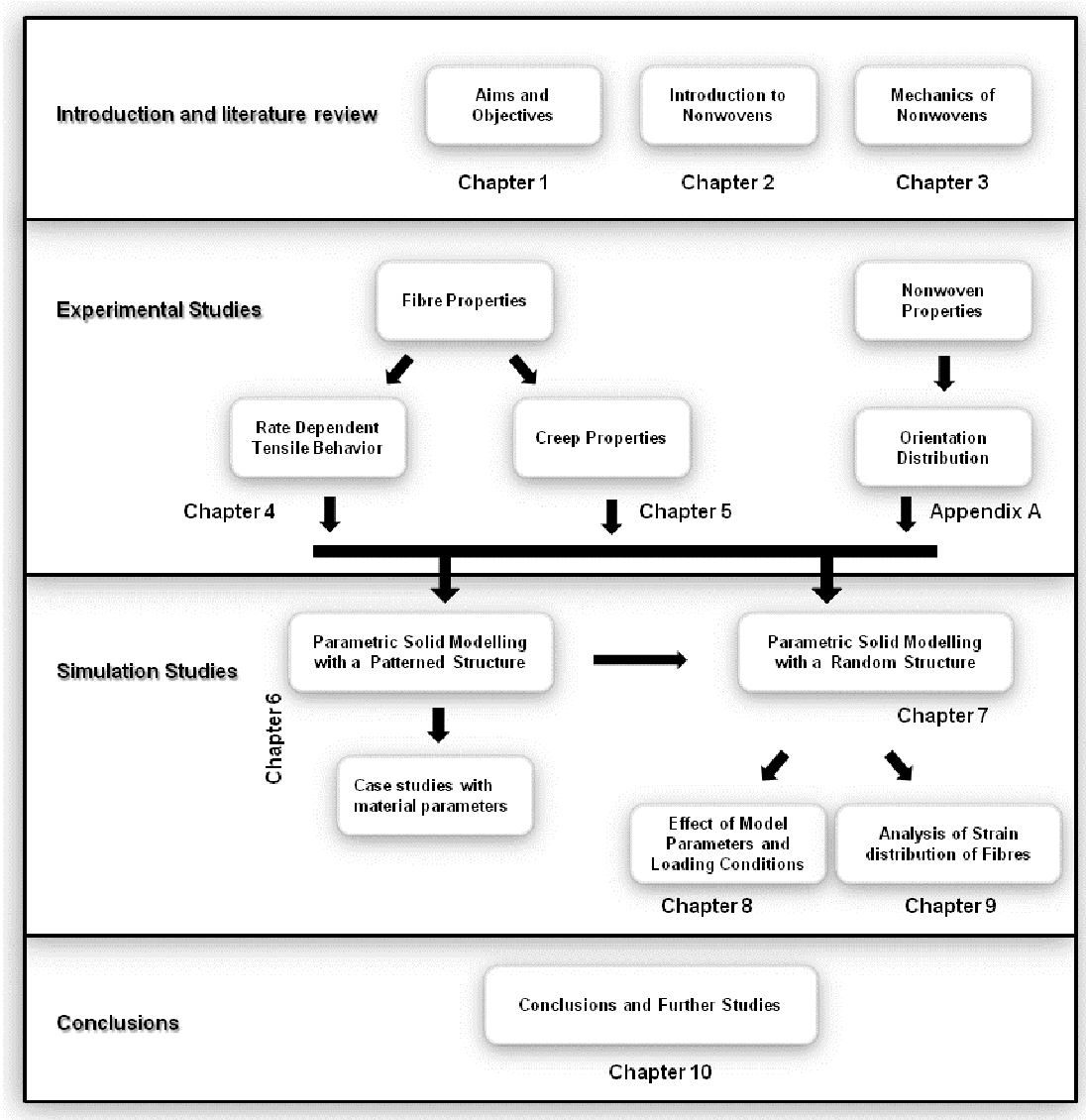

Figure 1.1. Research methodology of the study

1.3 Outline of the Study

The presented study consists of nine chapters excluding the current chapter. The summary of each chapter is given as follows:

Chapter 2, Introduction to Nonwoven Materials: A detailed introduction of nonwoven materials is given including their manufacturing methods and parameters affecting the structural behaviour.

Chapter 3, Mechanics of Nonwovens: The theories behind the mechanical behaviour of nonwovens are presented. The previous studies of the subject are reviewed. In addition, some principle concepts related to the current study are introduced.

Chapter 4, Rate-Dependent Tensile Properties of Polypropylene Fibres: The stress strain behaviour of polypropylene fibres in the nonwoven structure is determined at various loading rates. A procedure for implementing constant-true-strain-rate tests is introduced.

Chapter 5, Creep Properties of Polypropylene Fibres: The creep properties of polypropylene fibres are determined by means of a series of creep tests followed by application of data analysis techniques. The determined properties are implemented into the finite element software, MSC Marc Mentat. Some case studies are performed in order to verify the developed creep model.

Chapter 6, Parametric Modelling of Nonwovens with Patterned Structure: In this chapter, a novel parametric modelling method is proposed. The orientation distribution of fibres is applied by assigning various cross-sectional areas to the structure. The simulations are compared with tests and the effects of various material parameters on the structural behaviour are examined.

Chapter 7, Parametric Modelling of Nonwovens with Random Distribution of Fibres: Modelling of fibres with a patterned structure resulted in some significant weak points. In order to solve these problems, another parametric modelling technique is suggested. In this model, the individual fibres are distributed in the structure according to the given orientation distribution.

Chapter 8, Effect of Manufacturing Parameters and Loading Conditions on Stiffness of Nonwoven Materials: Parametric studies are performed to show the effect of manufacturing parameters and loading conditions with the proposed model in Chapter 7.

Chapter 9, Strain Distribution in Fibres in Nonwoven Structure under Tensile Load: The underlying mechanism on the strain distribution in the fibres of the nonwoven

structure is analyzed with various nonwoven models. The effect of each parameter on the distribution is discussed.

Chapter 10, Conclusions: The summary and the outcomes of the performed research studies are presented. Some further studies are suggested based on this research.

Appendix A: The orientation distribution of fibres, used in the entire study, was determined by scanning a representative nonwoven sample in an X-ray computed tomography machine and using an image analysis tool. In this section, the methodology is described in detail.

Appendix B: An additional study, which demonstrates the effectiveness of the model in simulating the deformation behaviour of high-density nonwovens, is presented.

CHAPTER 2

INTRODUCTION TO NONWOVEN MATERIALS

2.1 Definition of Nonwoven Materials

There are many different kinds of materials, which are really a part of our lives and we are ignorant of this and of their properties. Nonwoven materials are one of these types of materials. Although there are different kinds o definitions (Albrecht, 2003, Purdy, 1983, Truelove & Nordgren, 1981) we can consider nonwovens as a kind of low cost textiles in which fibres are bonded together by various methods. A sample image of a typical nonwoven is shown in Figure 2.1. The main difference between nonwovens and wovens arises from the fact that the yarn spinning stage is omitted in the nonwoven processing of staple fibres, while bonding of the web is accomplished by various methods such as chemical, mechanical or thermal ones instead of weaving and knitting, as in traditional textiles. The nonwoven industry as we know it today has grown from developments in the textile, paper and polymer processing industries. Today, there are also inputs from other industries including most branches of engineering as well as natural sciences (Albrecht, 2003, Russell, 2007). The biggest advantage of nonwovens is their low cost and flexibility of usage according to different areas. They could provide a comparable strength with a very soft structure. They are usually liquid repellent and can be used as a filtration media because of their porous structure (Hutten, 2007, Montefusco, 2005). The data on annual production of nonwovens in the world is shown in Table 2.1.

Nonwovens are produced in two main stages. First, a fibrous web is formed which is called the web formation process. Then the fibres in this web are attached to each other which is called the bonding process. The web formation process is divided into categories such as dry laying, wet laying and polymer laying. Bonding processes are divided mainly as thermal, chemical, needle punch, stitching and hydroentanglement

bonding (Russell, 2007). Current research is related with dry-laid, thermally bonded nonwovens. Thus, detailed information is given for these nonwovens only.

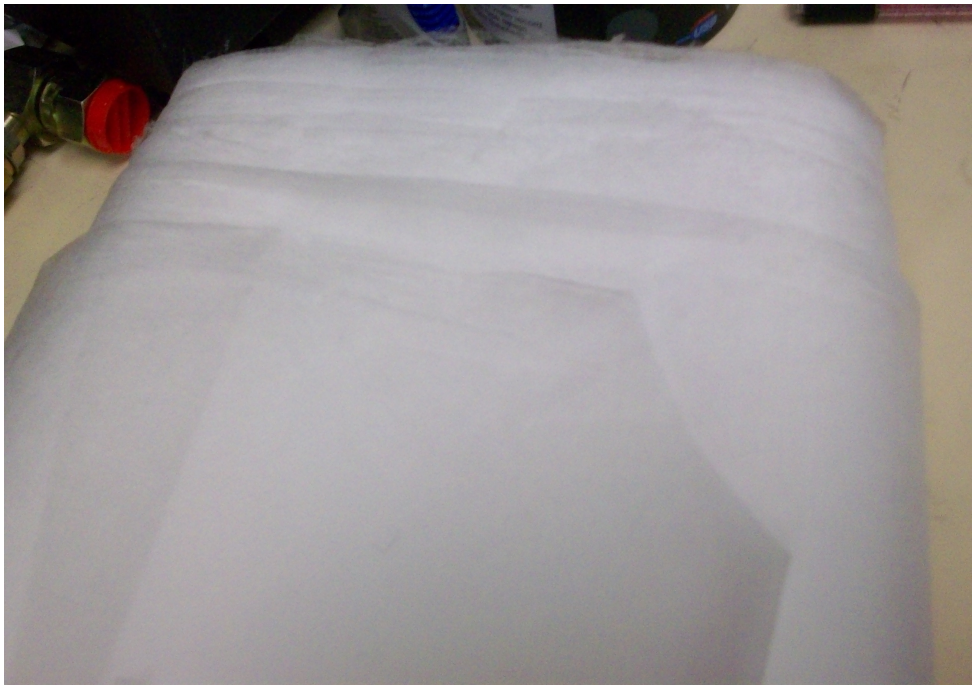

Figure 2.1. Image of thermally bonded nonwoven

Table 2.1. Worldwide Nonwoven Production (Pourdeyhimi, 2004)

Region	***Production, 2003 (m.tons)***	***Share (%)***
North America	1.2	30
Western Europe	1.1	30
Asia – Pacific	0.64	17
Japan	0.34	8
South America	0.24	6
Middle East	0.17	5
Rest of the World	0.16	4

2.2 Thermally Bonded Nonwovens

2.2.1 Manufacturing

Thermally bonded nonwovens are manufactured by two major methods: through air bonding and calendaring. In a through-air bonding process, a hot fluid, air, is forced through a pre-formed web. If the temperature of the fluid is high enough, the fibres may partially melt. In this case, they form bonds, where two or more fibres come into contact. The thermally bonded nonwoven in this research is manufactured with a calendaring method, in which the combination of web formation and the thermal bonding process feeds the formed web to the calendar, where it is condensed in the roller gap between two driven and heated rollers and melted at the contact points within a very short period (Figure 2.2). The use of a heated engraved roller and a smooth roller causes cohesive bonding of the web at the positive engraving points (Figure 2.3). The fibres are plastified and bonded with each other at the bonding points (Figure 2.4). The resulting bonded nonwoven is cut to the desired final width and wound up. The degree of bonding is influenced by the factors such as (Albrecht, 2003):

- fibre properties (Chand *et al.,* 2001, Dharmadhikary *et al.,* 1999);
- mass per surface area of the web to be bonded (density);
- roller diameter,
- compression pressure in the roller gap;
- bond pattern (Bhat *et al.,* 2004);
- bonding temperature (Michielsen et al., 2005);
- feeding speed of the web.

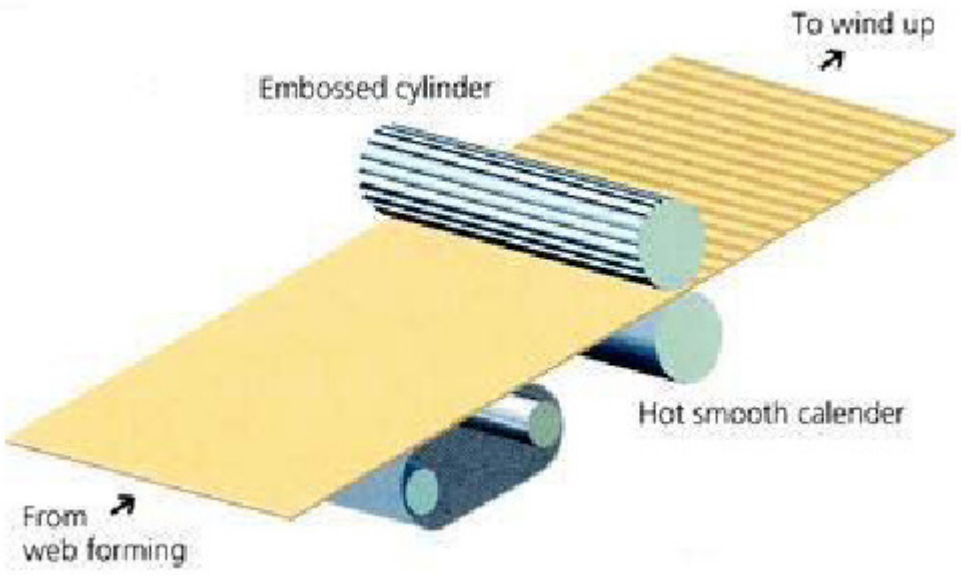

Figure 2.2. Nonwoven calendaring process (EDANA, 2007)

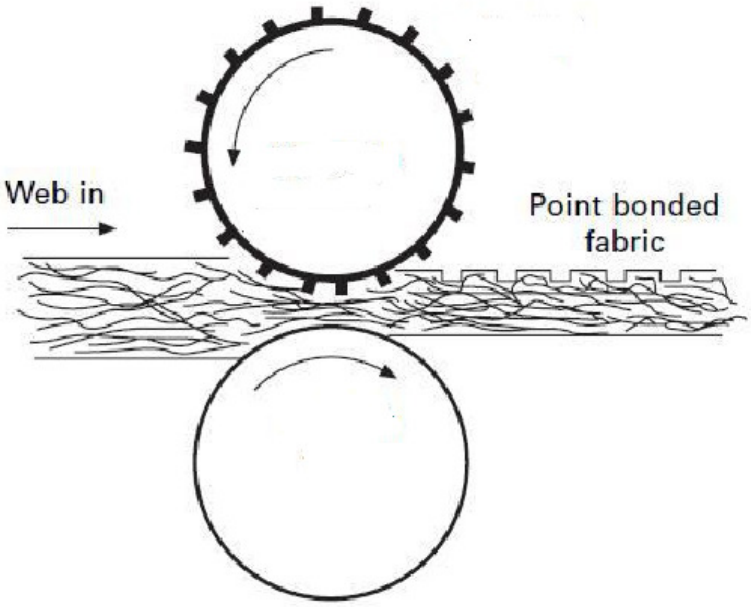

Figure 2.3. Engraved and smooth rollers (Russell, 2007)

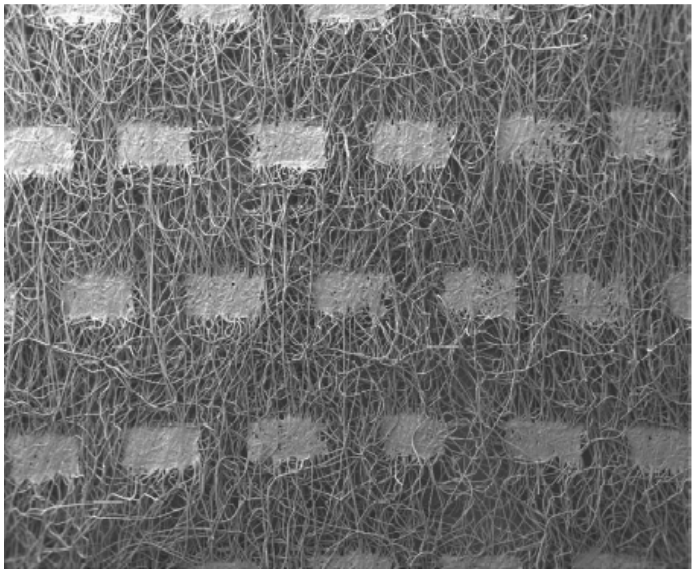

(a)

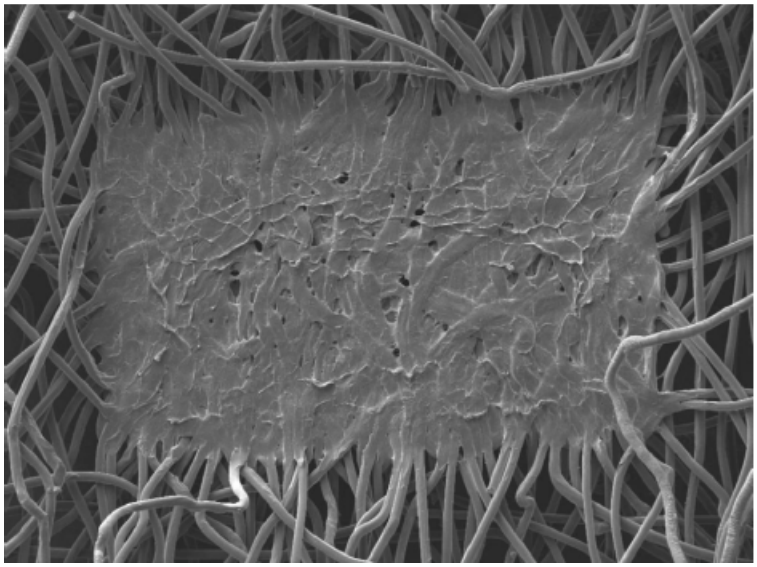

(b)

Figure 2.4. Bond points shown in SEM images: (a) bond points in a web (b) detailed sight (Hou *et al.,* 2009)

Thermal bonding is one of the most widely used bonding technologies in the nonwovens industry. Considerable efforts have been spent on trying to optimize the web-formation processes, bonding processes, and the fibre properties to achieve the desired end-use properties while reducing the cost of manufacture (Wang & Michielsen, 2001). Among these, the effects of compression pressure and

temperature are two of the factors in determining the mechanical properties. The effects of those are beyond the concept of the study but some of the previous efforts are shown to reflect the importance of those effects on the structural behaviour of nonwovens.

2.2.2 Compression Pressure

Sufficient pressure is needed to compact the web (decrease its thickness) so that efficient heat transfer through conduction can take place. In addition, pressure aids plastic flow at elevated temperatures, thereby increasing contact area between the fibres as well as decreasing thickness at the bond even further. Pressure also aids "wetting" of the surfaces by "melt" from the neighbourhood of the bond-point. Over the range of pressures commercially employed, higher pressures do not necessarily lead to higher performance. In calendar bonding, the bonding pressure appears to have little or no effect on fabric performance beyond a certain minimum (Figure 2.5). The temperature of the calendar together with dwell time would have an effect on the minimum pressure required to bond the web. Although no published research was found regarding the relationship between the bonding temperature and pressure, in general, when the temperature of the calendar is increased, the required minimum pressure should be decreased. It would be easier to compress the fibres as they will be softer due to high temperature, which in turn would lead to improved bonding. However, when the temperature is too high, high pressure can damage the fibres and the integrity of the bond points, consequently causing premature failure while forming the bond points.

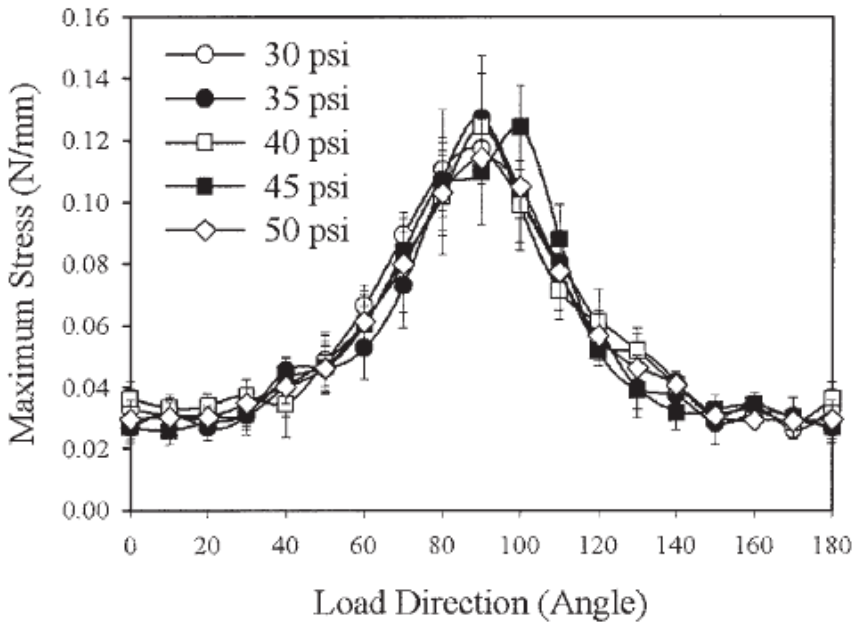

Figure 2.5. Mechanical properties in different angular directions as function of nip pressure (Michielsen *et al.,* 2005)

2.2.3 Bonding Temperature

Heating of the web must be done within the contact period in such a way that formation of bonding points takes place with simultaneous application of pressure. As shown in Figure 2.6, when the fibre-specific temperature is exceeded, a reduction of strength occurs (Michielsen *et al.,* 2005, Chidambaram & Batra, 2000). This can be attributed to the reduction of strength of fibres as a result of heat. Temperature must be selected carefully so that bonding of fibres results in optimum strength and the fibre structure in the bonding area is maintained. Insufficient compression pressure can also reduce the strength of nonwoven if the pressure is close to the minimum pressure required to compress the fibres after which further increase in pressure does not affect the strength required to bond the web together (indicated in section 2.2.2).

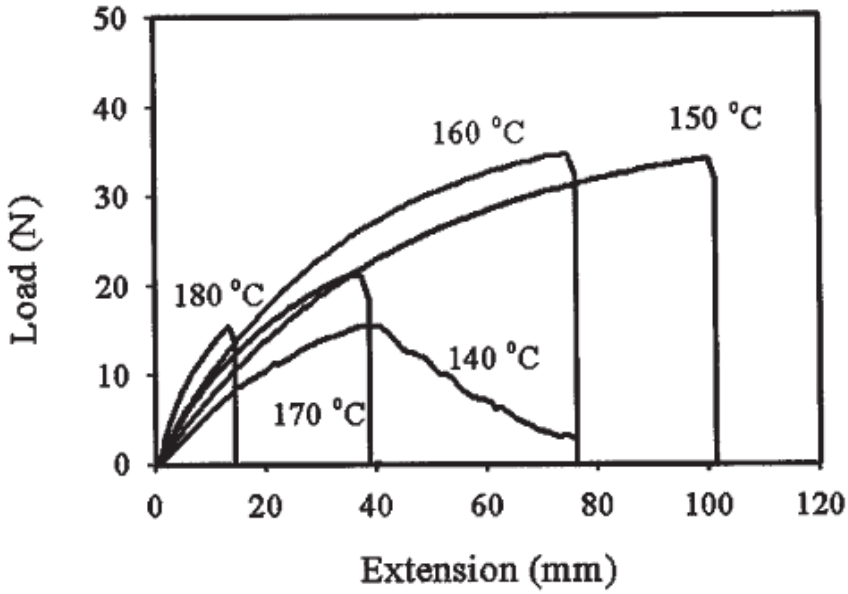

Figure 2.6. Effect of bonding temperature on stress–strain behaviour of nonwoven fabrics made of polypropylene fibres produced with a nip pressure of 40 psi (Kim *et al.,* 2001)

2.2.4 Fibres

Thermally bonded fabrics are produced both from entirely thermoplastic materials and from blends containing fibres that are not intended to soften or flow on heating. The non-binder component may be referred to as the base fibre component and commercially, a variety of base fibre types are used. The binder fibre component normally ranges from 5–50% on weight of fibre depending on the physical property requirements of the final product (Russell, 2007).

The base fibre contributes to key physical, chemical and mechanical properties of the fabric derived from the polymer from which it is constituted. This influences dyeing characteristics, flame resistance, tensile properties, hydrolytic resistance and biodegradability amongst many other properties (Bechter *et al.,* 1991). The commonly used fibres include natural fibres (regenerated cellulosic fibres, vegetable and protein fibres such as wool), synthetic fibres (polyester, polypropylene, acrylic,

nylon, aramid and many others), mineral fibres (e.g., glass and silica) and metallic fibres (Mezeix *et al.,* 2009). Sometimes the fibres (carrier fibre) are bicomponent with the core responsible for the strength and the sheath component for bonding. (Hamza *et al.,* 1986, Zhao et al., 2003, Demirci, 2010).

Depending on the manufacturing method, the fibres can be continuous or discontinuous (staple) in the nonwoven structure (Bhat & Malkan, 2000, Gong *et al.,* 2003). The layout of fibres for both cases is shown in Figure 2.7. A certain amount of crimp should be introduced in case the fibres are discontinuous for manufacturing requirements (Zheng, 2003).

(a) (b)

Figure 2.7. Layout of fibres in nonwoven structure; (a) continuous; (b) discontinuous (staple)

CHAPTER 3

MECHANICS OF NONWOVENS

As discussed in Chapter 1, one of the most important requirements is to understand the mechanical behaviour of nonwoven materials under the influence of external loads. In the last 40 years, many efforts have been made by researchers to understand the mechanical performance of nonwovens related to their structure. In this chapter, the factors related to the mechanical behaviour of nonwovens are discussed and the previous studies about the concept are reviewed. In addition, some principle concepts related to the mechanics of nonwovens are introduced.

3.1 Anisotropy and Orientation Distribution

The material properties of nonwovens are highly anisotropic. This behaviour is governed by distribution of connecting bond points that are distributed in the structure and their material properties of those. Figure 3.1 shows a stress – strain curve of 20 g/m^2 polypropylene nonwoven along machine and cross directions (MD and CD) (Hou *et al.,* 2009). These are the two perpendicular directions in the nonwoven that define its anisotropic structure.

As seen from Figure 3.1, there is a large difference in the behaviour of polypropylene nonwoven along two different directions; this behaviour is governed by orientation of fibres in the structure. This means that the orientation distribution directly influences the mechanical properties of materials (Pourdeyhimi *et al.,* 1996). The orientation distribution of fibres with respect to certain directions can be obtained by taking the microscopic image and analyzing the image by image analysis techniques (Figures 3.2, 3.3). In Figure 3.3, 0 degrees is the direction along CD and 90 degrees is the direction along MD. As it can be seen, more fibres are orientated towards machine direction. The determination of the orientation distribution makes use of advanced simulation techniques with implementing algorithms such as Fourier

transform (Pourdeyhimi & Kim, 2002), Fast Fourier Transform (Ghassemieh *et al.,* 2002), Hough Transform (Demirci *et al.,* 2009) etc.

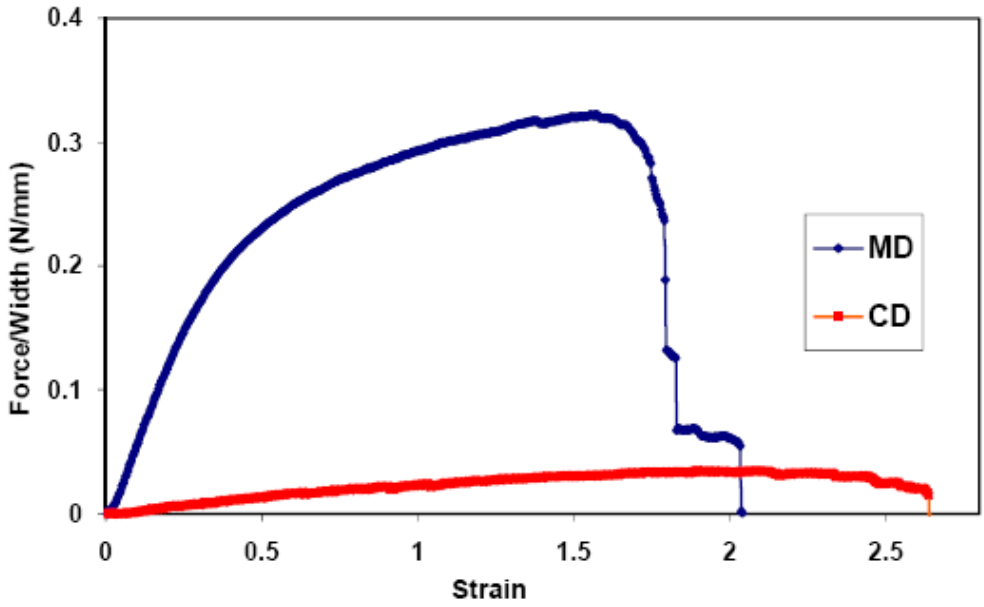

Figure 3.1. Different tensile behaviours of thermally bonded nonwoven fabric in MD and CD directions (Hou *et al.,* 2009)

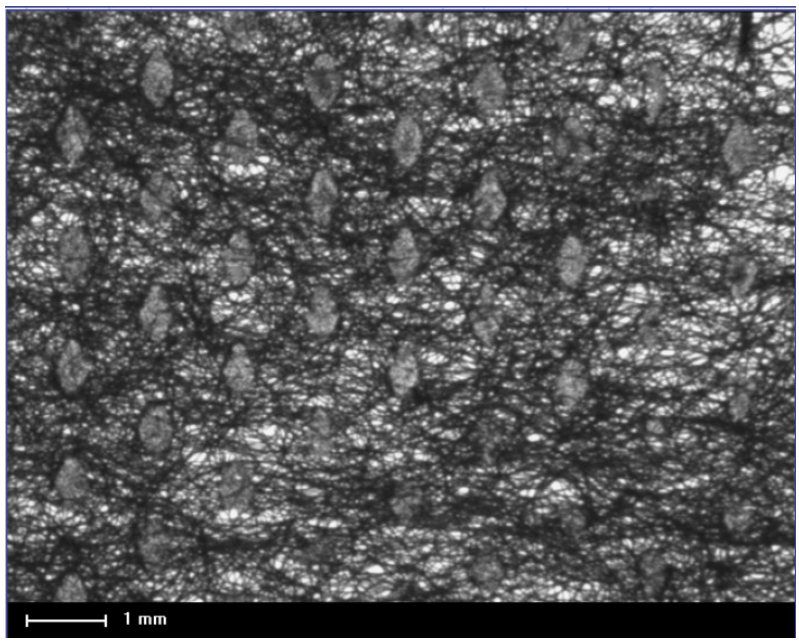

Figure 3.2. Microscopic Image of thermally bonded nonwoven (Maze & Pourdeyhimi, 2005)

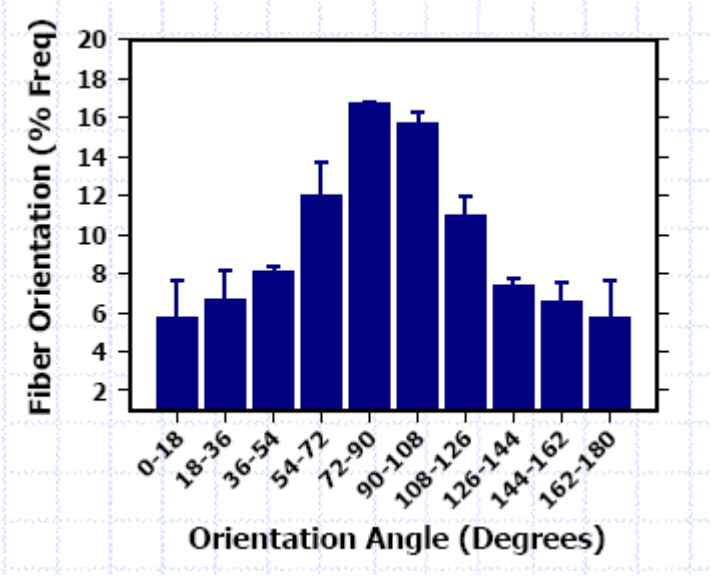

Figure 3.3. Orientation distribution with reference to cross direction (Maze & Pourdeyhimi, 2005)

3.2 Fibre Curl

When dealing with anisotropy and determination of the orientation distribution function, there is a factor that should always be taken into account – the curliness of fibres (Figure 3.4). It affects not only the initial deformation behaviour of nonwoven but also the accurate determination of orientation distribution function. It is introduced intentionally in the nonwovens having discontinuous fibre structure due to the manufacturing requirements. However, it is also present in the nonwovens having continuous fibre structure because of some misalignments during feeding the web into the calendar rollers.

The fibre curl has been studied since 1960s. The pioneering work by Backer & Petterson (1960) was extended by Hearle & Stevenson (1963) by introducing fibre curl into the structure. Since then many studies ignored the effect of fibre curl, especially dealing with nonwoven materials as it is difficult to implement it accurately. The tensile behaviour of nonwoven fabrics with introducing the fibre curl into a stress strain relationship of fibres was predicted by (Adanur & Liao, 1999). The fibre modulus is replaced by an equivalent one to include the effects of fibre curl

oriented in all directions. A curl in a fibre segment refers to its degree of curvature. They introduced the curl factor as follows:

$$C(\%) = \frac{L_c - L_s}{L_s} X100, \tag{3.1}$$

where L_c is the curve length of a fibre segment that spans two selected points. L_s is the straight distance between these two points. The distribution of curl factor was determined by some image analysis techniques. The results are shown in Figure 3.5.

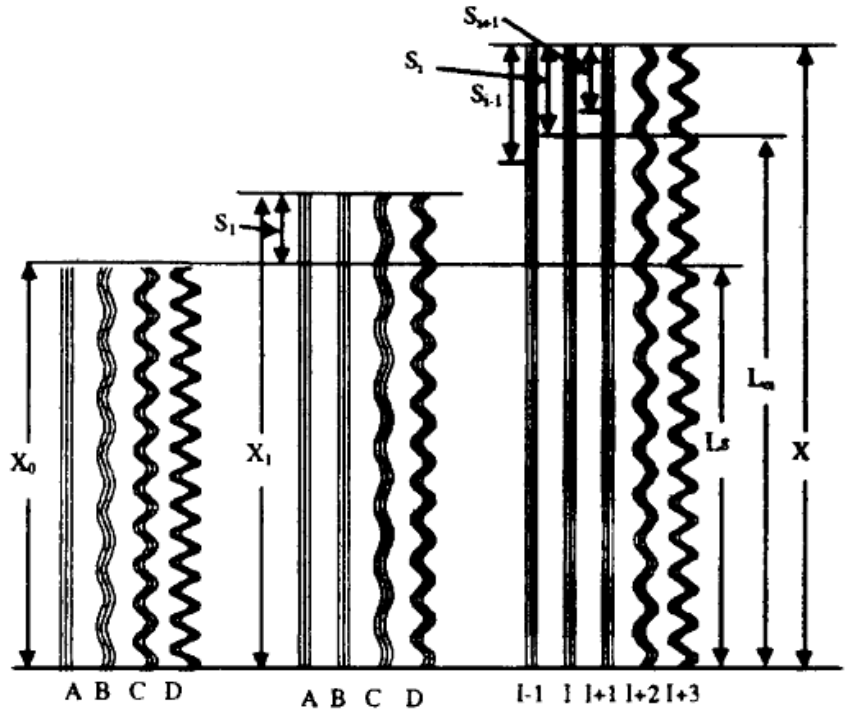

Figure 3.4. Schematics of fibre extension with different curls (Adanur & Liao, 1999)

In a recent work by Rawal (2007), the study of Adanur & Liao (1999) was extended with a new micromechanical model. The results were compared with those of experimental tests. However, a good correlation was not found with tensile behaviour of the nonwoven material (Figure 3.6). It was claimed that the reason was the contribution of bond strength. It is apparent that the predicted tensile stress curve was nearly parallel to the experimental one. This suggests that the distribution of fibre curl was not predicted accurately. As there should be a distribution of curliness of

fibres, some fibres having a low degree of curl were stretched in the very first time. Although there may be the effect of entanglement and friction between the fibres, it is thought that the main reason was the prediction accuracy in the fibre curl. The importance of fibre curl was also justified in the thesis which affected the tensile behaviour of nonwovens significantly.

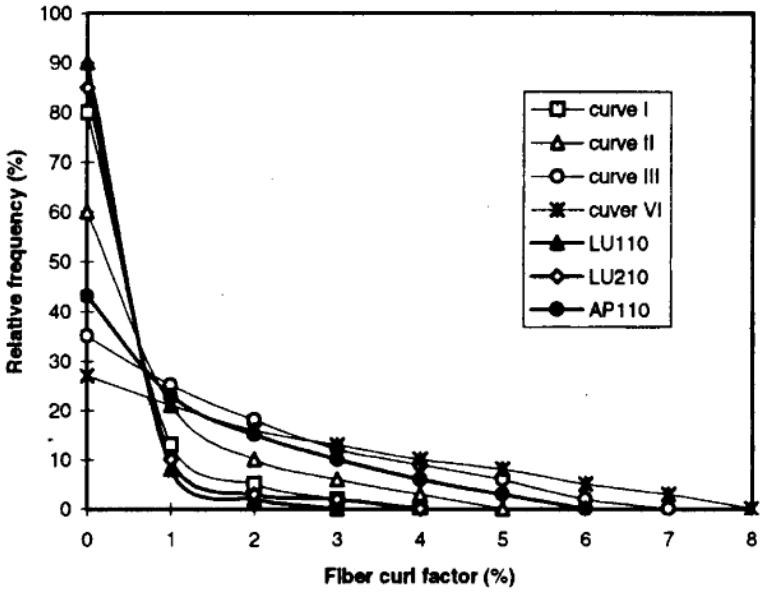

Figure 3.5. Relative frequency of fibre curl for different fabrics (Adanur & Liao, 1999)

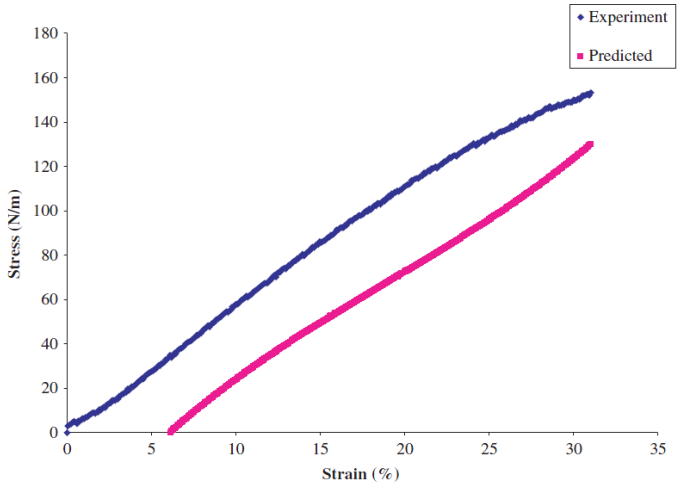

Figure 3.6. Stress strain curve of thermally bonded nonwoven (Rawal, 2007)

3.3 Mechanics of Fibre Materials

Materials of fibres used in nonwovens are generally polymers. The main reason of using polymers is their extraordinary range of accessible properties and their low cost (The national academy press, 1995).

Many studies were published during the last two decades on the laws governing the mechanical behaviour of polymer materials. Because of the structural complexity of these materials, several models are being developed and used. The phases present in the micro-structure of polymers, especially semi-crystalline ones, are the main reason for complexity of their mechanical behaviour. Several studies showed the existence of viscous contributions to the behaviour of polymers (Dijkstra *et al.,* 2003, Colak & Dusunceli, 2006, Zrida et al., 2009). The deformation behaviour of polymers is generally assumed to be as viscoelastic, viscoplastic or elastoviscoplastic behaviour (Lee *et al.,* 1993, Nikolov & Doghri, 2000, Van Dommelen *et al.,* 2003)

3.3.1 Viscoelasticity in Polymers

Viscoelasticity is the property of materials that exhibit both viscous and elastic characteristics when undergoing deformation. Viscous materials resist shear flow and strain linearly with time when a stress is applied. Elastic materials strain instantaneously when stretched and just as quickly return to their original state once the stress is removed. Viscoelastic materials have elements of both of these properties and, as such, exhibit time-dependent strain. There are two most important realizations of viscoelastic behaviour in nature. Firstly, if the stress is held constant, the strain increases with time (which is called *creep*). Secondly, if the strain is held constant, the stress decreases with time (*relaxation*) (Meyers & Chawla, 1999).

The stress-strain equations used in viscoelasticity are given in the documents of some of the finite element softwares (ANSYS, 2008, Marc Analysis Research Coorporation, 2007). They are not only dependent on the current stress and strain state but also on the entire history of development of these states. This constitutive behaviour is most readily expressed in terms of hereditary or Duhamel integrals. These integrals are formed by considering the stress or strain build-up at successive

times (Marc Analysis Research Coorporation, 2007). The behaviour can be expressed in creep or relaxation form.

Small Strain Viscoelasticity

One of the most extensively used models is the Generalized Maxwell Model in viscoelastic analyses (Lin *et al.,* 1995). This generalization is equivalent to arranging many of the dashpot-spring combinations with different values of viscosity and material elastic constant together in parallel, as shown in Figure 3.7.

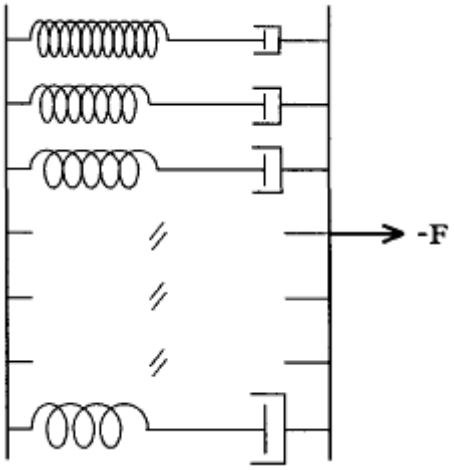

Figure 3.7. Generalized Maxwell Model represented by springs and dashpots (Lin, 2003)

Large Strain Viscoelasticity

For an elastomeric time-independent material, the constitutive equation is expressed in terms of energy function. For large-strain viscoelastic material different formulations are developed. One of the formulations used in finite element codes for large-strain viscoelasticity is derived by Simo (1987), who generalized the small-strain viscoelasticity material behaviour to a large-strain viscoelastic material. The derivation of stress strain relationship in this model is quite long. Further knowledge can be obtained from Marc Analysis Research Coorporation (2007).

3.3.2 Viscoplasticity in Polymers

There are some analytical models that define constitutive relationships for a plastic strain regime, and they all assume a linear elastic behaviour terminated by a yield point that is rate dependent. This means that the yield surface of the material is rate-dependent. Since the purpose of these models are to develop methods to calculate deformations, which are rate-dependent beyond the yield point of a material they are often referred to by the term *viscoplasticity* (Brinson & Brinson, 2008). More general theories of viscoplasticity have also been developed, in some of which no yield stress is necessary (Lubliner, 2006, Bodner & Partom, 1975). Deriving these equations would be very cumbersome and can be obtained from the relevant references.

3.3.3 Polymer Viscoelasto–plastic Behaviour

The determination of viscoelasto-plastic properties is a big concern and many researchers dealt with determining the viscoelastic mechanical parameters of polymers. In a recent study by Felhos *et al.,*(2008), the viscoelastic properties of ethylene, propylene and rubber are determined by dynamic mechanical thermal analysis (DMTA), and the Maxwell model was proposed in their structure. Rolling friction was simulated whereby a steel ball is rolling on the plate. A rolling test to compare the results was also performed. The test method is a very complex work and from the test results, it could be understood that the data were not scattered much. The master curve obtained in the tests is given in Figure 3.8.

In a study by Drozdov & Christiansen (2002), tensile relaxation tests were performed for post-yield regions, which is an alternative method to use DMTA. Although the results were not verified with simulations, their plots in the paper clearly show that polypropylene has a large ratio of viscoelastic behaviour that should not be discarded in finite element modelling especially during slow deformations.

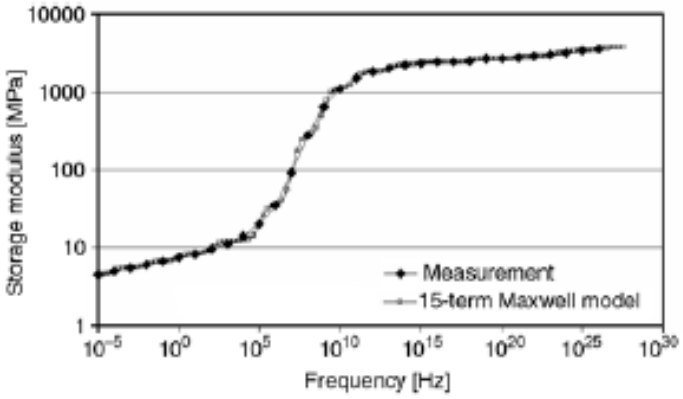

Figure 3.8. Master curve obtained in Felhos *et al.,*(2008)

Ambroziak & Kłosowski (2007) studied viscoplastic parameters of polypropylene – ethylene copolymer and their implementation into a numerical model. Uniaxial tests with different strain rates were performed to determine the parameters. Although the method is a rather efficient method to determine the viscoplastic parameters, the application of these parameters to a different loading condition is problematic, although the authors did not mention that. Still, this paper gives an effective tool to implement viscous parameters in a finite element model.

There are not many studies that reflect the viscoelastic properties of fibres in the general behaviour of nonwovens. Among many studies about the behaviour of fibre properties, Mishakov *et al.,*(2006) related the effect of viscoelastic properties of fibres to the deformation behaviour of nonwovens. An irreversible strain component was proposed from the tests. But the application of finite element programs is questionable and requires much effort when compared to readily available models in the commercial softwares.

Klosowski *et al.,*(2009) proposed a description for nonlinear viscoelastic behaviour of a textile material, made of two polyester thread families woven perpendicularly to each other with double-side PVC coating. The long-term uniaxial creep laboratory tests in the thread direction were conducted at five different constant stress levels. For the fabric behaviour a different viscoelastic constitutive model for threads was assumed. The results obtained were verified by simulation of laboratory tests.

3.4 Computational and Analytical Modelling of Mechanical Behaviour of Nonwovens

In order to predict the mechanical behaviour of woven textiles, researchers used many different approaches including analytical and computational models (Potluri & Manan, 2007). Similarly, many efforts were spent for nonwoven materials as well. In a work by Bais-Singh & Goswami (1995), an analytical model was presented and its results were compared with test data. The tests were conducted at a single strain rate which is a very doubtful assumption as polymer behaviour is considerably affected significantly by strain rate.

In a work by Kim & Pourdeyhimi (2004), an orthotropic theory was applied to the mechanical behaviour of nonwovens taking into account their orientation distribution. The results of tensile and shear tests reflected the orthotropic behaviour and confirmed the results. This was an important study, which proved that orthotropic modelling is well suited to point-bonded nonwovens. A similar study by Ostoja-Starzewski & Stahl (2000) also showed the orthotropic structure of different fibrous networks.

One of the principle computational models was developed by Mi & Batra. In that study, an incremental deformation principle was proposed. In that model, the bond points were assumed rigid and the fibre behaviour was taken from the nonlinear tensile response of fibre pull-out tests. The model did not include viscoelastic parameters, which would definitely have an effect if the loading speed was changed. However, the application of that model for a different range of nonwovens is questionable. In the second part of the study the results with actual nonwoven tests were compared (Mi & Batra). The result plots did not include the information on test speed, so again it should be mentioned that the results may differ for different loading speeds and conditions.

Kim & Pourdeyhimi (2001) proposed a computational model to study the role of the bond point geometry, distribution and fibre properties. Realistic results were

obtained according to fibre distribution and fibre strength. However, any results revealing the effect of bond point geometry were not presented.

3.5 Finite-Element Analysis of Nonwovens

3.5.1 Introduction to Finite Element Analysis

Many physical phenomena in engineering and science can be described in terms of partial differential equations. However, solving these equations by classical analytical methods for arbitrary shapes is almost impossible. The finite element method (FEM) is a numerical approach, with which these equations can be solved approximately. From an engineering standpoint, the FEM is a method for solving engineering problems such as stress analysis, damage, heat transfer, fluid flow and electromagnetic analysis by computer simulations (Fish & Belytschko, 2007, Ashcroft *et al.*, 2012). The basic idea of the finite element method is to divide the body into finite elements, connected by nodes, and obtain an approximate solution. Finite element studies are a very broad subject and it is impossible to discuss their every aspect here. Hence, in this section only some basic principles of finite elements in solid mechanics are presented.

3.5.2 Underlying Theory in Structural Finite Element Analysis

Regardless of geometry, material, boundary conditions and type of the problem, the finite-element method follows a general, well-defined step by step procedure (Tekkaya, 1999):

Idealization

The continuous medium is divided into a finite number of ideal elements bearing some simplifications. First, geometrical idealization takes place and the ideal geometry is obtained. Then, any curved boundaries are replaced with straight ones. Second, the real displacement field is approximated. Finally, other properties such as a material behaviour and loading conditions are approximated.

Discretization

The body is divided into parts, which are called *elements* that will be combined in the calculations. This operation is called *meshing* of the structure. The shape and number of these elements are directly related to how accurate the stress and strain related solutions are obtained.

Determination of Element Properties

The relationship between unknown displacements and known forces are written as:

$$\{f\} = [k]\{u\}, \tag{3.2}$$

Where $[k]$ is the element stiffness matrix, $\{f\}$ is the nodal force vector and $\{u\}$ is the nodal displacement vector. The stiffness matrix can be found directly or with a variational approach (ANSYS, 2008)

Assembly of Element Stiffness

After the element stiffnesses are determined, assembly is performed according to the nodal principles of discretization. These are compatibility and equilibrium of nodal forces. By this way an overall stiffness matrix is obtained for the whole structure.

Introduction of Boundary Conditions and Solution

The assembled equations are singular if boundary conditions are not introduced. With a sufficient number of known values of forces and displacements, the unknown displacements are obtained from,

$$\{u\} = [K]^{-1}\{F\}. \tag{3.3}$$

Computation of strain and stress values

With the known displacements, it is possible to compute the dependent variables like stresses and strains in the element by using the theories related to the material behaviour.

3.5.3 Nonlinearity in Finite Element Analysis

Nonlinearity is explained in detail in ANSYS (2008). Nonlinear structural behaviour arises from a number of causes, which can be grouped into three principal categories; a changing status, geometric nonlinearities and material nonlinearities. The changing status is related with the contact condition occurred in the structure causing a change in the stiffness matrix. In a case of geometric nonlinearities, the structure experiences large deformations, and the nonlinearity is governed by large displacements and/or rotations. The last one is the material nonlinearity, which is the main aspect considered in the study. There are generally factors influencing a material's deformation behaviour under stress such as load history, environmental conditions (temperature etc.) and the time-dependent behaviour. In the viscoelastic material to be modelled in the thesis, load history and time-dependent behaviour causes nonlinear behaviour in the structure.

When dealing with the nonlinear material behaviour, each finite element analysis software can use unique approaches. In general, the Newton – Raphson approach is the most commonly used method to deal with nonlinear problems (Figure 3.9). In this method, the load is divided into a series of load increments (iterations). The load increments can be applied over several load steps.

The procedure that was employed by Marc Analysis Research Coorporation (2007) is described here as it is the solver used in the study. For a small displacement case,

$$K(u)\delta u = F - R(u), \tag{3.4}$$

where u is the nodal-displacement vector, F is the external nodal-load vector, R is the internal nodal load vector (following from the internal stresses), and K is the tangent-stiffness matrix. The internal nodal-load vector is defined for the internal stresses from the following equation:

$$R = \sum_{elements} \int_V \beta^T \sigma dv, \tag{3.5}$$

where β^T is the differential operator which transforms displacements to strains. Supposing that the last obtained approximate solution is termed ∂u^i , where i represents the iteration number, Eq (3.4) can be written as

$$K(u_{n+1}^{n-1})\delta u = F - R(u_{n+1}^{n-1}). \quad \textbf{(3.6)}$$

Solution of this equation completes one iteration and the process can be repeated for further steps. When it is determined that the iterations are getting closer each time and at the end do not change too much, the solution is said to be converged and the solution is obtained (Figure 3.9). When the calculations do not show an improvement with the iterations, the calculations diverges. There are many techniques for dealing with this problem which have very detailed explanations elsewhere and not discussed here.

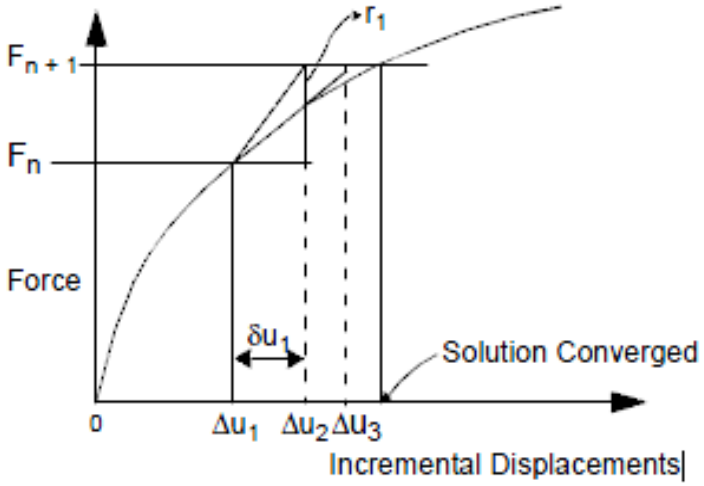

Figure 3.9. Newton – Raphson algorithm (Marc Analysis Research Corporation, 2007)

3.5.4 Previous Finite Element Studies of Nonwoven Materials

Regarding the finite element analysis of nonwoven materials, very few studies have been performed until recently. One is the study accomplished by Mueller & Kochmann, (2004). A discontinuous model for the analysis of tensile behaviour of nonwovens was generated there (Figure 3.10).

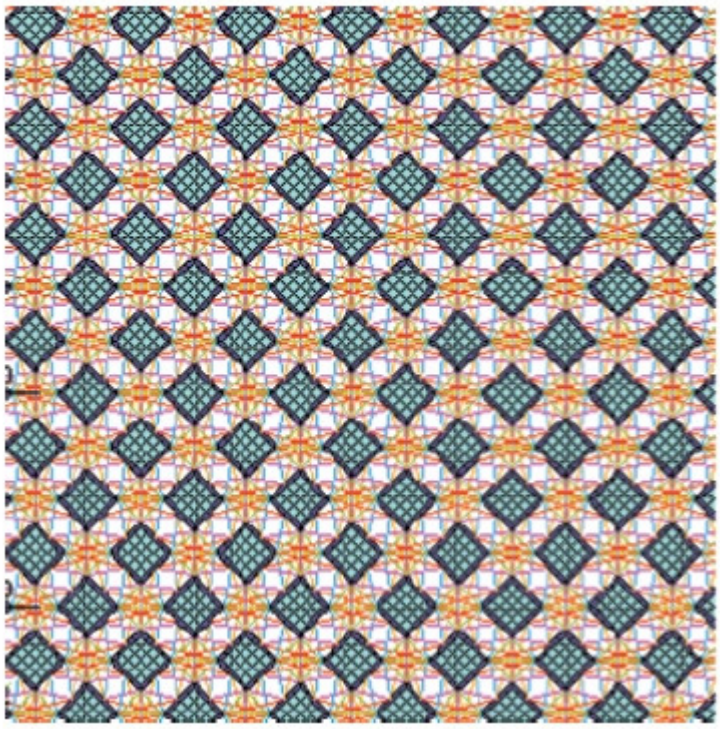

Figure 3.10. Discontinuous finite element model (Mueller & Kochmann, 2004)

In order to obtain the material properties, fibre and fibre-bundle tests were performed to determine the deformation behaviour and failure. However, the use of those failure results in the model and the failure behaviour was not presented. The orientation distribution function regarding the structure was presented. However, the explanation of its implementation into the finite element model was not clear. Besides, the model did not include the details of the material properties of bond points. The only information given was that they were modelled with isotropic properties. The effect of bonding temperature was added to the model. However, its effect was not implemented in the paper as a change in the deformation behaviour, though it was implemented as a change in the dimension of bond points according to bonding temperature. The model was verified by tests but when the results are examined, it is obvious that the stress – strain curve results in machine direction and cross direction were very similar to each other (Figure 3.11). Generally, nonwovens exhibit a high degree of anisotropic behaviour in tensile loading in cross and machine directions.

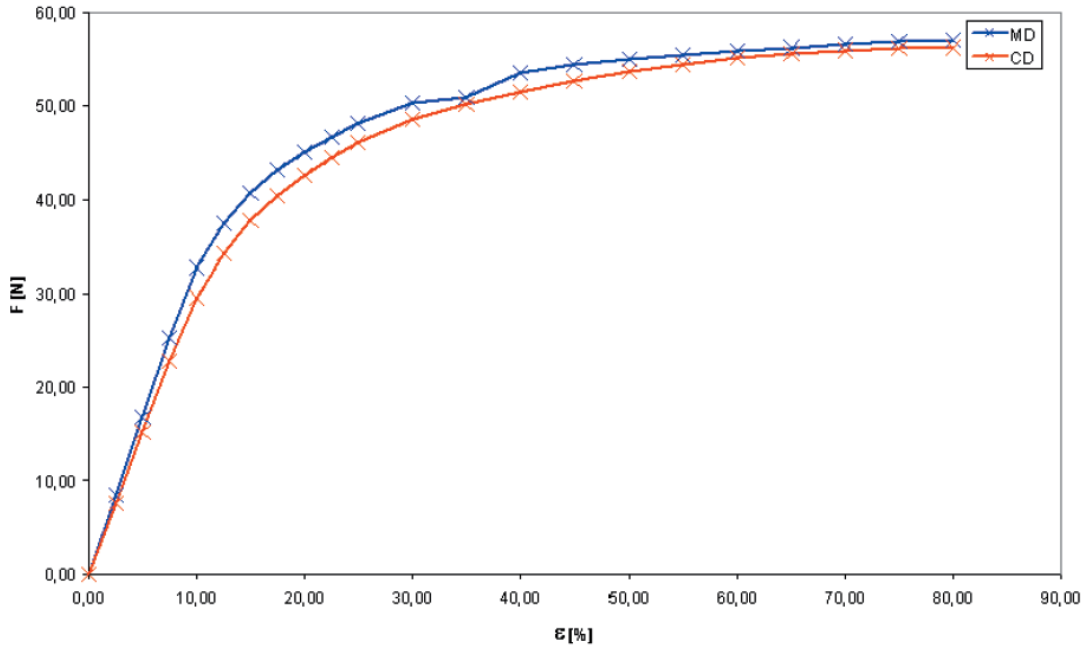

Figure 3.11. Stress-strain curves in the simulations (Mueller & Kochmann, 2004)

Another finite element model developed by Limem *et al.,* (2007) is also of interest (Figure 3.12). A discontinuous nonwoven model was suggested by connecting bond points with truss elements according to a certain pattern. While connecting the bond points, it was assumed that no fibres link bond points in cross direction as it is known that very few fibres were oriented along it (Figure 3.13). Although it may be a valid assumption, this may create convergence problems for the simulations in cross direction as too much rigid body movement would take place. The results in cross direction were not presented so this situation might have been experienced by them. The orientation distribution function was applied by assigning relevant cross-sectional areas to the truss elements. The methodology was observed and some assumption problems were recognised. Besides, it was realized that the equation of calculating average fibre length through the bond points was not correct. The methodology of assigning orientation distribution function to finite-element model was presented. However, the actual distribution was not shown. Hence, it is impossible to judge whether or not this is a realistic model that simulates the real behaviour.

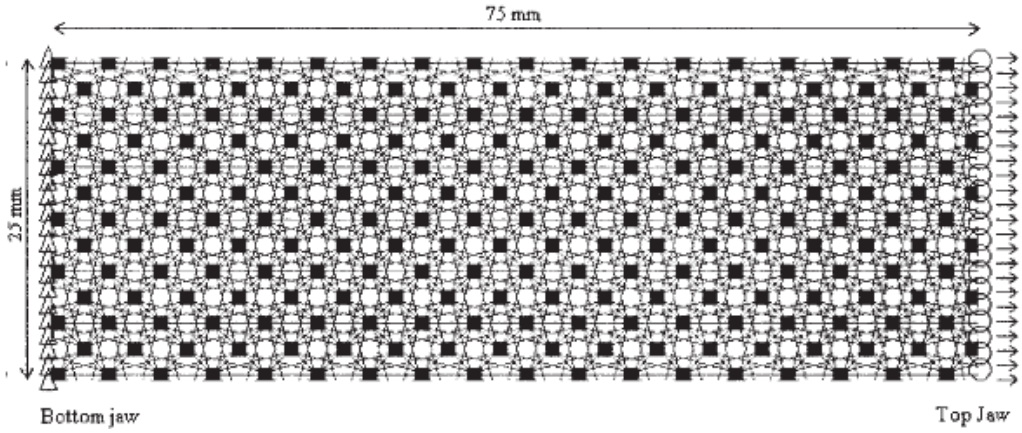

Figure 3.12. Finite element geometry for nonwoven simulation (Limem *et al.,* 2007)

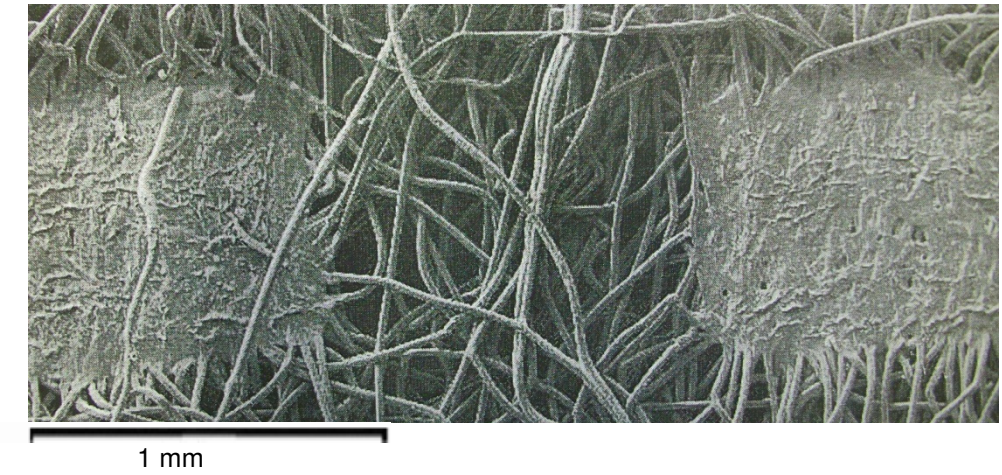

Figure 3.13. SEM picture of a nonwoven showing very few or no fibre connects bond points in cross direction

Recent models were developed by Hou *et al.,* (2009). Both discontinuous and continuous modelling were performed to reflect the tensile behaviour of low-density nonwovens. For the continuous model, the material properties were obtained from stress – strain curves of the fabric in cross and machine directions. The main problem in this model is that the material behaviour was valid only for specific type of nonwoven as the material properties are obtained from the tests performed to that specific nonwoven. If a different nonwoven type is required to be simulated, it would be impossible to judge how material properties are affected. Due to this reason, a

more realistic discontinuous model was developed where the properties of fibres (not the entire nonwoven) can be implemented into the model (Figure 3.14). In this method, a fibrous network was first constructed according to orientation distribution and then the bond points were introduced to the structure. This is a good method for implementation orientation distribution as it is utilized by the modelling of fibres. The problems with this method were first, the convergence was a big problem because it was impossible to model all the fibres in the structure. In this case the model becomes unstable with a limited number of fibres in the structure. Second, only linear elastic material properties were used for the fibres. Third, the model was constructed for one specific type of model. By using the utilized modelling technique, it is difficult to analyze another type of nonwoven.

In another recent study by Demirci (2010), the tensile behaviour of thermally bonded high-density nonwovens was simulated with a continuous finite element model (Figure 3.15). In this model, the fibre matrix and bond points were modelled as shell elements. Orientation distribution was implemented by assigning orthotropic material behaviour to shell elements representing fibres. Good correlation was observed between the simulations and tests. However, the model was specific for high-density nonwovens with a continuous fibre structure. The author mentioned that the model was not valid for nonwovens below a density of 50 g/m^2. The length of fibres was not modelled as the studied nonwoven had a continuous fibre structure. Though, with this modelling technique, it is not possible to model the length of fibres in case the nonwoven model had discontinuous fibrous network. The model is also not efficient to investigate the effect of dimensional parameters on the structural behaviour as it is not a straight forward procedure to modify the model parameters and the mesh structure together.

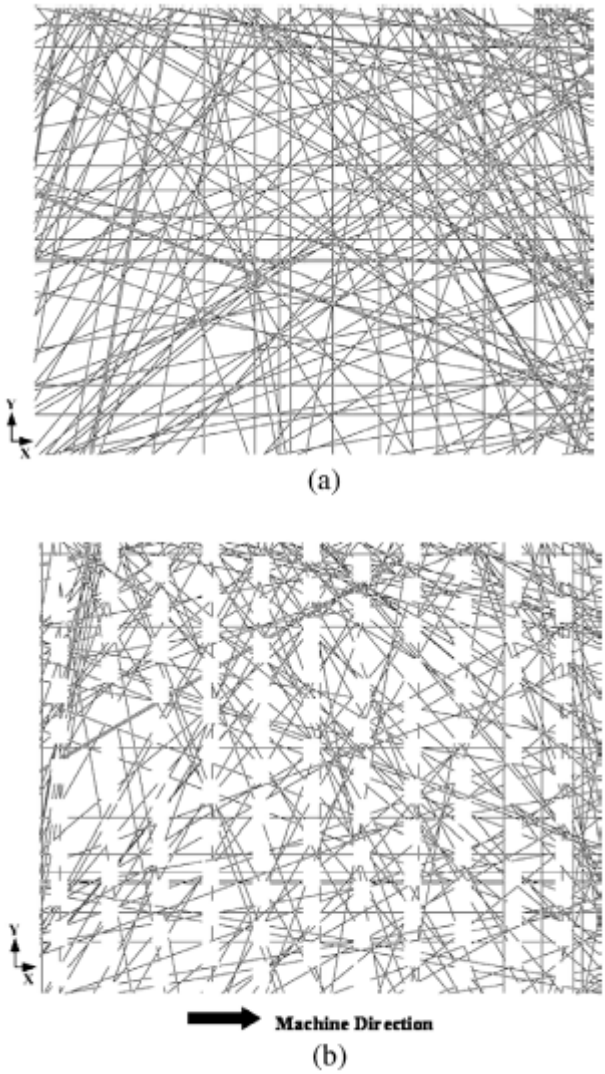

Figure 3.14. Discontinuous model (Hou *et al.*, 2009)**:** (a) fibrous network; (b) with the bond points

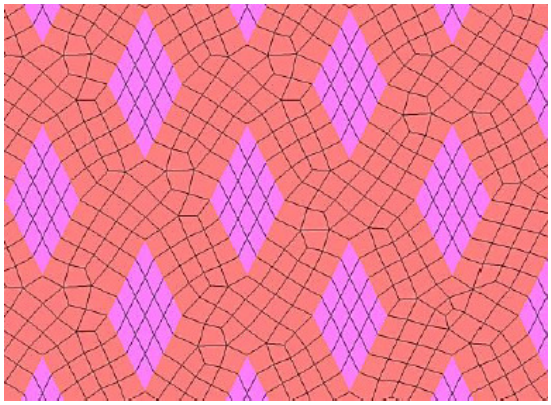

Figure 3.15. Continuous model (Demirci, 2010)

After the examination of previous finite element studies, the following points were noted:

- Generally, these studies simulate the deformation behaviour for a particular nonwoven. Their use for different kinds of nonwovens would require a lot of effort.
- In some studies, finite element simulations did not represent the realistic behaviour up to an acceptable level. In others, sufficient information was not given for the reader to understand the modelling details.
- None of the studies include the failure behaviour.
- Almost all finite element models were generated to simulate tensile behaviour
- The curliness of fibres was not considered in any of the studies.
- A continuous finite element model can be preferred only for the nonwovens employing high-density structure. It is generally not preferred for low-density nonwovens as it is hard to introduce the random behaviour. Besides, assigning material properties to a continuous model to represent the fibrous structure is another problematic task. As nonwovens generally show orthotropic behaviour, the number of material constants to be determined increases. The implementation of further studies such as failure of fibres is also a challenging task and requires additional assumptions.
- In discontinuous models, assigning material properties to the structure is easier as isotropic material properties could be used to model the fibres. However it is a challenging task to construct the finite element model that represents fibrous structure.

Finite element codes generally offer parametric modelling options which provide user capabilities to do automated tasks according to the parameters in the model. Thus, in this study, discontinuous modelling technique is preferred for the development of parametric finite element models. This allows modelling of different types of nonwovens in an easy manner. Material failure and application of various

boundary conditions were not studied here as well. However, the presented modelling method is very efficient to be developed for such further studies.

Assigning accurate material properties to material models is a significant task in finite element simulations. In discontinuous models, the properties of fibres that make the structure of nonwoven material should be determined. In the present study, the available nonwovens are made of polypropylene fibres As it is known that the tensile properties of polypropylene is dependent on the rate of loading, the studies start with understanding the deformation behaviour of polypropylene fibres in the nonwoven under tensile load with various strain rates.

CHAPTER 4

RATE-DEPENDANT TENSILE PROPERTIES OF POLYPROPYLENE FIBRES

4.1 Introduction

Assigning accurate material properties is crucial for finite element analyses and hence, needs significant efforts. The material of fibres used in this study is polypropylene. It is known that polypropylene shows viscoelastic deformation behaviour. But before dealing with the modelling of such an advanced behaviour, it is required to find the stress strain behaviour at various loading rates.

Tensile tests for polypropylene fibres used in this study, was performed by Hou (2010) at different test speeds. The results are shown in Figure 4.1.

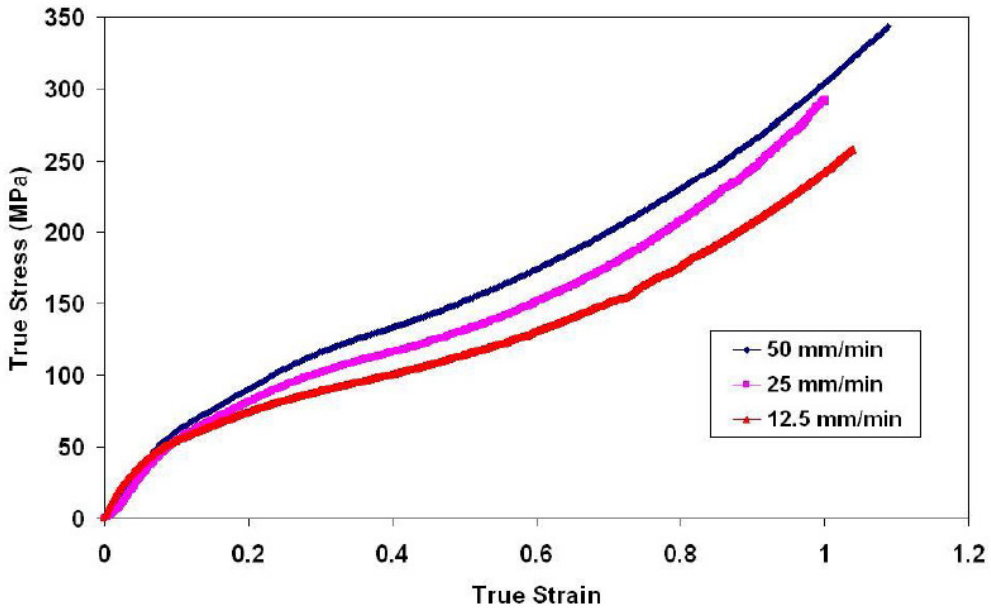

Figure 4.1. Stress – strain curves for single polypropylene fibre tests (Hou, 2010)

It can be seen from this figure that the stress-strain behaviour changes with the test speed. However these test results have some problems. Firstly, there is no information on gage lengths of specimens used. So it is impossible to convert the loading rates to strain rate values. Secondly, these curves have a constant engineering strain rate because of the constant cross-head speed. However, real deformation behaviour of the material for a given strain rate means that it should be defined for a constant-true-strain rate. When the engineering strain rate is held constant, the true strain rate value decreases with engineering strain. This can be shown by obtaining the expression for a true strain rate:

$$\varepsilon_{true} = \ln(1+\varepsilon_{eng}), \tag{4.1}$$

$$\frac{d}{dt}\varepsilon_{true} = \frac{d}{dt}\ln(1+\varepsilon_{eng}), \tag{4.2}$$

$$\dot{\varepsilon}_{true} = \frac{\dot{\varepsilon}_{eng}}{1+\varepsilon_{eng}}, \tag{4.3}$$

where, ε_{eng} and ε_{true} are engineering and true strain, respectively. The expression for true strain can also be found from the following equations:

$$\varepsilon_{eng} = \frac{u}{L_0} = \frac{L-L_0}{L_0}, \tag{4.4}$$

$$L = \varepsilon_{eng} L_0 + L_0, \tag{4.5}$$

where L_0 and L are initial and current lengths of the specimen, respectively, and u is the displacement of cross head. The true strain rate is the instantaneous rate. So;

$$\dot{\varepsilon}_{true} = \frac{V}{L} \tag{4.6}$$

$$\dot{\varepsilon}_{true} = \frac{\dot{\varepsilon}_{eng}, L_0}{L} \tag{4.7}$$

Then, the length of the specimen obtained from equation (4.5) is substituted into equation (4.7) to obtain expression (4.3).As it can be seen, the true strain is not only dependent on the test speed, but also on the current strain value. For example, for the test results obtained for a 25 mm/min test speed in Hou (2010), the true strain rate *vs.*

true strain curve is given in Figure 4.2 assuming that the gage length is 12 mm. This gauge length value is estimated based on the length of fibres in the structure. It is just used to show the reduction in true strain rate.

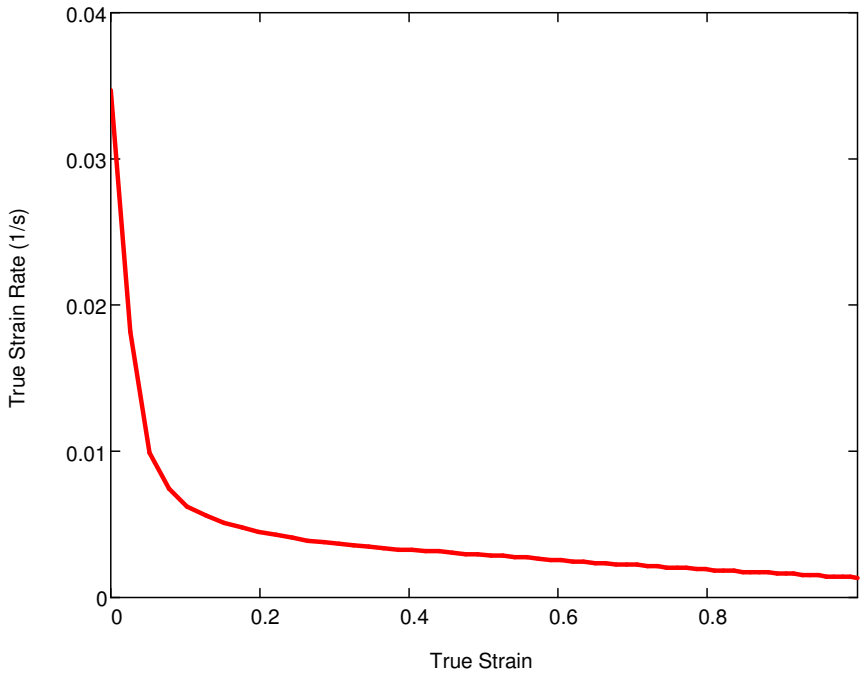

Figure 4.2. True strain rate *vs.* true strain curve for test speed 25 mm/min and assumed gauge length of 12 mm

As it can be seen from Figure 4.2, the strain rate value decreases to less than 1/5th of the initial value. In order to compensate for this reduction, the test speed should be increased gradually by introducing acceleration to the cross-head movement. This regime is not available for conventional test machine so it was decided to increase the speed incrementally until the end of the test.

Another concern about the tensile tests is the effect of the Poisson's ratio. Following is the equation for the calculation of true stress:

$$\sigma_{true} = \sigma_{eng}(1+\varepsilon_{eng}). \qquad \textbf{(4.8)}$$

The expressions for true strain and true stress values are valid for the condition that the material is incompressible (that means the Poisson's ratio is 0.5). Otherwise, the decrease in the cross-sectional area should be determined. The diameter of

polypropylene fibres in this study was previously determined by Hou (2010) as 0.02 mm. For the polypropylene fibres of this diameter, it is not possible to connect a device that can measure the decrease in the cross-sectional area. There are some techniques in the literature based on optical techniques in order to measure the decrease in the cross-sectional area (Krucinska & Stypka, 1991, Fathi *et al.,* 2012). However, the implementation of these techniques is not straightforward and need sophisticated equipment/experience which are beyond this study. Therefore, after conducting a literature survey, Poisson's ratio of fibres which is determined in Duffo *et al.* (1995), is assigned to the fibres in this study as 0.35.

Three expressions were found in the literature related to Poisson's ratio dependence of true stress. One was given by Arriaga *et al.,* (2007) that adds the effect of Poisson's ratio as

$$\sigma_{true} = \frac{\sigma_{eng}}{(1-\nu\varepsilon_{eng})^2}. \qquad \textbf{(4.9)}$$

It was thought that there is a mistake in this equation. Because it should give an expression equal to the equation (4.8) when ν is equal to 0.5, where as it does not. Another expression was given by Lin (2001) as

$$\sigma_{true} = \frac{\sigma_{eng}(1+\varepsilon_{eng})}{1+(1-2\nu)\dfrac{\sigma_{eng}}{E}}, \qquad \textbf{(4.10)}$$

where E is the modulus of elasticity. True stress values obtained from this equation are plotted along with the expression that assumes polypropylene as an incompressible material ($\nu = 0.5$) for a tensile test with 25 mm/min strain rate (Figure 4.3). It can be seen that the values are very close to each other. As a result, the true-stress expression that assumes polypropylene as an incompressible material can be used for the studied fibres

4.2 Test Methodology

In the light of these findings, the stress – strain curve for polypropylene was determined. Single-fibre tests were performed with the MicroTester with a 5 N loadcell. MicroTester is a small scale version of the traditional tensile test machines.

It has the ability to perform tension, compression and low-cycle fatigue tests with a load range of 2mN up to 2 kN with a very high precision drive system and load measurement (INSTRON®, 2012). First, a free fibre found at the edge of the fabric was extracted with tweezers (Figure 4.4). Its ends were stuck on a sticky paper (Figure 4.5). Then those stickers were attached to the jaws of the test machine (Figure 4.6). Some glue was spread inside the jaws to prevent them creating stress concentration. Then the crosshead was lowered until the jaws were nearly touching each other (Figure 4.7). At that time, the displacement value was reset. Then the top jaw was moved upwards again until a force increase was read from the load cell. At that time, the displacement value, which shows the gauge length, was read from the screen. Then the displacement value was reset again.

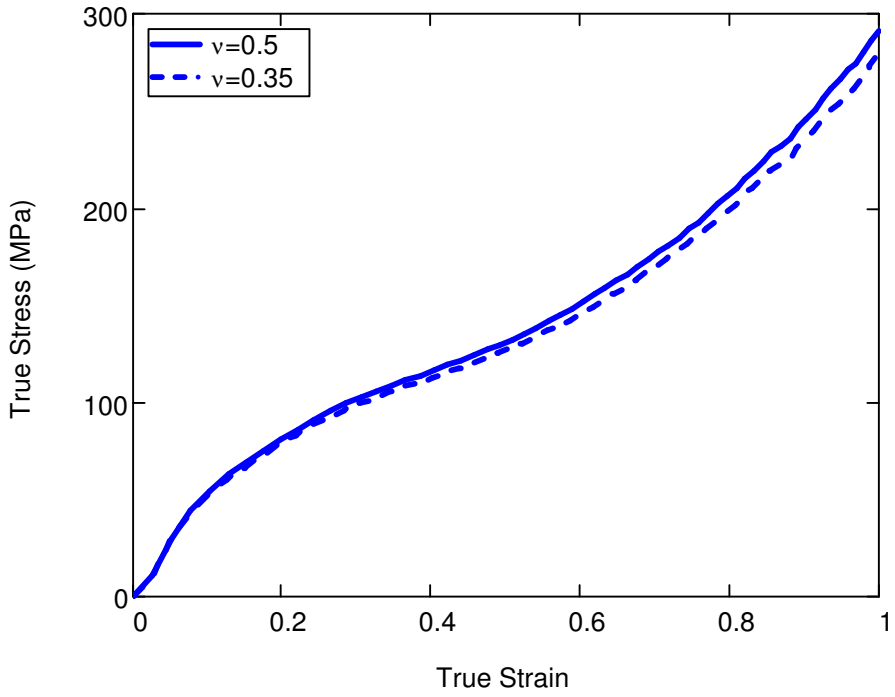

Figure 4.3. True stress *vs.* true strain curves for different Poisson Ratio's

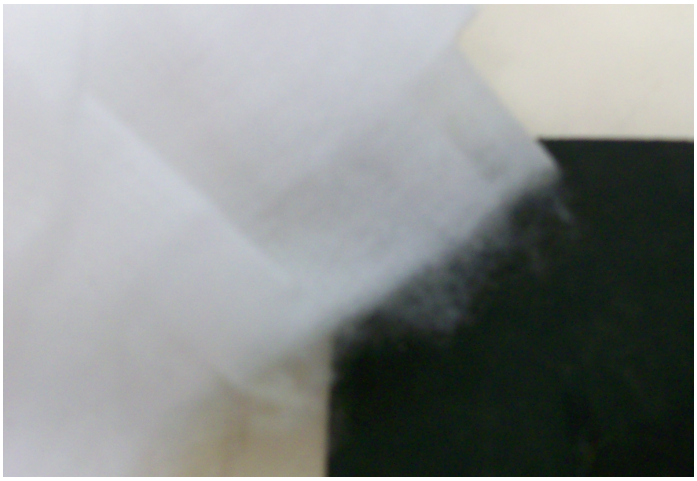

Figure 4.4. Free fibres

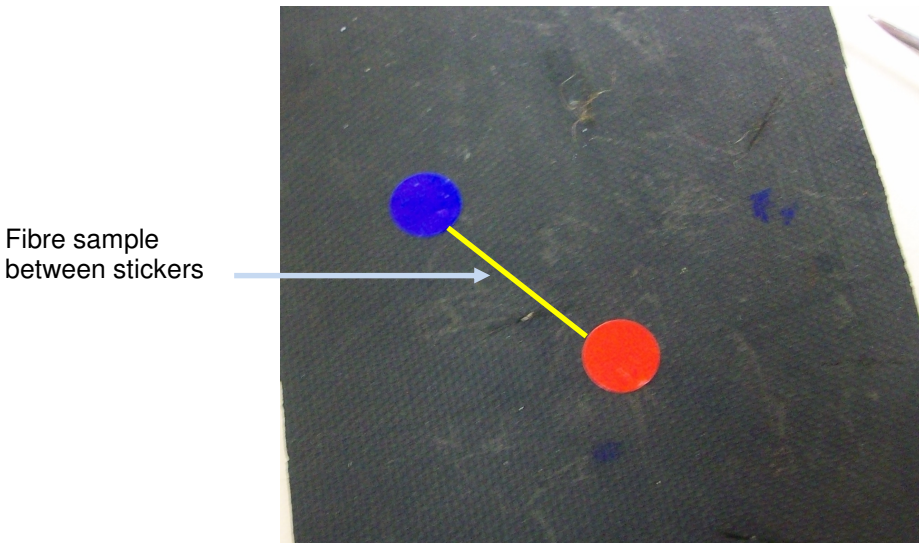

Figure 4.5. Sticking of stickers

Figure 4.6. Attachment of fibres to the test device

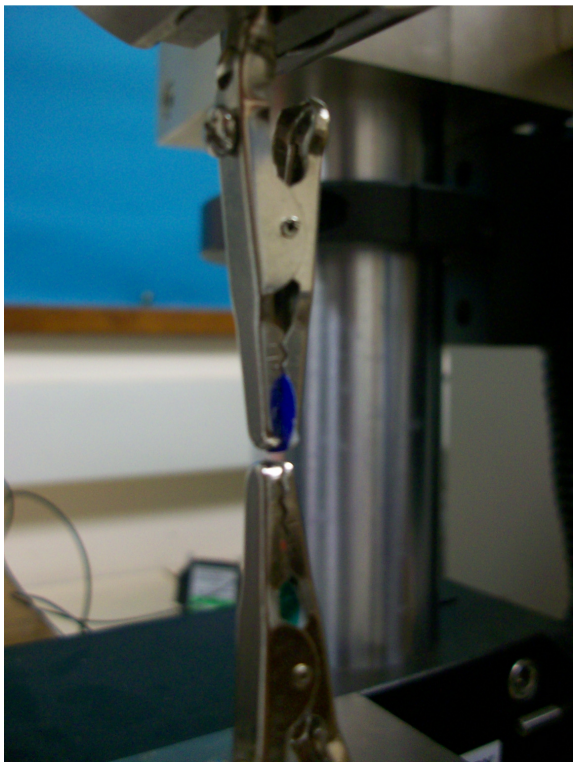

Figure 4.7. Jaws brought on top of each other

It was decided to perform the tests with true strain rates of 0.001, 0.01, 0.031, 0.1 and 0.31 s^{-1} considering the nonwoven simulations to be performed later. In logarithmic scale, these rate values are equal to -3,-2, -1.5, -1 and -0.5 respectively. The upper bound, 0.31 s^{-1} is linked to the maximum velocity of the loading device. The lowest speed to be utilized was determined to be 0.001 s^{-1} since it was found that a further decrease in the test rate does cause significant deviation.

4.2.1 Determination of Test Speed

As discussed earlier, in order to implement the tests with a constant-true-strain rate, the test speed is increased gradually. The test speed is determined for every test according to the gauge length measured and the required constant true strain rate. First, the displacement values are determined with respect to time to obtain a constant-true-strain rate for the sample. In order to do this equation 4.6 is written as

$$\dot{\varepsilon}_{true} = \frac{\frac{du}{dt}}{L} = \frac{\frac{du}{dt}}{u + L_0} \tag{4.11}$$

When this equation is rearranged a first order ordinary differential equation is obtained as

$$\frac{du}{dt} - \dot{\varepsilon}_{true} u = L_0 \dot{\varepsilon}_{true} \tag{4.12}$$

If $\dot{\varepsilon}_{true}$ is held constant and the initial value is 0, the solution of this equation is as follows:

$$u = -L_0 + L_0 e^{\dot{\varepsilon}_{true} t} \tag{4.13}$$

It was decided to increase the speed by 6 steps. The stepped displacement profiles obtained are compared with the profiles as if the displacement was applied according to the nonlinear equation given in (4.13). The result for $\dot{\varepsilon}_{true}$ = 0.31 s^{-1} and a gage length of 12 mm is shown in Figure 4.8. Apparently, the curves are very close to each other. The slopes of these 6 linear parts are the respective velocity values that are given as input to the tensile test machine together with the duration of steps (Table 4.1).

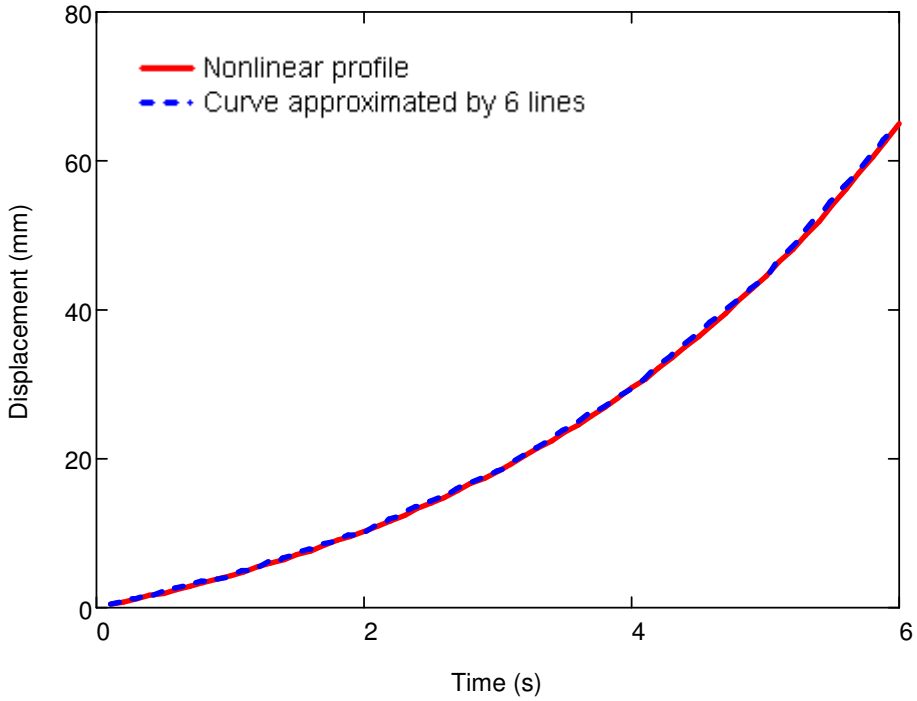

Figure 4.8. Comparison of theoretical and piecewise linear curves

Table 4.1 Profile data for MicroTester

Time increment (s)	Velocity (mm/s)
1	5.8
1	7.6
1	10.5
1	14.4
1	19.7
1	27.1

The velocity profile in Figure 4.9 was obtained as output from the tensile test machine when the velocity values in Table 4.1 were introduced; they were calculated as a displacement increment divided by time increment. Evolution of true strain rate with time calculated for this implementation of velocity profile is given in Figure 4.10

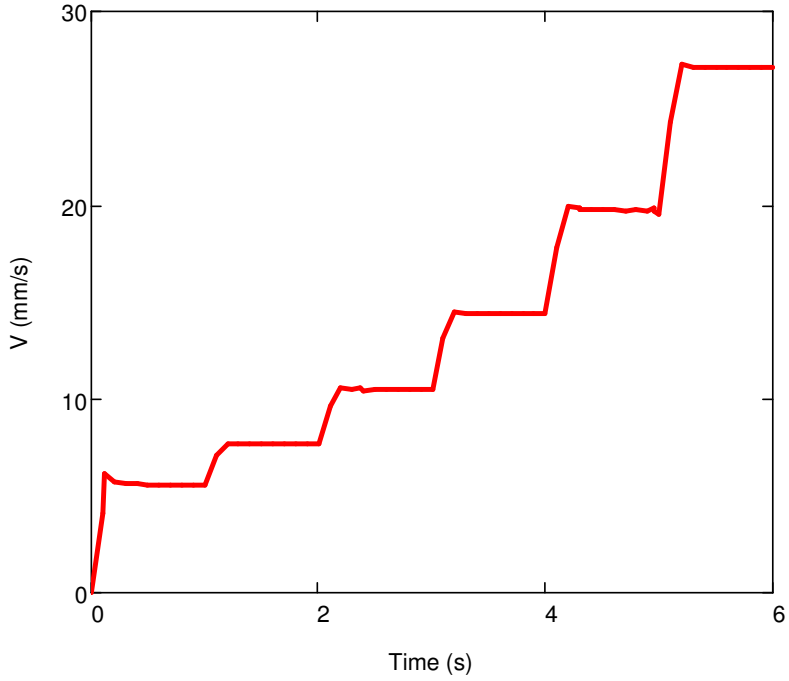

Figure 4.9. Time versus velocity of the cross head

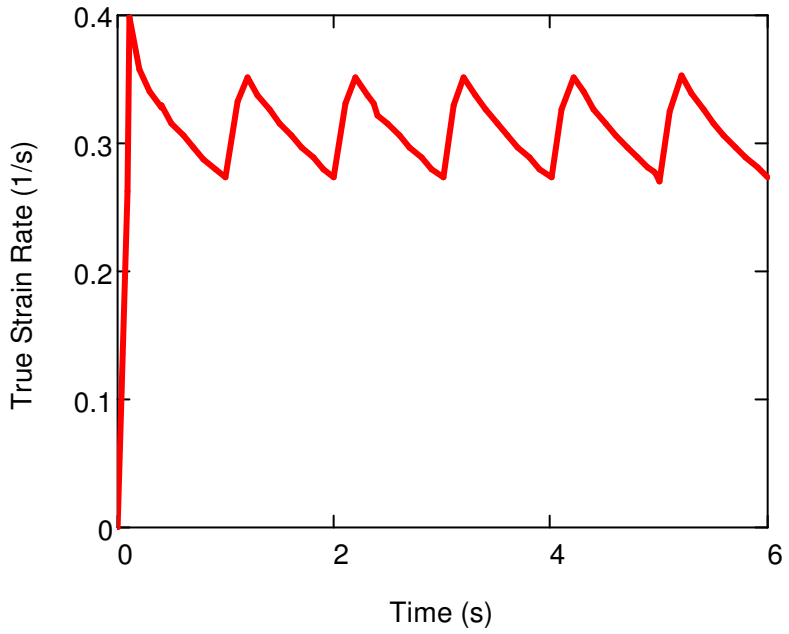

Figure 4.10. Evolution of true strain rate with time

It can easily be seen from Figure 4.10 that although the strain rate values are fluctuating between 0.34 and 0.27 s^{-1}, the values of average true strain rate are about 0.31 s^{-1}. It was considered that the fluctuations in the curve would not affect the

materials behaviour too much. After obtaining the strain-stress curves with different strain rates, it was confirmed that those fluctuations would cause minor deviations.

4.3 Tensile Test Results

The test inputs were calculated for different values of gauge length and different strain rate requirements. Each test was repeated with four samples. The stress-strain curves obtained in those tests are shown from Figure 4.11 - 4.15. The average values from these curves are calculated for each 0.1 true strain steps and plotted in Figure 4.16 to show the effect of strain rate on the tensile behaviour.

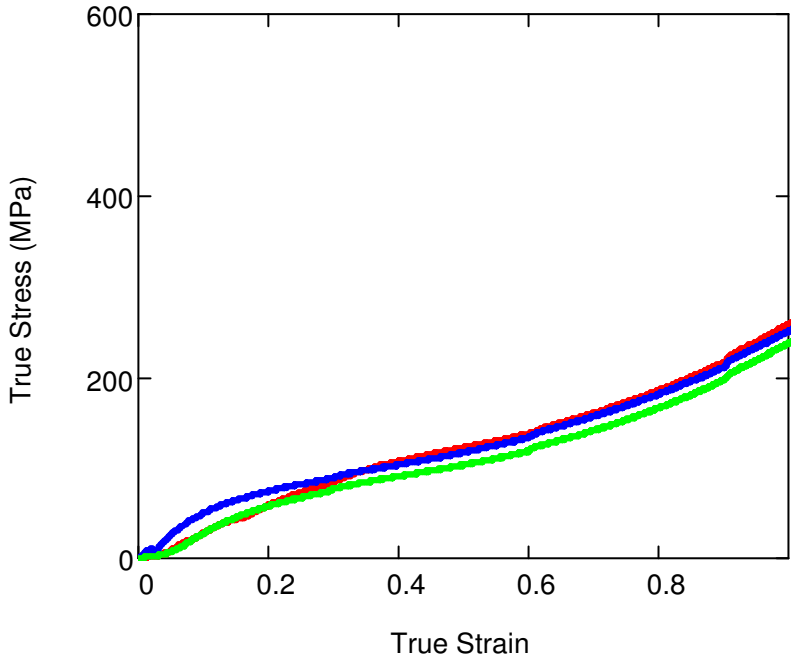

Figure 4.11. True strain *vs.* true stress curve for true strain rate 0.001 s^{-1}

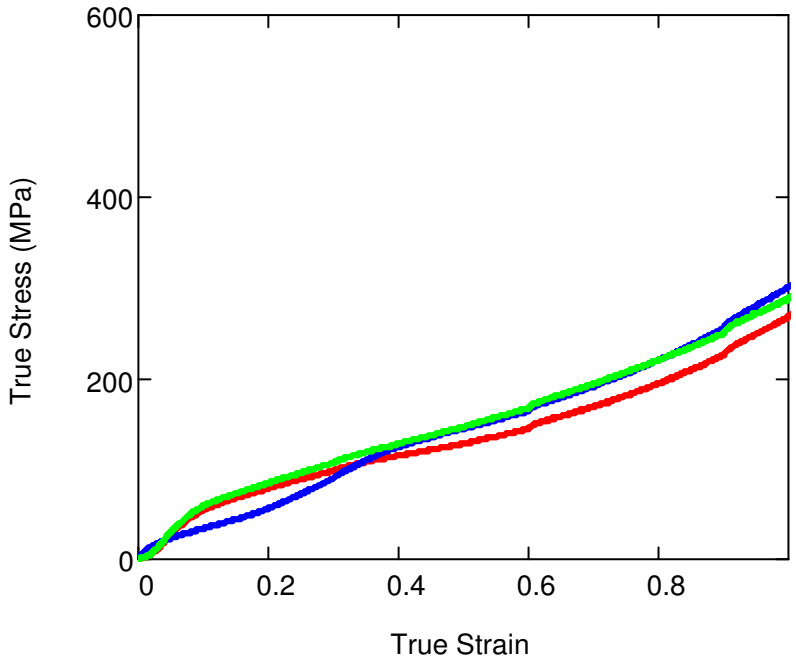

Figure 4.12. True strain *vs.* true stress curve for true strain rate 0.01 s^{-1}

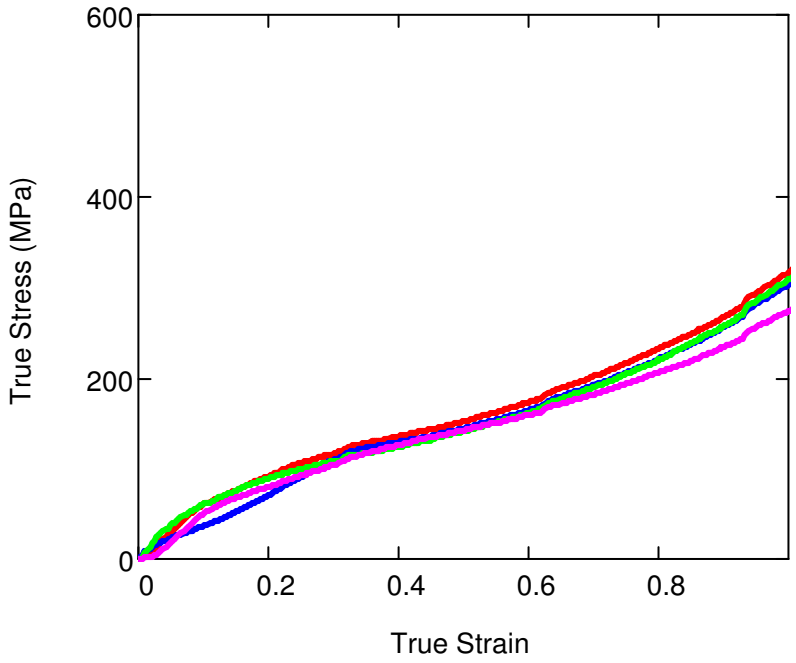

Figure 4.13. True strain *vs.* true stress curve for true strain rate 0.031 s^{-1}

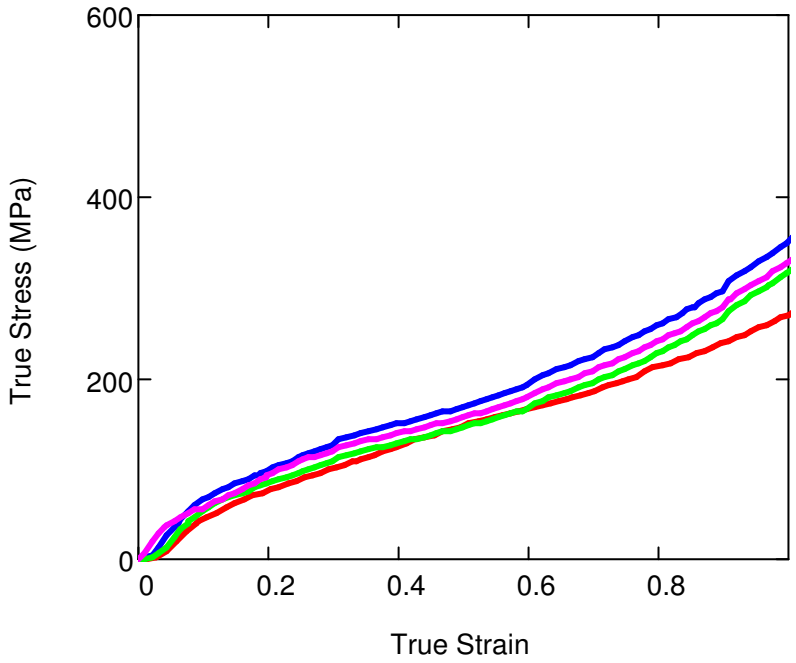

Figure 4.14. True strain *vs.* true stress curve for true strain rate 0.1 s^{-1}

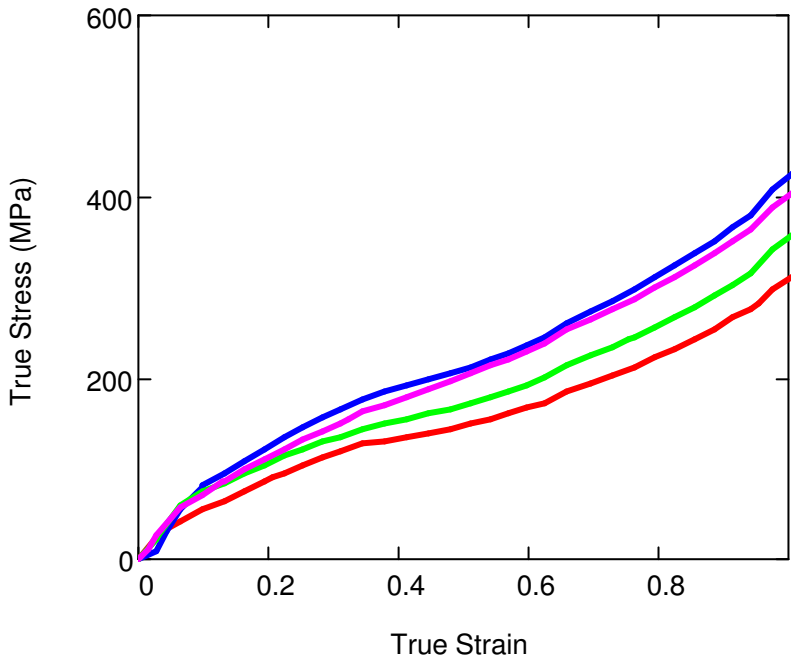

Figure 4.15. True strain *vs.* true stress curve for true strain rate 0.31 s^{-1}

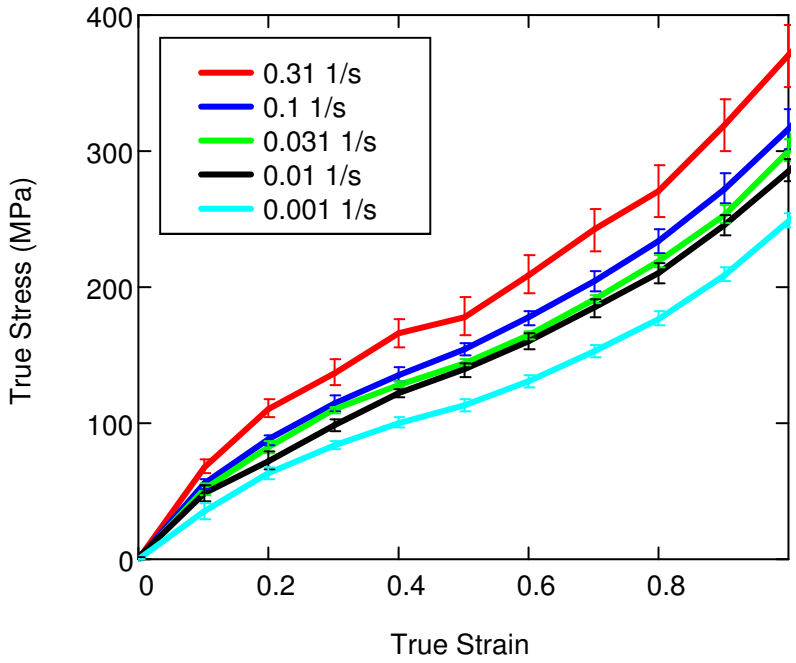

Figure 4.16. Average true strain – true stress curves for different true strain rates

According to the results, it is apparent that the strain rate has an effect on the deformation behaviour although it is not very strong. As expected, the higher the strain rate, the steeper the stress strain curves are as the material is hardened at higher strain rates.

In Figure 4.17, the test results close to average values are shown for until the true strain of 0.3. When the curves for strain rates of 0.01 s^{-1} and 0.001 s^{-1} are observed, it was seen that there is a low-stress region of the initial stage of the curves with a parabolic like shape (indicated by black arrows in Figure 4.17). This behaviour is attributed mainly to the crimp on the fibres. In all the tests, first, the fibres are extended to fully straightening until some load is measured before starting the tests in order to avoid the effect of crimp. However, some samples still have a crimpled structure, which cannot be seen with a naked eye, even after applying some load. An example of a crimpled fibre which cannot be detected by naked eye is shown in Figure 4.18. Thus, in the first stages, a different material behaviour is observed linked with fibre extension and straightening of crimpled fibres. This behaviour was

not observed in higher tensile rates because the machine was not able to capture enough points in the early stages of loading when the test speed was higher.

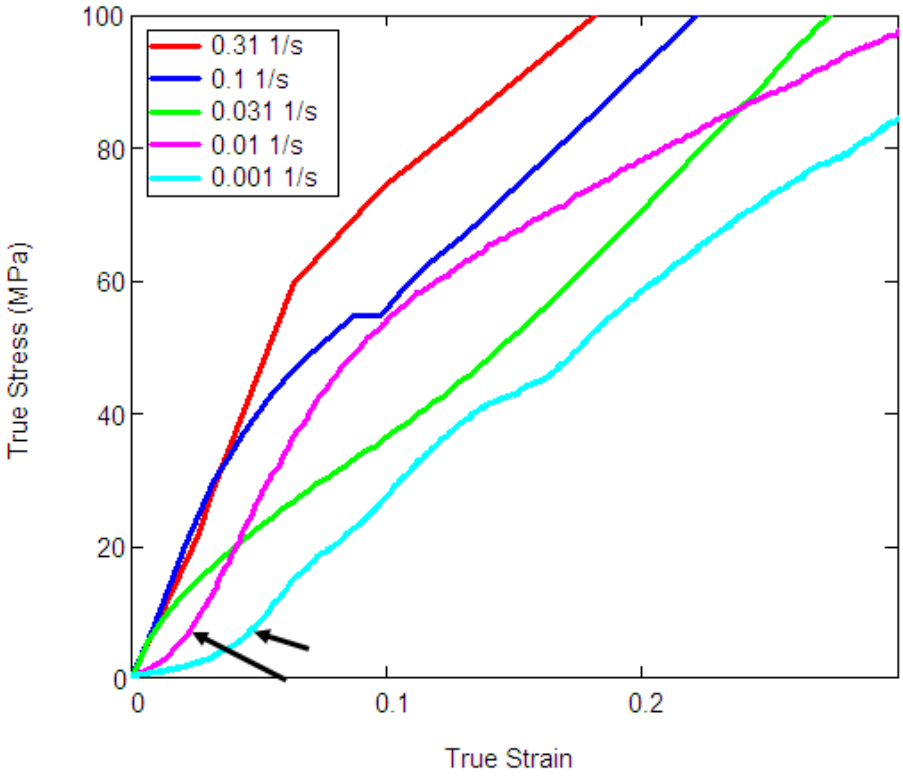

Figure 4.17. Initial portions of average true strain – true stress curves with different true strain rates

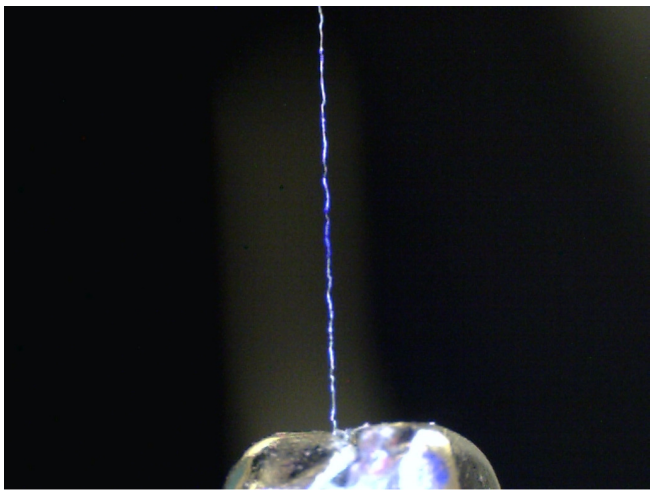

Figure 4.18. Fibre sample of the test given in Figure 4.17 showing the crimp on the specimen

4.4 Comparison of Constant-True-Strain-Rate Tests with Constant-Engineering-Strain-Rate Tests

As discussed, performing constant-true-strain-rate tests requires implementing acceleration to the crosshead displacement. If this option is not available, it is required to increase the test speed step by step. The application of this procedure requires implementation of a test-speed profile for each sample separately which is time consuming. In this section, the necessity to perform constant-true-strain-rate tests was checked. Tensile tests with constant-engineering-strain rates of 0.1, 0.01 and 0.001 s^{-1} were performed in order to compare with the tests performed with the same values of constant-true-strain rate. Tests were repeated for four specimens in order to consider the consistency of the results. Figures 4.19 to Figure 4.21 show the test results with engineering-strain rates compared with the test results with true-strain rates. The notation "E" in the scales represents engineering-strain rate whereas the notation "T" represents true-strain rate. The selected average results representing average values are shown in Figure 4.22 to Figure 4.24.

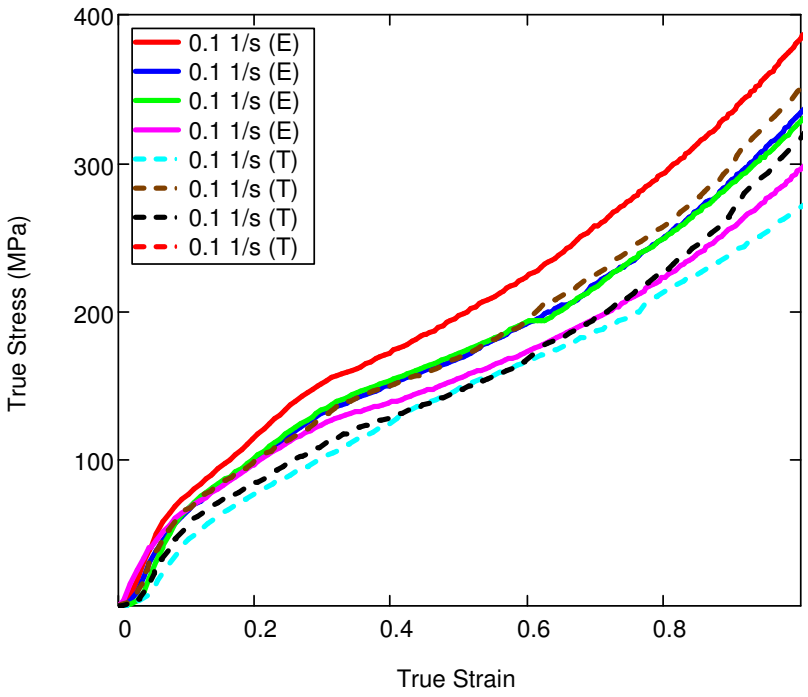

Figure 4.19. Comparison of constant true strain rate tests with constant engineering strain rate test (0.1 $\mathbf{s^{-1}}$)

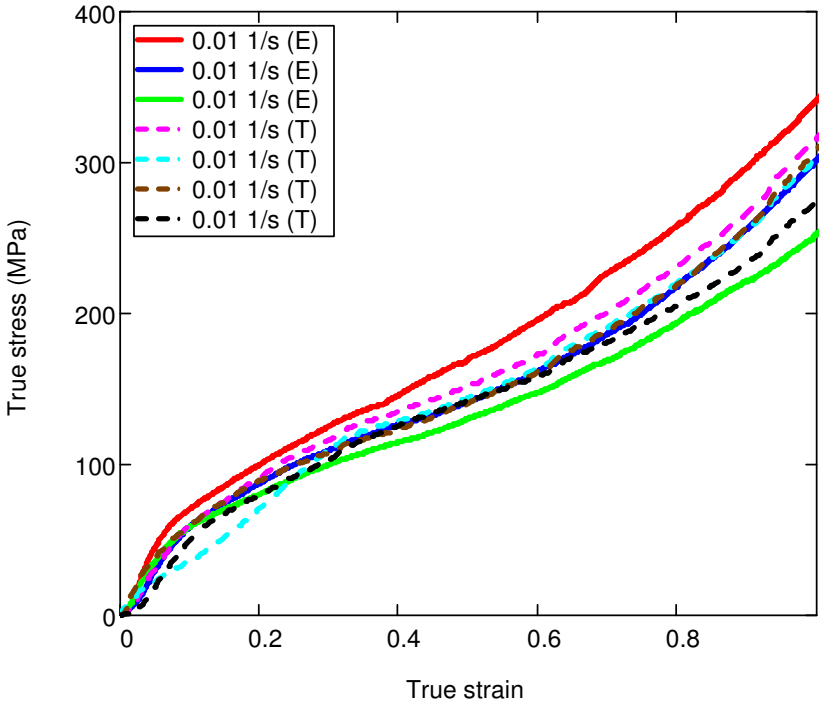

Figure 4.20. Comparison of constant-true-strain-rate tests with constant engineering strain-rate tests (0.01 $\mathbf{s^{-1}}$)

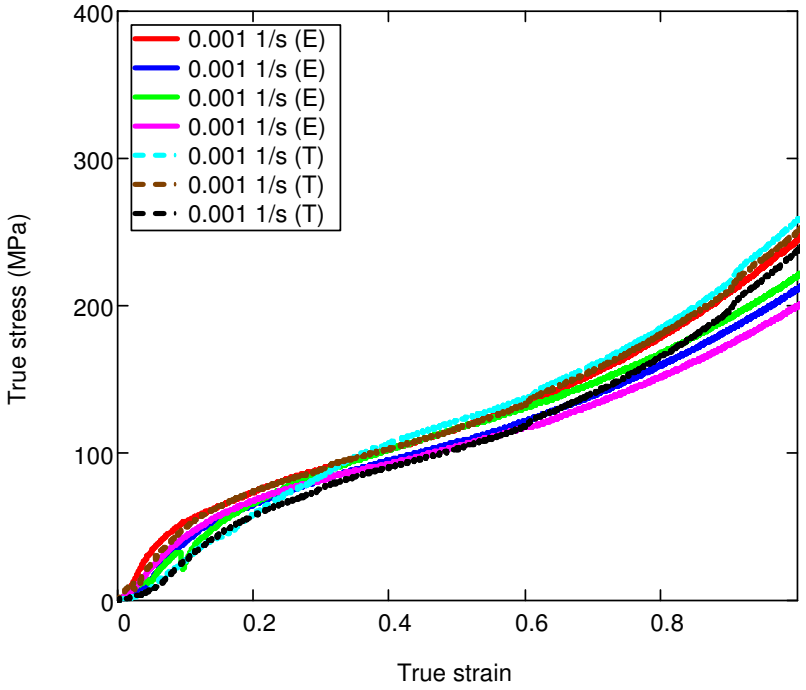

Figure 4.21. Comparison of constant-true-strain-rate tests with constant engineering strain rate tests (0.001 $\mathbf{s^{-1}}$)

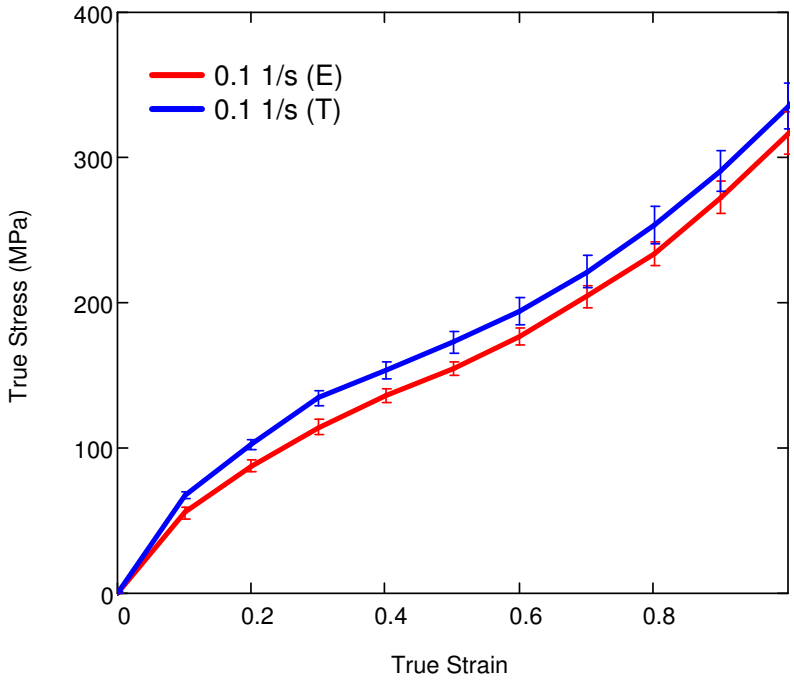

Figure 4.22. Comparison of constant-true-strain-rate tests with constant engineering strain-rate tests (average values,0.1 s^{-1})

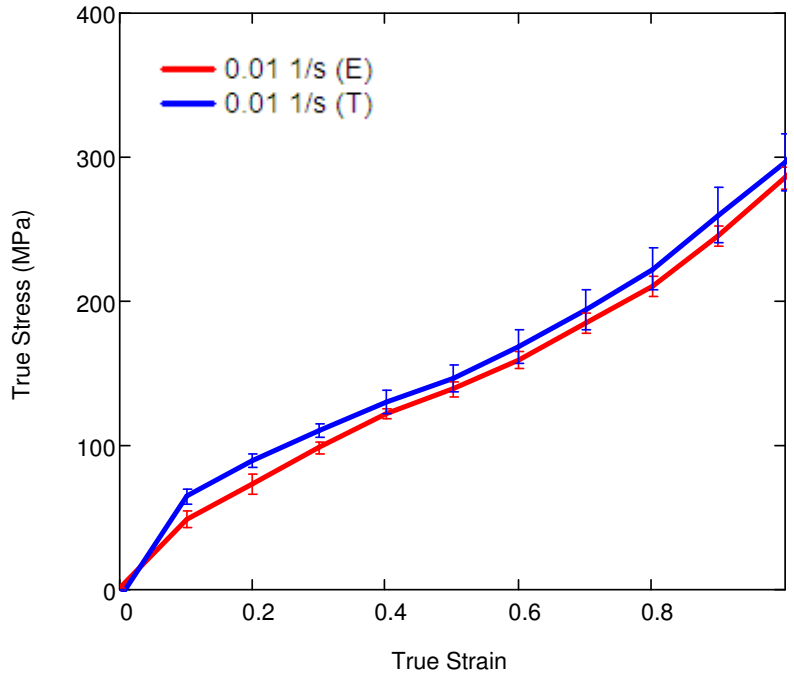

Figure 4.23. Comparison of constant true strain rate tests with constant engineering strain rate test (average values, 0.01 s^{-1})

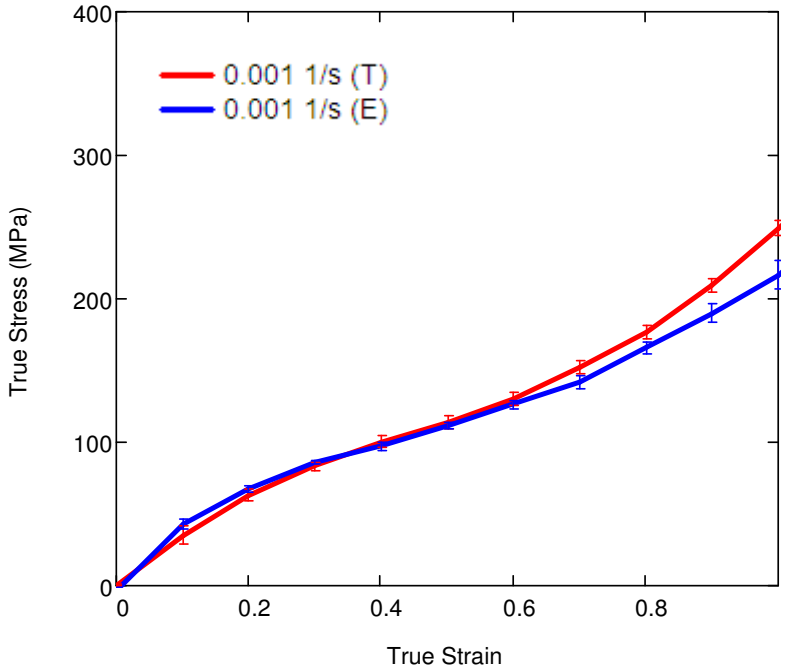

Figure 4.24. Comparison of constant-true-strain-rate tests with constant engineering strain-rate tests (average values, 0.001 $\mathbf{s^{-1}}$)

According to the test results, it was observed that the tests with constant true strain rates and engineering strain rates result in similar plots. It can be said that there is no need to use constant-true-strain-rate results instead of constant-engineering-strain-rate results as they both give similar results. Still, a procedure was developed for the implementation of constant true strain rate in the tensile tests. It may be important for testing a different kind of material which shows a larger strain-rate dependency, especially in the plastic region.

The evolution of engineering and true strain rates in the tests in Figure 4.22 are shown in Figure 4.25 and Figure 4.26. Apparently, the test speeds are similar in the initial stages for constant engineering and true strain rate tests. The difference increases after several seconds. Thus it can be concluded that the rate-dependant tensile behaviour shown in Figure 4.16 was due to the difference of the strain rates only in the initial stage of loading. This demonstrates that the viscous behaviour is generally effective in the initial stage of loading which was also confirmed by Demirci (2010). In the next chapter, the viscous behaviour of polypropylene fibres is

studied in the elastic range to determine the rate dependent properties of fibres in the initial stage of loading.

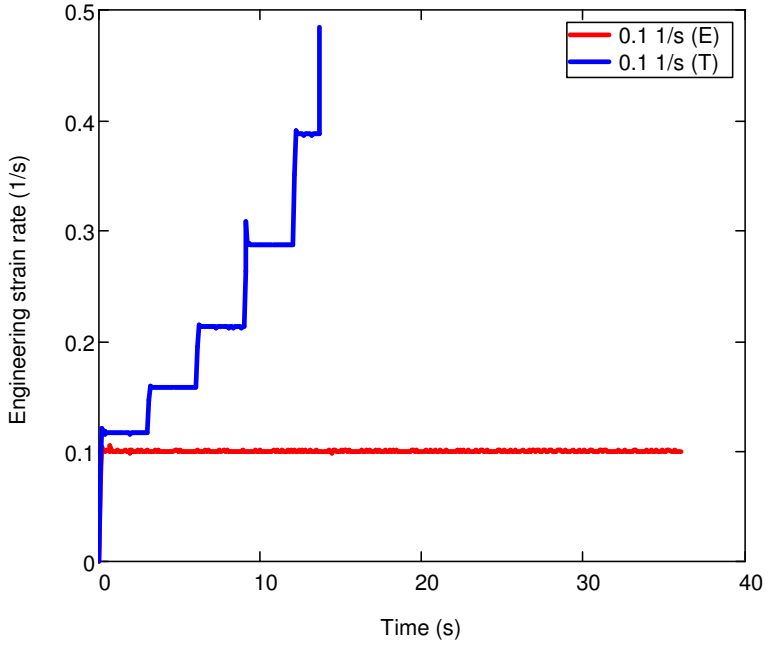

Figure 4.25. Engineering strain rate results for the tests in Figure 4.22

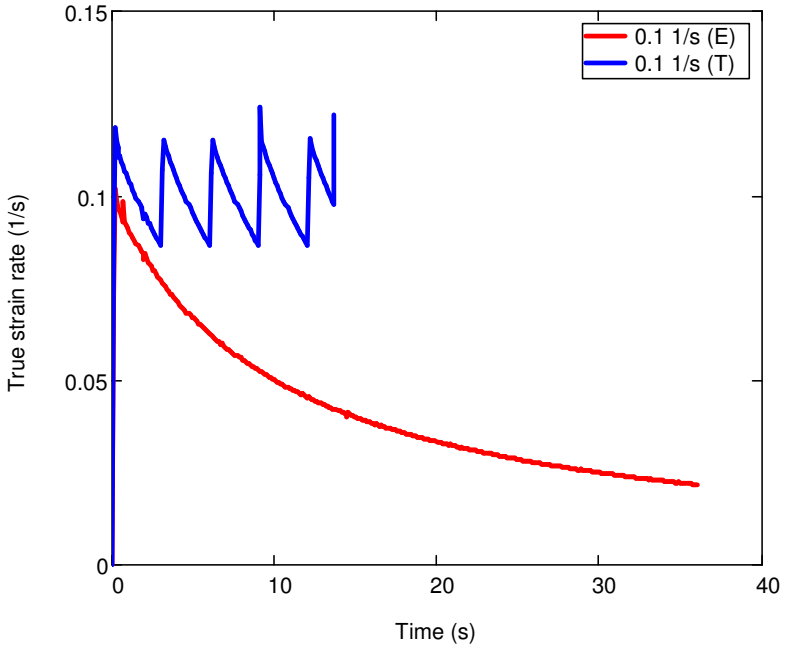

Figure 4.26. True strain rate results for the tests in Figure 4.22

CHAPTER 5

CREEP PROPERTIES OF POLYPROPYLENE FIBRES

5.1 Introduction

It was understood from Chapter 4 that polypropylene fibres' response to tensile load is dependent on the rate of loading. This shows that the viscous features of this material are effective under the influence of stresses. In this chapter, the viscous properties of polypropylene fibres were determined by means of a series of creep tests followed by application of data analysis techniques. The determined properties were implemented into the finite element software, MSC Marc Mentat. Some case studies were performed in order to verify the developed model. The tests were performed with single polypropylene fibres of the thermally bonded nonwoven. Time-dependent creep properties also reflect the viscoelastic behaviour as they can be converted into viscoelastic ones (Dropik *et al.,* 2002). Creep or relaxation properties of a material can be determined in several different ways:

Constant-strain relaxation: In this procedure, the load is applied until a constant strain level is reached. After that, the strain level is kept constant and the decrease in the tensile load is observed. This is the most traditional method of determination of viscous properties of materials. However in the fibre tests, the pre-determined strain level is not always accurate in especially low strains below the yield point of fibre. This situation occurs because of the test procedure explained in section 4.3. Sometimes a small level of load is observed not only as a result of stretching the fibre, but also as a result of friction occurred while unfolding the crimp in the fibre (see section 4.3). This can create an error in the determination of the gage length of the fibre to be tested. Therefore, this may result in the inaccuracy of stretching the specimen to the pre-determined strain level.

Constant-stress relaxation: In this procedure, the specimen is stretched to some stress levels and the strain values are held constant when those stress values are

reached. Compared to the case of stretching the specimen to a pre-determined strain level, this method is more reliable as the determination of the point to be stretched is disconnected from the calculation of gage length. The problems with this procedure; first, the machine has no closed-loop control so that there is a difficulty attaining the pre-determined stress level. Especially at higher test speeds, the stress value, shown on the screen passes beyond this stress level. When the software detects this, the cross head movement stops later than expected. Secondly, it is difficult to interpret the results to be used in the finite element software. In MSC Marc, there is no option for relaxation based on a stress level in the material properties section.

Constant-strain creep: In this procedure, the specimen is stretched until certain strain levels are reached. The load at this level is read at this point, and the machine tries to hold this stress level constant by adjusting the displacement of the crosshead. Same problems as in constant strain relaxation tests are valid for this case as well.

Constant-stress creep: In this method, the material is extended to a stress level and this stress level is held constant. Same disadvantages in constant stress relaxation case are valid for this procedure with the exception of MSC Marc having the option of implementing creep properties according to stress levels.

5.2 Test Procedure

After assessing the methods described above, constant-stress creep tests were determined to be the most feasible method in order to study the viscous behaviour of polypropylene fibres. A general outline of the study is presented in Figure 5.1. First, creep tests were performed with different initial stress levels. The data obtained from the tests were analyzed to determine stress and time-dependency of creep, and the obtained data were implemented into the finite element software. Then, the model was verified and updated using the relaxation test and simulations. Finally, tension tests with low strain rates were performed to present the applicability of the developed creep model.

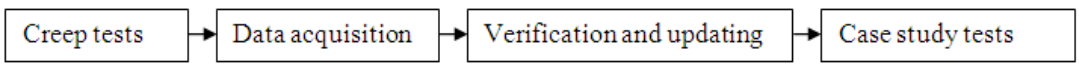

Figure 5.1. Procedure used in the creep study

5.3 Creep Tests

As discussed above, in creep tests, the test samples are stretched until a predetermined stress level is reached and this stress level is held constant. The predetermined stress levels should be selected carefully in order to obtain the required creep parameters.

5.3.1 Creep-Stress Levels

Creep tests are performed below the yield stress of the material in order to eliminate coupling with plastic strains. Thus, the yield point in the tests should be determined initially. Constant-true-strain-rate tests that were performed in Chapter 4 were used in order to determine the yield point of polypropylene fibres. The tests shown in Figure 4.17 were plotted as engineering stress *vs*. engineering strain values (Figure 5.2).

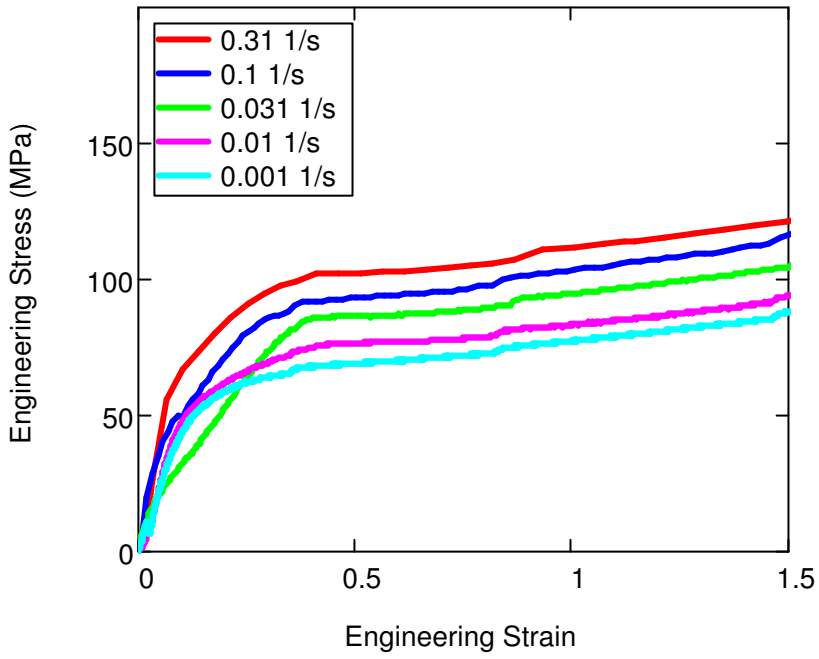

Figure 5.2. Average values of engineering strain *vs*. engineering stress

It is assumed that the yield stress is reached when there is a significant variation in the slope of stress-strain curves (Mallick & Zhou, 2003, Gomez-del Rio & Rodriguez, 2010). According to Figure 5.2, the slope variation is observed between 70 - 100 MPa depending on the test speed. As discussed above, the specimens are

stretched until a constant stress level is reached. The test rate to reach constant stress levels is determined as $0.01s^{-1}$ (explained in section 5.3.2). Thus, the change of the slope of stress – strain curve obtained from the curve with 0.01 s-1 true strain rate is used to determine the yield point, which is around 75 MPa. The maximum engineering stress level for creep tests is determined to be 80 MPa, which is slightly beyond this yield point (Dropik *et al.,* 2002). It was decided to perform the tests for various stress levels with 10 MPa increments up to the previously determined 80 MPa engineering stress value.

5.3.2 Test Speed and Duration

During the tests, fibre samples were stretched until a certain stress level was reached and held constant at this level. The speed to reach this constant stress level should be as fast as possible in order to prevent too much creep in the first stages. But if the speed is too high, the machine misses the required stress level to be held, stops at a higher stress and waits for some time to reach to the acquired stress level by relaxation. After reaching this level, it tries to reach the desired stress value by decreasing the stress level and stabilize the level by increasing the strain continuously. This will result in a mixture of creep and relaxation, before the start of the actual test.

In order to prevent this situation, for each test, the test speed were determined so that it was low enough not to pass the desired stress value but high enough to reach the stress level without significant initial creep . After performing some trial tests, it was decided to reach the desired stress levels in 10-15 seconds. The crosshead speed was adjusted for each stress level separately by taking into account the gage length of the specimen so that the predicted stress level is reached approximately in 10-15 seconds. In order to determine this speed, the plots of tensile test for fibres with different strain rates are analyzed (Figure 5.3) and the strain rates to be applied were determined (Table 5.1) The test speed was determined for each test according to the specimen gage length and their strain-rate values.

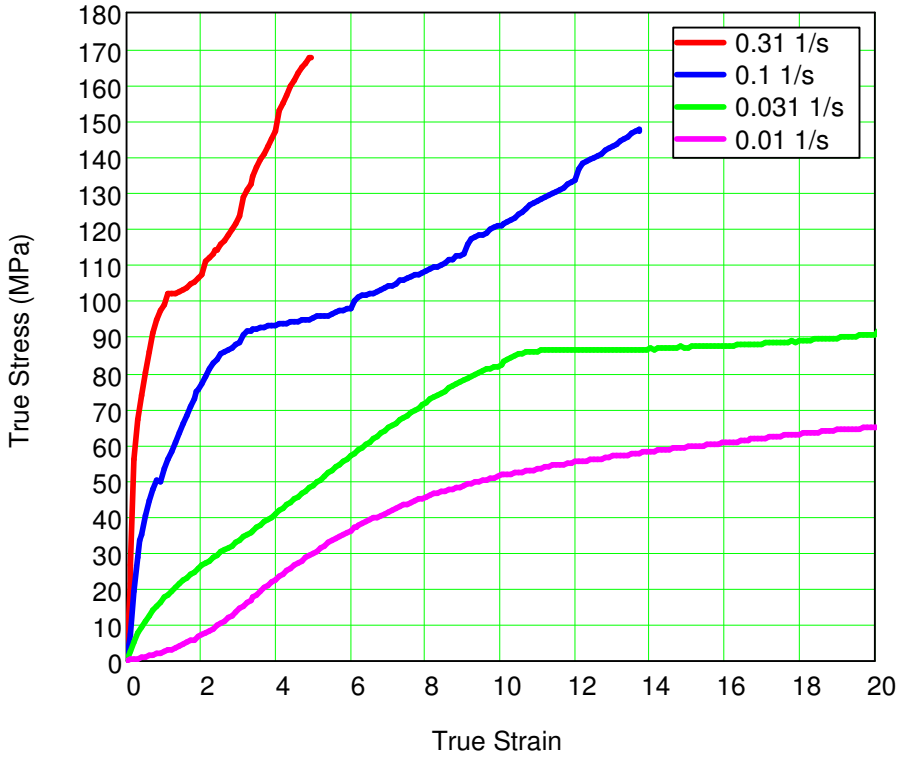

Figure 5.3. Stress evolution for different true strain rates

Table 5.1. Defined strain rates for different constant stress levels

Stress Level (MPa)	**Strain Rate (s^{-1})**
80	0.025
70	0.018
60	0.012
50	0.008
40	0.006
30	0.004
20	0.002
10	0.001

Creep tests are generally performed for long times, at least 1 hour (Drozdov & Yuan, 2003, Bhunavesh & Gupta, 1995, Dropik *et al.,* 2002). The primary stage of creep is

generally ignored in the analysis, and the respective equations are developed predominantly for the secondary region of creep, in which the logarithm of the creep curve is a straight line Figure 5.4

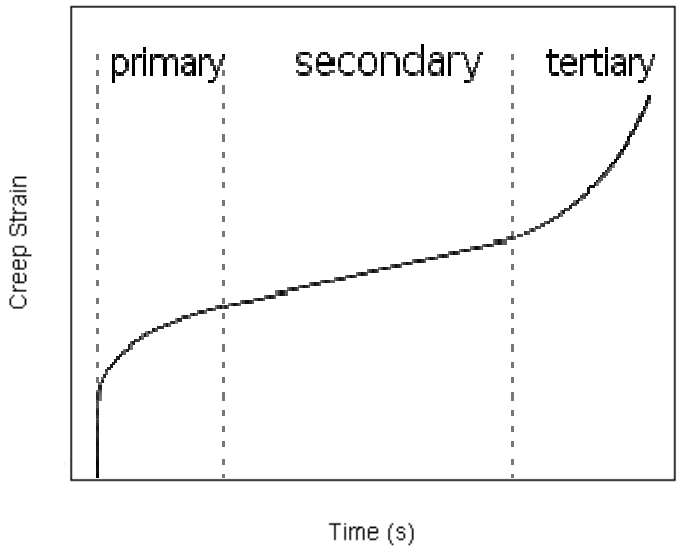

Figure 5.4. Logarithmic creep strain versus time curve for viscoelastic material that has creep properties

In this study, it was decided to concentrate on the primary region of creep with the maximum creep strain rate. Hence, it was decided to do the tests for 5 minutes only instead of some hours. This test duration is determined to be low enough to catch the initial stage of creep, high enough to observe the stress relaxation clearly.

5.3.3 Creep Tests Results

Tests for all stress levels were conducted with three specimens each. The test for 10 MPa of engineering stress gave inaccurate results because of the load values that were low even for 5 N loadcell (around 0.003 N). On the other hand, some preload was applied during fixing the fibre into the jaws. Thus a small difference below 10% was observed between the desired and actual stress value. The tests that replicated other tests were not taken into account in the calculations. The creep test results are shown in Figure 5.5. Respective changes in cross-head displacement are shown in Figure 5.6 which reveals a significant creep component in the deformation behaviour of the material.

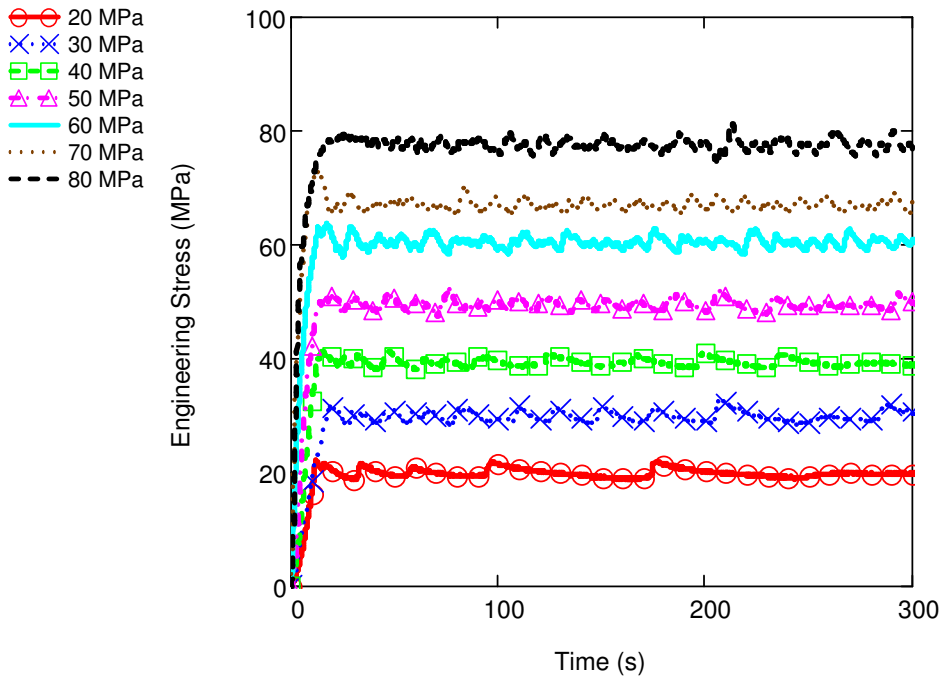

Figure 5.5. Evolution of engineering stress values in creep tests, for various nominal stress levels (MPa)

As it can be seen, because of its displacement-control feature, the machine switches on and off the crosshead displacement in order to stay close to the pre-defined stress values. At the point, where the machine first switches off, generally, the stress value is higher than the required stress level because of the effect of initial continuous extension stage. After this peak stress value is reached, the machine remains switched off until the machine detects that the stress value is lower than the expected level. Then, the machine switches on again after relaxation from this much higher peak stress value that can introduce some error. Thus, it was decided to determine the creep behaviour by omitting the initial "switching off and on stage" of the tests. The initial extension stage should also be omitted for creep behaviour as the stress is not constant during this stage. It was observed that for all the tests, it would be suitable to analyze the data after about 20 seconds, which was enough for all tests to omit the initial extension, initial switching off and switching on stages.

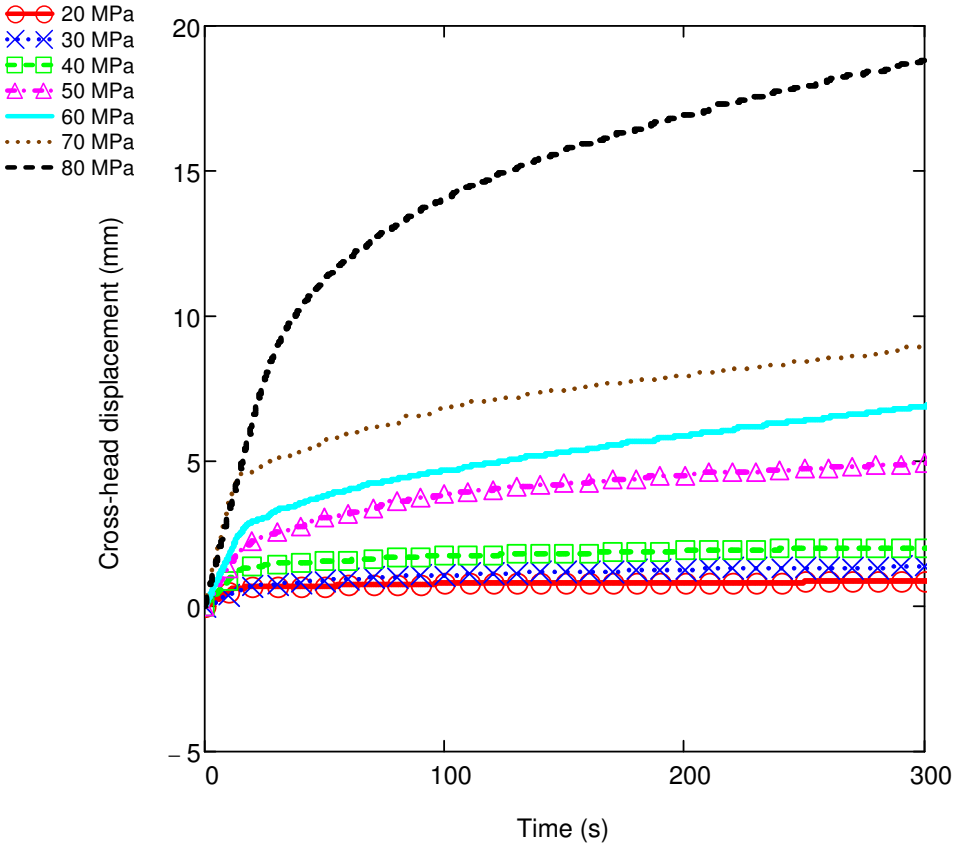

Figure 5.6. Crosshead displacement with time for different stress values

5.4 Data Acquisition

5.4.1 Calculation of True Stress Values

Engineering-stress values were converted into true-stress values using equation (4.8) and using the strain data obtained during the tests (Figure 5.7). The creep time represents the time after 20 seconds of the initial stage which was determined previously.

As it can be seen, although, the engineering stress values were held nearly constant, the true stress values were increasing with time because of the variation in the creep strain. Especially, the tests for the constant engineering-stress value of 80 MPa were changing from about 110 MPa to 200 MPa. So it was decided not to use the test data for 80 MPa. Mean true-stress values from the rest of the tests were calculated by

taking the average of all the tests and assigning as the new constant stress values for those tests (Table 5.2).

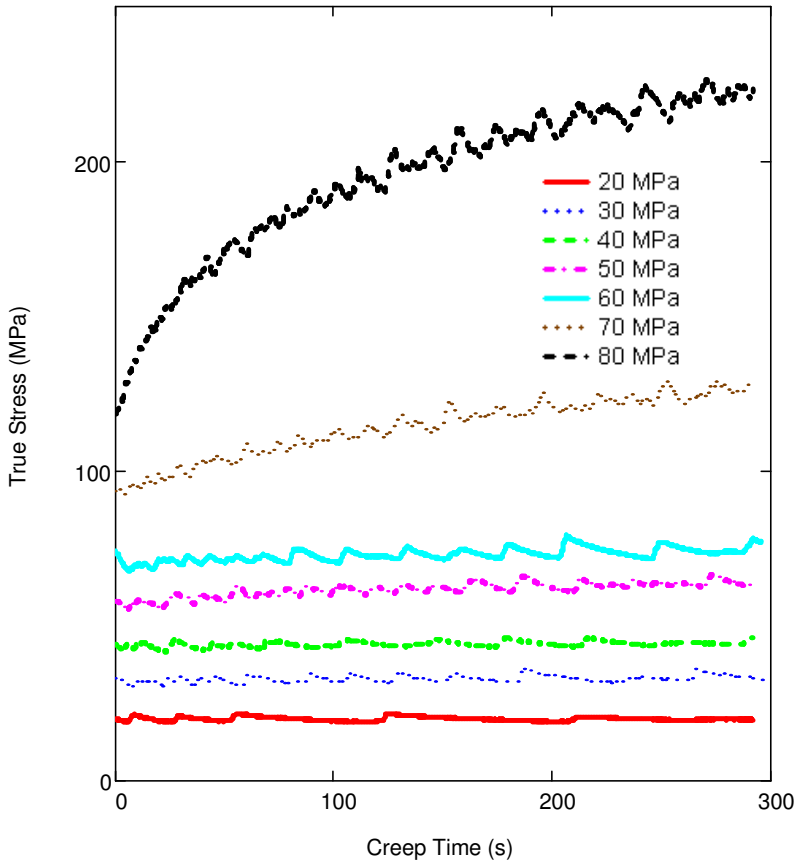

Figure 5.7. Calculated true stress vs. time curves of creep tests.

Table 5.2. Creep test constant-true-stress values

Test number	True stress (MPa)
1	19.9
2	32.6
3	44.1
4	60.8
5	73.1
6	82.8
7	91.3
8	96.9

5.4.2 Creep Strain *vs.* Time

True strain *vs.* time plots for all the tests were obtained for the selected stress values. It was determined that the data could be approximated with the following logarithmic equation:

$$FIT_i(x) = C1_i(\ln(x) + C2_i) + C3_i \quad \textbf{(5.1)}$$

In this equation, i donates different stress levels; $C1$, $C2$ and $C3$ are fitting function coefficients that are different for each test. Fitting is performed for curves beyond 20 seconds of time. An example of such fitting is shown in Figure 5.8.

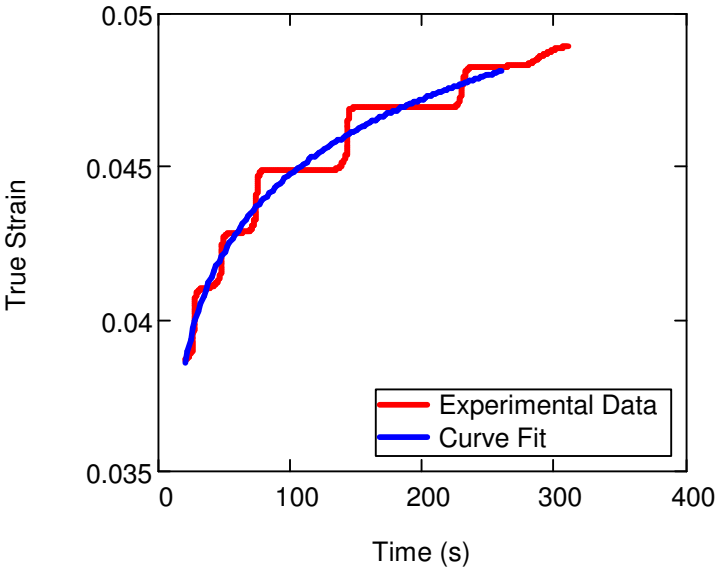

Figure 5.8. True strain-time plot (true stress, 19.9 MPa)

Apparently, the stepwise behaviour of the true strain curve was improved with the logarithmic curve fit. Similar curves were obtained for each stress levels mentioned in Table 5.2 (Figure 5.9). The curves for 91.3 MPa and 82.8 MPa stress levels cross each other. This may be attributed to the variation of mechanical properties of individual fibres and inaccuracy during sample installation. In the Chapter 4, it was told that about 10% error can be present during the tests because of sample alignment. Thus, this kind of behaviour can be expected for stress levels close to each other.

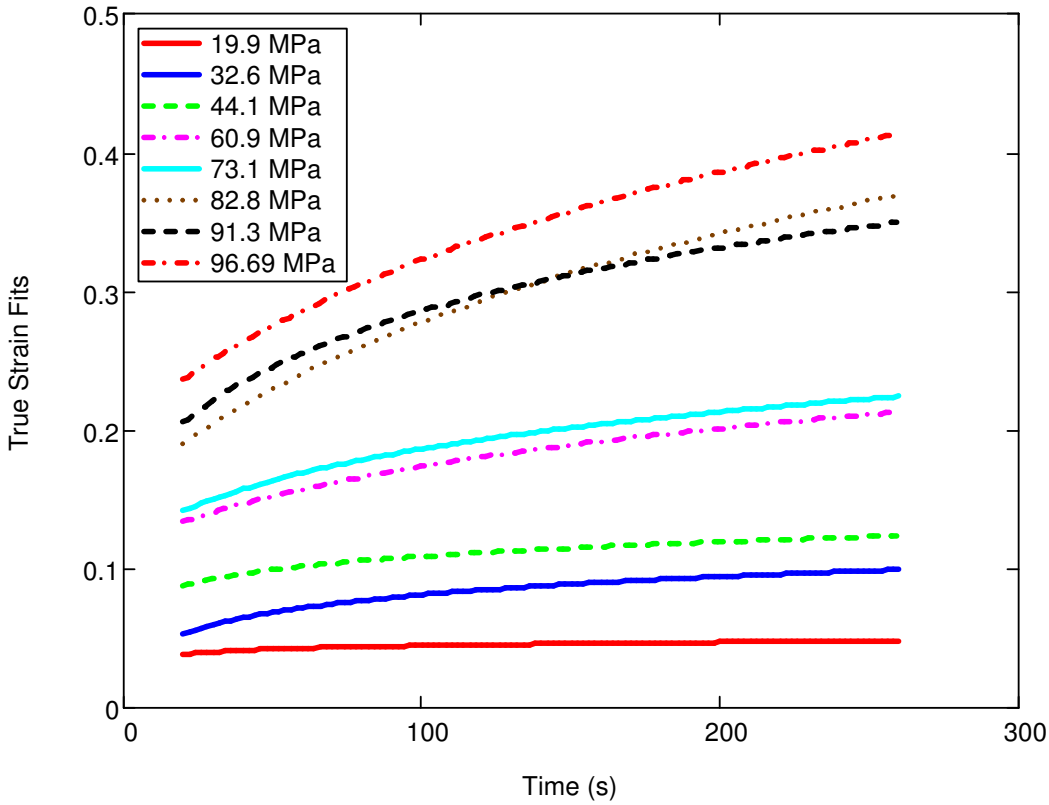

Figure 5.9. True-strain fitting curves for various levels of true stress

The presented true strain curves include both elastic and creep components. In order to compare the creep behaviour for different stress levels, creep strain curves for different stress levels should be obtained. Creep strain curves were obtained by subtracting the elastic part of strain (i.e. the initial value of true strain in Figure 5.10). In this way, it was assumed that there occurs no creep during the initial omitted stage (the behaviour until 20 seconds of initial time is considered to be fully elastic). However, it is known that creep strain rate is very large in the first few seconds of loading time. The creep in the first region will be added in the later stage after the creep strain curves are fitted according to stress (see section 3.3). The creep strain curves after subtracting the initial values are shown in Figure 5.10.

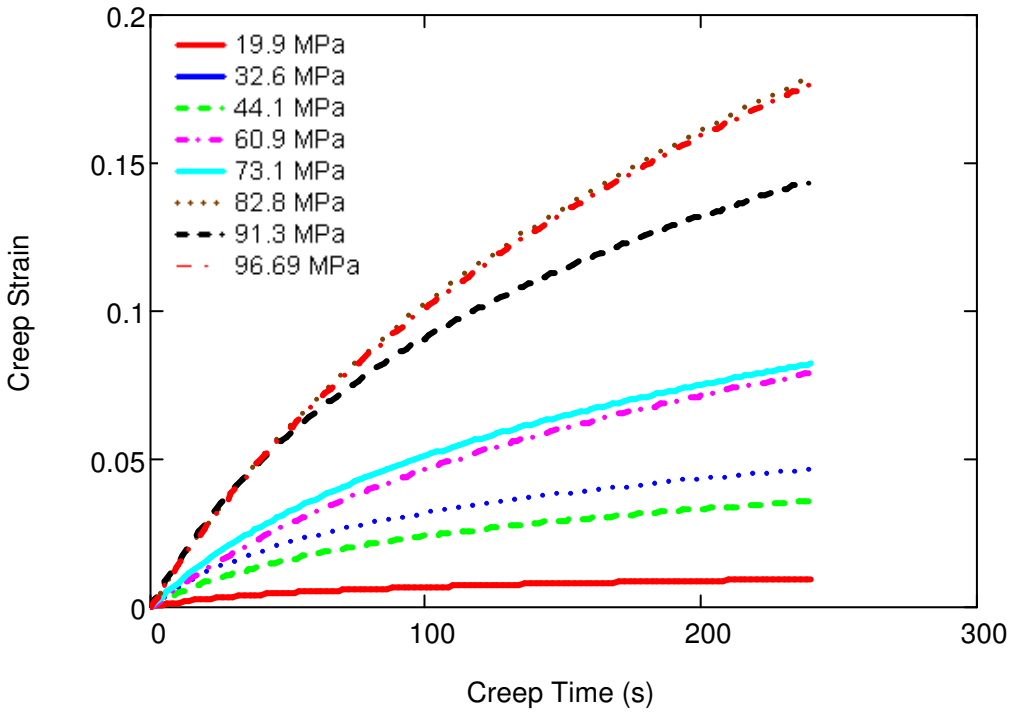

Figure 5.10. Evolution of creep strain for different stress levels (see legend in Figure 5.10)

5.4.3 Creep Strain vs. Stress

The creep behaviour changes not only with time; it also depends on the stress level. The true strain *vs.* stress plots were obtained for each time value. Then, curves were fitted for each moment of time according to the power function,

$$FIT(\sigma)_i = D1_i \sigma_i^{D2_i} + D3_i, \tag{5.2}$$

where σ is the nominal stress value, $D1$, $D2$ and $D3$ are the coefficients of the fitting function. The number of used stress data points is the same as the number of time data points as the finite element software requires a square matrix to be implemented for the analysis. Two of these stress-dependent creep strain data for particular times are shown in Figure 5.11 with the fitted functions.

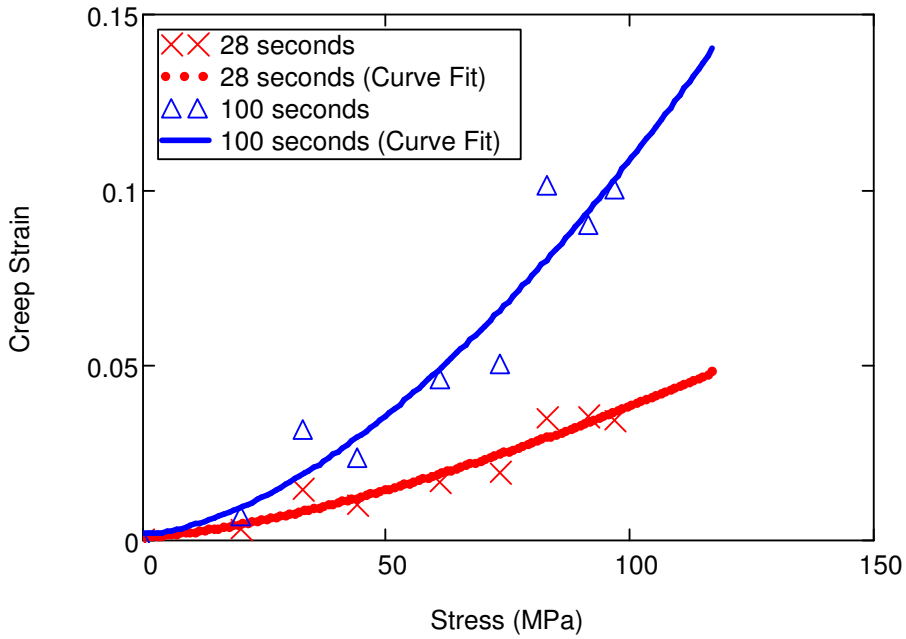

Figure 5.11. Creep strain vs. stress plots for different moments of time

The fitted curves in Figure 5.11 should start at zero creep strain value when there is no stress, as creep cannot be present without the application of stress on the sample. Hence, the initial values of all fitted curves were adjusted to zero. When fitting the creep strain data according to stress values, the values of creep strain curves according to time, which was determined in previously was changed unavoidably. So, the creep strain values for different stress states are obtained and new curves are fitted for the time values with other power functions such as in Eq. 5.1. Also, the curves were shifted to the right by the time, t=20 seconds in order to add the creep behaviour in the initial stage mentioned in section 5.4.4 (Figure 5.12).

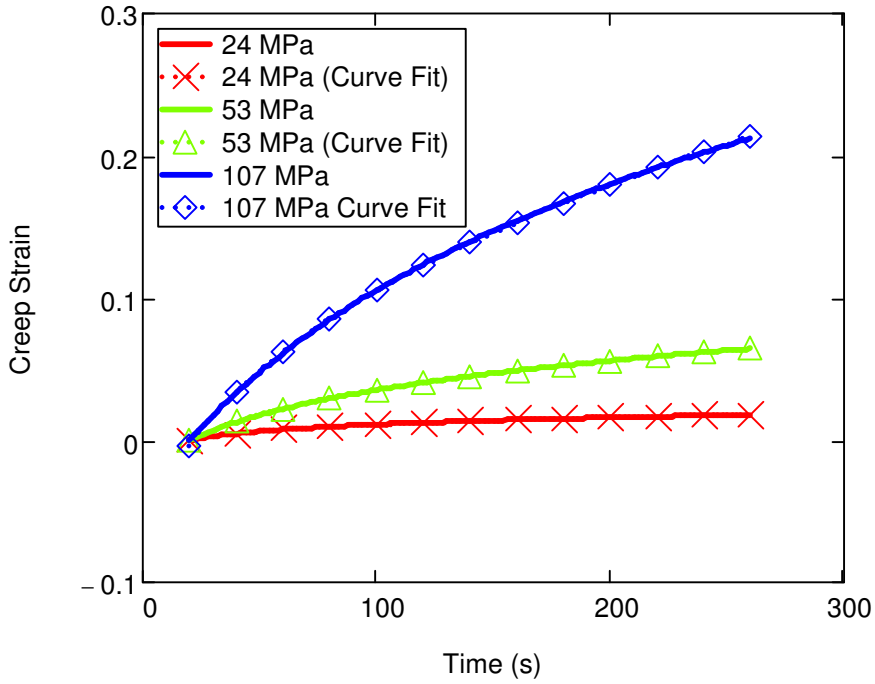

Figure 5.12. Evolution of creep strain after fitting operation of creep strain with time

5.4.4 Creep Strain of Initial Loading Stage

The creep behaviour until this stage was obtained after the initial time of 20s which was determined previously. However, there was also creep until the specimen was stretched to the pre-determined stress levels. During this stage, the creep strain increases together with the elastic strain. Thus, creep strain should be separated from elastic strain. The simplest solution was to extrapolate the creep behaviour to this initial stage. The result of extrapolation for the stress level of 53 MPa is shown in Figure 5.13. This modification results in negative creep strain values which is impossible as there is no compression. This situation occurred because of the operation performed in Figure 5.10. This is corrected by shifting the curves upwards. (i.e. creep strain starts to evolve immediately after the start of the test). This modification does not cause any error because at the end, the creep strain rate is implemented to the software. The values of creep strain rate do not change by shifting of the curves vertically (i.e. addition of constant parameter).

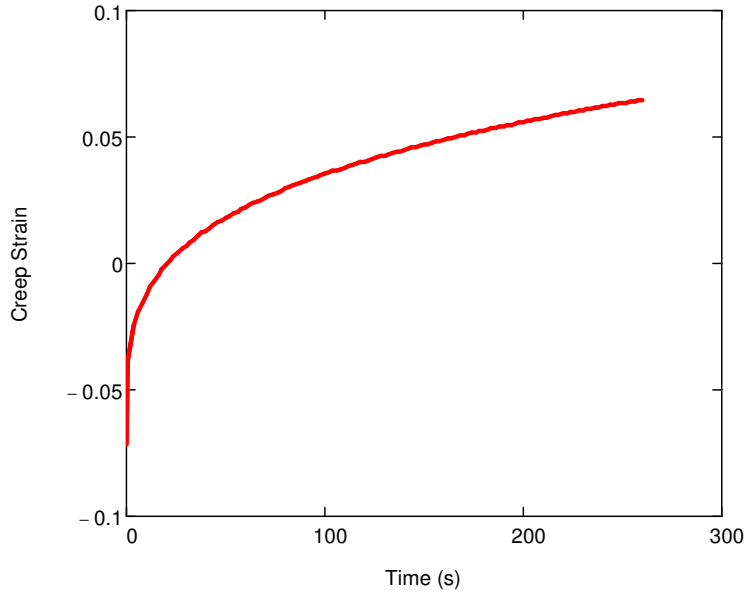

Figure 5.13. Evolution of creep strain after extrapolation of fitting function towards initial stages

Obviously, after the modifications for the initial stage, the fits of the creep strain - stress are affected. Thus, another fitting operation is performed with the power function in Eq 5.2 (Figure 5.14).

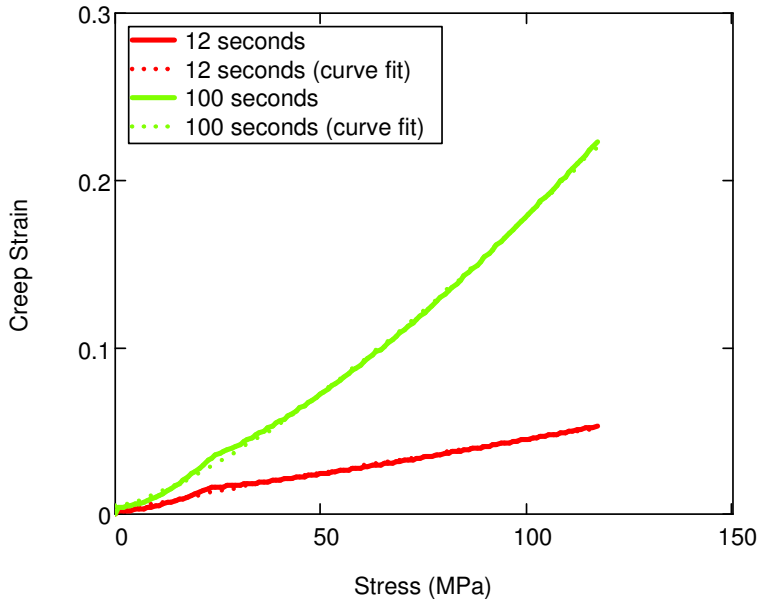

Figure 5.14. Creep strain *vs*. stress data for different moments of time with account for initial stage

After this fit, it was decided not to implement another fit for time values because it was noticed that the values did not change too much. A new matrix is formed that shows the creep strain values for various levels of time and stress (Figure 5.15). The analysis software requires the creep strain rate data instead of creep data. Thus, the following section explains the method of obtaining these data.

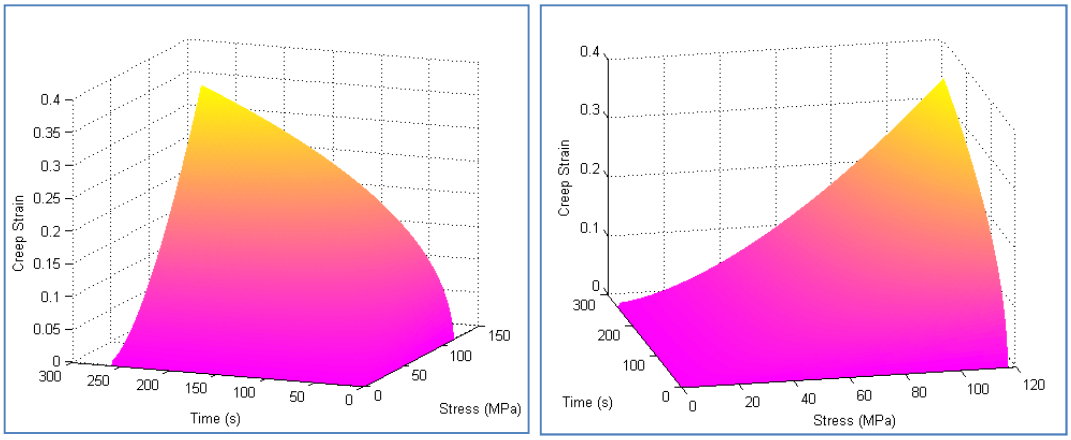

Figure 5.15. Creep strain plot according to stress and time (view from two different directions)

5.4.5 Creep Strain Rate

The matrix of creep strain rate was formed by dividing the creep strain data with time increments. The creep strain rate for the creep value at $t = 0$ was calculated by subtracting the second creep value from the creep value at $t = 0$ and dividing by the first time increment:

$$\dot{\varepsilon}_{creep_{1,\sigma}} = \frac{\varepsilon_{creep_{2,\sigma}} - \varepsilon_{creep_{1,\sigma}}}{t_2 - t_1}, \tag{5.3}$$

where t_1 and t_2 denote the first and second time data. The creep strain rate for the final creep value was obtained by subtracting the final creep value from the creep value just before the final creep value and dividing with the final increment:

$$\dot{\varepsilon}_{creep_{f,\sigma}} = \frac{\varepsilon_{creep_{f,\sigma}} - \varepsilon_{creep_{f-1,\sigma}}}{t_f - t_{f-1}}, \tag{5.4}$$

where f is the total number of data points. The creep strain rates for other data were found by middle-averaging method which is using the creep strain and time values

before and after the data analyzed. The plot of creep strain rate matrix for different time and stress values are shown in Figure 5.16.

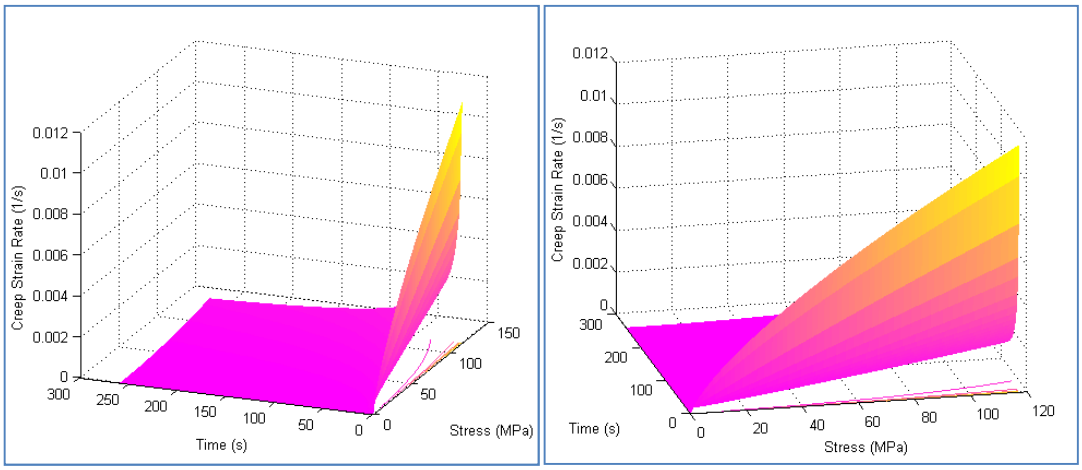

Figure 5.16. Creep-strain rate according to stress and time (view from two different directions)

According to Figure 5.16, in general, the creep strain rate increases with stress and decreases with time as expected. On the other hand, the behaviour is similar to the behaviours of the primary stage of creep of polymers shown in Figure 5.4.

5.5 Verification and Updating

5.5.1 Relaxation Tests and Simulations

In order to verify the model at the end of the study, some relaxation tests were performed and compared with the simulations employing the creep data. A model used for these studies was composed of one truss element with the same gage length as that measured during the test. The exact displacement profile introduced to the crosshead was also applied in the simulated model. A true stress-true strain curve obtained form a fast tension test (15 mm/s, Figure 5.17) was introduced into the model with the creep strain-rate data obtained in the previous section. Figure 5.18 shows two of those test results compared with the simulations. In this figure rapid extension was applied until the specimen reached the predetermined engineering stress value with a speed which was fast enough to minimize the relaxation during the initial loading stage, but slow enough not to reach a stress value beyond the predetermined engineering stress value of 75 MPa. The tensile extension was

stopped at that point, and the decrease in the loading is recorded. The same procedure was also applied for the stress states values of, 65, and 55 MPa. The crosshead movement of the machine cannot be stopped without the engineering stress reading on the specimen exceeding beyond 55 MPa unless the test speed is decreased below 1mm/s. In that case, the relaxation would be effective during the initial loading stage, which can affect the accuracy of results. Thus, relaxation tests with the stresses below 55 MPa were not performed.

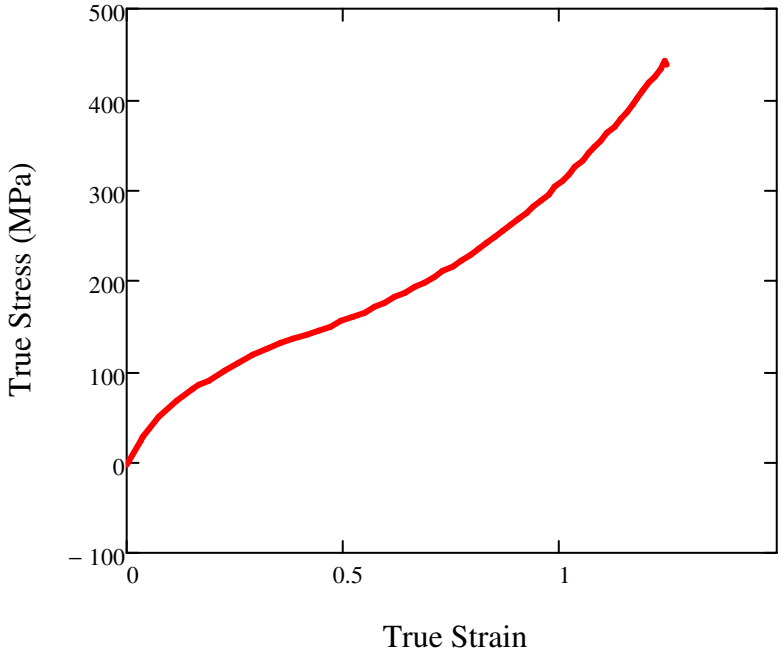

Figure 5.17. True stress – true strain data (test speed, 15 mm/s)

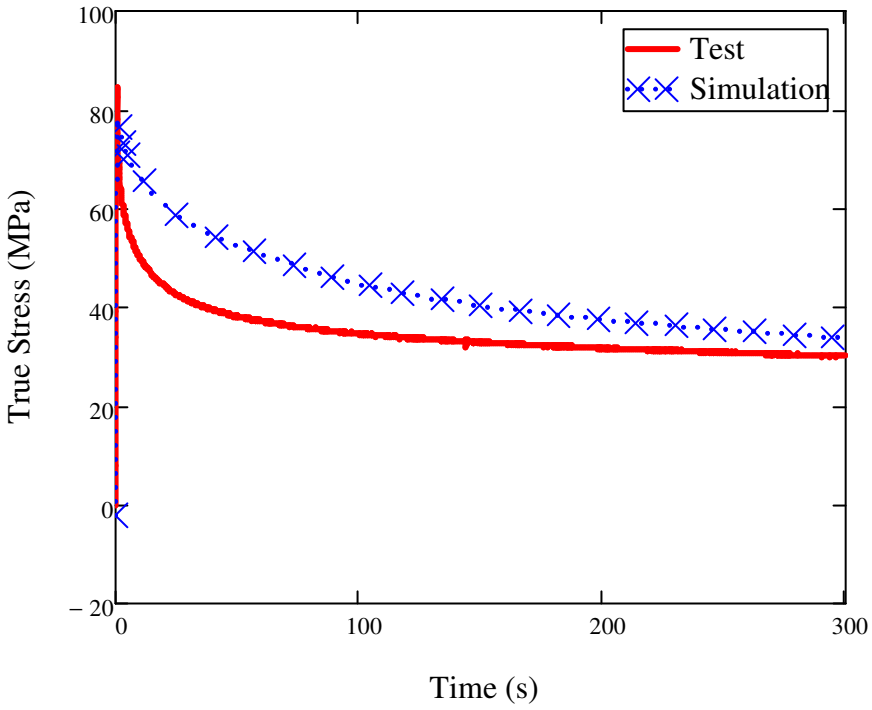

(a)

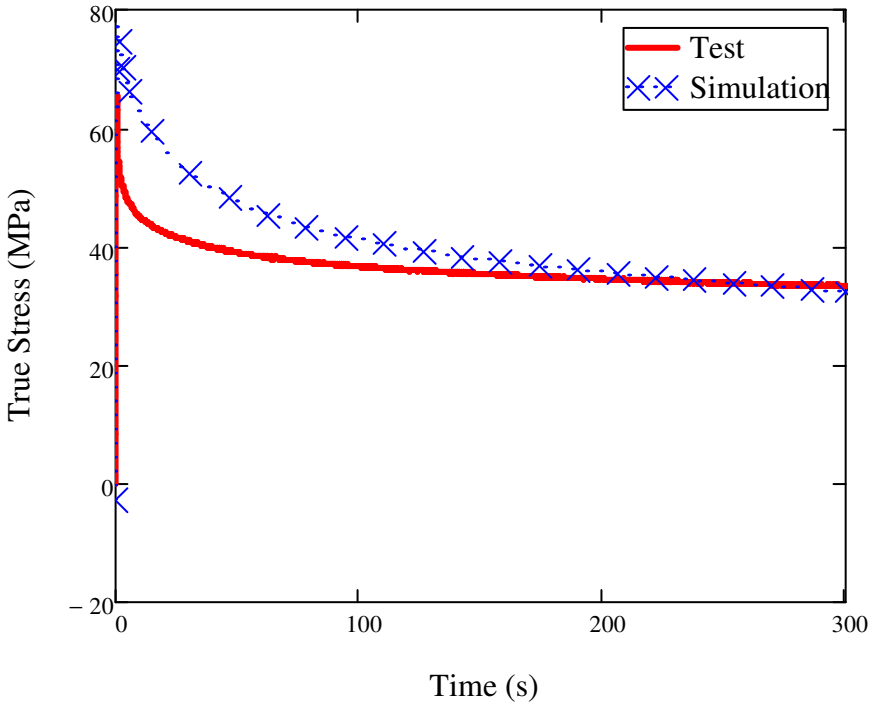

(b)

Figure 5.18. Results of relaxation tests results for initial engineering stress of 75 MPa (a); 55 MPa (b)

According to Figure 5.18, it was found that, the calculated stress magnitudes for the initial stages of relaxation were higher than those in the test. It means that the creep behaviour modelled was not fully adequate for the initial stages of loading. Hence, it was decided to increase the creep strain rate at the initial stages of loading. As discussed before, all creep strain curves were determined after the initial loading stage of 20 seconds. For this stage, the values were extrapolated to the initial time. However it is obvious that a different creep profile should be introduced for the initial stage.

5.5.2 Updating Creep Model

In order to update the profile for the initial stage, the results for creep strain rate obtained from the relaxation tests and in the simulations were compared with each other. To obtain the creep strain from the actual test, the elastic strain should be subtracted from the true strain because true strain involves both the elastic and creep components of strain (it can also include other strain components due to damage, which cannot be accounted in this study).

In order to determine the creep component of strain, first of all, true stress values *vs.* time plots of each relaxation test were obtained. The time to reach the constant stress (tc) was obtained from each graph. The strain values were read starting from the end of the data until a difference of 5% in the strain values was observed. The time reached at that strain level was recorded (tc). Then the true strain and true stress values were obtained at that time. The modulus of elasticity was calculated from the following equation:

$$E_i = \frac{\sigma_{true_{i(tc)}}}{\epsilon_{true_{i(tc)}}}, \tag{5.5}$$

where i denotes the individual tests. The elastic part of the relaxation tests was found from the following equation:

$$\epsilon_{elastic_i} = \frac{\sigma_{true_i}}{E_{i(tc)}}. \tag{5.6}$$

The creep part of the true strain was found by subtracting this elastic part from the true strain values:

$$\epsilon_{creep_i} = \epsilon_{true_i} - \epsilon_{elastic_i}. \quad \textbf{(5.7)}$$

The creep strain rate was calculated for each time increment using the procedure described in the previous section. Then creep strain rate *vs.* time data were plotted for each figure after the constant strain value is reached. Figure 5.19 shows the results for a stress level of 75 MPa. As it can be seen, the creep strain rate obtained from the simulations predicts the test results except for several initial seconds. Thus, the creep strain rate should be increased for the first few seconds. Taking into account other simulation results, it was decided to increase the creep strain rate further at about 4 seconds. After several trial and errors, it was noticed that increasing the exponent *D*2 in equation (5.2) with two-fold during 0-4 second of time and extrapolating the predetermined creep curves from 20 seconds to 4 seconds would be enough for simulating the initial stage of creep with a reasonable approximation. The time step size in this stage was decreased to simulate the creep behaviour in this region more accurately. However, after the modification was made, the continuity of the creep strain curves was broken. So the value at the 4^{th} second was brought to the same values by shifting the initial stage accordingly. This is explained in Figure 5.20. As it can be seen in this figure, during the stage between 0-4 seconds, the curve that is not shifted lies separately because of the modification of the fitted function. Thus, the curve in the initial stage is shifted downwards until it is continuous with the rest of the curve. It is important to note again that shifting the curves vertically do not change the creep behaviour as the rate of creep strain is implemented in the model.

After the above operation, the rest of calculations and relaxation simulations were repeated. The respective results are shown in Figure 5.21 and Figure 5,22. As it can be seen from these figures, after this modification, the relaxation curves obtained from simulation fit better to the experimental data for the stress level of 75 MPa. Some difference between experimental and simulation data was observed for the stress level of 55 MPa especially in later stages. However, this difference was determined to be acceptable since even in tests with the same configurations, such an

error can be experienced (Figure 5.23). The reason may be due to the mechanical operations that were applied to the polypropylene fibres during production. The fibres are drawn and attached to each other by means of certain pressure and heat. Thus, in fact, the viscoelastic behaviour had already been initiated. As the distribution of pressure and heat is not even throughout the structure, it is natural to obtain different results for different fibres. Other reasons can be specimen alignment which can contribute about 10% error. Also, damage strain may cause some discrepancy as it could not be separated from the total strain obtained during the test. In addition, damage strain could have been present during the manufacturing operations of fibres.

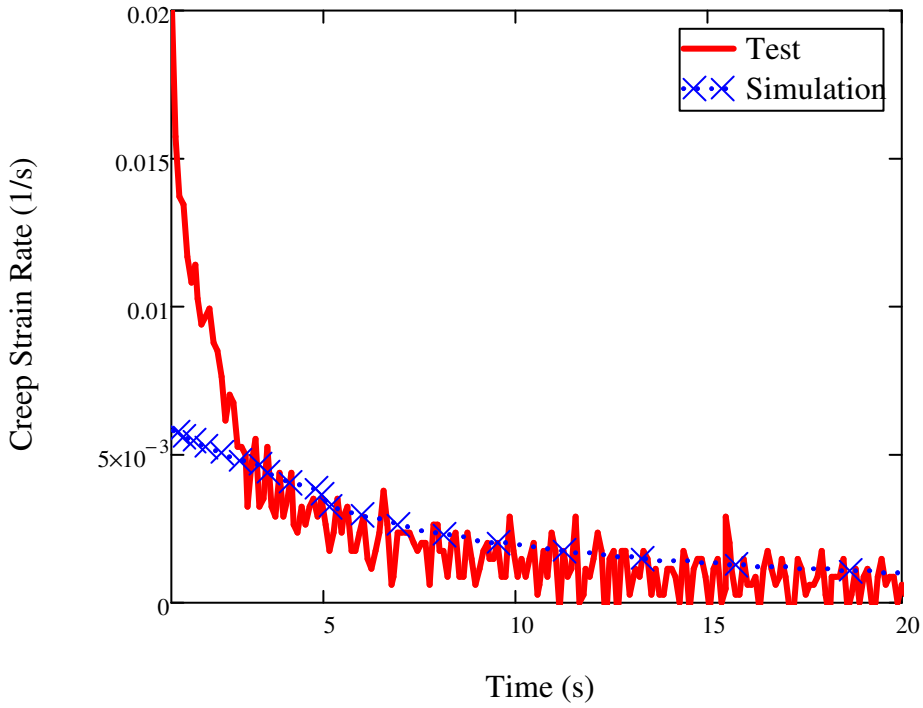

Figure 5.19. Creep strain rate *vs.* time plot (initial engineering stress, 75 MPa)

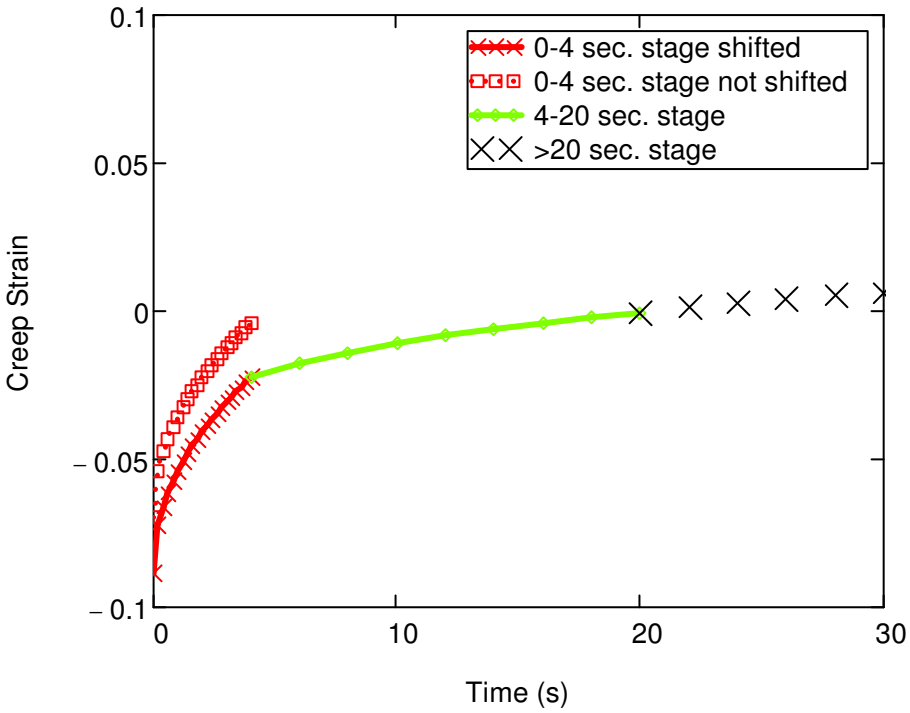

Figure 5.20. Time *vs*. creep strain curve (stress, 50 MPa)

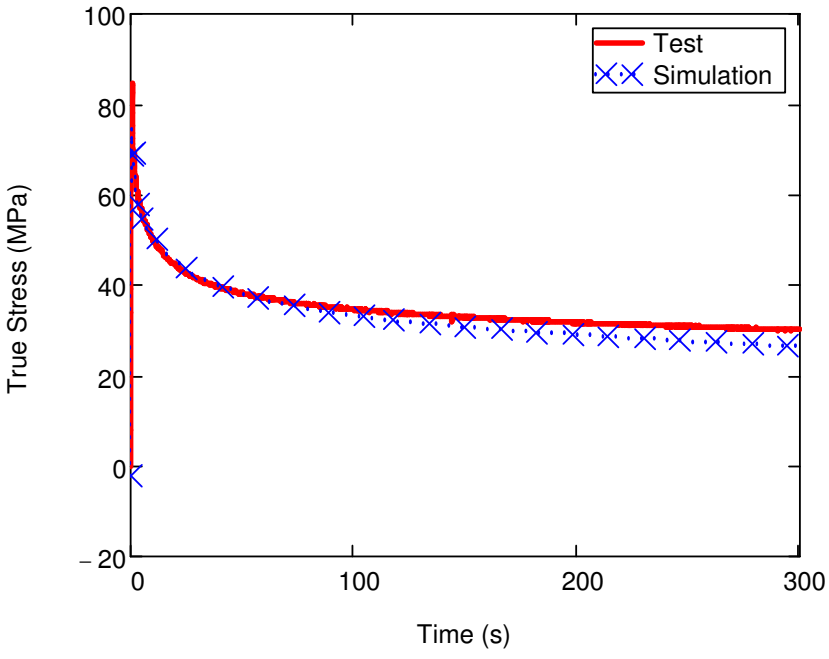

(a)

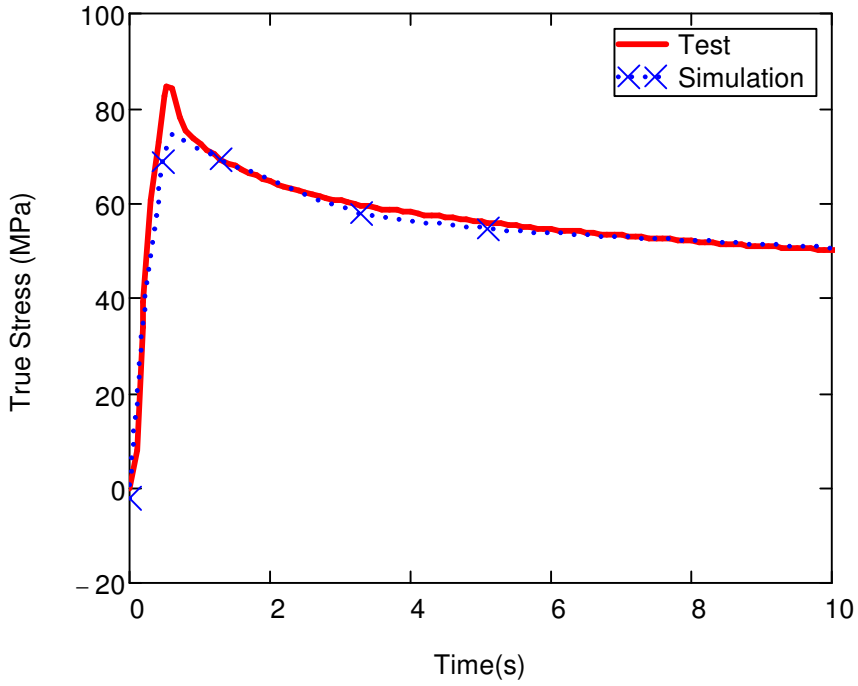

(b)

Figure 5.21. True stress *vs*. time data for entire interval (a) and initial stage (b) of creep curves (stress, 75 MPa)

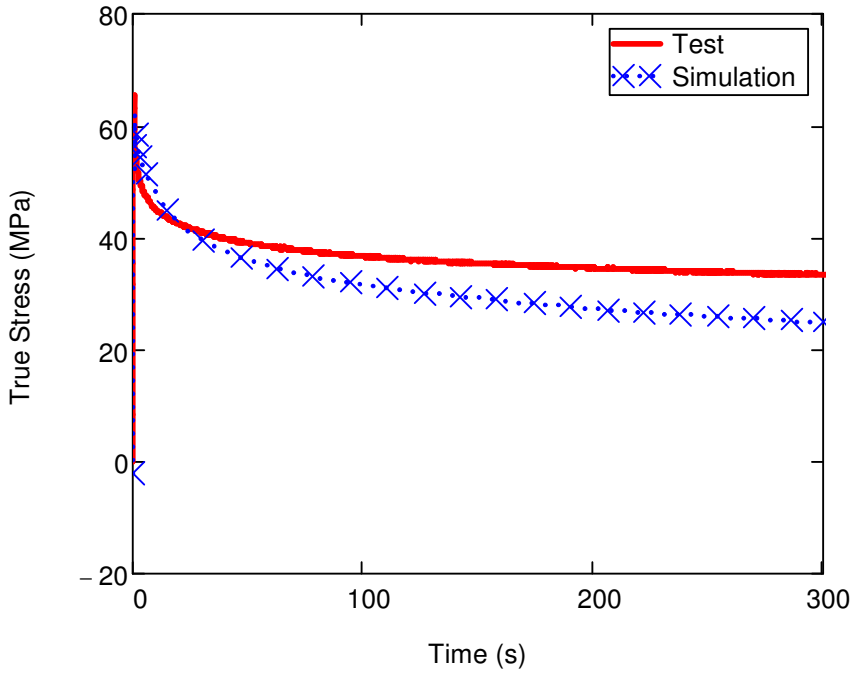

(a)

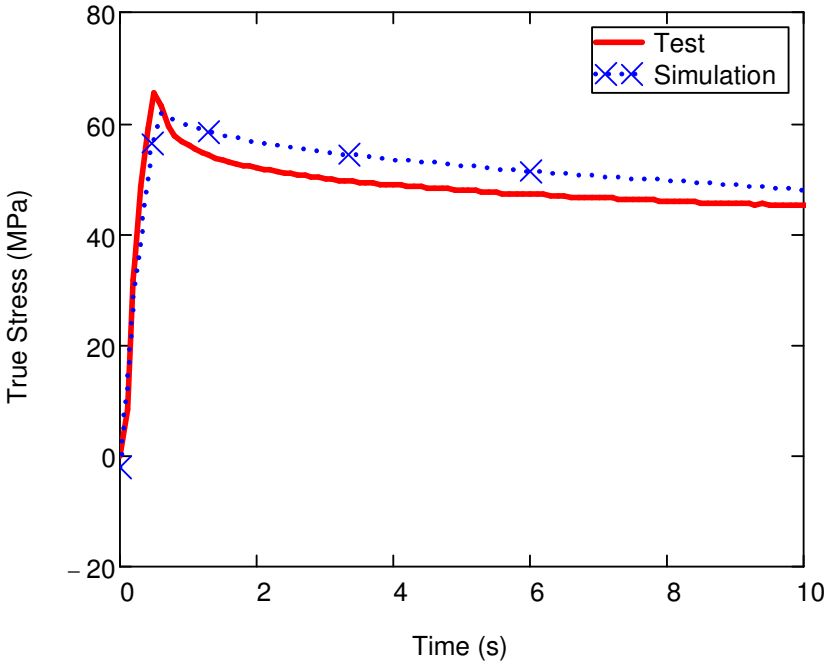

(b)

Figure 5.22. Force *vs*. time data for entire interval (a) and initial stage (b) of creep curves (stress, 55 MPa)

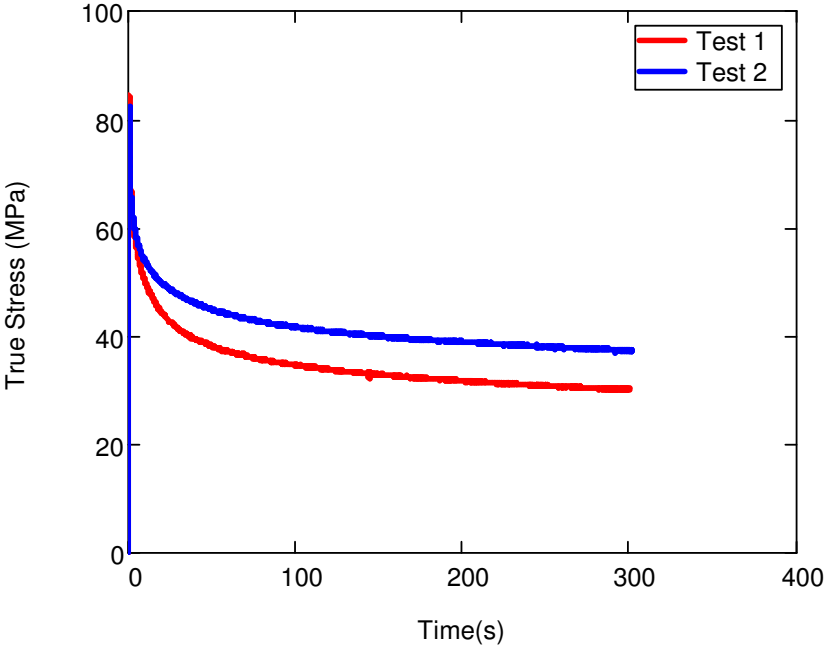

Figure 5.23. True stress *vs*. time curves for two relaxation tests from a stress value of 75 MPa

5.6 Case Study Tests

Tensile tests with a true strain rate of 0.001 s^{-1} were performed to study how well the simulations based on viscoelastic model with creep can predict a low-speed tensile behaviour. These simulations were performed by combining the data obtained from a high-speed tensile test (used in the previous section) and the creep behaviour determined in this study. In another simulation, the creep option was turned off to assess the contribution of creep in the model. Results of the test and simulations are shown in Figure 5.24. The figure demonstrates the importance of implementation of creep behaviour in order to achieve more realistic results for this test speed. Another test was simulated similarly with the same test speed (Figure 5.25). This time, the simulations were not as close of the first one due to crimpled fibres, as discussed in Chapter 4.

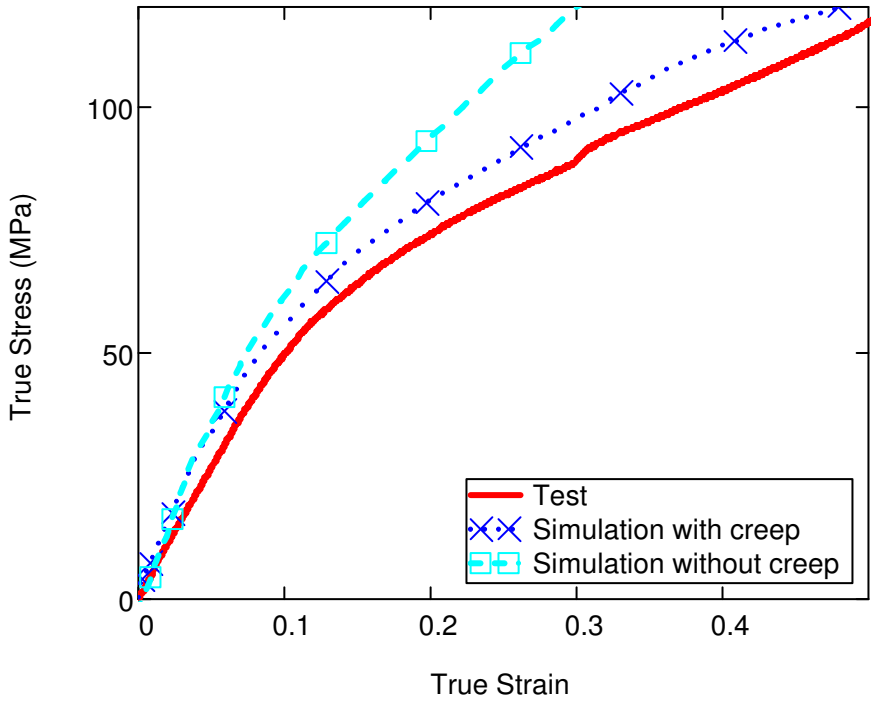

Figure 5.24. Tensile test for true strain rate of 0.001 s^{-1} compared with simulations

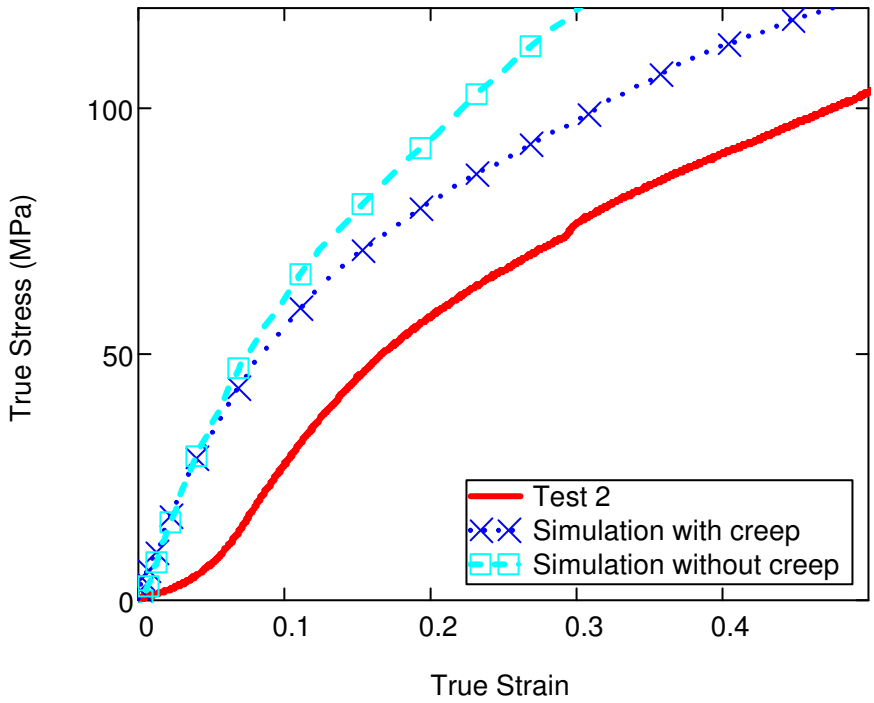

Figure 5.25. Tensile test for true strain rate of 0.001 s^{-1} compared with simulations (Test 2)

A tensile test with ten times higher true-strain rate (0.01 s^{-1}) was also simulated and compared with the test data to observe the effect of test speed. The results are shown in Figure 5.26. It can be seen that the simulations with and without creep gave similar results for this test speed. This shows that the implementation of creep behaviour was not crucial for this speed level.

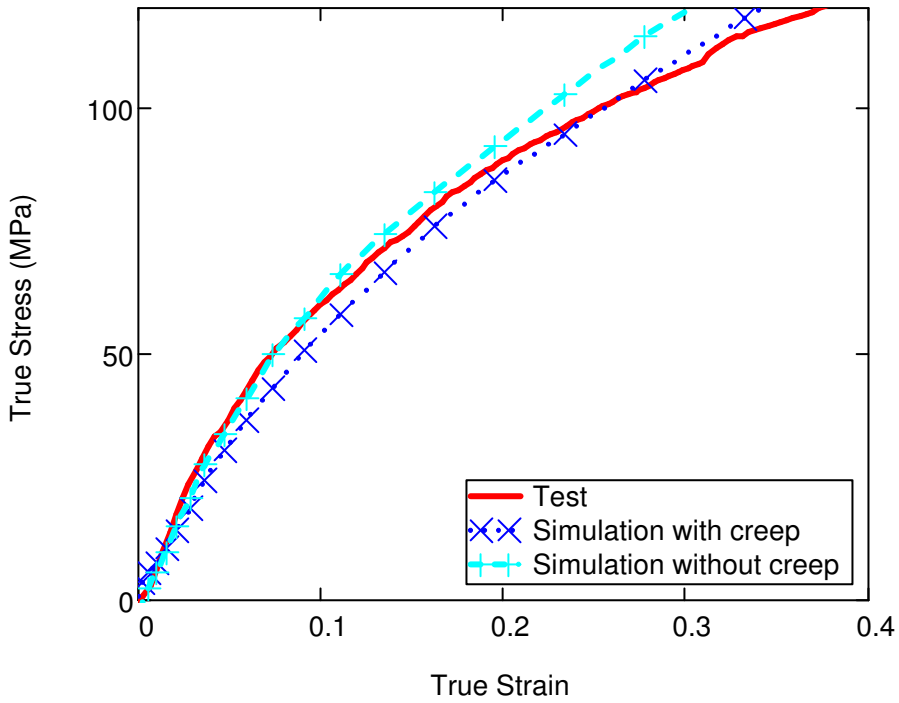

Figure 5.26. Tensile test for true strain rate of 0.01 s^{-1} compared with simulations

Another study was performed to observe the effect of creep modelling in the plastic region. In order to do this, the plastic region of the fast tensile test was implemented with approximated linear elastic data of this test instead of the nonlinear elastic (hypoelastic) stress *vs.* strain option because the software does not allow implementation of a nonlinear elastic behaviour with plasticity. Normally, the creep data for undetermined stress and time values are extrapolated by the software. As this extrapolation could result in strange material behaviours, two more models were generated by preventing extrapolation options. In one of the models, the extrapolation in time values was prevented. In the other, the extrapolation in stress values was prevented. The results are shown in Figure 5.27. It was observed that creep modelling with extrapolation causes a high level of relaxation in the plastic region. Apparently, the best approximation was with preventing the extrapolation in stress values.

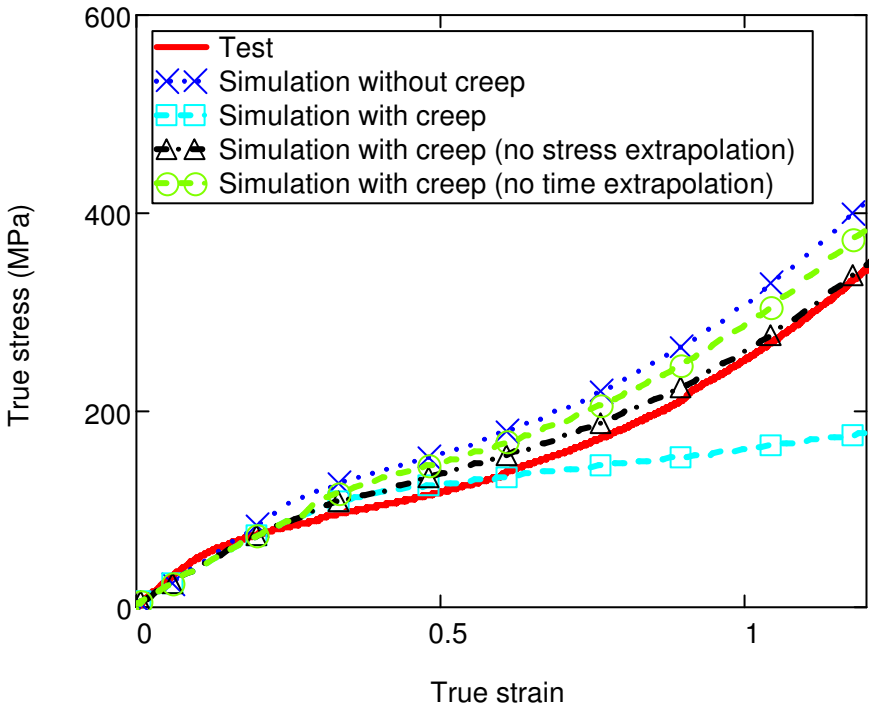

Figure 5.27. Tensile test for true strain rate of 0.001 s^{-1} compared with simulations

5.7 Conclusions

In this study, a methodology was developed to determine the creep behaviour of polypropylene fibres that are used in nonwoven materials. Creep tests were performed with different stress levels, and the obtained test results were analyzed in order to implement the behaviour in the finite element software MSC Marc Mentat. It was observed that the creep behaviour of fibres can be simulated reasonably well. However, it is difficult to judge about its accuracy for the studied polypropylene fibres that demonstrate a scatter in their material behaviour.

The procedure given here can be used for the stress levels below the yield point. After this point, the extrapolated values give inaccurate results when compared with tests. It was demonstrated that preventing the extrapolation option towards stress values gives the best approximation. However, a material model should be implemented in plastic region. Many studies focussed on the viscoplastic behaviour to simulate the creep in the plastic range (see Section 3.3.2). Thus, it is still too early to simulate the tensile properties accurately by implementing the data from tensile

tests at high strain rates directly and implementing the creep behaviour, especially for the stresses beyond the yield point. It is necessary to consider the effects of damage and viscoplastic components for more realistic results.

The crimp in the fibres is still a problem as mentioned earlier in Chapter 4. It affects the determination of the viscoelastic behaviour. Some other inaccuracies in this study can be related with the following factors:

- The crosshead movement in tests cannot be fixed at the predefined stress value. The machine turns on and off the crosshead movement in order to hold the stress constant.

- Adjusting the alignment of fibre ends in the jaws is accomplished by using only a naked eye (i.e. without any instrument). It was observed that an error of about 3-4% can be introduced because of the alignment problems. Keeping the gage length as long as possible reduces the error as, for example, a 1 mm alignment difference will alter the vertical orientation of the sample with less error when the gage length is larger.

- Fibre properties demonstrate a scatter; one of the reasons could be various stress levels experienced during manufacturing processes.

CHAPTER 6

PARAMETRIC MODELLING OF NONWOVENS WITH PATTERNED STRUCTURE

6.1 Introduction

The modelling method used in this chapter is a more comprehensive version described by Limem *et al.* (2007), Mueller & Kochmann (2004) which involves the distribution of fibres according to a certain pattern. As discussed in Chapter 2, the structure of nonwovens consists of two distinct regions called bond points and fibres. Bond points are the continuous regions where fibres are attached together in calendaring operation. Thus, they are modelled with thin shell elements with a certain thickness similar to the mentioned studies. Fibres are modelled as truss elements which can carry axial load but not transverse load. This resembles the behaviour of fibres under loading conditions. The number of fibres to be modelled is a concern here as there can be thousands of fibres in the nonwoven structure (Figure 6.1). This problem was solved by parametric modelling technique described in the proceeding sections.

As discussed in the previous chapter, in order to be able to model different types of nonwovens with a significant number of fibres, a parametric model should be formulated by employing finite element techniques. This requires the model to be constructed by using arrays and subroutines that the software could read instead of using its graphical user interface. This gives the opportunity of modelling more complex models with less effort. Parametric modelling was performed with the finite element software, MSC. Patran. The program has its own script language called Patran Command Language (PCL), which can be utilized for parametric modelling. The solver used in the study is MSC. Marc Mentat, which is a widely used commercial software in finite element studies.

6.2 Modelled Nonwoven Sample

A 20 g/m^2 thermally bonded polypropylene nonwoven with rectangular bond points was simulated in this section which was also used in Hou *et al.* (2009) (Figure 6.1). The dimensions of bond points as well as the distances between them are given in Figure 6.2 and Table 6.1.

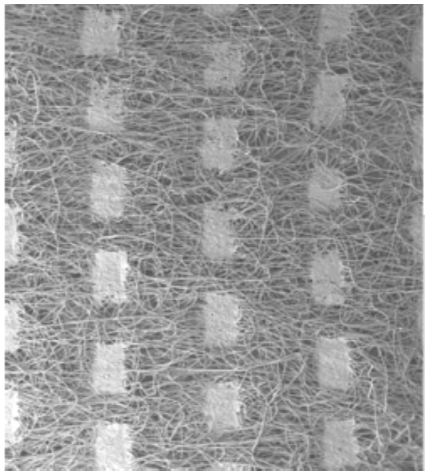

Figure 6.1. Nonwoven material used in (Hou *et al.,* 2009)

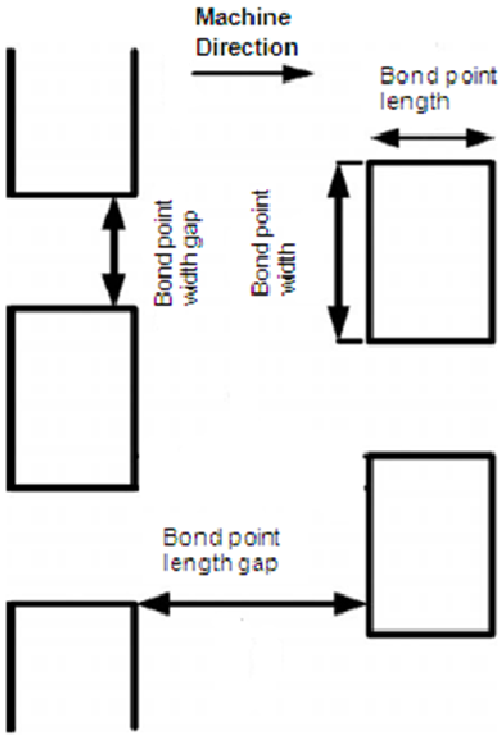

Figure 6.2. Layout of bond points in (Hou *et al.,* 2009)

Table 6.1. Bond point dimensions (mm)

Bond point width	1.1
Bond point length	0.75
Bond point width gap	0.7
Bond point length gap	1.5

6.3 Modelling Methodology

Finite element models are generally constructed in the following sequence: First, the solid geometries are generated. Then those geometries are meshed with appropriate element sizes. Material properties are defined and assigned to the relevant elements. Boundary conditions and loading states are defined. Lastly, the analysis parameters are determined, and the analysis is sent to the solver. In this technique, especially the generation of solid geometry stage requires significant effort. The generated model should take into account, the orientation distribution, fibre and bond point properties, and other parameters related to manufacturing. Especially, the application of orientation distribution is an important concern in this type of modelling. During the explanation of the procedure, the fabric dimensions (fabric length and width) were kept as 10 mm x 8 mm in order to show the procedure more clearly (Figure 6.3).

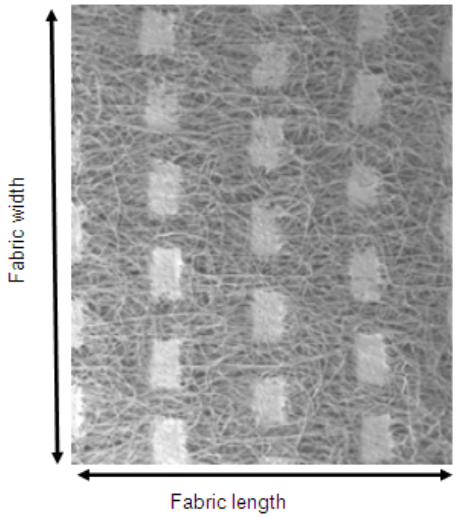

Figure 6.3. Representation of fabric length and width

6.3.1 Generation of Planes on Fabric Borders

Fabric width and length was read from the code and planes were generated on the corners of these fabric limits. These planes not only show the fabric dimensions, but also they were used to cut the fibres and bond points which were generated in the further stage (Figure 6.4).

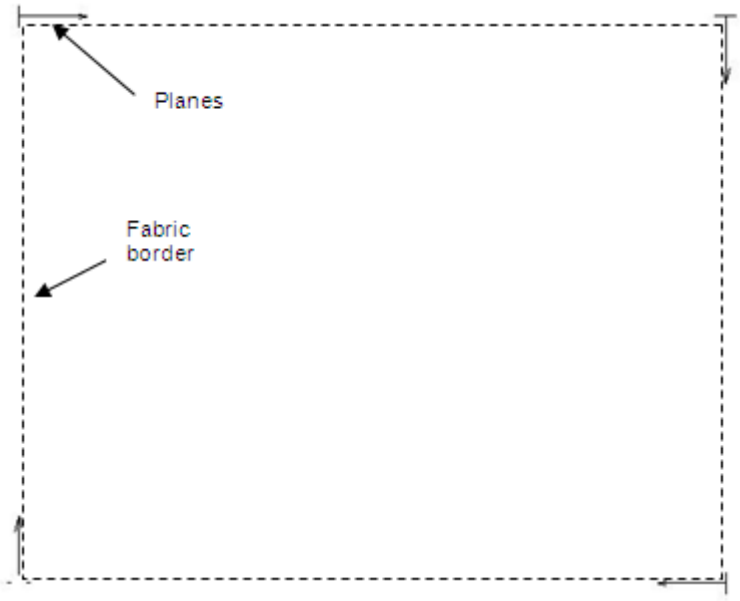

Figure 6.4. Planes on fabric borders

6.3.2 Modelling of Bond Points

At the initial stage of modelling, it was decided to connect the bond points with each other from different locations without taking into account the orientation distribution. It was assumed that 12 locations along the periphery of the bond points were enough to represent the behaviour. The models of Limem *et al.* (2007) and Mueller & Kochmann (2004) had only four connections from the four corners of bond points. It was thought that modelling fibres with only 4 corners would be insufficient to model enough fibre connections along machine direction. In addition modelling fibres from only 4 corners may cause the bond points to rotate unnecessarily and cause the analyses to diverge. Thus, three intermediate connections on the longer sides of the bond points and one extra connection were added to the shorter sides. Eventually,

twelve connections were introduced to the model and, the bond points were generated by connecting those points (Figure 6.5).

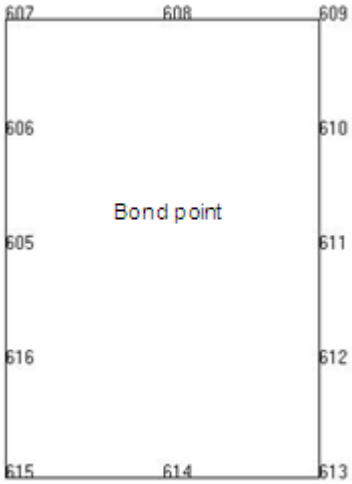

Figure 6.5. 12 points along the periphery of a bond point with point numbers

All the bond points were generated according to the fabric dimensions (Figure 6.6). As seen, bond points were drawn in a much larger area. Here, the criterion was given so that there were enough bond points to prevent any missing fibres in the area of interest. Otherwise, some fibres connecting single bond points could be missed (Figure 6.7), causing a problem at the stage of application of boundary conditions. Surfaces were generated on the bond points, part or all of which fall into the fabric limits. The reason is that, the software can only mesh surfaces (will be shown later). The surfaces that lie on the fabric limits were cut and the ones left outside the fabric limits are deleted.

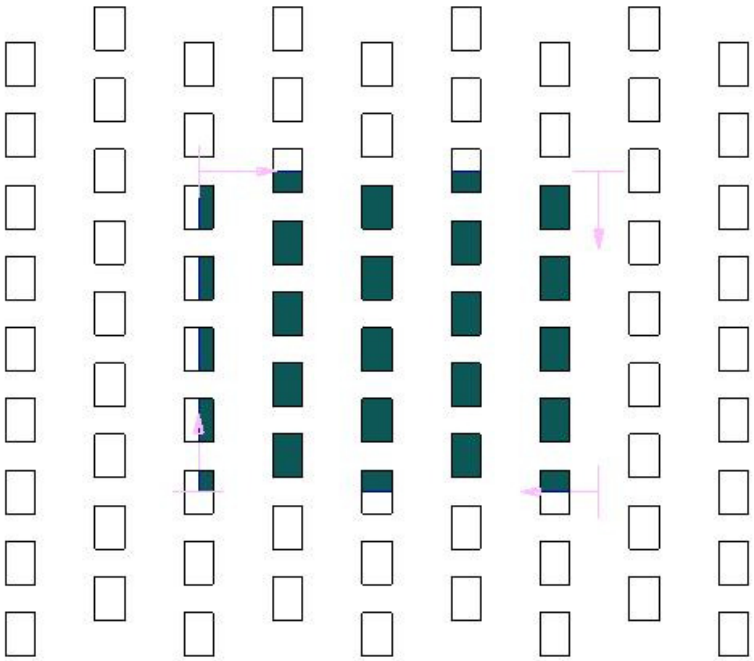

Figure 6.6. Modelling bond points (dark ones show the surfaces generated)

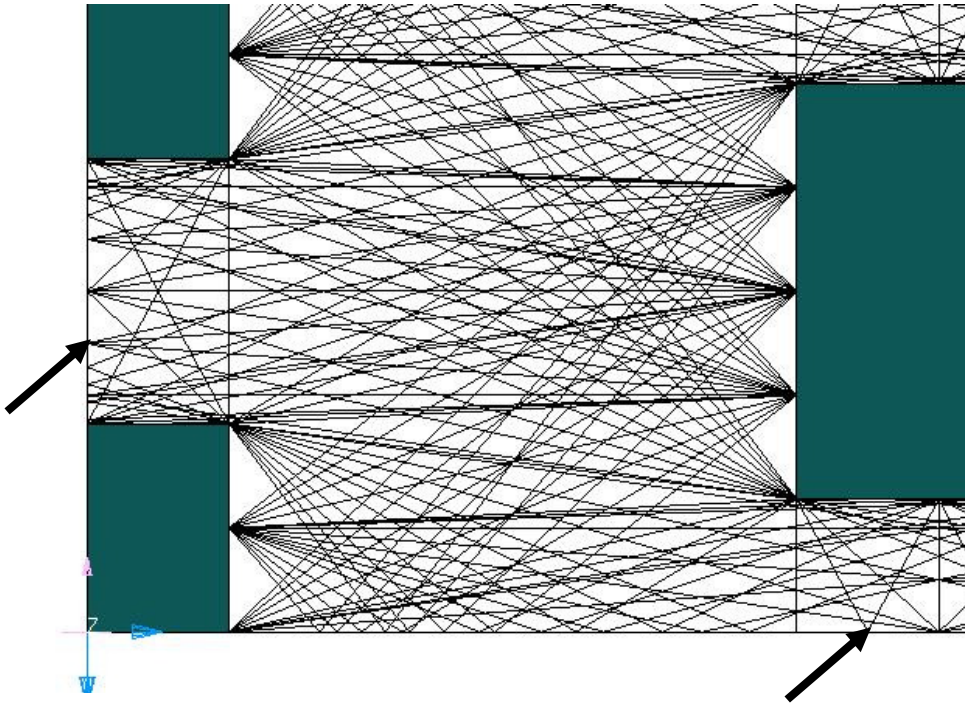

Figure 6.7. The lower left corner of the modelled fabric that shows the importance of fibres connecting single points

6.3.3 Modelling of Fibres

The fibres in the model were drawn by connecting 12 points on the bond points with each other by considering some criteria. The first criterion was that, the points on the same bond point should not be connected. Secondly, the fibres should not cross through the bond points. Lastly, the bond points situated very far from each other were not connected. The first one was easy to be implemented via a subroutine. The implementation of the other two criteria is explained in the following two sections

Control of Intersection of Fibre Lines with Bond Point Borders

The intersection of lines was checked by a method presented by Cawsey (1998). It was accomplished by a subroutine that checks the location of line points. Firstly, given three points, a function (CW) was written that determines whether to turn clockwise or counter-clockwise while travelling from the first, to the second and the third point. The function returns the value "true" if the direction is clockwise whereas it will return "false" if the direction is counter-clockwise. In order the two lines, *L1* and *L2*, to intersect each other, both of the conditions given below should be satisfied (Figure 6.8):

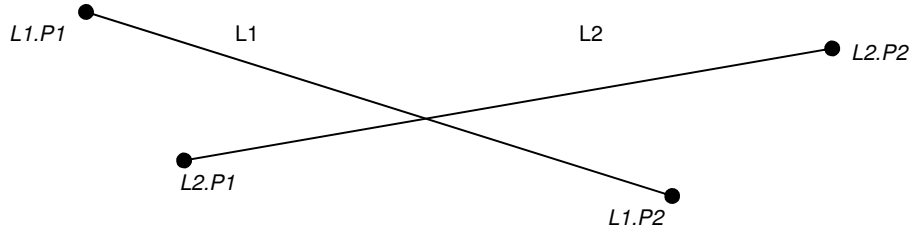

Figure 6.8. Notation used for line intersection conditions

$$CW(L1.P1, L1.P2, L2.P1) \neq CW(L1.P1, L1.P2, L2.P2) \quad \textbf{(6.1)}$$

$$CW(L2.P1, L2.P2, L1.P1) \neq CW(L2.P1, L2.P1, L1.P2) \quad \textbf{(6.2)}$$

There are 4 points to be checked with two lines, but the function takes into account 3 points. So in order to take into account all the points, four combinations should be given as input (Eq. 6.1). The problems occur in special cases when one of the end points of the lines coincides with the end points of the other line. To take into

account this, additional conditions were added in the subroutine such as checking the length of the fibre lines to be created between particular points of bond points.

Prevention of Connecting Far Bond Points

Some bond points which were very far from each other can still be joined without intersecting any other bond points (Figure 6.9). Connecting these bond points with fibre lines would be very unrealistic and unnecessary. It can be observed from the SEM image of the studied nonwoven that there are no such connections between bond points. In order to prevent that, additional constraints were introduced to the model. First, it was assumed that fibres do not connect bond points with centres separated by a distance exceeding the limit equal to a sum of half bond point width and half bond point width gap (distance *d* in the figure) distance if the bond point connection candidate is in the next row (Figure 6.10)

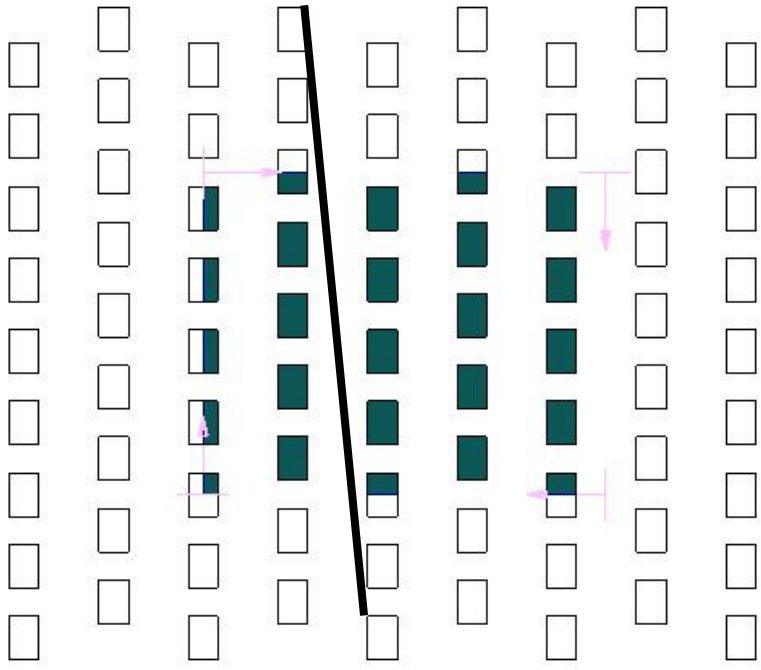

Figure 6.9. Unrealistic connection of far bond points

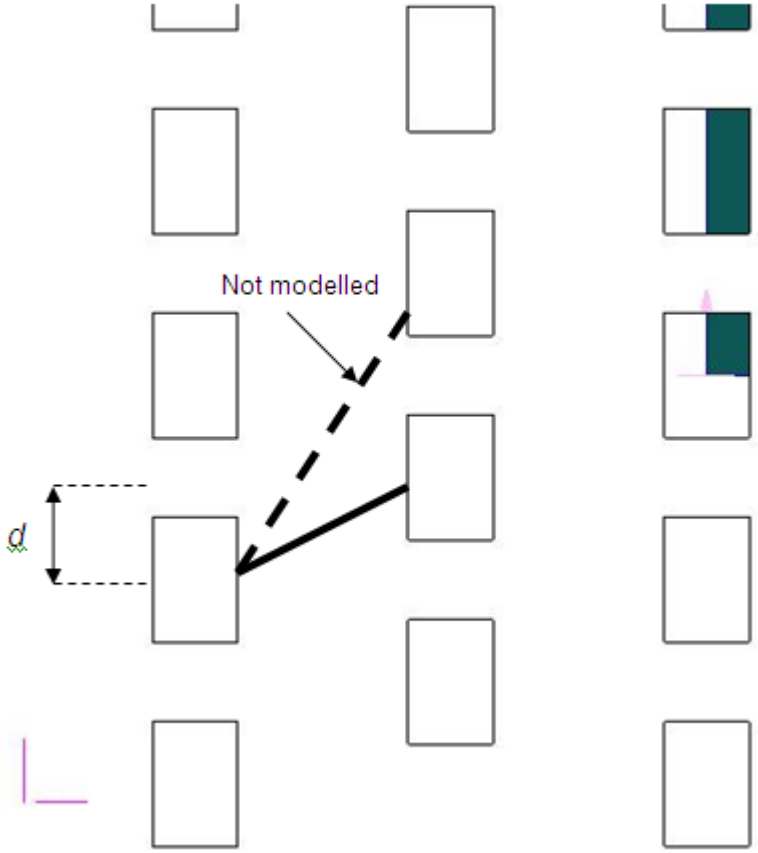

Figure 6.10. BP connection conditions (*d* represents distance limit)

Fibre Lines Generation Procedure

The usual way to connect the fibre lines is to scan all the bond points and connect them with each other. However, in a full-scale model, which has fabric dimensions of 25 x 20 mm, there are 240 bond points, having 12 points each, making the total number of connecting points, 2880. It would require 4,145,160 combinations to check all the bond point connection points whether it should be connected to all other bond points. Such checks would require a lot of time for the software even in a case of relatively small fabric dimensions. In order to prevent this, BP points were handled one at a time; an example is shown in Figure 6.11. Initially, an attempt was made to connect BP1 in the bottom left corner to all other bond points. When the first loop is completed, (connection of BP1 points finishes), it is the time for BP2 to be checked for connections with other bond points. But this time BP1 points were neither connected nor checked for intersection. For BP3, two previously connected

bond points (BP1 and BP2) were not checked for intersection and connection, and so on. This procedure not only prevents generation of double lines between bond points, but also reduces number of loops to be passed in the code (thus decreasing modelling time). In this method, the number of loops is decreased by one for each new BP and no loops were required for the last bond point in the upper right – hand corner. In order to decrease the fibre-connection combinations, it was decided to create two new arrays: one, storing the bond point number together with the number of bond points to be connected to it. In addition, another array stores the bond point number versus bond point numbers to be checked for intersection. In such a way, a certain number of BP points were scanned instead of checking all the BP points in the model. Thus, the CPU time is decreased. An example of implementation of this algorithm is shown in Figure 6.12. For BP3, only the bond points shown with arrows are considered for connections with fibres and checked for intersection. Fibres in the structure are generated by taking account for all those conditions mentioned (Figure 6.13).

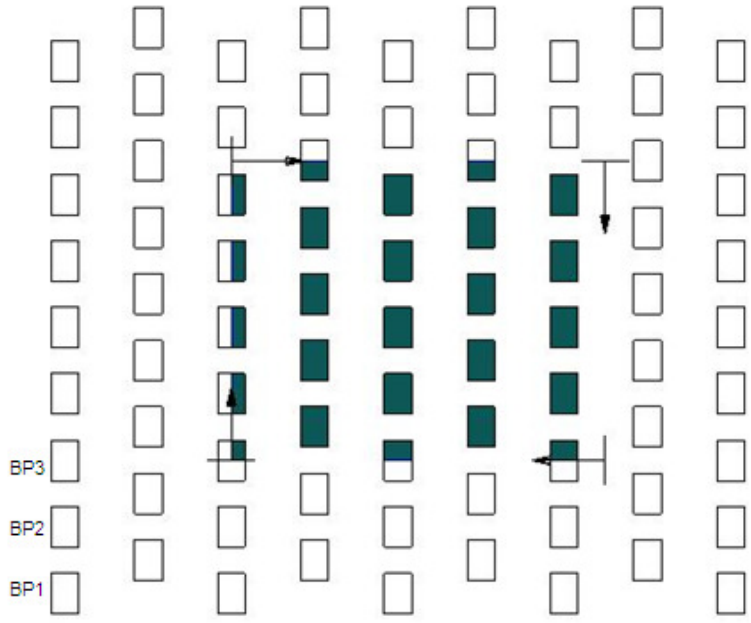

Figure 6.11. Representation of bond point connection and scanning procedure (step 1)

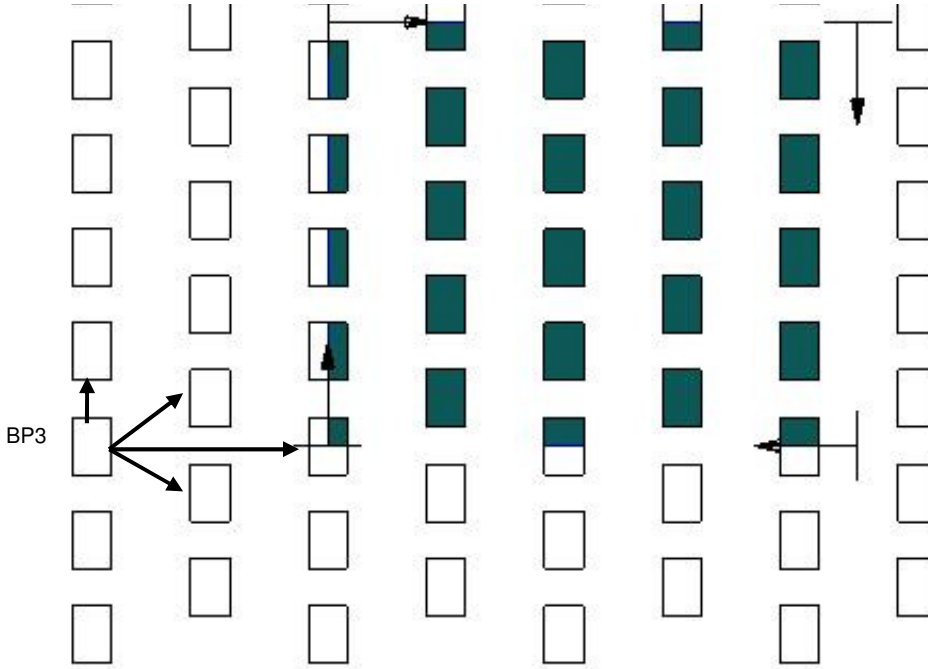

Figure 6.12. Representation of bond point connection and scanning procedure (step 2)

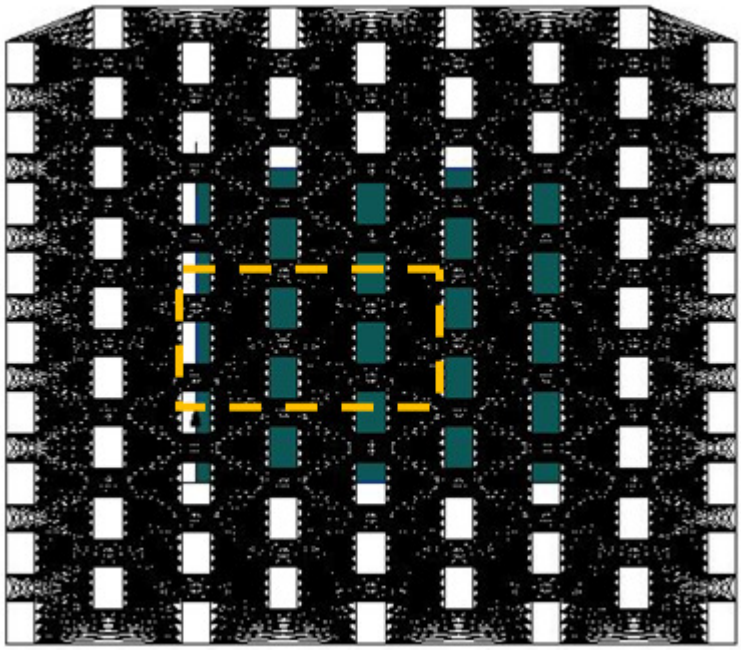

(a)

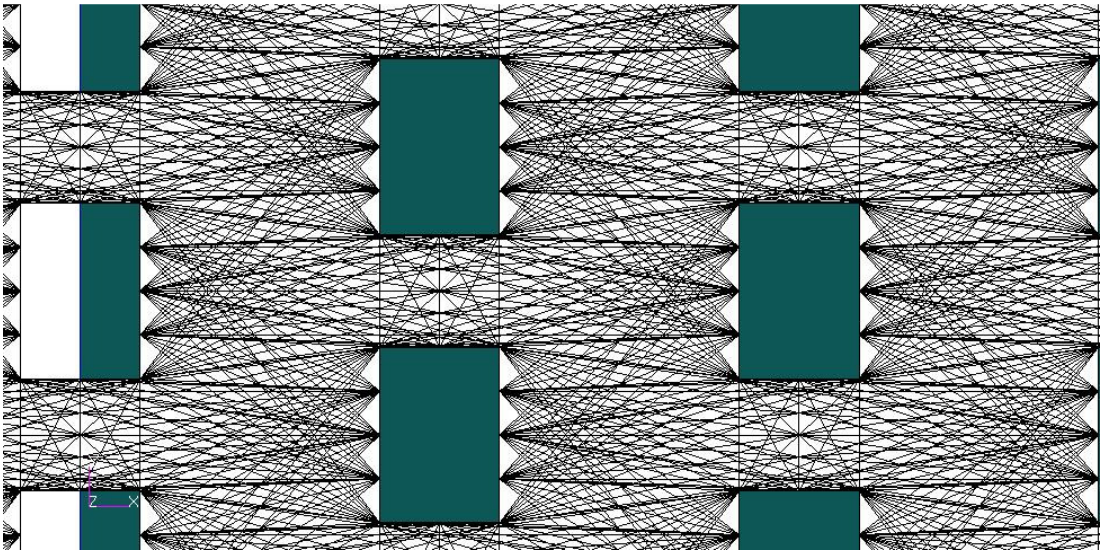

(b)

Figure 6.13 Created fibre lines: (a) general view; (b) closer view

6.3.4 Extraction of Fabric

After the generation of fibrous model, the part of fabric to be analyzed is extracted from this general model (Figure 6.14).

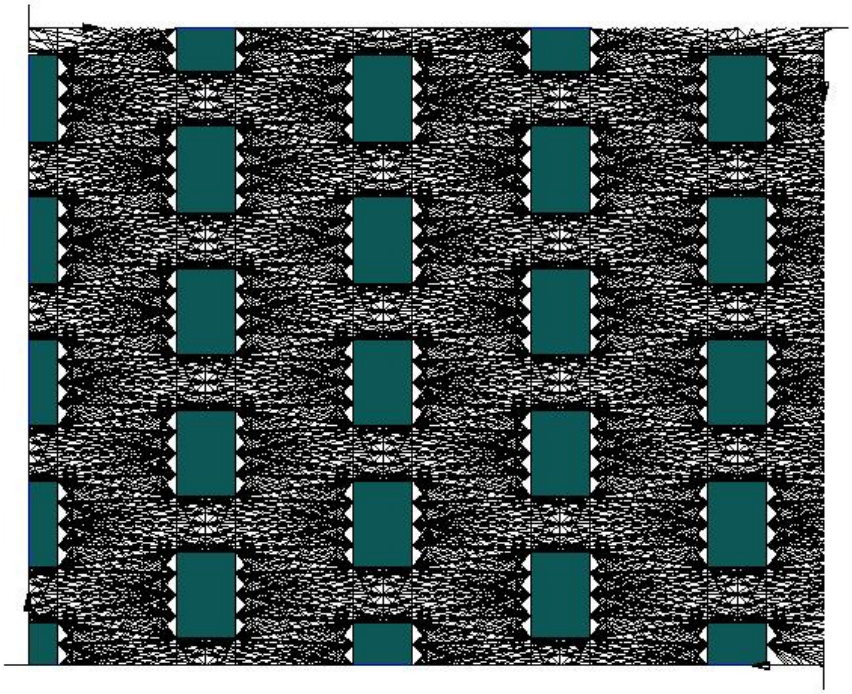

Figure 6.14. Extraction of fabric

6.3.5 Implementation of ODF

The orientation distribution function of the fibres was determined by a procedure described in Appendix A. It was implemented in the developed model by assigning various cross-sectional areas to the fibres in the structure based on the orientation distribution. First, the coordinate system was adjusted to make use of the output obtained from the orientation distribution software. Then, an angle for each fibre in the current structure was calculated and stored in an array. Angle bands of 10º were used in the software so all the fibres in the structure are classified according to their angle. This means, for example, if the angle of a fibre is 25º, it belongs to the third band of angles corresponding to fibres with orientations between 20º – 30º. Some adjustments in the code were made to obtain the angles as positive for comparability with the output obtained from the orientation distribution software. Also, a special care was taken for the fibres that are close to 0º and 180º. In principle, they represent the same orientation so the angle of fibres very close to180º orientation was changed to 0º orientation.

After this procedure, a new array was created to show the number of lines (*NL*) currently modelled for each orientation distribution intervals. Besides, the magnitudes for angles from the output of orientation distribution software are also written into an array. The ODF values and number of lines in the model belonging to certain angle bands are given in Table 6.2.

Table 6.2. Sample ODF values and representative number of lines in the model

Angle band(º)	***ODF (%)***	***NL***
0-10	1.1	111
40-50	7.54	249
90-100	10.04	483

In order to generate a relationship between the ODF and the model, the number of lines in the angle intervals and the angle of each fibre were determined. It was assumed that the total fibre mass in the model was the same as in the modelled

fabric. Thus, the total fibre mass of the fabric should be found; it can be calculated by subtracting the total mass of bond points from the fabric mass. The fabric mass was found from the following equation

$$m_{fabric} = d_{fabric} A_{fabric}, \quad \textbf{(6.3)}$$

where d_{fabric} is the fabric's density (20 g/m^2). A_{fabric} can be calculated easily as the product of fabric length and width. In order to find the mass of bond points, a computed tomography image obtained in Hou (2010) was used (Figure 6.15). As it can be seen from this image, the thickness of bond points is about 0.02 mm and the empty spaces between fibres vanished. So, the bond point mass was found by the following equation:

$$m_{BP} = d_{polypropylene} A_{BP} t_{BP}, \quad \textbf{(6.4)}$$

where $d_{polypropylene}$ is the density of polypropylene; A_{BP} is the area of a bond point and t_{BP} is the thickness of the bond point. Mass of bond points can also be found by assuming that fabric density is same inside the bond point as;

$$m_{BP} = A_{BP} d_{fabric}, \quad \textbf{(6.5)}$$

In the case of present nonwoven the density of polypropylene (0.98 gr/cm^3 (Fibrevisions®, 2009) multiplied by the thickness (0.02 mm) is nearly equal to the thickness of fabric (20 g/m^2) so either of these methods can be used to determine the mass of bond points for the studied nonwoven. However, for a different type of nonwoven, it should be discussed further because equation 6.4 has the assumption that there are negligible spaces in the structure of bond points whereas equation 6.5 assumes that the density of fabric is valid inside the region of bond points.

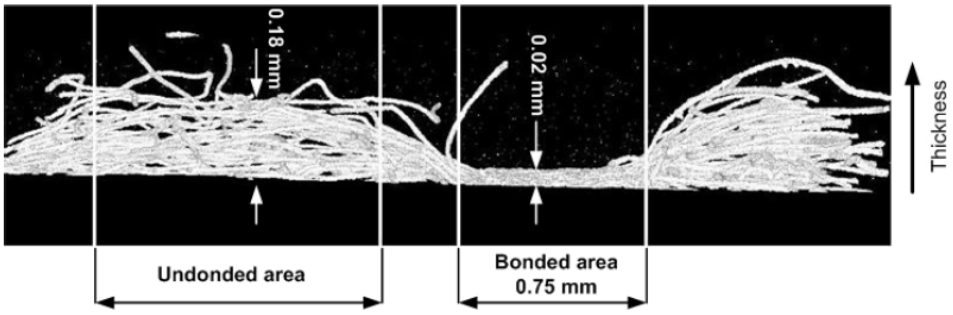

Figure 6.15. CT image of 20 g/m^2 nonwoven (Hou, 2010)

In the finite element model, it was aimed that the cross-sectional area values of fibres should be such that, when multiplied by the fibre's length and added together, the total fibre mass should be obtained. This means that

$$\sum_{i=1}^{NF} CA(i)length(i) = m_{total\_fibre}, \tag{6.6}$$

where $CA(i)$ and NF represent the cross-sectional area of i^{th} fibre and number of fibres in the model, respectively. A cross-sectional area was assumed to be directly proportional to the respective ODF and inversely proportional to the number of fibres in that interval.

$$CA(i) = k\frac{ODF(i)/100}{NL(i)}, \tag{6.7}$$

where $NL(i)$ is the number of lines that have the same orientation as fibre i. $ODF(i)$ is divided by 100 as it is given as a percentage. The value of k can be found by inserting Eq. (6.6) into Eq. (6.5).

6.3.6 Element properties

The cross-sectional area of each fibre was assigned as a separate truss property in the model by implementing a subroutine. Bond points were assigned as thin shell elements with thickness value shown in Figure 6.15.

6.3.7 Deleting Unnecessary Fibres

After the fabric is extracted, some fibres were left in the boundary of fabric dimensions to be analyzed. If no boundary condition is applied to these fibres, there is no point in keeping these fibres in the model as they do not affect the structural behaviour. Besides as they are redundant, they can increase the analysis time or cause diverging of the results. An example of such fibres is shown in Figure 6.16. One of the tips of Fibre A is located on the left boundary whereas one of the tips of fibre B is located on the bottom boundary. If the boundary conditions are applied to the left boundary and the top boundary is free, fibre A is kept and fibre B is deleted. The opposite operation is performed if left boundary is free and boundary conditions are applied to the top region. First, all the fibres were divided into five groups by scanning their point locations. First four groups represent the fibres which have a point in any of four sides. The last group represents the fibres located away from the boundaries. According to the boundary conditions, necessary fibres were deleted from the model. As an example, when the tensile behaviour along the machine direction is analyzed, the top and the bottom fibres are deleted as shown in Figure 6.17.

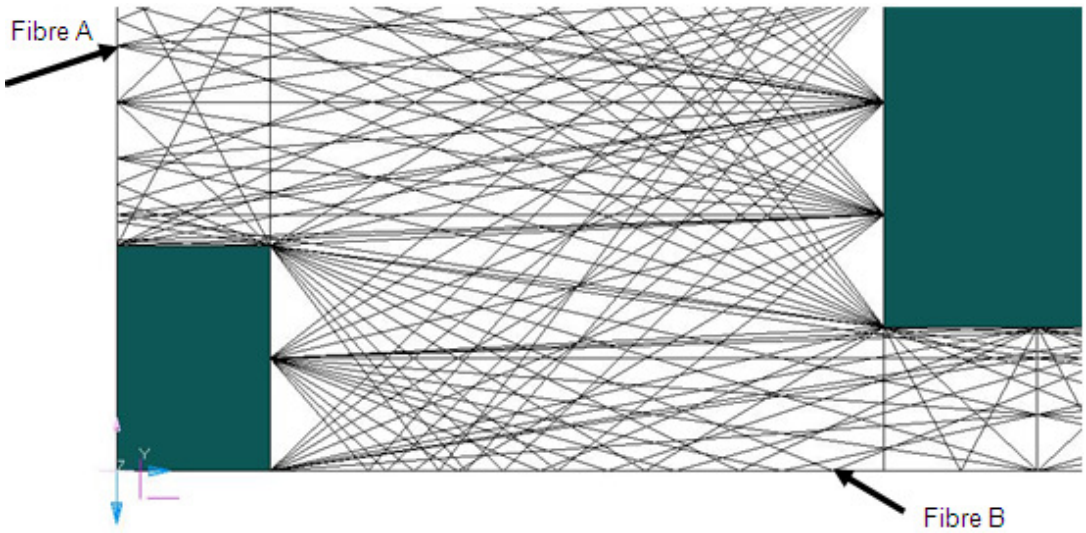

Figure 6.16. Deletion of unnecessary fibres

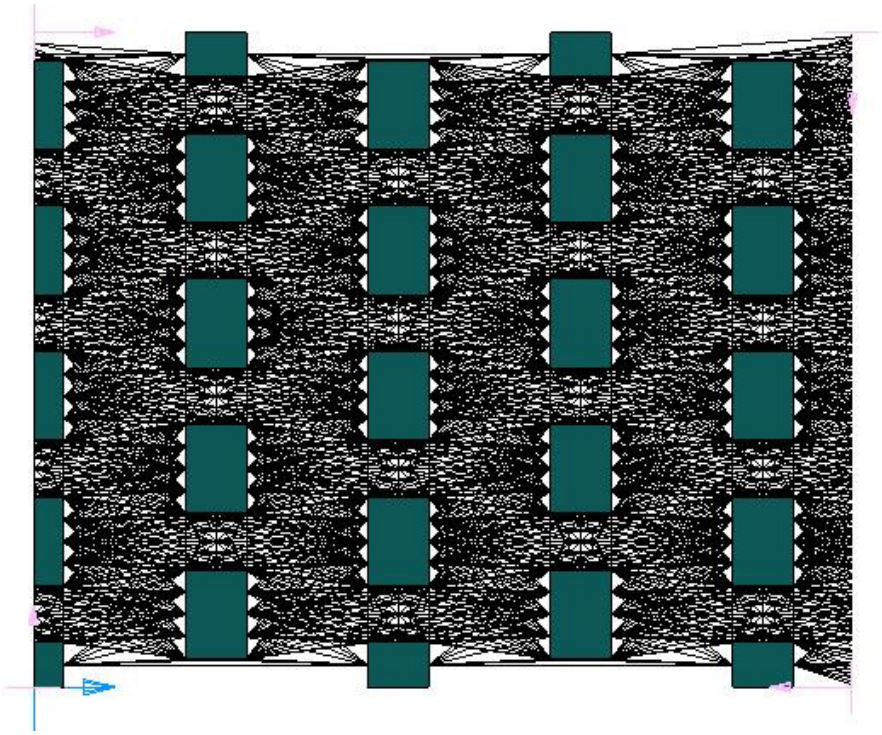

Figure 6.17. Fabric structure for tensile behaviour along machine direction

6.3.8 Associating and Meshing

The fibre lines are associated to bond points for bond point nodes and fibre nodes to coincide during meshing. By running loops for the fibres and bond points, the entire model was meshed (Figure 6.18).

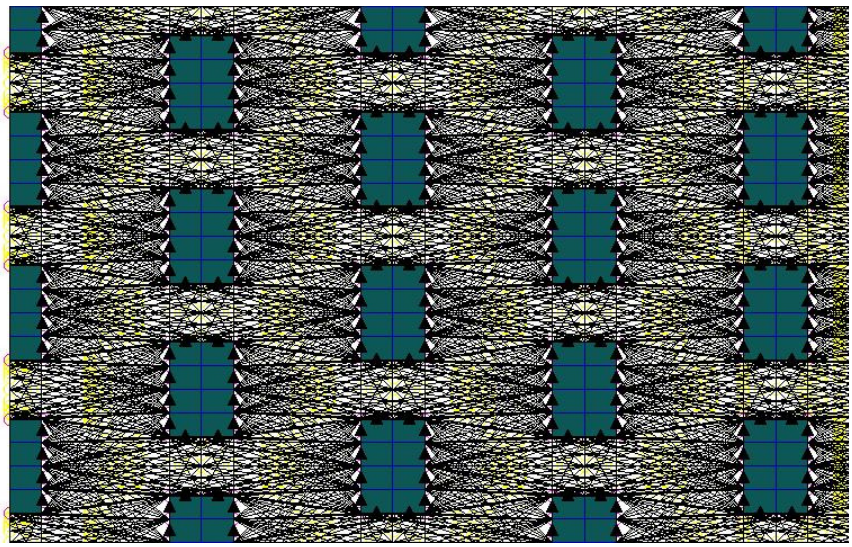

Figure 6.18. Meshing of the model

6.3.9 Boundary Conditions

In the analysis of tensile behaviour along the machine direction, boundary conditions should be applied to the nodes located along the left and right boundaries of the model. In this study, the nodes on the left boundary were fixed and the displacement is applied to the right nodes while fixing the movement in other directions to reflect fixture conditions in experiments. Boundary conditions were applied via multi-point-constrain (MPC) elements which connects all the nodes on left or right boundary to a single node (Figure 6.19). In this way, it was possible to apply boundary conditions to a single node. It was also convenient to get the total force applied to the model, as all the forces to these nodes were merged to this single node.

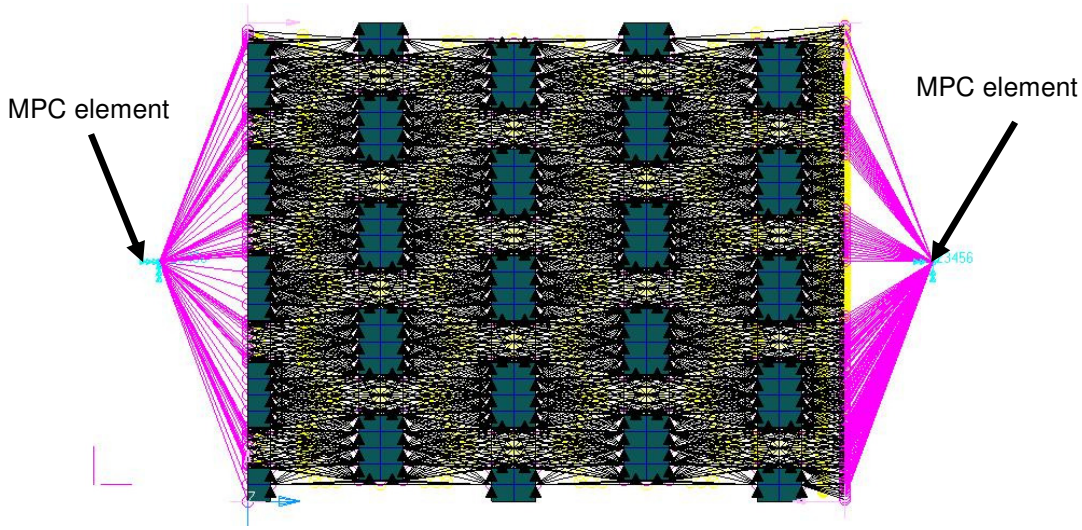

Figure 6.19. Fabric structure with MPC elements (shown with arrows)

6.4 Tensile Tests to Compare with Simulations

In order to compare the simulation results with the tests, several tensile tests were conducted with the present nonwoven. The dimensions of the specimen were 25 mm gage length with 20 mm width which selected previously by Hou (2010) considering the attachment of test device and representative are. The crosshead speed were 25 mm/min. Tests were repeated with 5 different samples and the average is plotted with the error bars (Figure 6.20). The definition “stress” in the plot is the “specific stress” which is the force divided by the width of the test sample. This stress term measure is often used by the nonwoven industry because it is difficult to measure the

exact thickness of the textile specimen (Hou, 2010). The definition "strain" is the crosshead displacement divided by the gage length which is 25 mm in this case.

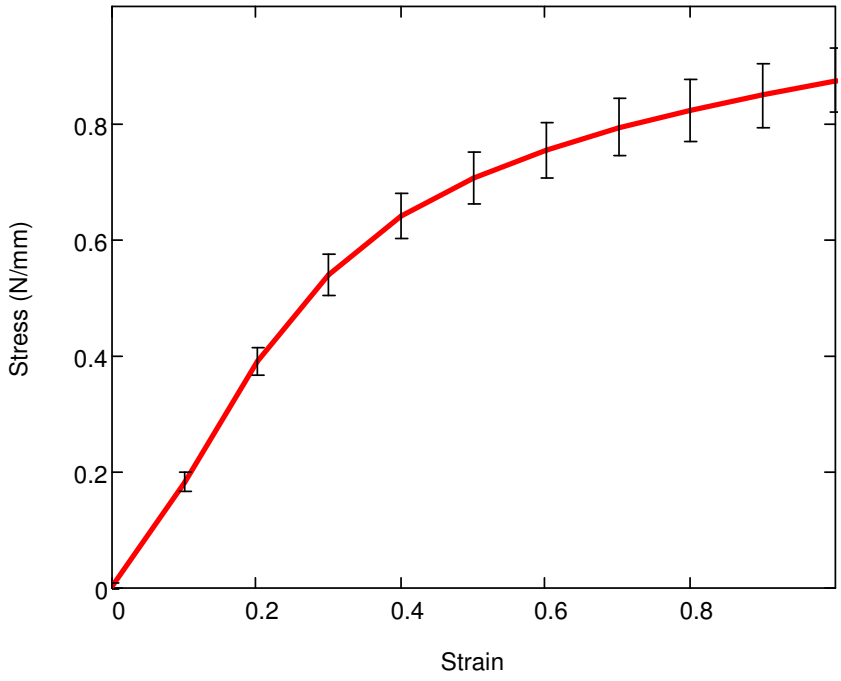

Figure 6.20. Comparison of stress-strain plots of present study

6.5 Simulations with Various Material Properties

The tensile tests of nonwovens were simulated with various material formulations assigned to the fibres and bond points. The simulations were performed with the results of the fast tensile test presented in Chapter 5. Creep properties were implemented by preventing the stress extrapolation option. The obtained results were compared with each other and with the test results in order to observe the effect of material formulation. Bond points were assumed as isotropic having the same material property of fibres. The following material property conditions were studied:

Model A: Elastic fibres and bond points;

Model B: Elasto-plastic fibres and elastic bond points;

Model C: Elasto-plastic fibres and bond points;

Model D: Elasto-plastic fibre and bond points with creep model.

Figure 28 shows stress-strain curves for various cases studied and the test result. It can be seen that all the results demonstrate a stiffer behaviour compared to the test. The case of totally elastic behaviour not only demonstrates very stiff results, but it also cannot reproduce the displacement behaviour. Introduction of plastic formulation for fibres shows better results with the slope of the nonlinear part is closer to that in the actual behaviour. When bond points are also modelled with plastic behaviour, the total fabric's behaviour does not change too much compared with the previous case confirming the expectation that the properties of fibres dominate the model as response. It was also found that an account for the creep behaviour has a little effect for this case of simulation and hence can be ignored.

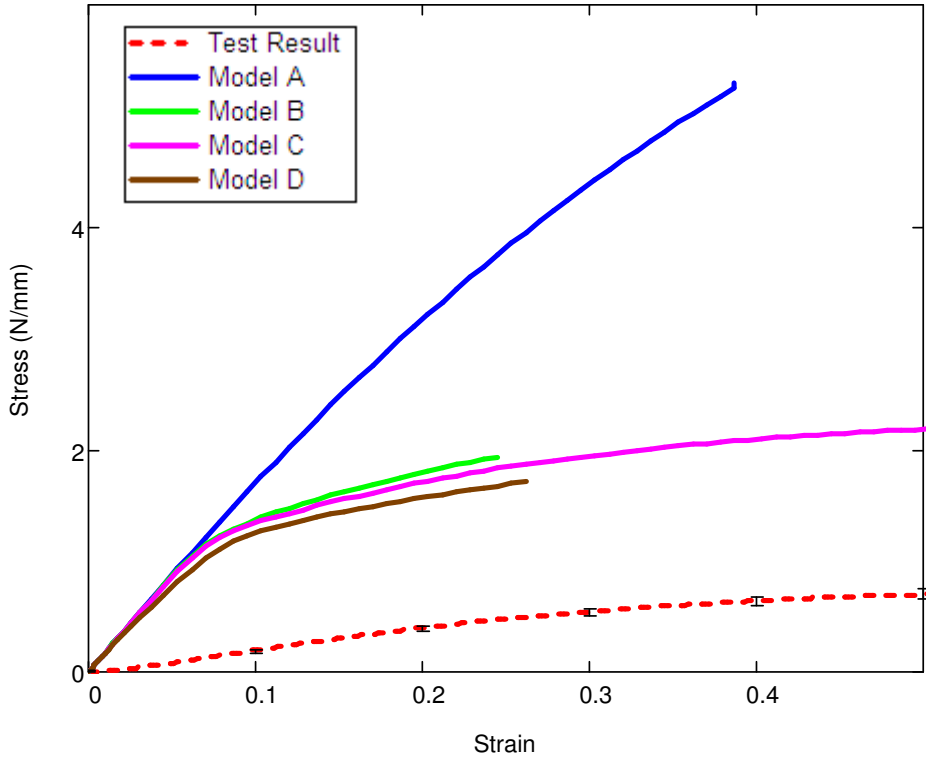

Figure 6.21. Comparison of the simulations with tests

6.6 Case Studies

In order to study the effect of each material parameter in a more detailed way, various analyses were performed with respective material property, changing within broad limits. These changes were implemented using multiplication factors applied

to Young's modulus and the stress-strain curves beyond the yield point. Figure 6.22 shows the effect of different multiplication factors for elasto-plastic properties of fibres, demonstrating its large effect on the deformation behaviour. In Figure 6.23, the material properties of bond points were multiplied by different factors. Apparently, the deformation behaviours for multiplication factors of 10 and 100 were very similar. The latter factor means that the material of bond points has elastic properties close to those of aluminium, which can be treated as rigid, compared to polypropylene. The original elastic deformation behaviour was also very close to the multiplication factors 10 and 100. This implies that it could be possible to model bond points as rigid bodies. Still, this assumption may not be valid for cases of bi-component fibres, damage analysis and different density levels of the nonwoven material.

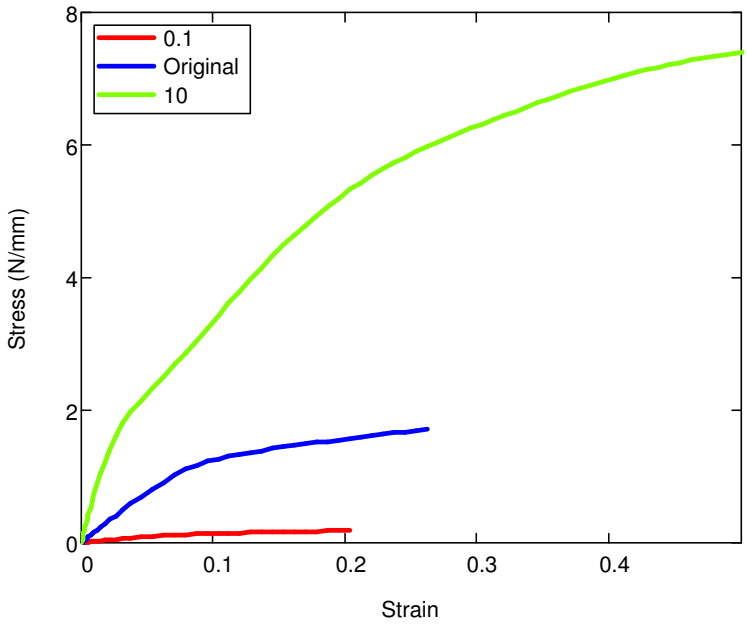

Figure 6.22. Stress-strain plots for models of fibres with different multipliers for elasto-plastic material behaviour

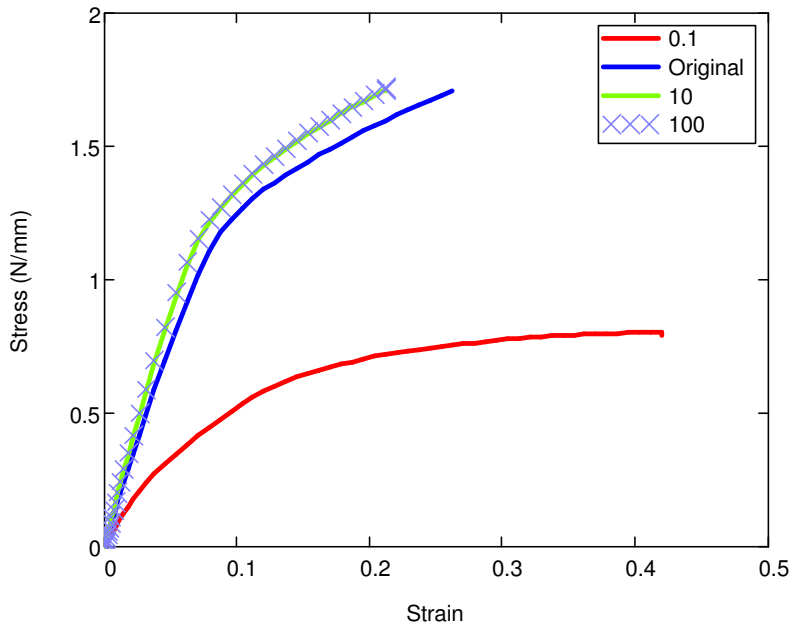

Figure 6.23. Stress-strain plots for models of bond points with different multipliers for elasto-plastic material

6.7 Discussions and Conclusions

A novel modelling technique was implemented for a low density nonwoven in this study. It was shown that the simulations based on the developed approach give stiffer results when compared with those of the tests. This can be attributed mainly to the curliness of fibres in the structure. When the computed tomography image shown in Appendix A was analyzed, it was determined that there were fibres that were curled as much as 40%. This means that fibres begin to carry load only after they are fully straightened under tensile load. In order to show this effect, an analysis was performed by giving 40% curl to all the fibres (procedure explained in section 7.4). The simulation results for this curl factor were compared with the test data and initial simulation (Figure 6.24). The simulation with 40% curl gives less stiff values than those in test results. Here, the same curl factor was assigned to all fibres whereas in reality there should be a distribution of fibre curl (with some having 40%, some having 20% etc.). It can be the reason why the actual test result lies somewhere between the simulated two extreme cases.

At the later stage of deformation, even simulations with the fibre curl of 40% gave results stiffer than in the tests. This can be due to another mechanism encountered in the test, – continuous damage of bond points during the deformation process – that was not been incorporated into the developed model. Figure 6.25 shows a microscopic image of the studied nonwoven under tensile strain of 15%. Even for this relatively low-strain value, which is close to the deflection point of slope of the tensile force-deformation curve, there were some bond points (marked by a circle in Figure 6.25) that lost their integrity as fibres started to be pulled out one by one. The strength of bond points is governed by the temperature and pressure applied during the manufacturing stage, which was not accounted in this model.

Another reason of this behaviour can be related to the determination of orientation distribution. The software was developed recently and its accuracy should be verified with further studies.

According to the parametric finite element studies for different material behaviours, it was shown that bond points can be modelled as rigid for the studied low-density nonwoven. The results of analysis also demonstrate that fibre properties are crucial for accurate modelling of the deformation behaviour. Modelling of the elasto-plastic material behaviour makes the slope of the obtained deformation behaviour close to that of the test demonstrating its importance for realistic simulations. The creep properties are not so effective in this type of loading but should be taken into account for lower strain rates.

It was concluded that with this type of modelling technique, there are three major problems: First, the effect of fibre length cannot be taken into account though it can also affect the deformation behaviour. Second, assigning orientation distribution with the distribution of cross-sectional areas may not reflect the realistic behaviour. Thirdly, the model is not efficient to be used for further studies such as damage modelling or implementation of fibre curl. As a result, instead of performing parametric studies related to bond point and fabric dimensions with this model, efforts were spent to develop an alternative modelling method which can handle the orientation distribution function and fibre length more realistically. However, as

some crucial parameters such as fibre curl, damage behaviour, bonding temperature and pressure were not studied in the entire thesis, a difference between the test and simulation results are still expected.

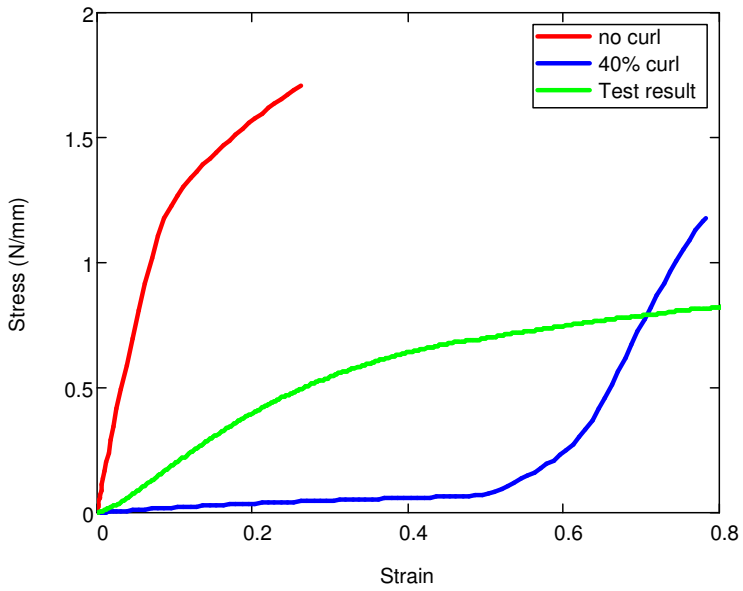

Figure 6.24. Simulation with curl factor of 40% compared with original simulation and test data

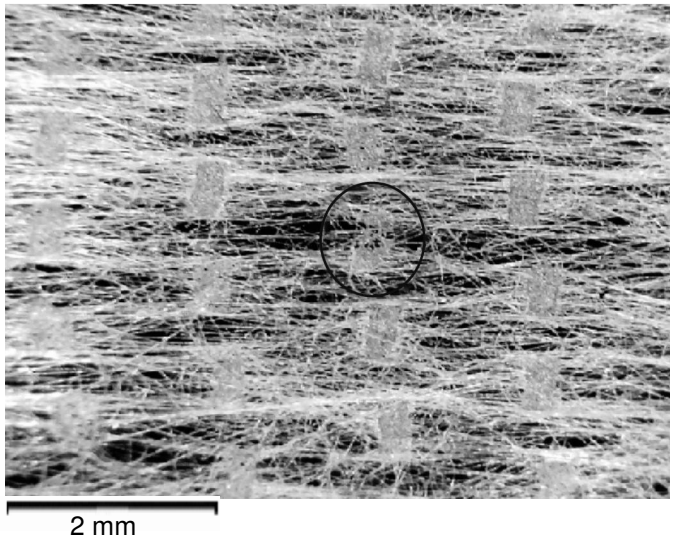

Figure 6.25. Damage in bond points under a tensile strain of 15%

CHAPTER 7

PARAMETRIC MODELLING OF NONWOVENS WITH RANDOM DISTRIBUTION OF FIBRES

7.1 Introduction

Modelling of fibres with a patterned structure discussed in the previous section resulted in some important conclusions. This method is efficient to study the dominant effects of fibres (compared to bond points) and the effect of material property variations. However, it demonstrated that the model had some weak points.

First of all, the assumption of applying different cross-sectional areas to the structure introduces the necessity of additional assumptions for further studies. For example, in order to implement the damage behaviour of the structure, new assumptions should be made to determine the fibres to be deleted from the model. Secondly, with this kind of modelling, the length of fibres cannot be taken into account. Thirdly, introduction of curliness of fibres is another concern for the use of the modelling technique presented in the previous chapter.

In order to solve those problems, another parametric modelling technique was suggested based on the previous model developed by Hou (2010). In this model, the fibres were distributed in the structure according to their orientation distribution. Thus, no additional assumption was needed to implement different cross-sectional areas regarding to the orientation distribution. The problems with those models were first, the number of fibres in a standard low-density nonwoven can be around 30000 within a fabric with dimensions of 25 mm x 20 mm. As it is impossible to model all the fibres, a certain percentage of them was modelled, and the cross-sectional areas of modelled fibres were scaled up accordingly. However, with the use of parametric modelling technique, it is possible to model large numbers of fibres automatically. Another missing point was that, the length of individual fibres was not taken into

account, which makes it impossible for the designers to decide using a continuous or staple fibre structure. This problem can be also solved by randomly distributing the fibres with a certain length.

As discussed before, the parametric modelling technique gives the opportunity to solve the problems related with repeated tasks and lengthy procedures in a short amount of time. This gives the designers the chance to observe the effect of design parameters on the structural behaviour. In this manner, the parameters given in Table 7.1 can be altered by using the model developed in this section.

Table 7.1. Variable parameters in the present modelling technique

General model parameters	Model coefficient (*), random numbers (*)
Fabric properties	Fabric length, fabric width, fabric density, bond area percentage (**)
Fibre properties	Fibre diameter, fibre length, fibre material
BP properties	BP length, BP width, BP length gap, BP width gap, BP material
Orientation distribution	Orientation distribution function, angle intervals
Mesh parameters	Bond point element size
Boundary conditions	Tensile direction, tensile speed, tensile strain rate (**)

(*) explained in the following sections

(**) can be calculated from other parameters

7.2 Modelling Methodology

A general outline of the parametric modelling procedure in this study is shown in Table 7.2. In order to explain the procedure clearly, a low-density nonwoven was used as an example. The same table shows parameters used for this sample nonwoven model (referred as *EX*). The details of the modelling procedure are explained in the following sections.

Table 7.2. General outline of modelling technique

Procedure	**Inputs**	**Model *EX***
Modelling of bond points	Fabric length	10 mm
	Fabric width	8 mm
	Bond point shape and dimensions	See Chapter 6
Modelling of raw fibres	Orientation distribution	See Appendix A
	Model scale	10
	Fabric density	20 g/m^2
	Fibre density	0.98 gr/cm^3
	Fibre diameter	0.02 mm
	Fibre length	25 mm
Editing fibres for proper modelling	No input	No input
Editing fibres for proper meshing	Shift tolerance	0.05 mm
Association of bond points and fibres	No input	No input
Meshing	Mesh size for bond points	0.05 mm
	Equivalence tolerance	1e-4 mm
Boundary Conditions	Boundary Conditions	MD tensile
Analysis Properties	No input	No input

7.2.1 Modelling of Bond Points

As the first stage of simulations, the dimensions of the fabric, bond point dimensions and fabric dimension were read from the input file. The bond points that lay inside the fabric dimensions were modelled as surfaces, and parts of surfaces crossing the fabric boundaries were trimmed similar to the model presented in Chapter 6 (Figure 7.1).

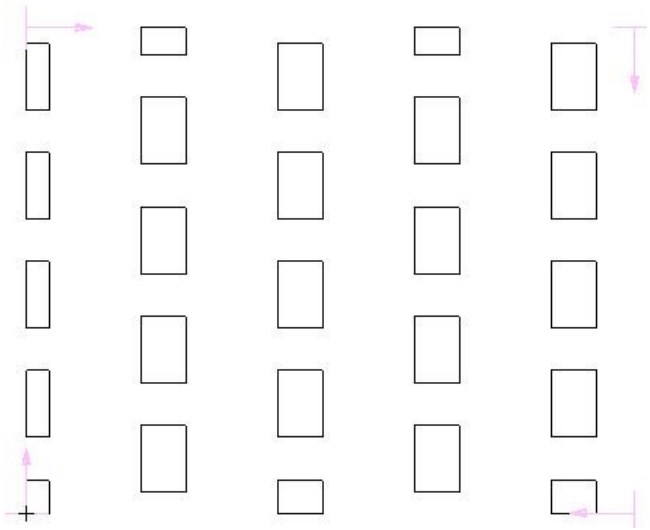

Figure 7.1. Modelling bond points

7.2.2 Modelling of Raw Fibres

Randomness

The fibres are located randomly in the structure, characterized by the orientation distribution function. This means that individual fibres can be located anywhere in the fabric. So, first, three columns of random real numbers varying between 0 and 1 are generated. The first two columns of random numbers represent the x and y coordinates of the fibre in the fabric structure. The numbers in the third column show the position of the fibre at that point. For example, if this number is 0 or 1, one tip of the fibre passes through that location. If it is 0.5, the midpoint of the fibre is located at that point (Figure 7.2). Each row represents the individual fibre which would be generated in the next stage. The values were stored in the array called $RANDOM$, which has three columns and a large number of rows.

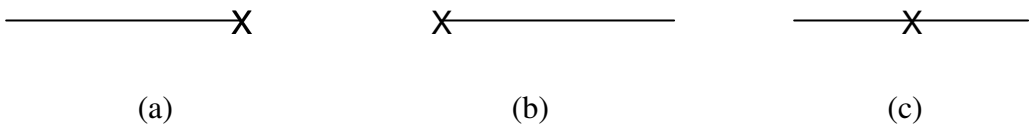

(a) (b) (c)

Figure 7.2. Modelling of fibres with different random numbers from third column: (a) 1.0; (b) 0.0; (c) 0.5

An exception was introduced if the user wanted to model continuous fibres instead of fibres with a certain length (staple fibres). In this case all parts of all the fibres should be inside the fabric borders. It was found that assigning a very large fibre length (e.g. 1000) creates some editing problems during modelling stage. Thus, in continuous modelling, the third column of random numbers was assigned as 0.5 and the fibre length was automatically adjusted to a value slightly larger than the diagonal of the fabric. By this way, it was guaranteed that all the fibres were located inside the fabric without having a free end (Figure 7.3).

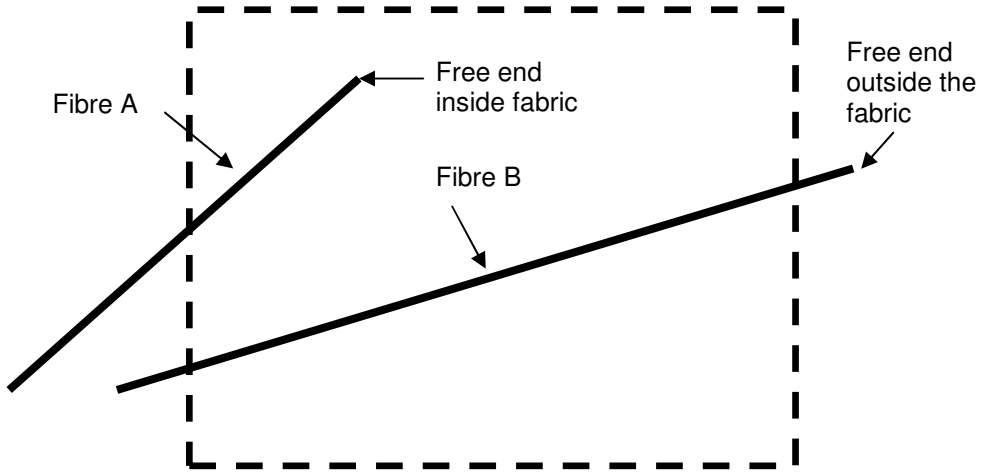

Figure 7.3. Representation of fibres; fibre A, having a free end in the fabric; fibre B, a continuous fibre.

Total minimum number of fibres

The mass of all the fibres in the model (m_{fabric}) is calculated by multiplying fabric area density with the fabric area that was input previously. From the mass-volume-

density relation, the total length of fibres (TL_{real}) in the model is calculated as follows:

$$TL_{real} = \frac{m_{fabric}}{\pi \frac{d_{fibre}^2}{4} \rho_{fibre}}. \quad \textbf{(7.1)}$$

TL_{real} is the length of all the fibres in the specified fabric region. The number of fibres (NF) is found by the following equation;

$$NF = NINT(\frac{TL_{real}}{l_{fibre} MC}), \quad \textbf{(7.2)}$$

where l_{fibre} is the average length of fibres; $NINT$ operation is used to acquire the nearest integer value from the argument in the brackets. MC is the model coefficient that defines the scale of the model. It determines the ratio of fibres to be modelled. When it is assigned as 1, all the fibres are modelled. In the example shown here, it is 10 so that $1/10^{th}$ of the fibres are modelled. Increasing this coefficient can be very useful in case of modelling high-density nonwovens or when the computer power is limited.

The number of fibres calculated in this way assumes that all the fibres lie completely inside the specified fabric region. However, some fibres can be located at the edge of the fabric, and part of them can be outside of the fabric (Figure 7.4). Thus the number of fibres determined is the minimum number of fibres that can be present in the fabric. The calculation of the exact number of fibres is presented in the proceeding sections. This determined minimum number of fibres will be the first iteration for the calculation of exact number of fibres in the model

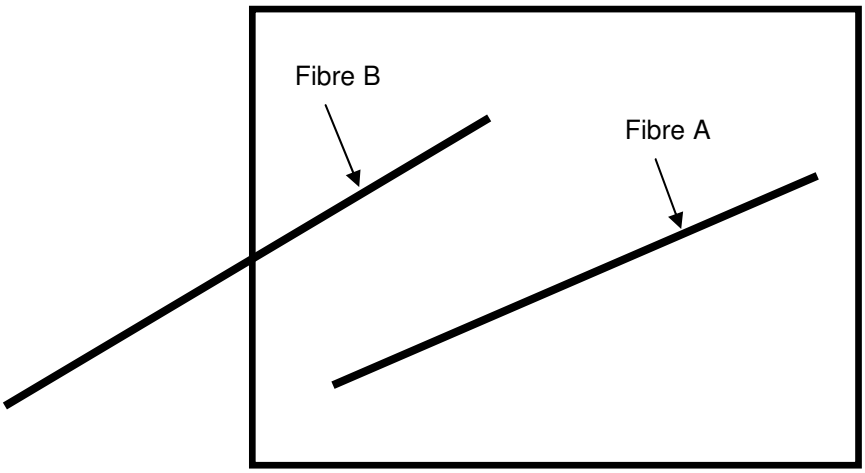

Figure 7.4. Two fibres: Fibre A is located completely inside the fabric whereas fibre B is partially out of the fabric

Orientation Distribution

Orientation of fibres measured for a real fabric is read from a file and an array is formed named as *ODF(p)*. Here *p* shows the angle band of ODF file. In this example, the parameter varies between 1 to 18 for the angles, 0-10º, 10º -20º, …., 170º-180º (see Appendix A).

Virtual Modelling of Individual Fibres

After the random numbers, ODF, and the minimum number of fibres were determined, the modelling procedure can be started. This procedure is performed virtually because initially, the real number of fibres in the model is unknown. It will be modelled in Patran after the real number of fibres is determined. The total length of fibres, which is achieved by this virtual modelling procedure, is compared with the total length that should be present in the model (see Eq. 7.1). The number of fibres in the model is increased until the former one reaches latter one. Note that the initial number of fibres cannot be greater than the real number of fibres as the former one is calculated by assuming all the fibres are entirely inside the fabric. After a certain amount of fibre length inside the fabric is reached (compared to the real length), the virtual modelling is stopped and the number of fibres to be modelled is stored. The

procedure can be explained more clearly in Figure 7.5. In this figure, *TF* is the number of fibres in the model. The important steps (underlined) shown in this figure are explained in the following section.

Begin
Loop on modelling iteration (Loop 1)
    Loop on angle interval of ODF file (Loop 2)
        Total number of fibres in a particular interval
        Angle to be used in that interval
        Loop on individual fibres in that interval (Loop 3)
            Fibre orientation and location
            Length of fibre inside the fabric
            Total length of fibres inside fabric
        End (Loop 3)
    End (Loop 2)
    If Total length of fibres $TL_{simulated} < TL_{real}$ then
        $TF = TF + 1$
    Else
        Break
End (Loop 1)
        Real modelling
End

Figure 7.5. Fibre modelling procedure

Total Number of Fibres in a Particular Interval

The total number of fibres to be modelled (*TF*) is divided into orientation groups according to the array, *ODF* . An array, *NFA* is formed that stores the number of fibres in a particular angle interval by using the following equation.

$$NFA(p)=NINT(ODF(p) \ X \ TF \ / \ 100). \qquad \textbf{(7.3)}$$

The operation *NINT* is used as the elements of *NFA(p)* should always be integer (The ODF file can contain decimal numbers). The ODF file gives the distribution in terms of percents so the argument is divided by 100.

Angle for a Particular Band

The fibre angles are calculated by taking the average of mid-point of the respective band. They are stored in the array, $AU(p)$**.** For example, for the second interval, 10º-20º

$$AU(2) = \frac{10^\circ + 20^\circ}{2} = 15^\circ. \tag{7.4}$$

Fibre Orientation and Location

The fibres are modelled as lines connecting two points. First, the location of fibre is found by using three columns of random numbers that were generated in the previous stage:

$$rpc_x = RANDOM\ (i,1)\, fl, \tag{7.5}$$

$$rpc_y = RANDOM\,(i,2)\, fw, \tag{7.6}$$

where rpc_x and rpc_{yx} represent the x and y coordinates of a point located in the line representing the fibre. fw and fl are the fabric width and length, respectively. The following equations are used to determine the location of start and end point of the fibres using the third column of random numbers:

$$sp_x = rpc_x + RANDOM\,(i,3)\cos(AU(p))l_{fibre}, \tag{7.7}$$

$$sp_y = rpc_y + RANDOM\,(i,3)\sin(AU(p))l_{fibre}, \tag{7.8}$$

$$ep_x = sp_x - \cos(AU(p))l_{fibre}, \tag{7.9}$$

$$ep_y = sp_y - \sin(AU(p))l_{fibre}, \tag{7.10}$$

where sp_x and sp_y represent the x and y coordinates of start point of the line; ep_x and ep_y represent the x and y coordinates of its end point.

Length of Fibre inside the Fabric

When the coordinates *rpc* are close to the fabric boundaries, the locations of *sp*, *ep* or both can lie outside of the fabric. In order to determine the length of the part of fibre inside the fabric, the portions outside the fabric are subtracted from the fibre length. The procedure is explained below:

A parameter *c* is defined so that if the coordinate x or y is larger than fabric length or width, respectively, the parameter *c* is 2. If, the coordinate is negative (showing that it is located left hand side or below the bottom of the fabric depending on if it is x or y coordinate), the parameter *c* is 1. If it is located inside the fabric limits, the parameter *c* is zero. Figure 7.6 shows an example. The parameter *c* takes the numbers shown in Table 7.3 for this example.

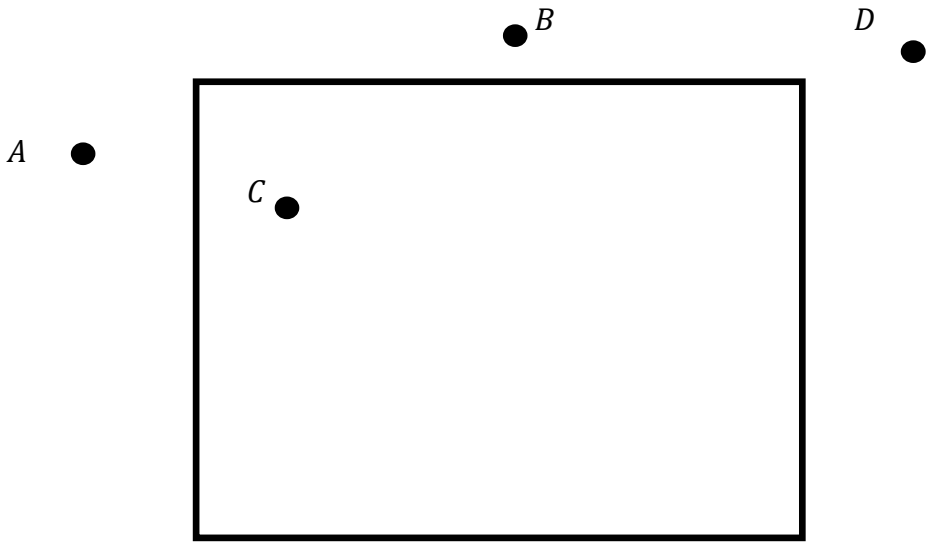

Figure 7.6. Example of points with various magnitudes of parameter *c*

Table7.3. Values of parameter *c* for the points shown in Figure 7.6

Point in Figure 7.6	***c (for x-coordinate)***	***c (for y-coordinate)***
A	1	0
B	0	2
C	0	0
D	2	2

An example of a fibre, part of which is located outside the fabric is shown in Figure 7.7. The aim is to determine the length lo, which is the portion of the line outside the fabric. The dimensions a and b are found from the following equations for the start point of fibres:

$$a = ABS(sp_x - CR), \tag{7.11}$$

$$b = ABS(sp_y - CR), \tag{7.12}$$

where the operator ABS is the absolute value. CR takes the values in Table 7.4 according to the parameter *c*.

Table7.4. Values of parameter CR

c (for x-coordinate)	***CR***
0	Not calculated
1	0
2	Fabric length
c (for y-coordinate)	***CR***
0	Not calculated
1	0
2	Fabric width

The dimension lo is calculated by the following expression:

$$lo = MAX\left(\frac{a}{\cos(AU(p))}, \frac{b}{\sin(AU(p))}\right), \tag{7.13}$$

where the operator MAX is the maximum of arguments. Thus, either the magnitude a or b determines the length outside the fabric. In case of Figure 7.7, lo is determined by a. In this figure, both *x* and *y* coordinates of the point lie outside the fabric so that both dimensions a and b exist. In case where the point is outside in terms of only one coordinate (such as point *B* in Figure 7.6), either a (if it is y-coordinate) or b (if it is x-coordinate) is assigned as zero. . In the case of point *B*, the parameter a is assigned as zero as the this point is outside the fabric limits due to its y-coordinate only. Thus, the fibre location is determined by using the parameter b in Eq. 7.13. The

last calculation to perform is the determination of the length inside of the fabric (li) with the following equation:

$$li = l_{fibre} - lo. \tag{7.14}$$

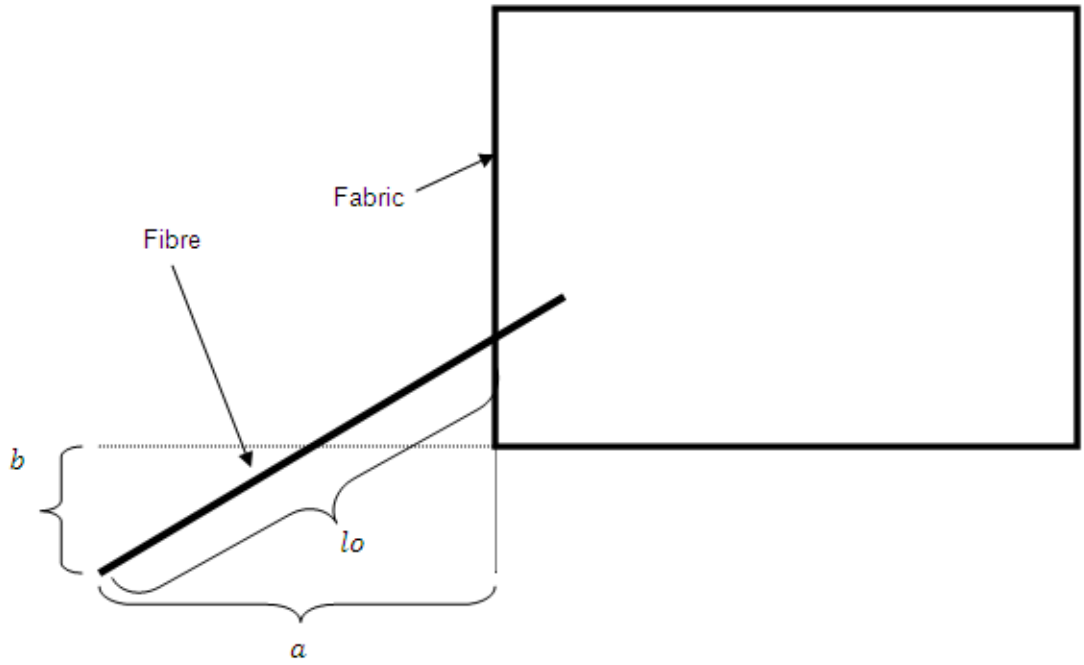

Figure 7.7. Representation of a fibre whose portion is located outside the fabric

Total Length of Fibres inside the Fabric

In a loop, the li values of all the fibres are added up, and the total value ($TL_{simulated}$) is compared with the real total length of the fibres TL_{real} .If $TL_{simulated}$ is lower than TL_{real} then the total number of fibres is increased by one and the whole procedure is repeated again until**,**

$$TL_{simulated} > TL_{real}. \tag{7.15}$$

In case, the modelling coefficient is different than unity, TL_{real} is divided with this value which reduces to total number of fibres to be modelled. The effect of modelling fewer numbers of fibres than the actual one is compensated by adjusting the fibre cross-sections at the later stage.

Real Modelling

After the number of fibres to be modelled is determined, the real modelling takes place with running the same loop for the final total number of fibres. Figure 7.8 shows the fibre distribution in the model generated for *EX*

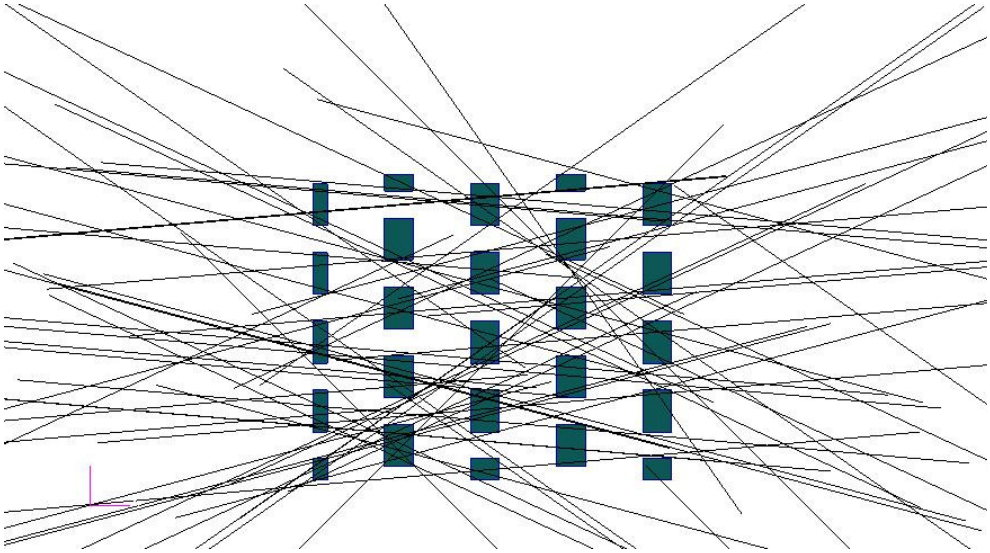

Figure 7.8. Distribution of generated fibres for *EX*

7.2.3 Editing Fibres for Proper Modelling

The fibres generated in the preceding section were the "raw" fibres, it means they are present in the model as if they are not bonded. The following operations are performed with fibres to link them with bond points already present in the model.

Trimming Fibre Lines along Fabric Borders

The fibres are cut along the edges of fabric as the region to be analyzed is inside the fabric limits (Figure 7.9)

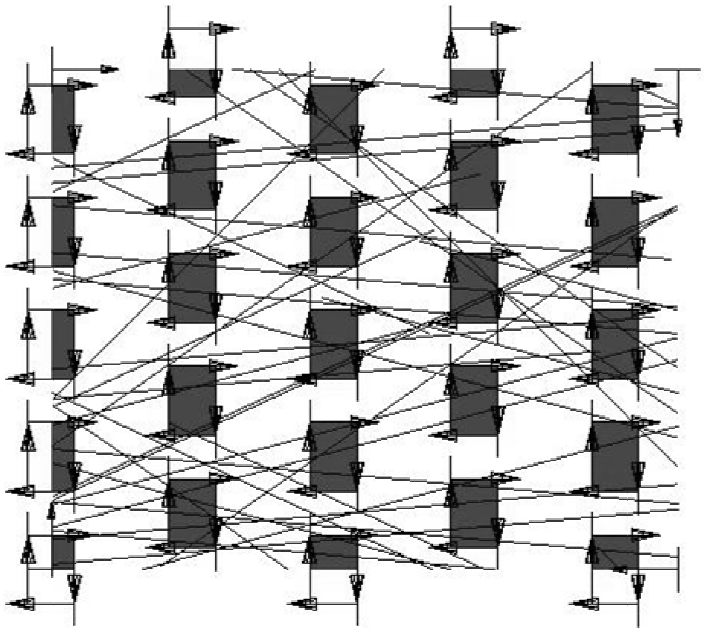

Figure 7.9. Fibres after trimming from fabric limits

Dividing the Fibre Lines inside the Bond Points

The fibre lines inside the bond points are divided along the bond point borders. This is performed by checking all the bond points whether any fibres cross them. When it is detected, the lines are divided along the edges of the bond points by using the cutting planes generated previously (Figure 7.10). The fibres left in the bond points are trimmed in a further stage.

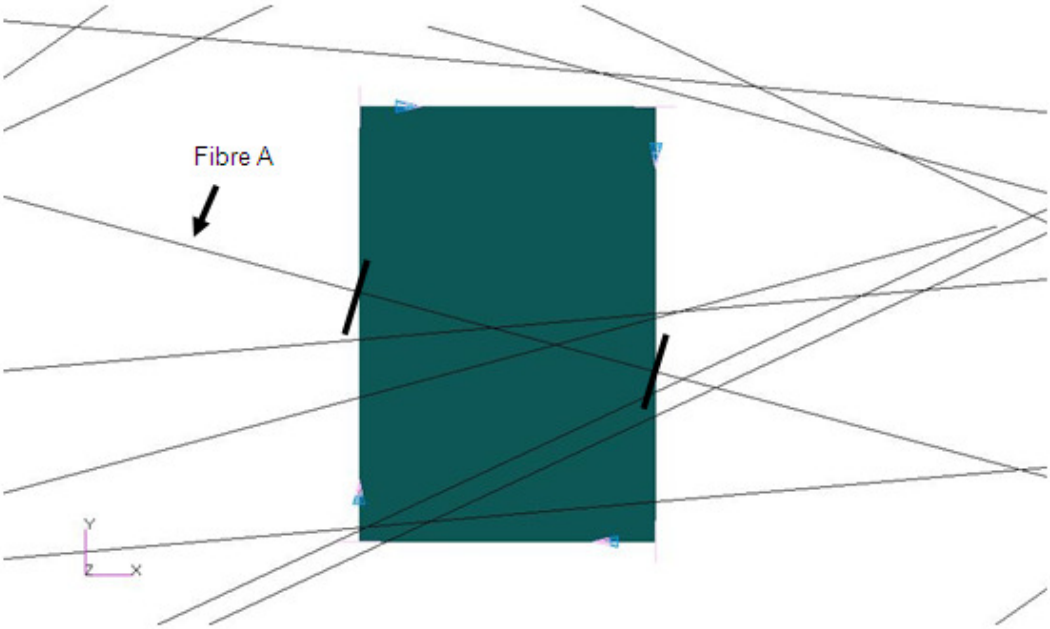

Figure 7.10. Fibre A is cut from marked locations

Deleting Fibres along Borders without Boundary Conditions is Present

The procedure performed in this section is the same as described in Section 6.3.7.

Deleting Fibres not Connecting Bond Points

The fibres, whose tips are left in the matrix (between regions of bond points) also do not carry any load and should be removed due to the reasons mentioned in Section 6.3.7. In order to do this, all the end points of the fibre lines are scanned. If any of those points are found to be located outside the bond points, the respective fibre is deleted (Figure 7.11). Such fibre tips exist in the model only if the fibres are discontinuous (staple fibres).

Deleting Fibres inside Bond Points

The fibres divided in the previous operation and located inside the bond points are deleted in this stage

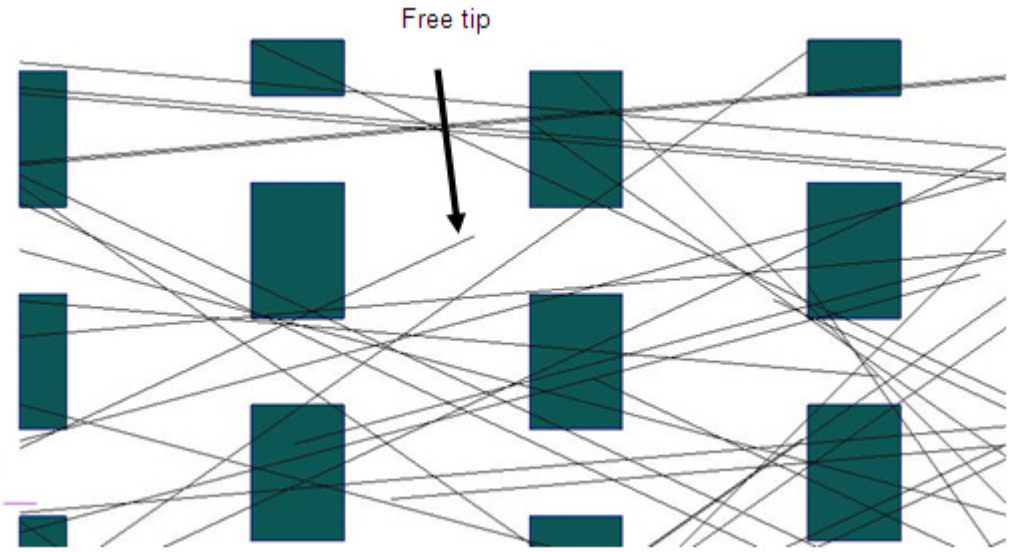

Figure 7.11. A free fibre tip in the matrix

7.2.4 Editing Fibres for Proper Meshing

As the fibres are attached to the bond points, the nodes of the fibres should coincide with the nodes of the bond points for element-connectivity requirement. However, the fibres are located randomly in the structure and this may result in distorted elements in the bond points during meshing if two or more fibre tips on a bond point are very close to each other or close to a corner of bond points (Figure 7.12). In order to prevent this situation, the sides of bond points are divided (virtually) to equal pieces each having the length of the mesh size. The tips of these pieces are called "imaginary hard points" (Figure 7.13). Then, all the fibre tips are shifted towards the closest imaginary hard point. As it can be seen in Figure 7.14, the fibre tips close to an imaginary hard point at A1 are shifted to that imaginary hard point, A2. The fibre tips close to the corner (see B1 and B2 in Figure 7.14) are shifted towards the corner of the bond point. After this operation, a regular mesh is obtained on the bond points (Figure 7.15). The orientations of all the fibres are varied as a result of this operation. It was calculated that maximum less than 1% angle change was observed with the current mesh size. As the orientation distribution is given in an interval of 10 degrees, this amount of angle change can be assumed as negligible.

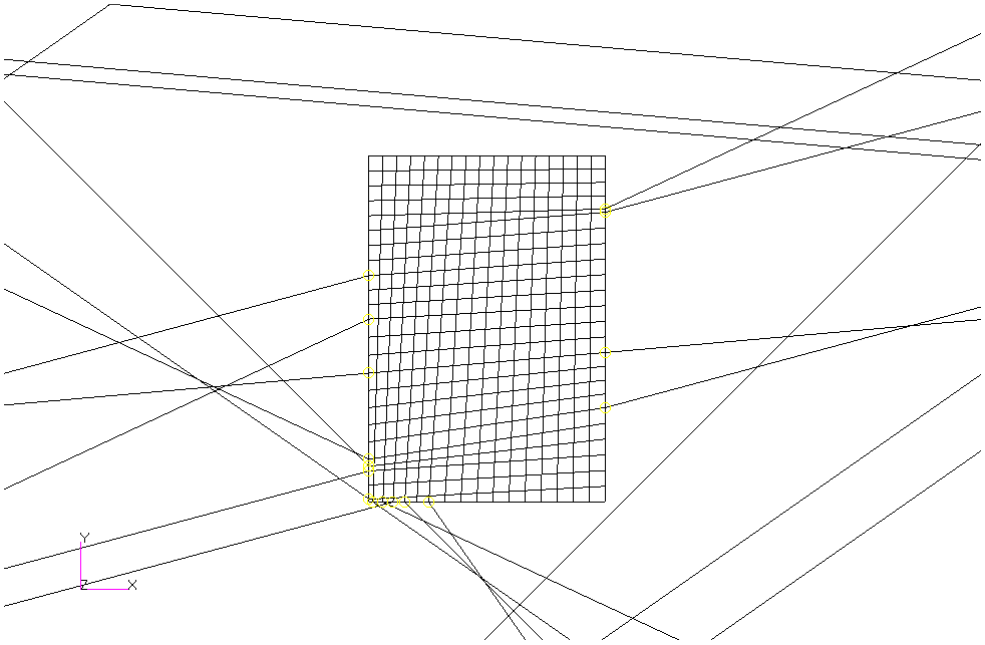

Figure 7.12. Distorted elements in a bond point

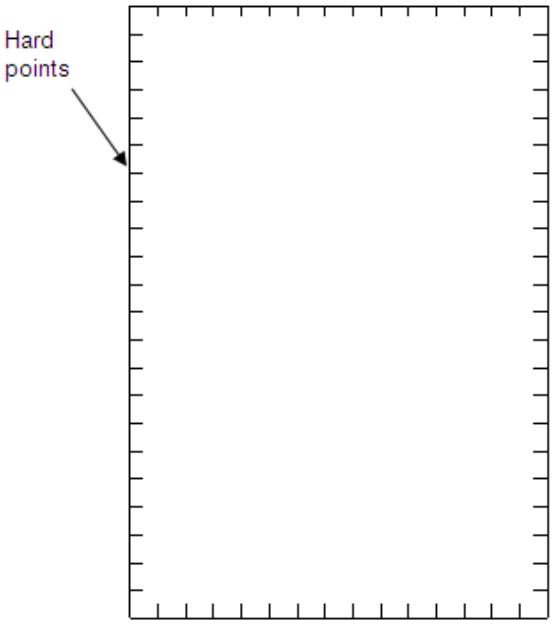

Figure 7.13. Hard points on bond points

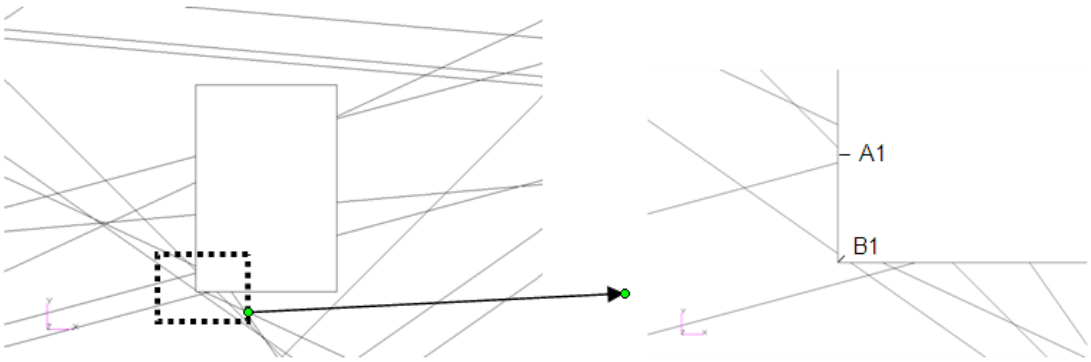

(a)

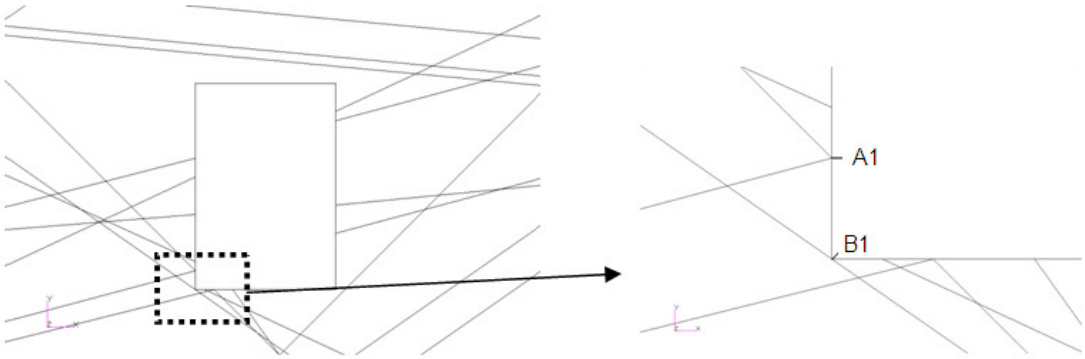

(b)

Figure 7.14. Fibres around a bond point: (a) before; (b) after editing for meshing

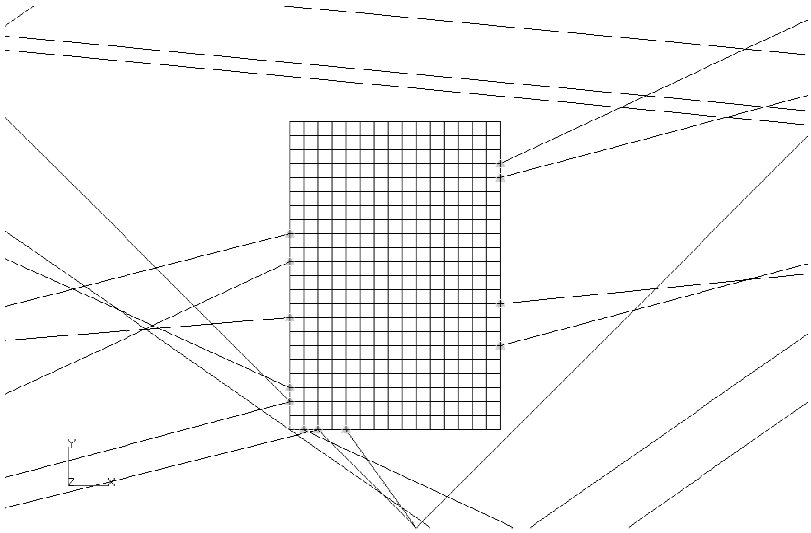

Figure 7.15. Element structure in the bond point after shifting of fibres

7.2.5 Other Modelling Steps

The rest of the procedure is similar to the one in Chapter 6. It includes the association of bond points and fibres; meshing, assignment of material properties, boundary conditions and the analysis properties. The only exception is the implementation of different fibre cross-sectional areas. As the orientation distribution is handled during the modelling of fibres, the real cross-sectional areas of fibres are assigned to the fibre curves multiplied by the modelling coefficient (*MC*) which indicates the scale of the model. The final model obtained is shown in Figure 7.16 for model *EX*.

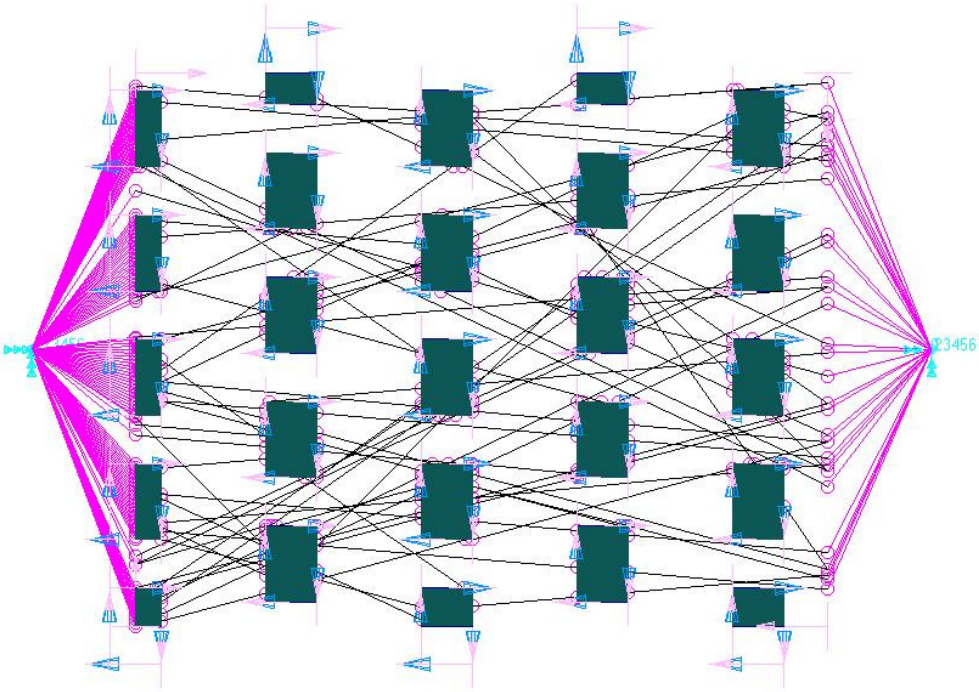

Figure 7.16. Generated model *EX*

7.3 Results

7.3.1 Comparison with Model in Chapter 6

The model generated with the random distribution of fibres was compared with the simulations and test results presented in Chapter 6. In order to do this, the plastic and creep material properties were implemented into the model. Initially, the model was generated with the same dimensions as in Chapter 6 (25 mm x 20 mm) with *MC*

value of 10. If *MC* were chosen as 1, the modelling would require too much CPU time. However, convergence problems were observed this time, and this was attributed to *MC* being too large. When 1/10 of fibres are modelled, there are some bond points having only a few fibres (Figure 7.17). As the model consists of trusses, (i.e. not beams) the attached nodes act like hinges carrying no moment. This can result in unconverged solutions.

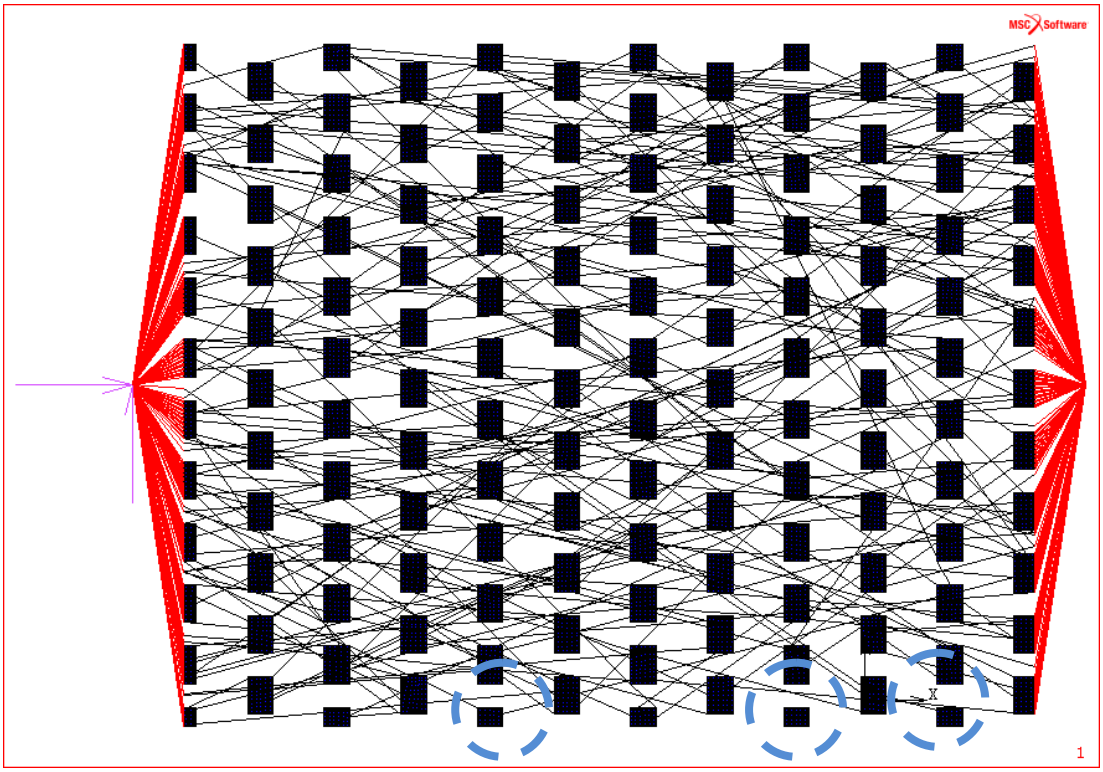

Figure 7.17. Bond points with few fibres

In order to solve this problem, the model was generated with smaller fabric dimensions and large number of fibres. A model with fabric dimensions of 10 mm x 8 mm was generated with the model coefficient of 1. The validity of using this model instead of that with real fabric dimensions was verified by performing simulations with each model and assigning linear elastic material properties (Figure 7.18). The term “stress” in the figure is the “specific stress” mentioned in section 6.4. Apparently, the behaviours of both models were close to each other. This means that the small-scale model can be used for comparison with the previous model. The

stress–strain result of the current modelling technique was compared with the model generated with patterned structure and the test result (Figure 7.19). Apparently, the simulation with the modelling technique with random distribution of fibres gave better results compared to the previous one. Because of the fibre curliness and damage of bond points described in Chapter 6, there was still a difference between the test and simulation results. However, the slope of the curves of present modelling technique and the test results were very similar after a certain extension. This implies that if fibre curliness is avoided, the behaviour in the simulation could be similar to the one in the test.

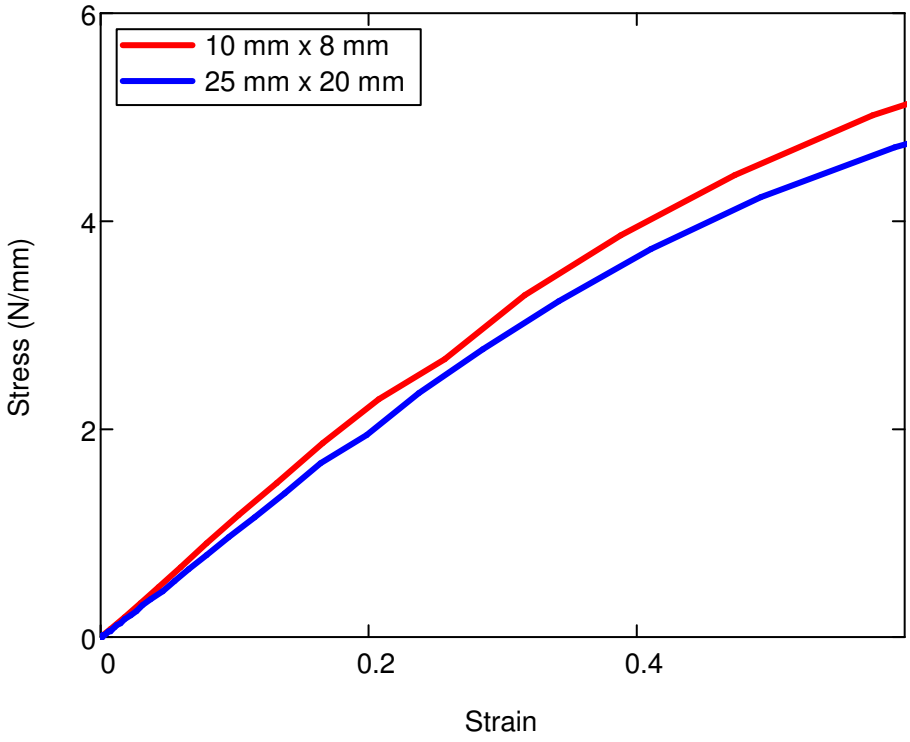

Figure 7.18. Stress-strain behaviour of tensile simulations with different fabric dimensions

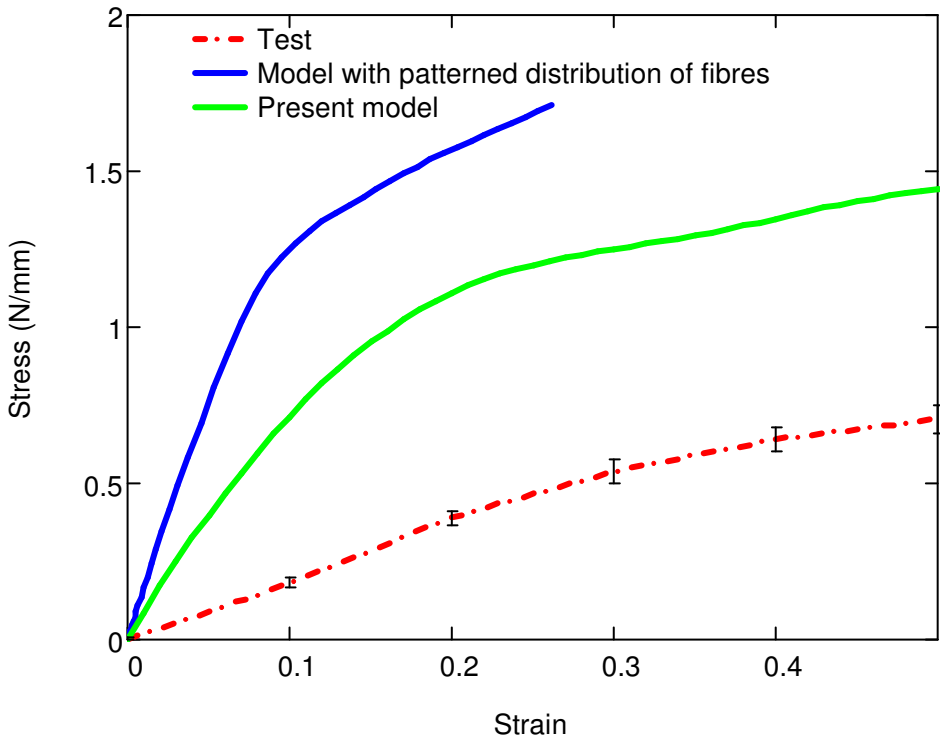

Figure 7.19. Comparison of stress-strain curves with different modelling techniques and test

7.3.2 Deformation Behaviour

The distribution of total strain in the fibres is shown in Figure 7.20. As it can be seen, a significantly large strain values were observed (larger than fabric strain) in some of the fibres. There was also a highly non-uniform distribution of strains in the fibres throughout the fabric structure. The factors governing this distribution are discussed in detail in Chapter 9.

The distribution of strains in the bond points is shown in Figure 7.21. Apparently, the regions of high strain in the bond points are the regions where fibres stretch the bond points. Thus, failure is expected in those regions. A similar behaviour was observed in previous studies as well (Hou, 2010, Demirci, 2010).

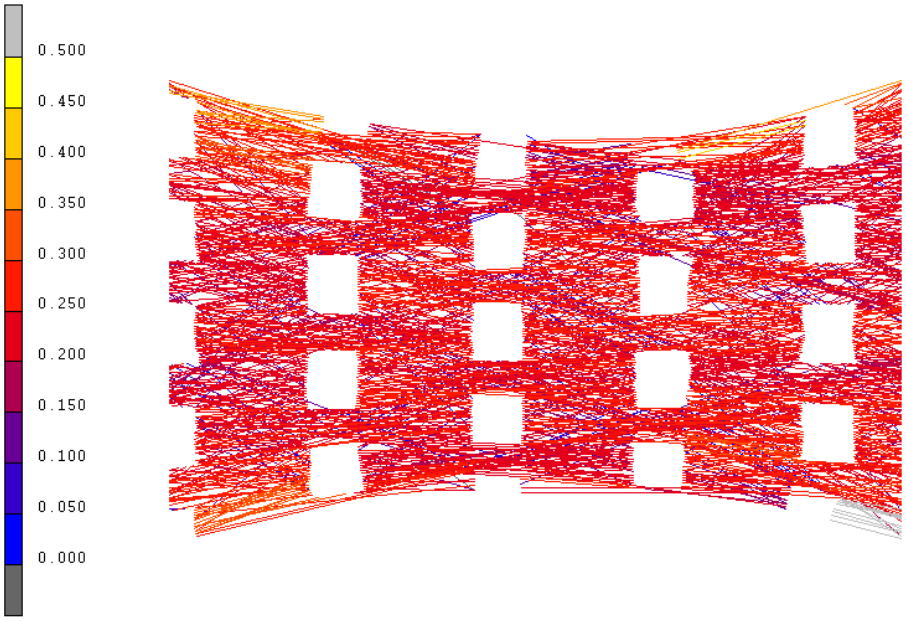

Figure 7.20. Distribution of total strain in fibres

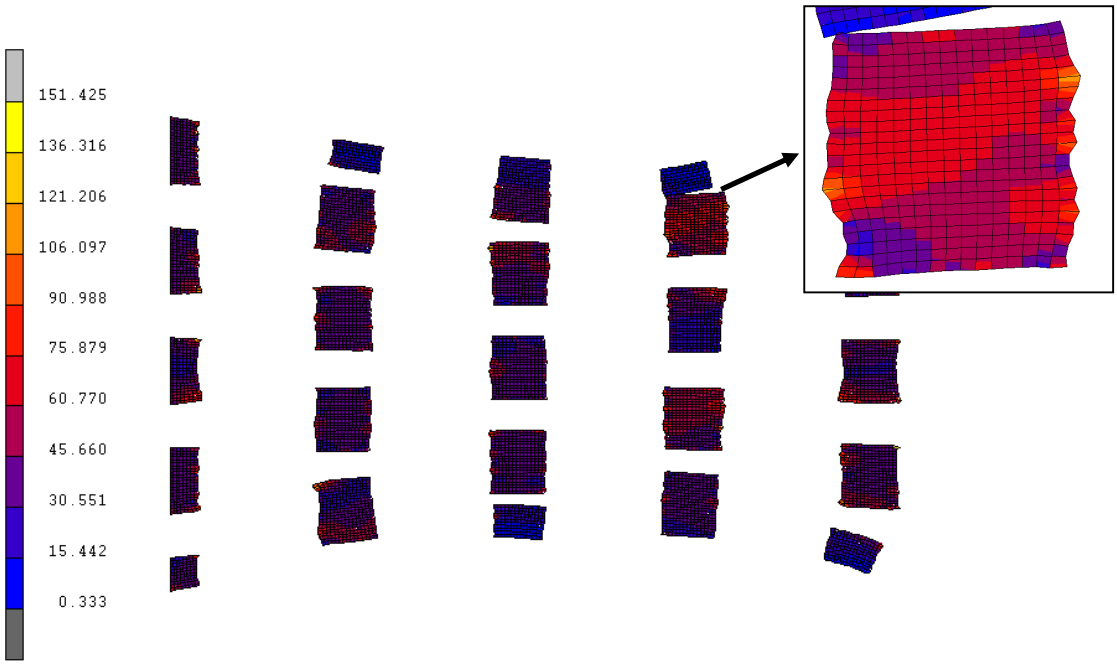

Figure 7.21. Distribution of von Mises stress in the bond points

7.4 Implementation of Fibre Curl

Even for the advanced model presented in this chapter, there is still a large gap between the deformation results of tensile tests and simulations. As was discussed in Chapter 6 this can be due to the curliness of fibres and damage of bond points, which have not been utilized in the current model as well.

In this section, the benefit of implementation of a distribution of fibre curl into the model is presented. Determination and quantification of the amount of curliness of fibres requires extensive research and sophisticated image-analysis tools, and it was not studied here (Rawal (2007), Adanur & Liao (1999)). Therefore, in this study, a fictitious curl distribution is used. As discussed in Chapter 6, it was determined that there were fibres curled as much as 40%. Taking into account this information, a curl distribution is introduced into the model employing the data presented in Error! Not a valid bookmark self-reference..

Table 7.5. Distribution of fibre curl introduced into the FE model

Fibre curl group	*Fibre curl*	*Frequency*
1	0 %	25%
2	20%	50%
3	40%	25%

7.4.1 Introducing Fibre Curl

Curl distribution is implemented by introducing a stress-free region into the material's stress-strain behaviour. The procedure is as follows:

First, the tensile test data is divided into three groups based on the curl distribution. For the curled fibres, it was considered that the tensile test was performed without fully stretching the specimen until the load was read from the screen of the MicroTester. The amount of unstressed length in the test was calculated by the following equation,

$$U_{free_i} = GL_{origin} \frac{CF_i}{100}, \tag{7.16}$$

where GL_{origin} is the gage length of the specimen during the test with a fully stretched specimen and CF_i is the curl factor of the ith fibre curl group. In order to prevent unconverged solutions during the simulations, it was assumed that a relatively small force (0.001 N) acts at the stage before the fibres are fully stretched. The engineering stress-engineering strain graphs obtained by this modification are given in Figure 7.22. When these values are converted to true-stress and true-strain values and introducing some smoothness during the transition of unstressed region to stressed region, the stress-strain curves presented in Figure 7.23 are obtained.

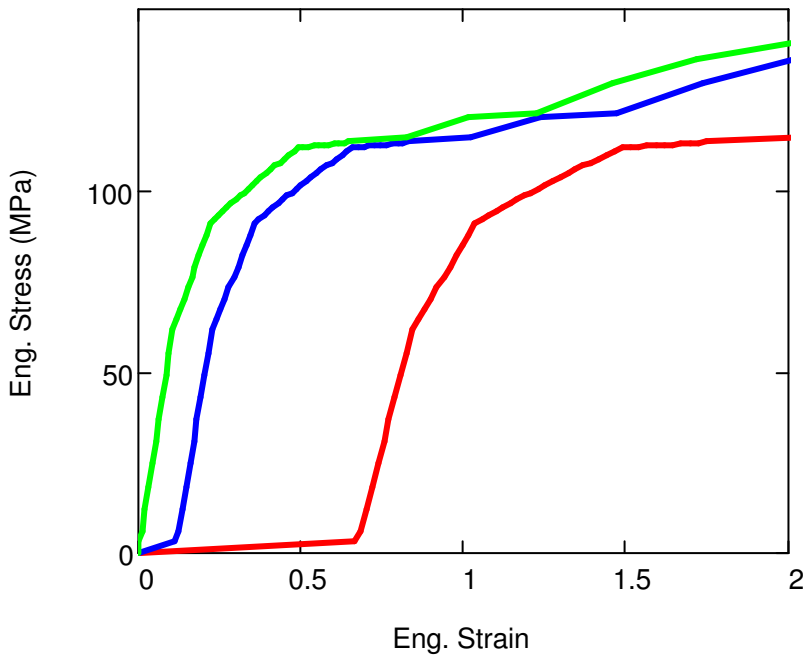

Figure 7.22. Engineering stress *vs*. strain for fibre groups with various curls presented in Table 7.5

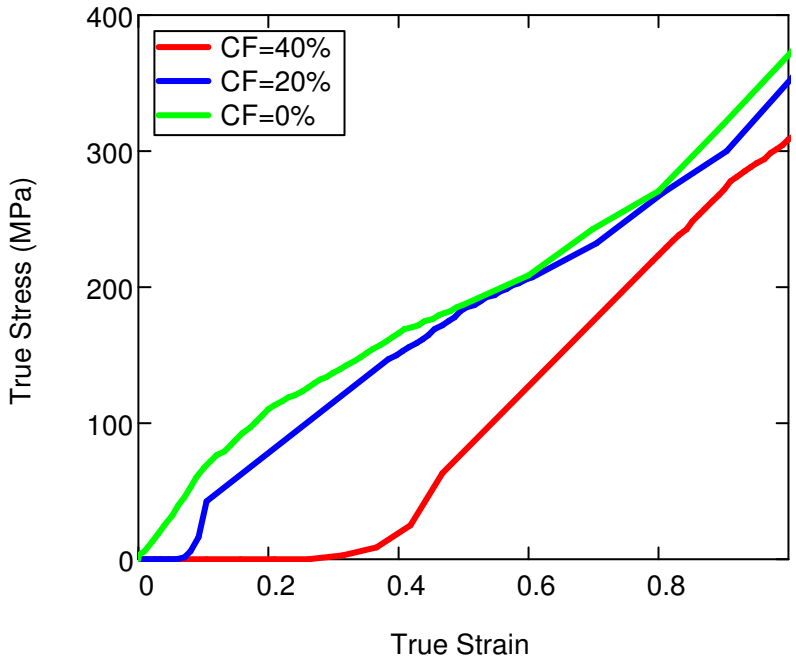

Figure 7.23. True stress *vs*. true strain for fibre groups with various curls presented in Table 7.5

7.4.2 Implementation of Fibre Curl into the Parametric Model

The curl factor is allocated to fibres of the parametric model using a specially written additional subroutine. First of all, three groups of material properties are generated, with respective stress-strain curves presented in Figure 7.23. After that, the number of fibres with each curl distribution is determined by considering the percentages linked to the groups as well as the total number of fibres in the model. Then fibres are chosen at random, and the first fibre curl group is assigned to them until the number of the fibres exceeds the defined number for this group. This procedure then continues with the curl factors for the second and third groups If the randomly chosen fibre was already assigned a curl factor, then fibre's number is increased incrementally by one until a fibre without an assigned factor is found. If it is the fibre with the maximum line number, then the search for a previously unselected fibre starts from the fibre with line number 1. The procedure is explained schematically in Figure 7.24.

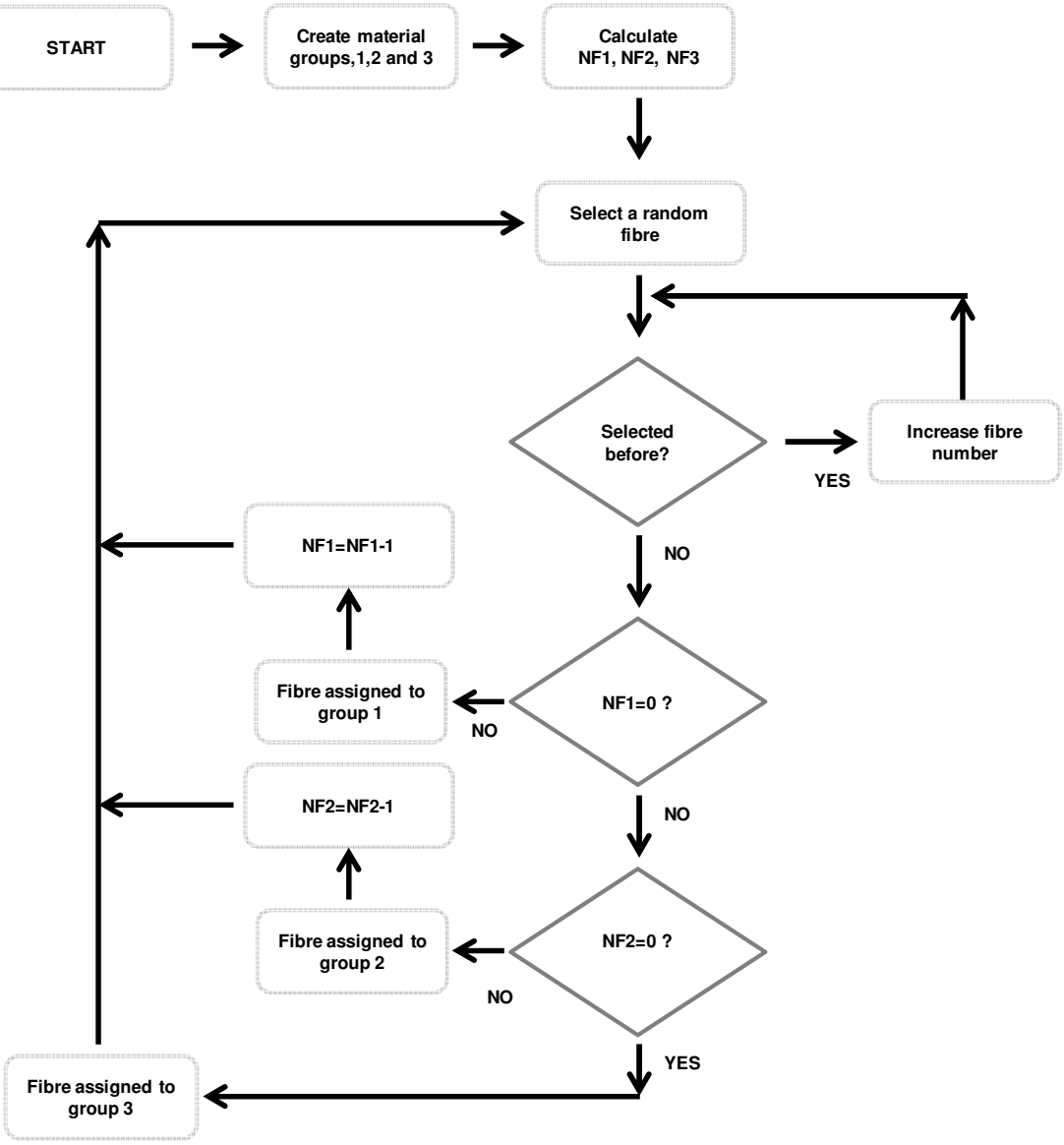

Figure 7.24. Schematic drawing of the procedure to implement fibre curl distribution ("NFX" means "number of fibres in group X")

The distribution of fibre curl groups in the fibrous network of the studied nonwoven is shown in Figure 7.25; indicating a successfully random distribution throughout the fibrous network, of which fibres with a curl of 20% dominate the structure with 50% (see Table 7.5).

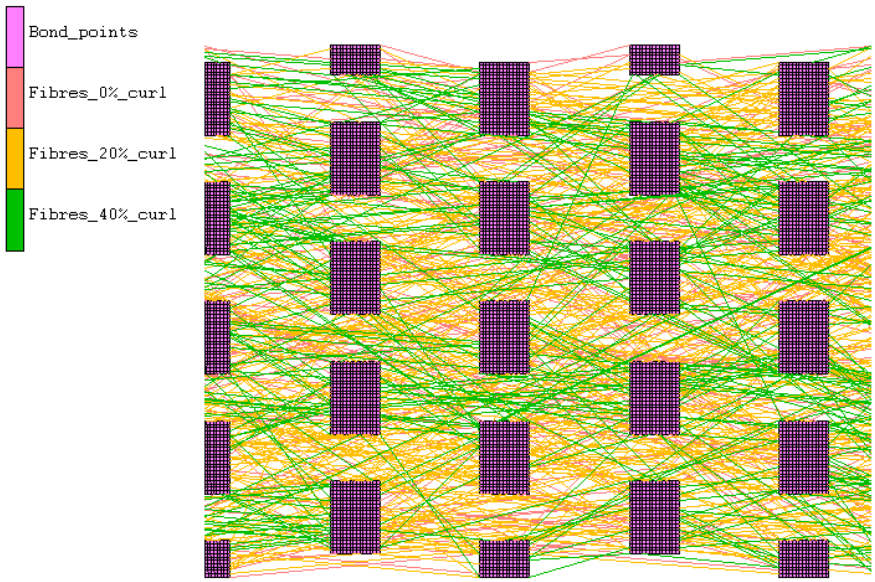

Figure 7.25. Distribution of fibre curl groups in fibrous network

7.4.3 Results and Discussions

The results obtained with the developed model and the model without curl distribution are shown in Figure 7.26 in comparison with the test data. As it can be seen, the behaviour gets closer to the tensile test results when the curl factor is accounted for. Especially during the initial stage, at which the curled fibres were not fully extended, the behaviours in tests and simulations are very close, indicating that introduction of fibre curl was beneficial to reproduction of a realistic response of the nonwoven to stretching. After a certain extension, the simulation again becomes stiffer since the damage in the fibre-bond point interfaces is not modelled and the stiffness of bond points is still taken as equal to that of the fibres. Hence, another group of simulations was performed with multiplying the bond point stress-strain curve with various coefficients less than unity in order to represent the damage in the bond points. The respective results are shown in Figure 7.27. Apparently, the curve gets closer to the test results as the stiffness of bond points is decreased. Further implementation of damage behaviour will probably result in a more realistic model.

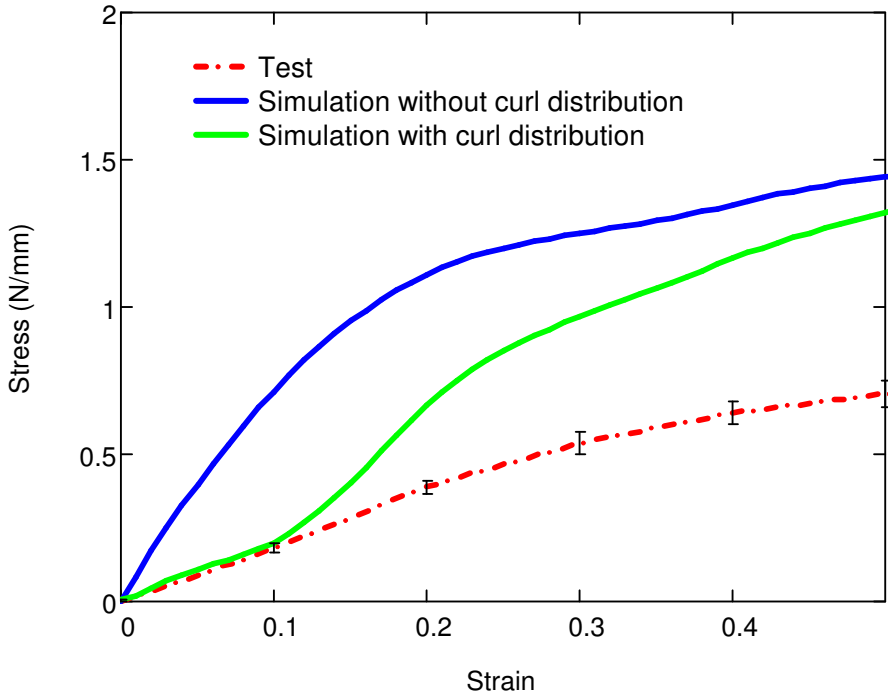

Figure 7.26. Comparison of simulations with and without implementation of fibre curl

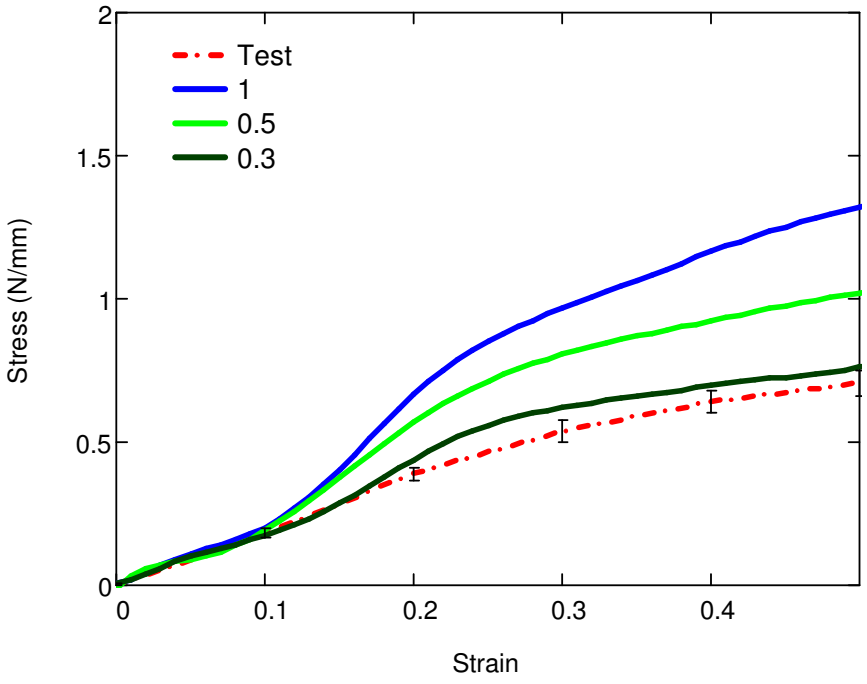

Figure 7.27. Simulations with various multiplication factors of bond point material properties to account for damage

7.5 Discussions and Conclusions

A parametric finite element modelling technique is introduced in this chapter based on random arrangements of fibres according to the orientation distribution function. This model has several advantages compared to the previous modelling technique and previous studies. First, this technique gives better results than the previous one when compared to the tests. It is shown that when fibre curliness and damage behaviour is introduced, the model is more likely to give closer results to the tests. However, it should be noted that nonwoven fabrics will always have some irregularities due to the manufacturing. The effect of temperature and pressure during production was also not included in the study. Therefore, trying to reach exactly the same deformation as in the tests should not be the final aim of this study. Secondly, this technique is closer to representation of the production method for thermally bonded nonwovens because the fibres are distributed in the model randomly. Consequently, the model handles the orientation distribution without any extra assumptions such as the one introduced in Chapter 6.

The last advantage of the current model is that, it is more open for further studies such as damage modelling since the fibres are modelled more realistically. Also it is more convenient to introduce fibre curliness into the structure. However, before this, an image analysis tool should be developed or used to determine the curliness distribution of fibres in the structure. Two suggestions are given to introduce the curliness of the fibres. The first one, given at the end of Chapter 6, is the modification of stress-strain curves of fibres. It should be noted that the fibres with a curl should be modelled shorter than their real length according to their amount of curliness. Another option is modelling the fibres with some curliness, directly. For example instead of fibre lines, fibre arcs, with their radii depending on the amount of curliness, can be introduced into the model. In that case, one fibre line in the model would consist of more than one element. The nodes of trusses act as hinges in finite element models (i.e. they do not carry moment) and convergence problems would be unavoidable. Instead of truss elements, the use of beam elements could be a solution.

In that case, the bending stiffness of these beams should be given as low as possible in order to represent the behaviour of fibres adequately.

The modelling technique proposed in this study was developed for the analysis of low-density (below 50 g/m^2) thermally bonded nonwovens. However, it can be used for the analysis of high-density nonwovens as well. This is shown in Appendix B with the simulation of a high-density nonwoven which was studied recently in Demirci (2010).

CHAPTER 8

EFFECT OF MANUFACTURING PARAMETERS AND LOADING CONDITIONS ON STIFFNESS OF NONWOVEN MATERIALS

8.1 Introduction

Nonwoven materials are manufactured in various methods due to the available equipment and the design needs. One of the crucial needs is to understand the effect of various design elements on the structural behaviour of nonwovens. In this chapter, several analyses were performed by altering the dimensions of the elements with the use of the model developed in Chapter 7. The evolution of reaction force and the displacement of the free MPC node were read from the analysis results and converted to stress-strain behaviour. Some analyses were also performed by changing the load direction and speed to see their effect on the stiffness. There were some additional parameters used in the developed model just related with only modelling efficiency. At the end of this chapter, their effect on the deformation behaviour was shown by performing analyses with various parameter values.

8.2 Reference Model

In these studies the fabric dimensions of the reference model were still kept small in order to save the CPU time. In addition, the fibre and bond point materials were all modelled as linear elastic in order not to couple the time dependent effects with those due to manufacturing parameters. The properties are given in Table 8.1. The parameters not given are the assigned as the same in Table 7.1. In all the models, the specimen is stretched along its machine direction.

Table 8.1. Properties of the model used for case studies

Fabric density (g/m^2)	*Fabric length (Gage length-mm)*	*Fabric width (mm)*	*BP width (mm)*
20	10	8	1.1
BP length (mm)	***BP width gap (mm)***	***BP length gap (mm)***	***MC***
0.75	0.7	1.5	5

8.3 Effect of Manufacturing Parameters

8.3.1 Density of Fabric

Simulations were performed with fabric densities of 10, 20 and 30 g/m^2. As expected, the density of fabric had a considerable effect in the deformation behaviour. The response to loading behaviour is theoretically linearly proportional to the fabric density, and the simulations show this feature (Figure 8.1).

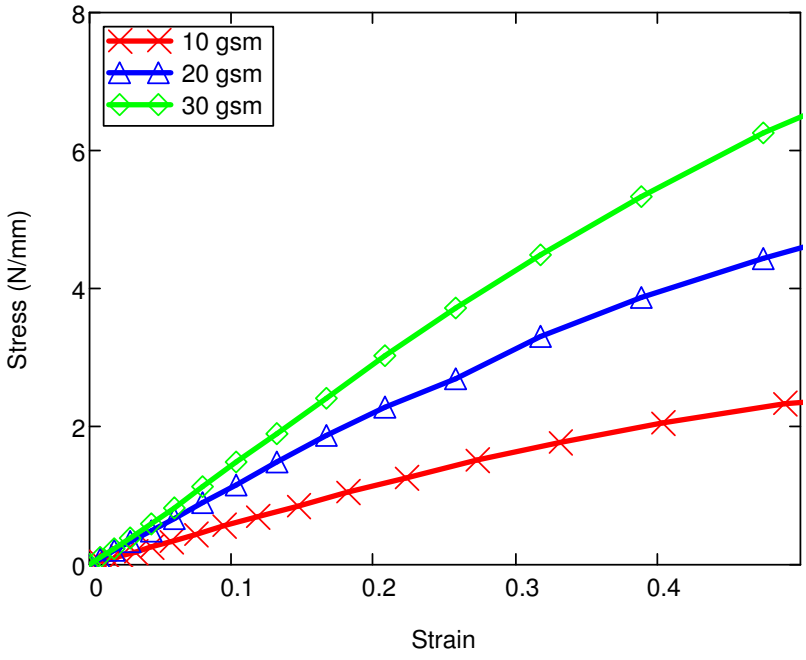

Figure 8.1. Stress-strain simulation results with various fabric densities

8.3.2 Bond Point Width

In these simulations, the width of bond points was increased and the width gap between the bond points was decreased by the same amount in order not to change the locations of bond points. The results for this case are shown in Figure 8.2. As it can be seen, when the BP width is increased, the model gives stiffer response under tensile load. Obviously, when the width of bond points increases, the percentage of bond point area increases as well. It was shown by Bhat *et al.* (2004) that the fabric samples with larger bond point area had a higher peak load value. This structural feature is confirmed with this study as the models with larger bond points give stiffer results.

It was also observed that the effect of increasing the width of the bond points was diminishing as the BP width is increased. The reason is that, in the simulation with BP width increase of +36%, the gap between the bond points in vertical direction is only 0.3 mm; i.e. very close to the case of bond points continuous along the vertical direction. Thus, the effect is converging to the behaviour of continuous bond point structure along the vertical direction.

8.3.3 Bond Point Length

The effect of varying the bond point length can be seen in Figure 8.3. The increase in the BP length also increases stiffness of the nonwoven as expected. There is still a large gap between the bond points even for the sample with the maximum length. Therefore, no convergence is noticed in these models like the one in the previous study.

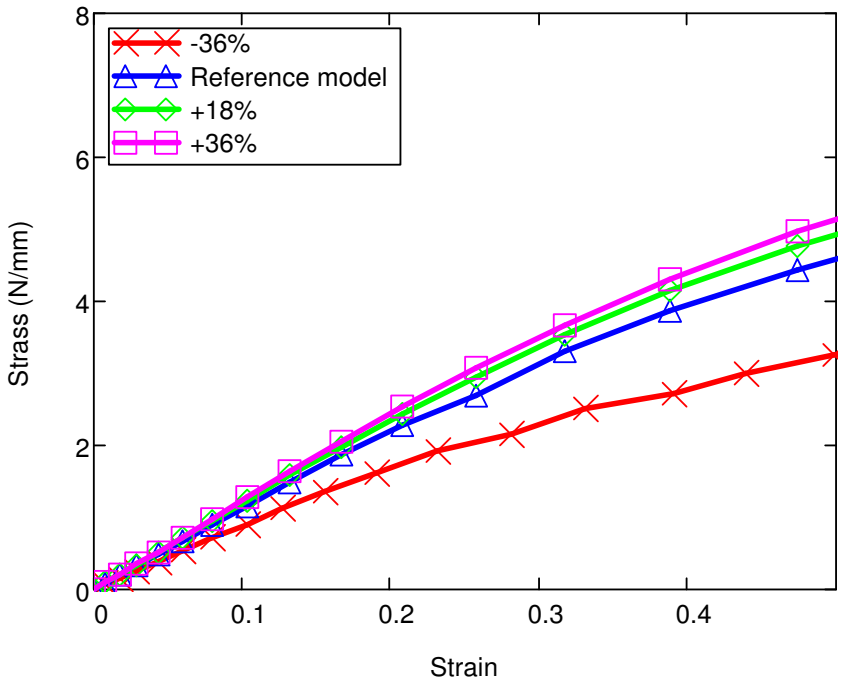

Figure 8.2. Effect of width of bond points on the stress-strain simulation results

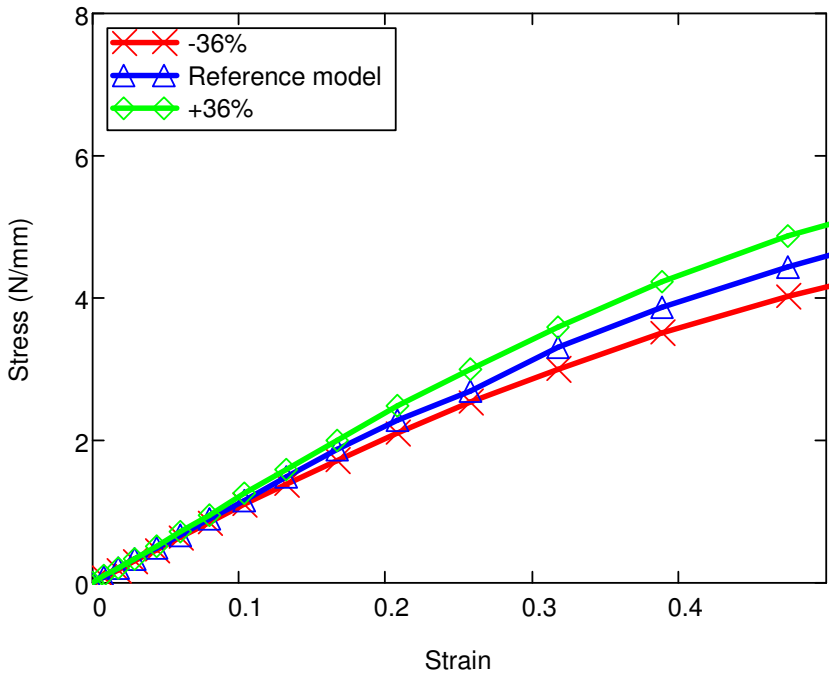

Figure 8.3. Effect of length of bond points on stress-strain simulation results

8.3.4 Length of Fibres

Various analyses were performed by decreasing the fibre length as the fibres were already quite long for the current model (fibre length was 25 mm, fabric dimensions were 10 mm x 8mm). An analysis with continuous fibres was also carried out to compare with the other results (Figure 8.4). As it can be seen, the fibre length plays a very significant role in the tensile behaviour and should not be ignored. The fibre length in the reference model was more than twice the diagonal length of the fabric. Thus, the model with continuous fibres and reference model with 25 mm fibre length gave very similar behaviours.

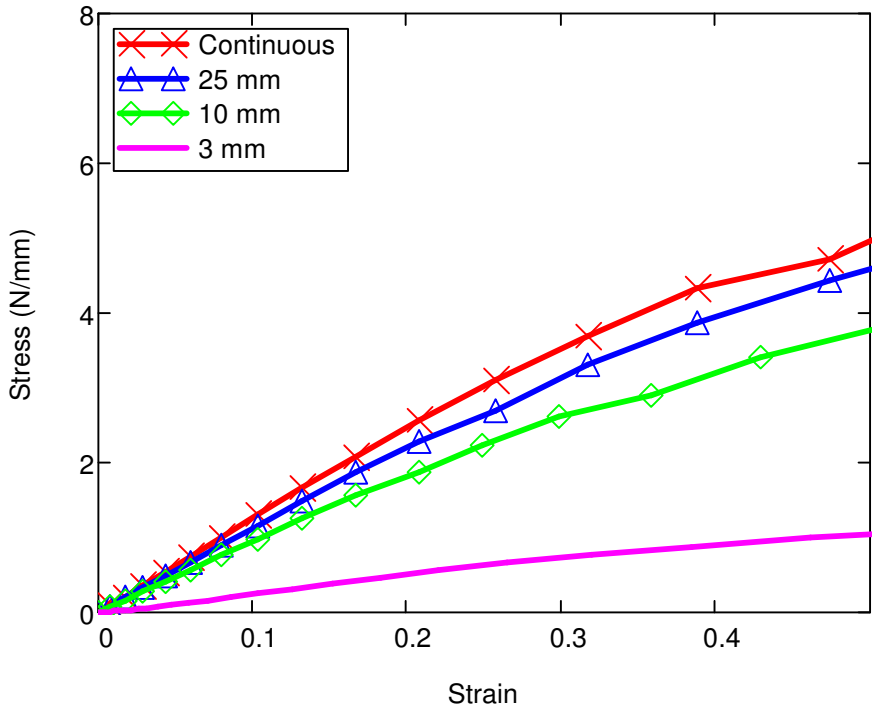

Figure 8.4. Effect of fibre length on stress-strain simulation results

8.3.5 Effect of Fabric Length (Gage Length)

The length of the fabric was varied to analyse its effect on the deformation behaviour. In the analysis of homogeneous materials, this parameter does not have any effect on the stress-strain behaviour. However, it may affect the results in the

present model because of the limited fibre length in the structure. In order to study this, an analysis was performed decreasing the length of fibres in the reference model to 10 mm. Two more analyses were performed by changing the fabric length (Figure 8.5.). As it can be seen, the stiffness of fabric decreases slightly with the increase in the fabric length. When the length is large, more fibres have free ends in the structure. This means more discontinuous fibres are present along the tensile direction. The models with 10 and 25 mm fabric give similar results as the fibre length of 10 mm is quite large for both of them (i.e. fewer fibres have free ends in the structure). This feature can be very useful for the designers to decide the length of fibres according to the dimensions of the fabric.

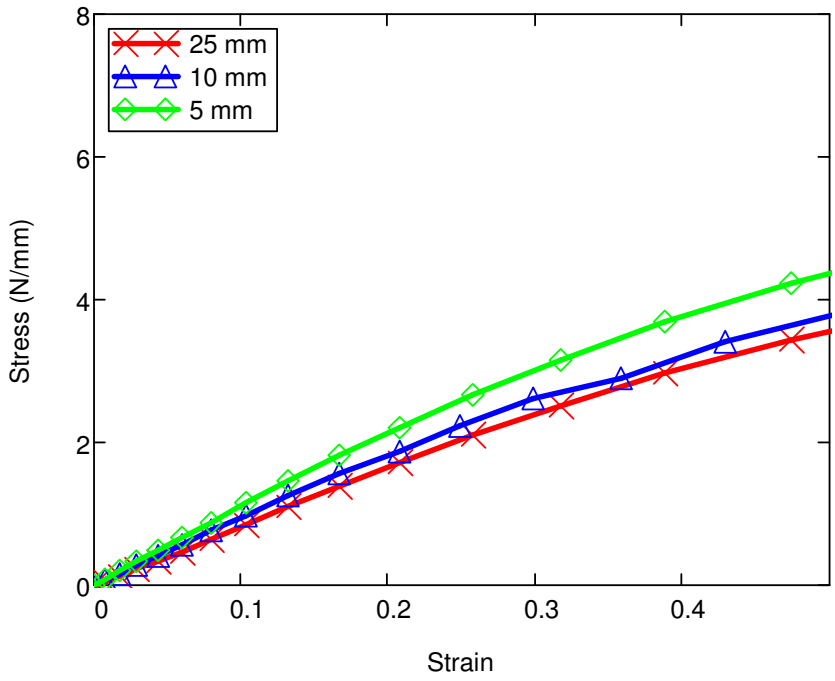

Figure 8.5. Stress – strain plots for various fabric lengths

8.3.6 Effect of Fabric Width

Similarly, the width of the fabric was varied, and the results of these simulations are presented in Figure 8.6. Obviously, varying the width of the fibres does not have the

same effect that the case of varying the fabric length. Secondly, the orientation distribution of fibres is not dominant along the width of the fabric.

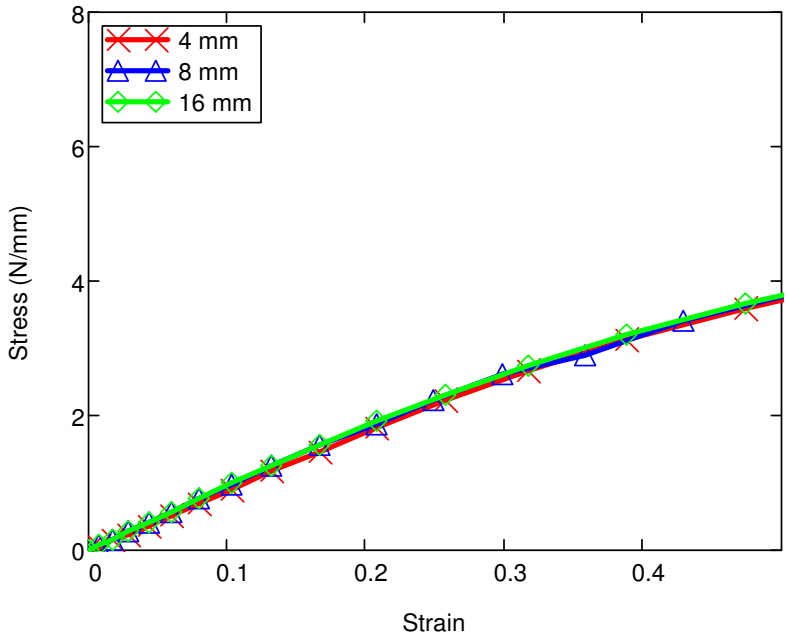

Figure 8.6. Stress – strain plots for various fabric widths

8.4 Effect of Loading Conditions

8.4.1 Test Speed (with Creep)

This group of analyses were performed to observe the effect of tensile strain rate. In order to achieve this, the creep behaviour was introduced to the model. The respective results are shown in Figure 8.7. In order to be able to comment on them, , nonwoven tensile tests were performed with the same strain rates, and the obtained results are shown in Figure 8.8. Although there were significant differences in the stress values between the tests and simulations, the levels of stiffness in both models was changed by nearly the same ratio. This confirms that the model was also capable of predicting the rate-dependent behaviour of nonwovens. From Figure 8.8, the inaccuracy of the test during the initial extension stage can also be observed indicating that curliness of fibres plays an important role.

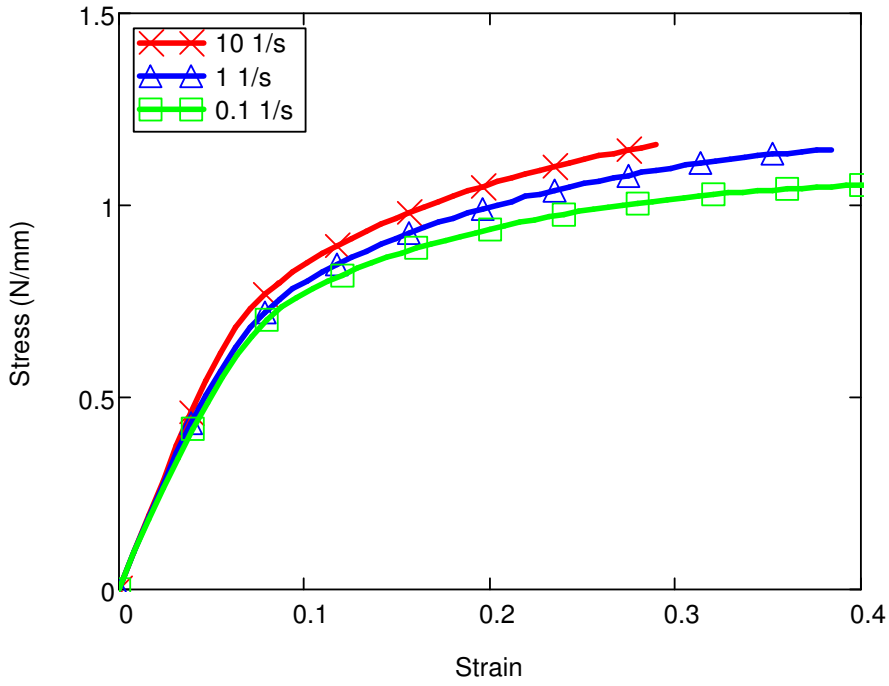

Figure 8.7. Stress – strain simulation results for various test speeds

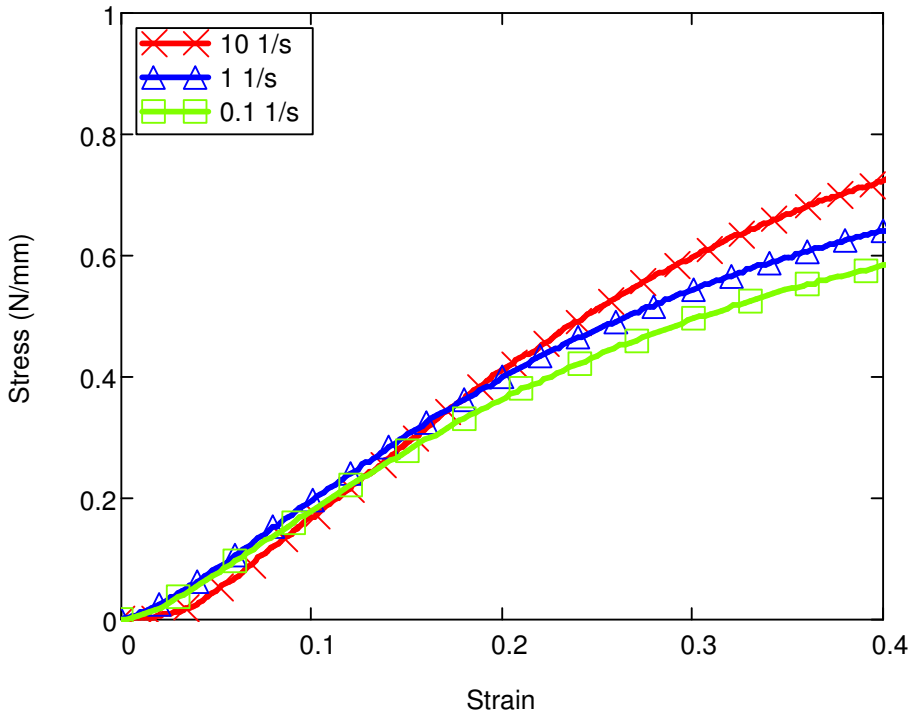

Figure 8.8. Experimental stress – strain results for various test speed

8.4.2 Tensile Direction

One of the most significant features of this model is the handling of orientation distribution in a very efficient way. The comparison of deformation behaviours along the machine (MD) and cross (CD) directions is shown in Figure 8.9. Apparently, deformation along the cross direction is less stiff compared to that of the machine direction as expected.

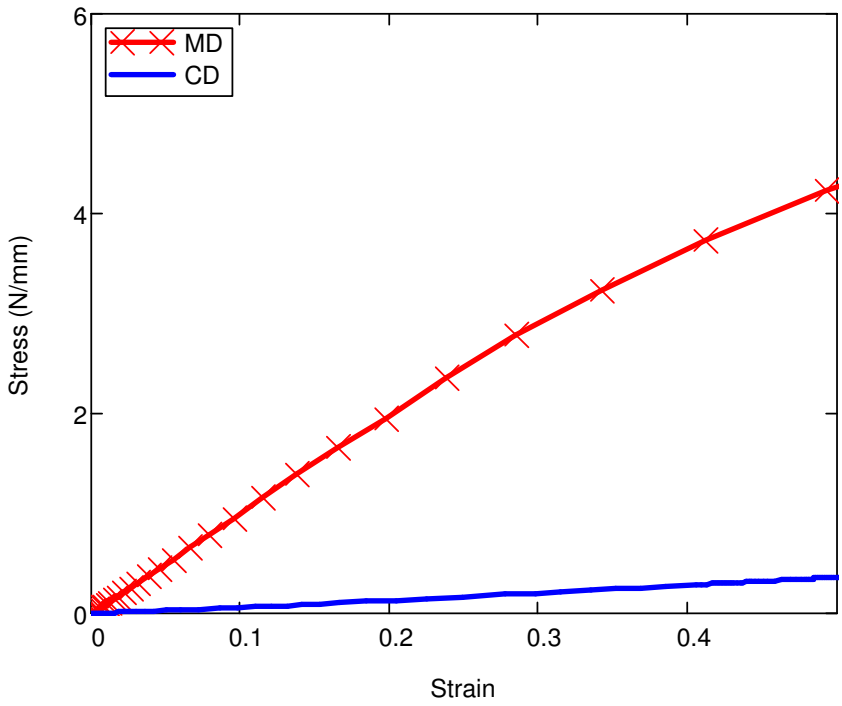

Figure 8.9. Stress-strain simulation results for deformation along MD and CD

8.5 Effect of Model Parameters

8.5.1 Randomness

The model was generated by fibres being located randomly according to the orientation distribution function. The random numbers that determined the location of fibres were varied to study the dependence of not only on orientation, but also on location of fibres. Two more sets of random numbers were generated and the models using these numbers were analyzed likewise (Figure 8.10). Apparently, all three

models gave similar results; meaning that it does not contribute to the results significantly. However, it may affect in the case of nonwoven with a lower fabric density.

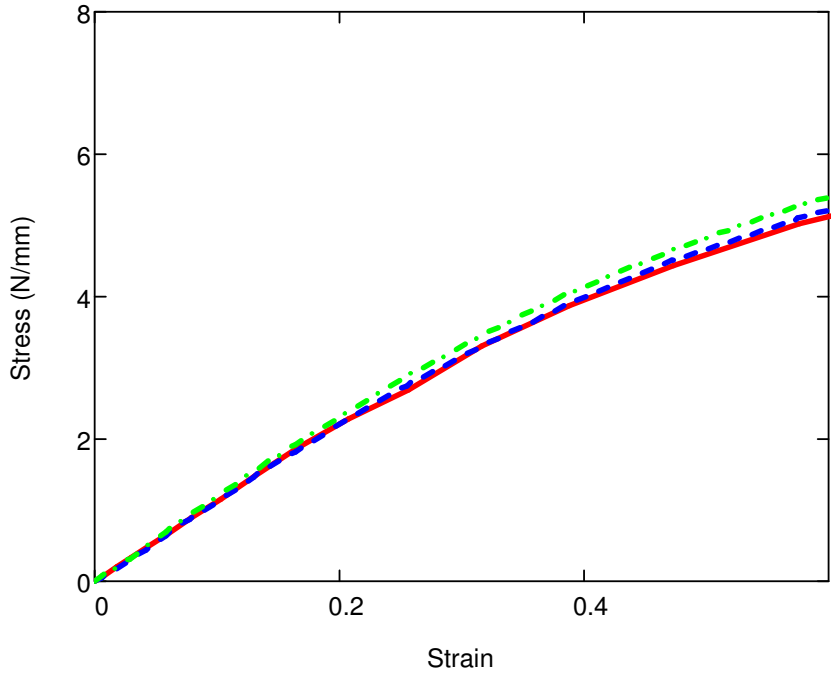

Figure 8.10. Stress-strain results obtained for three different sets of random numbers

8.5.2 Model Coefficient

The model coefficient, explained in Chapter 7 was varied to see if the size is suitable for the model (Figure 8.11). Apparently, the models give similar results with various model coefficients up to 10 indicating that the *MC*=5 was suitable for this model.

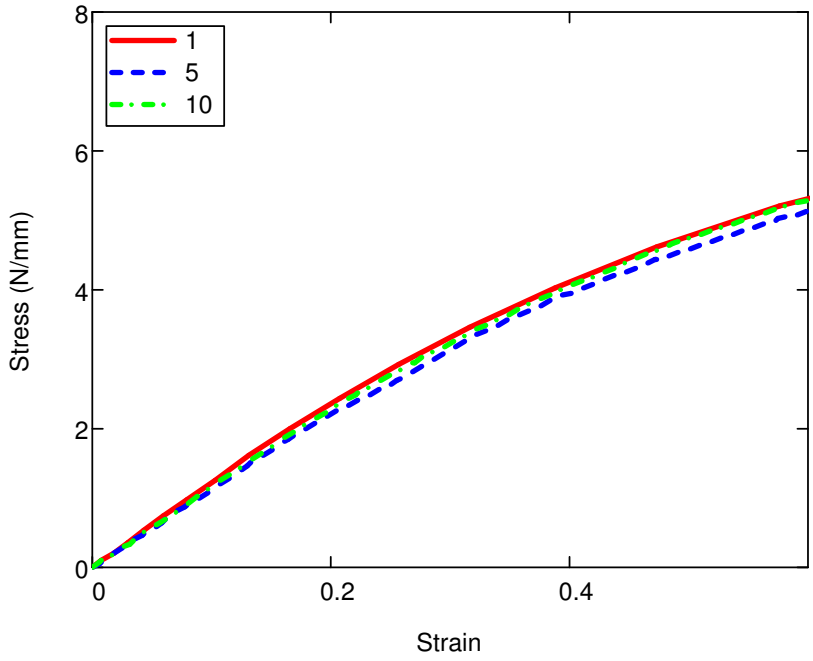

Figure 8.11. Stress – strain plots for various levels of *MC*

8.6 Conclusions

In this chapter, the effect of manufacturing parameters, loading conditions and model parameters were studied by using the developed model in Chapter 7. The parametric studies show that the dimensions of bond points and the fabric have a significant effect on the deformation behaviour of nonwoven materials.

According to the author's knowledge, this study is the first finite-element model in the literature that handles the effect of fibre length in a nonwoven structure. This feature can be crucial for designers to choose the length of the fibres to be used according to the dimensions of the final product.

The efficiency of the developed model was further shown by altering some model parameters used in the study. It was shown that the model coefficient and the randomness level is enough for the simulation; thus validating the use of the reference model. Further studies can be performed under different types of loading such as bending.

CHAPTER 9

STRAIN DISTRIBUTION IN FIBRES IN NONWOVEN STRUCTURE UNDER TENSILE LOAD

9.1 Introduction

In Chapter 7, a novel parametric finite element model was generated taking into account the distribution of fibres. In Chapter 8, the response of the model to applied extension was analyzed and the effect of manufacturing parameters on the model was shown.

One of the results, observed in Chapter 7, was the non-homogeneous distribution of strains throughout the fibres. In this chapter, the microstructure of nonwovens was analyzed more deeply by investigating the strain distribution in the nonwoven structure. The study reveals the distribution of applied load within the fibrous structure of nonwovens. The use of developed finite element model gives the opportunity to investigate the response of individual fibres under various loading conditions.

In the previous study by Hou (2010), the distribution of strains and stresses were studied for two different versions of nonwovens in cross and machine directions. The results demonstrated the difference between the studied models on the distribution of strains. However, the underlying mechanisms causing these differences were not presented. Even in a single nonwoven model, there were many fibres having very large and very low strains compared to the average and the reason for this behaviour was not explained. In addition, the effects of tensile rate and material properties, which may have an effect on the distribution, were not studied. Thus, the aims of this part of the study are:

1. Understand the mechanisms affecting the distribution of strains inside the fabric;

2. Determine the effect of model parameters on the strain distribution;

3. Observe the effect of varying the tensile strain rate.

9.2 Methodology

In the present study, first, the distribution of strains was investigated for a reference model without random orientation distribution and with linear-elastic material properties assigned to the fibres. Then the strain distribution for fibres of nonwoven models with various parameters, material models and tensile strain rate were compared with the reference model. Such a procedure reveals the underlying mechanism of the effect of each parameter. It also demonstrates the reason of some fibres having higher strains than the others which would be difficult to understand from a nonwoven with randomly distributed fibres. Finally, the distribution of strains in a nonwoven having an orientation distribution was analyzed.

Before starting the analyses, the tensile profile to be applied to the model and the intervals of the results to be analyzed are determined.

9.2.1 Tensile Profile Applied to Nonwoven Models

The main aim of this study is to analyze the distribution of strains in fibres with respect to fabric strain intervals. However, especially for high deformation cases, the true stain and engineering strain differs significantly. As shown in Figure 9.1, when constant velocity for extension is applied to the model, the true strain becomes around 67% of the fabric engineering strain at 100% extension. In order to obtain constant true strain through the time intervals, the displacement profile was introduced to the models according to the following equations (Figure 9.2);

$$\varepsilon_{eng} = \exp(\varepsilon_{true}) - 1, \tag{9.1}$$

$$u = \varepsilon_{eng}\, gl, \tag{9.2}$$

where, ε_{eng} and ε_{true} are the engineering and true strain respectively; gl is the gage length of fabric and u is the displacement applied to the model.

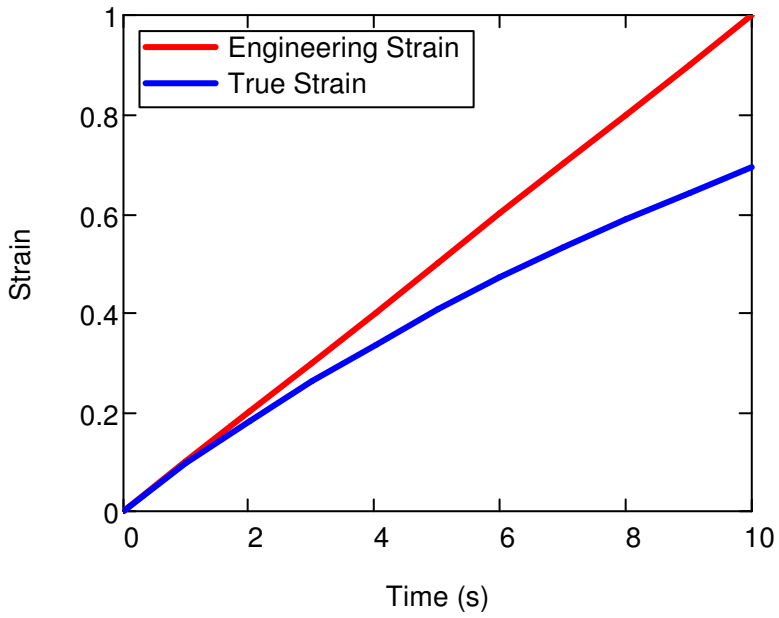

Figure 9.1. Difference between engineering and true strain of fabric when constant velocity is defined under tensile load

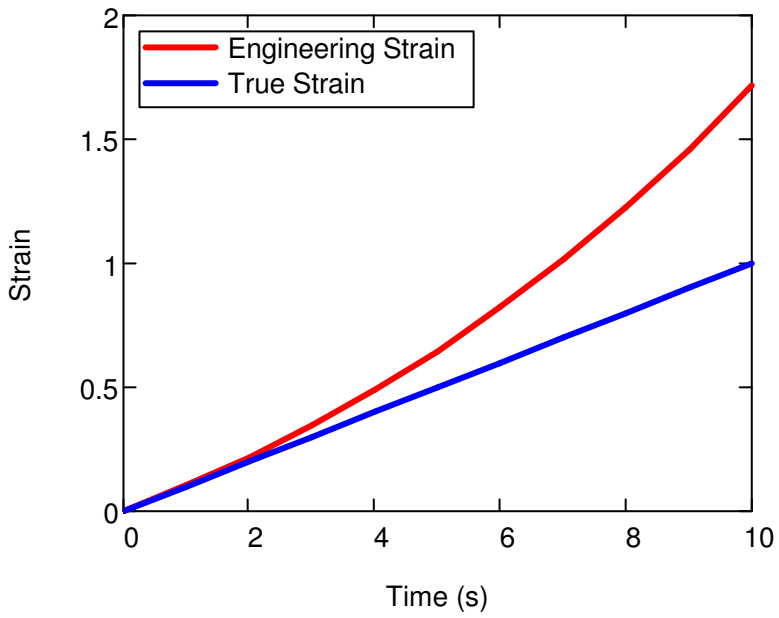

Figure 9.2. Difference between engineering and true strain of fabric when extension velocity is varied in order to obtain constant true strain rate

The results were obtained for fabric strain values of 0.1, 0.2, 0.3....1. Thus the strain distribution of fibres was analyzed at 6, 12, 18 ... 60 seconds of analysis time.

9.2.2 Reference Model

The model used until now was generated according to the orientation distribution determined with an image analysis software (Demirci et al. 2009). In the nonwovens having random distributed fibres, there are many fibres in the structure in arbitrary locations and orientations. In order to access the behaviour more accurately, a reference model was generated with all the fibres oriented along machine direction. This reference model has the following additional features:

1. Bond points were modelled as rigid bodies in order to avoid their deformation to interact with fibre strains to be investigated. In order to do this, a very high Young's modulus value was assigned to the bond point elements. The effect bond point stiffness was also analyzed during this study.

2. The fabric's dimensions were chosen as 10 mm x 8 mm, i.e. small enough to earn computational speed, large enough to have enough bond points and to simulate global response (shown in Chapter 7).

3. Linear elastic material was used for the fibre material to separate the effect of nonlinear material model.

4. Fibres were assumed as being continuous.

5. The model coefficient (*MC*, presented in Chapter 7) was chosen to be 1 in order to assess the results by investigating all the fibres that would be present in the nonwoven.

The finite-element implementation of the reference model is shown in Figure 9.3

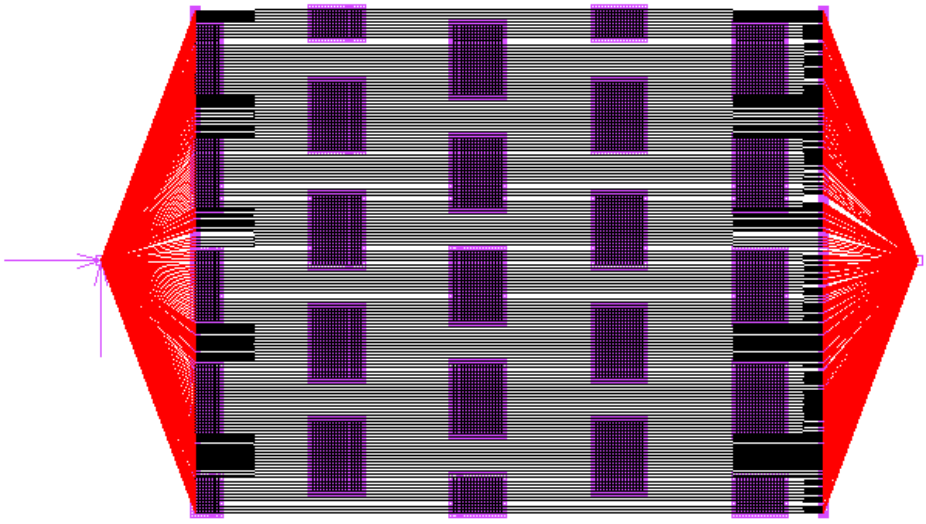

Figure 9.3. Finite element implementation of reference model

As it can be seen, the model was generated by fibres, all aligned parallel to the machine direction. The black parts along the borders near MPC elements are the fibres whose one coordinate was not shifted during "editing fibres for proper meshing" procedure explained in Chapter 7 (Figure 9.4).

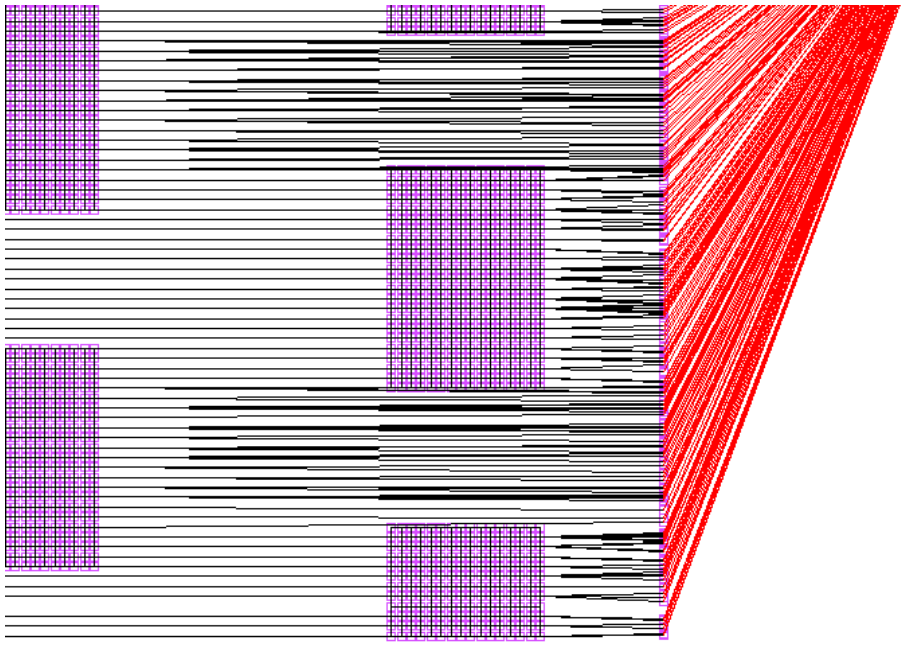

Figure 9.4. Fibres near boundary conditions for reference model

9.2.3 Studied Model Parameters

By using the parametric model presented in Chapter 7, many types of nonwovens can be analyzed by changing its parameters. In addition, the material properties can be varied to observe their effect on the distribution. Furthermore, it is also possible to vary the tensile strain rate. The model parameters considered in this study is shown in Table 9.1. The properties given under the heading "Ref" indicate the properties of characteristics of the reference model. In order to define various models clearly, a code is assigned for each parameter which is indicated in brackets. Parameters for which, the code is not indicated are the same as in the reference model. For example, a model with a code FL-I indicates that the length of fibres in the model was 10 mm whereas all the other parameters were the same as in the reference model.

Table 9.1. Model parameters and codes, used in the study

Model Parameter	**Ref.**	**I**	**II**	**III**
Mesh size of bond points (MESH)	0.05 mm	0.02 mm		
Density of fabric (DF)	20 g/m^2	10 g/m^2		
Bond point length (BPL)	0.75 mm	1.022 mm		
Bond point width (BPW)	1.1 mm	1.5 mm		
Fibre length (FL)	Continuous	10 mm		
Bond point material, rate-independent property (BPM)	Linear elastic, E=100000 MPa	Linear elastic, E=1000 MPa	Linear elastic, E=100 MPa	
Fibre material, rate-independent property (FM)	Linear elastic, E=1000 MPa	Linear elastic, E=100	Elasto-plastic (Chapter	

		MPa	7)	
Fibre material, rate dependent property (FV)	No creep model	Creep model (Chapter 5)		
Orientation distribution (ODF)	All fibres along machine direction	Appendix A		
Tensile strain rate (TSR)	1 min^{-1}	0.1 min^{-1}	0.01 min^{-1}	0.001 min^{-1}

9.2.4 Assessment of Results

The results of simulations were assessed by using the respective advantages of softwares, MSC Patran and Marc. The distribution of fibres was obtained by implementing a subroutine in MSC Patran which writes the fibre number *vs.* strains for increasing levels of fabric strain. The graphical results showing the fibres were obtained by another subroutine written for MSC Marc Mentat. While assessing the results, the strain magnitudes for fibres were isolated from strains of bond points by creating a group of fibres and selecting the "isolate elements" option (Figure 9.5a). In such a way, the averaging of strains of bond points with those of fibres was prevented. However, there can be fibres sharing a common node. The nodal results give the average strains of the fibres in that case. This was prevented by turning off the nodal averaging option in results menu (Figure 9.5b).

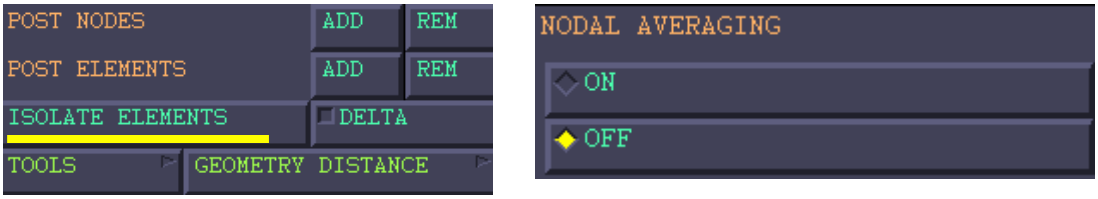

(a) (b)

Figure 9.5. Selection of result options in MSC Marc-Mentat: (a) isolating elements; (b) turning off nodal averaging

9.3 Results of Analyses

9.3.1 Results for Reference Model

The statistical distribution of strains for fibres for various levels of strain applied to the nonwoven fabric is shown in Figure 9.6. The results are given in three separate plots in order to make the figures clearer to viewers. The last curve of each plot is included at the beginning of the next one to allow comparison of all curves with each other. The y-axis presents the percentage of fibres in the nonwoven structure, which belong to a certain strain group, while the x- axis presents strain group, which was calculated as follows.

First, the strain values for each interval were multiplied by 1000 and rounded up to the closest integer in order to make them integer with precision of 10^{-3}. Then the strain groups are calculated using the following equation:

$$Strain\_group(i,j) = \frac{R_{i,j} - \mathrm{mod}(R,25)}{25}, \tag{9.3}$$

where $R_{i,j}$ shows 1000 times the rounded strain value for each fibre at each strain interval of fabric. Some of the calculated values are shown in Table 9.2. The strain group "-1" shows that the fibre is in compression.

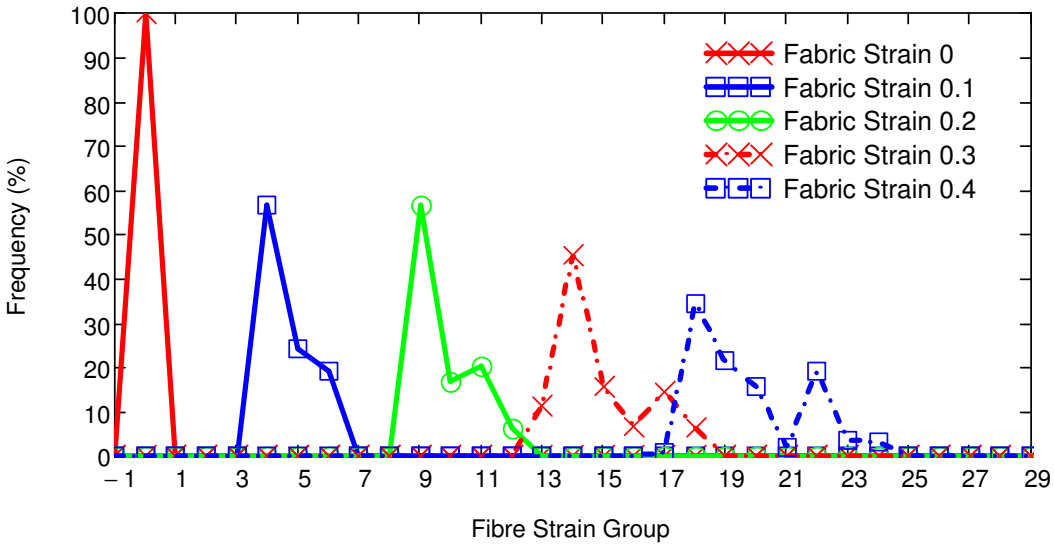
Frequency (%)
Fibre Strain Group
Fabric Strain 0
Fabric Strain 0.1
Fabric Strain 0.2
Fabric Strain 0.3
Fabric Strain 0.4

(a)

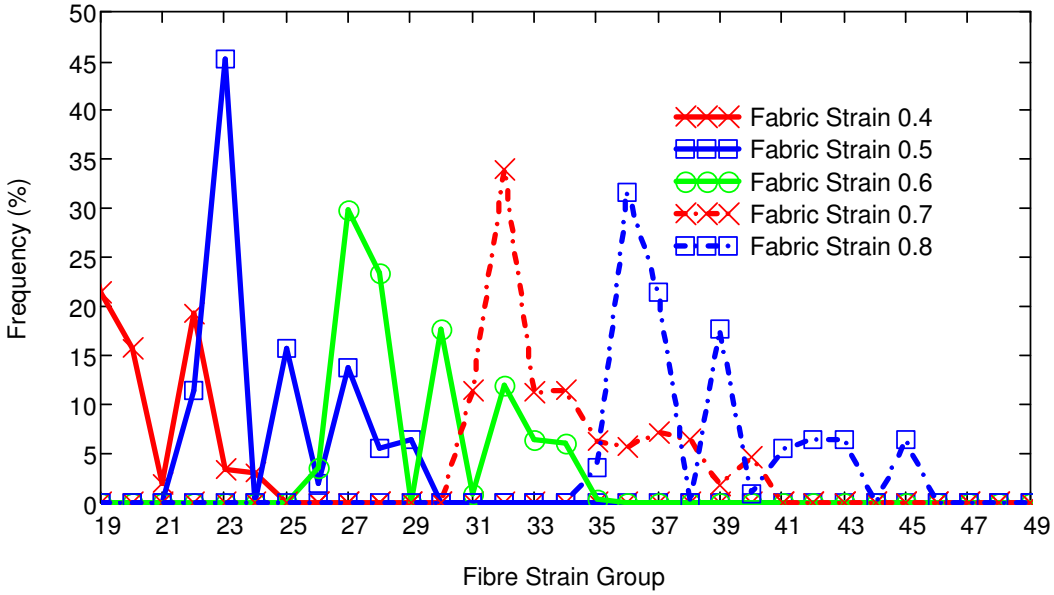
Frequency (%)
Fibre Strain Group
Fabric Strain 0.4
Fabric Strain 0.5
Fabric Strain 0.6
Fabric Strain 0.7
Fabric Strain 0.8

(b)

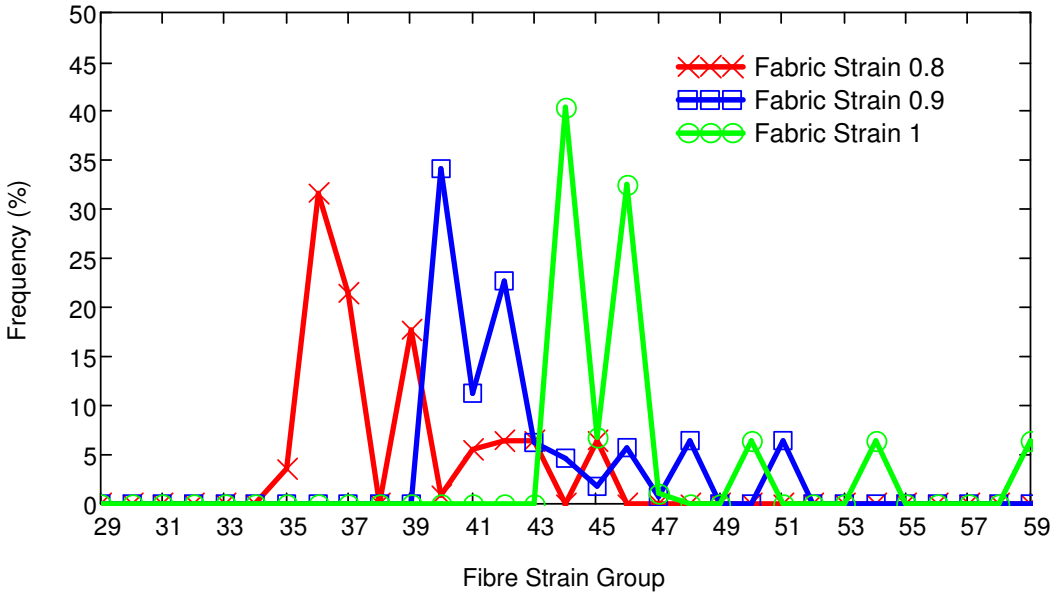

(c)

Figure 9.6. Distribution of strains for fibres for various values of fabric strain (reference model): (a) 0-0.4; (b) 0.4-0.8; (c) 0.8-1

Table 9.2. Strain groups for various intervals of true strain

Strain Group	*Interval*
-1	$\varepsilon_{true} < 0$
0	$0 \le \varepsilon_{true} < 0.025$
1	$0.025 \le \varepsilon_{true} < 0.050$
2	$0.050 \le \varepsilon_{true} < 0.075$
3	$0.075 \le \varepsilon_{true} < 0.1$
...	...
58	$1.450 \le \varepsilon_{true} < 1.475$
59	$1.475 \le \varepsilon_{true}$

It can be seen that at fabric strain of 0.1, most of the fibres had strain value close to that of the fabric (at group 4). However, some fibres started to be stretched to levels higher than that of fabric. At 0.3, nearly all of the fibres had strain higher that of the fabric (i.e. they should have been in the group 11-12 in order to have the same strain as the fabric). In addition there were fibres having more than 0.425 strain at this

level. At the fabric strain of 0.6, some fibres had strain levels between 0.85 and 0.875 of strain (strain group, 34). This behaviour continues until the end of analysis.

The deformation behaviour at fabric strain of 0.1 reveals the information about the reason of this distribution (Figure 9.7). In the direction of fibres having the smallest gage length, the rigid bond points occupy most of the space in the horizontal direction. This causes these fibres to stretch more than the others. The light-grey fibres show that they have strain value higher than the upper limit defined in the legend. These fibres are short ones connecting adjacent bond points. Here, the legend of the figure is given with keeping the fabric-strain value in the middle of the scale.

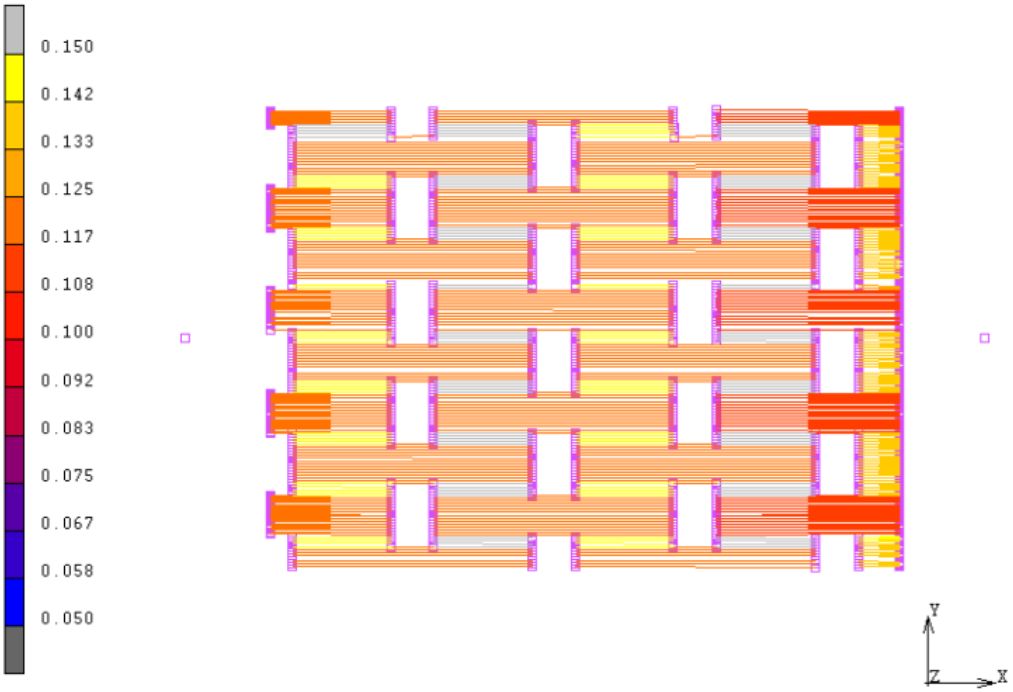

Figure 9.7. Strain distribution of fibres in fabric at fabric strain of 0.1

In order to understand the reason for this behaviour more clearly, two very simple models were built (Figure 9.8). Both of these models were composed of two truss elements connected end to end. In the first model, Young's Modulus value of 1000 MPa was assigned to both elements. In the second model, same Young's modulus value was assigned to the element on the left whereas a Young's modulus value of 100GPa was assigned to the second element which can be considered as a rigid

structure compared to the other element. In both models, the node at the left hand side was fixed and displacement was applied to the element on the right hand side. Displacement was applied so that the whole strain in the combination of two elements respond as constant total strain level in each increment. The strain values at the nodes at the time when the fibres are stretched for a true strain of 1 are shown in Figure 9.9.

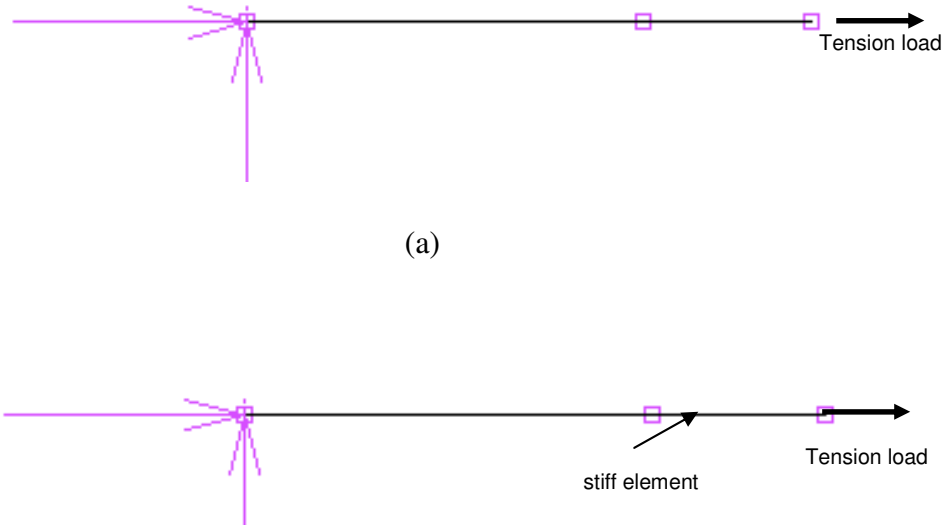

(a)

(b)

Figure 9.8. Simple truss models; (a) without stiff element, (b) with stiff element.

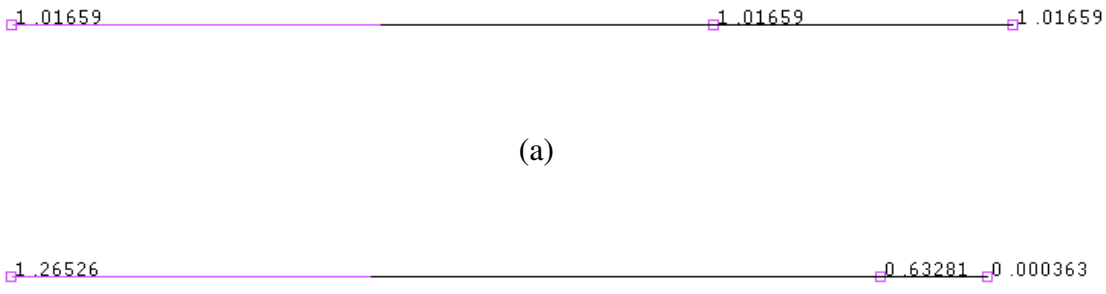

(a)

(b)

Figure 9.9. True strain distribution in simple truss models (a) without stiff element (b) with stiff element.

As it can be seen, in Figure 9.9(a), the strain values at the nodes were 1.01659 close enough to the strain value of 1. The small difference was due to the fact that the displacement to be applied for constant true strain was based on the equation which assumes that the material is incompressible (see section 4.1). In Figure 8(b), the stiff element (the right one) had a true strain value of 0.000363 which is far below the applied strain. As it is much stiffer compared to the left one, the total extension was mostly provided by the elastic fibre (left one). This fibre had a much higher value of true strain (1.2653) than the applied true strain (1). The strain value in the middle node (0.6328) is the average of the strains of two fibres, thus, should be ignored.

The result from this simple model explains the reason for the higher strain values in the fibres which are shorter than the others in the nonwoven structure. As the original length of short fibres is small, the same total displacement causes higher strain in them. The rigid bond points occupy more space in lines with these fibres resulting in their smaller initial length. With the same displacement introduced to the model, these fibres carry more strain because of their initial length.

Another observation is that fibres, including the long ones, start to take more and more strain than the fabric strain as the fabric strain is increased. This can be seen in picture showing the distribution of fibre strains for the fabric strain of 0.2 (Figure 9.10). As it can be seen, the strain of most of the long fibres is close to the limits of the scale compared to the case of fabric strain of 0.1. In the case of fabric strain of 0.3 (Figure 9.12), one can see that nearly all fibres are above the limits specified in the scale. It is obvious that as the strain of the fabric increases, the fibres are stretched more than fabric and the difference between strain of fibres and fabric increases. Thus, there is no sudden change of distribution of strains at certain levels of fabric strain, which can be a misleading conclusion obtained from Figure 9.6. The relative increase of the strain of fibres with the strain of fabric happens gradually.

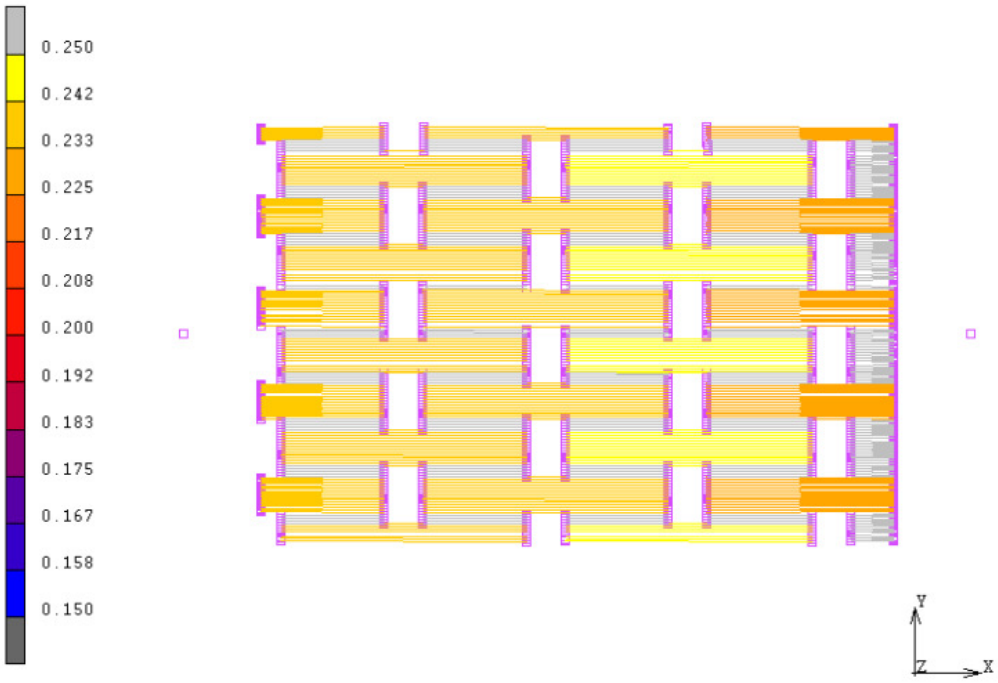

Figure 9.10. Distribution of strain of fibres in fabric at fabric strain of 0.2 (reference model)

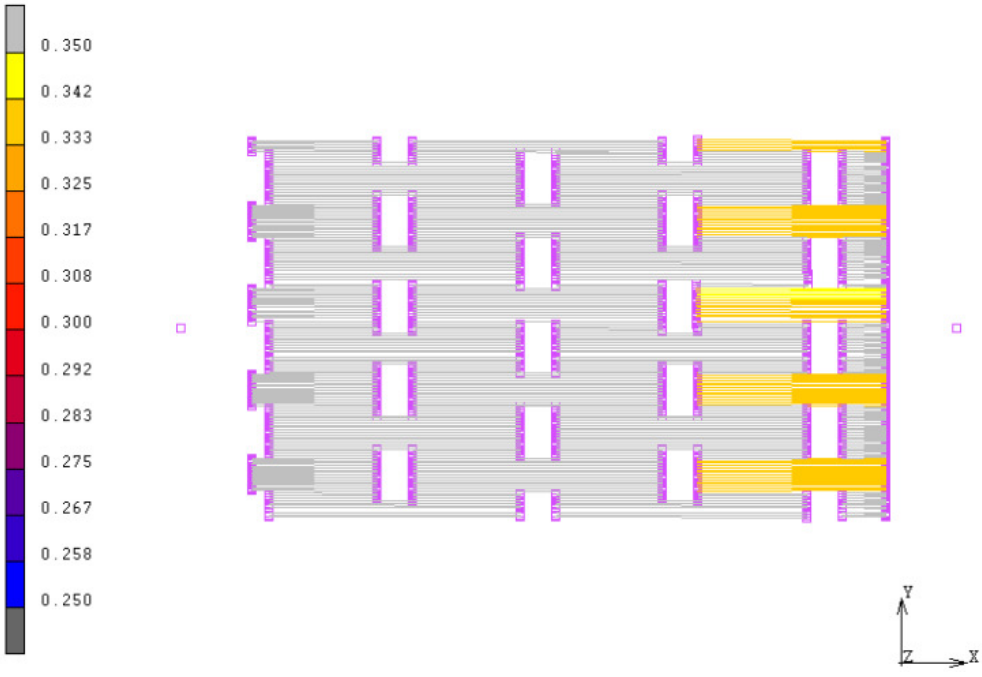

Figure 9.11. Distribution of strain of fibres in the fabric at the fabric strain of 0.3 (reference model)

The reason for this behaviour can again be explained by the simple truss models. The evolution of true strain with rigid and without rigid truss elements are shown in Figure 9.12. As it can be seen, the difference in the level of true strain for the models with rigid and non-rigid fibres increases with time (extension). This explains why strains of fibres in the fabric exceed the level specified in the figures as the fabric strain is increased.

The deformation at the last step (fabric strain of 1) is shown in Figure 9.13. Apparently, at this strain level, the bond points are still aligned in vertical columns as the entire fibres align along the machine direction. Small difference can be observed in a closer view to the fabric; this is due to the difference of number of fibres passing through each bond points (Figure 9.14).

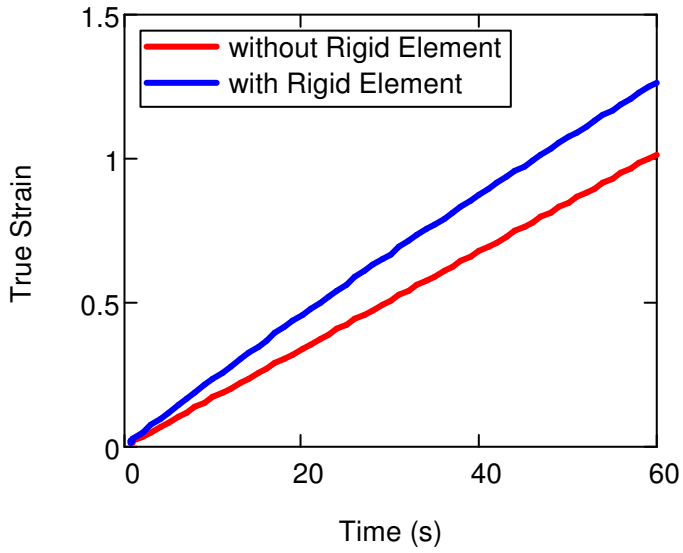

Figure 9.12. Evolution of true strain values in simple truss models

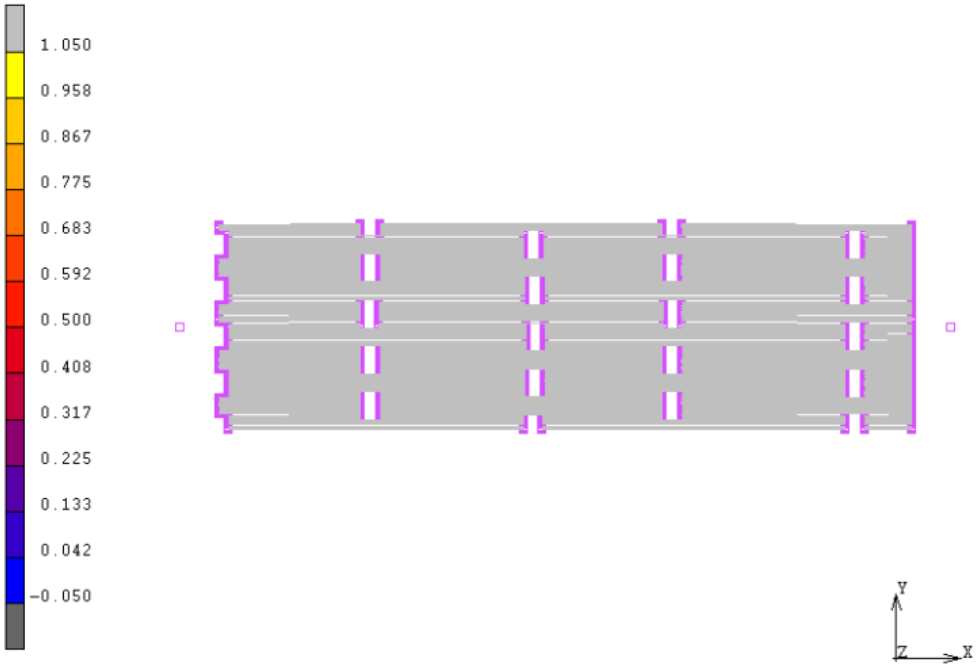

Figure 9.13. Distribution of strain of fibres in fabric at fabric strain of 1 (reference model)

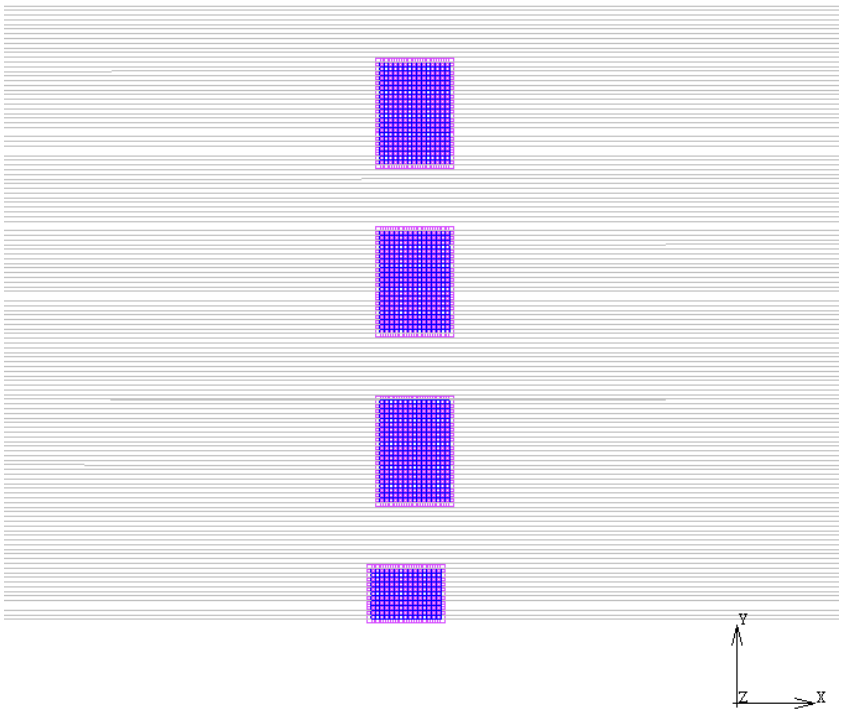

Figure 9.14. Alignment of bond points in fabric at strain of 1 (reference model).

The normal and cumulative distribution functions of strains for each interval of fabric strains are shown in Figure 9.15. As it can be seen from Figure 9.15a, the difference between fibre strains of the fibres at the peak value and corresponding fabric strain values are increasing, confirming that the distribution was shifting to the right. As the difference in strain levels for short and long fibres was increasing, the randomness of distribution increases as observed in these figures.

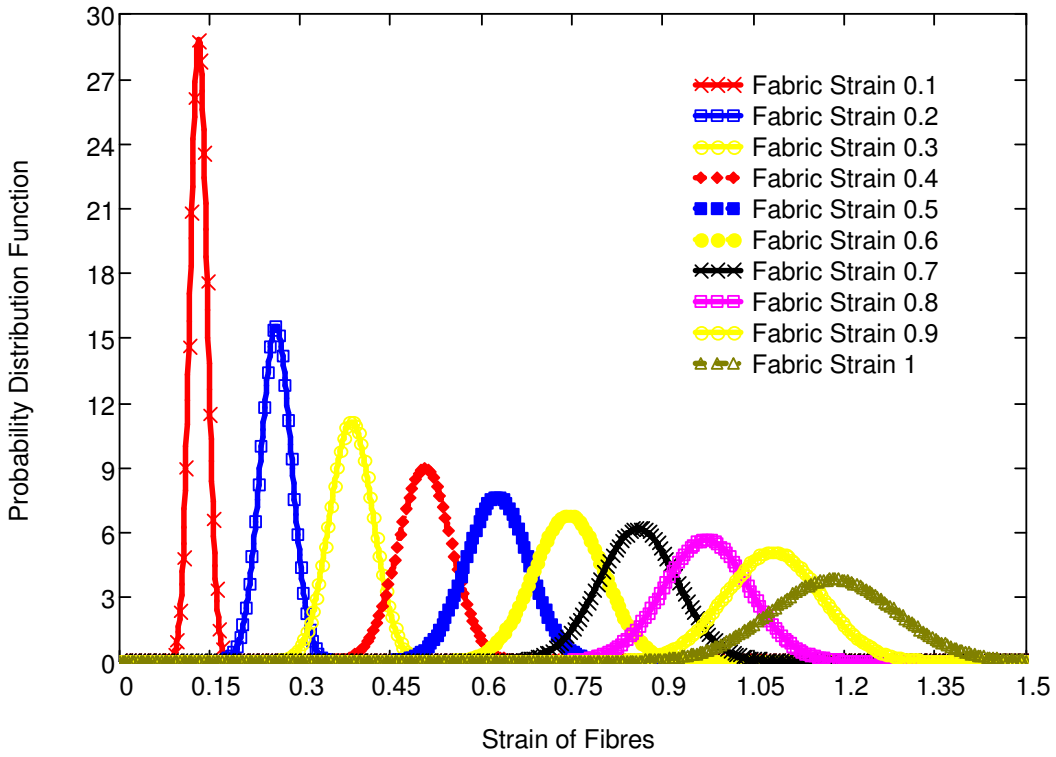

(a)

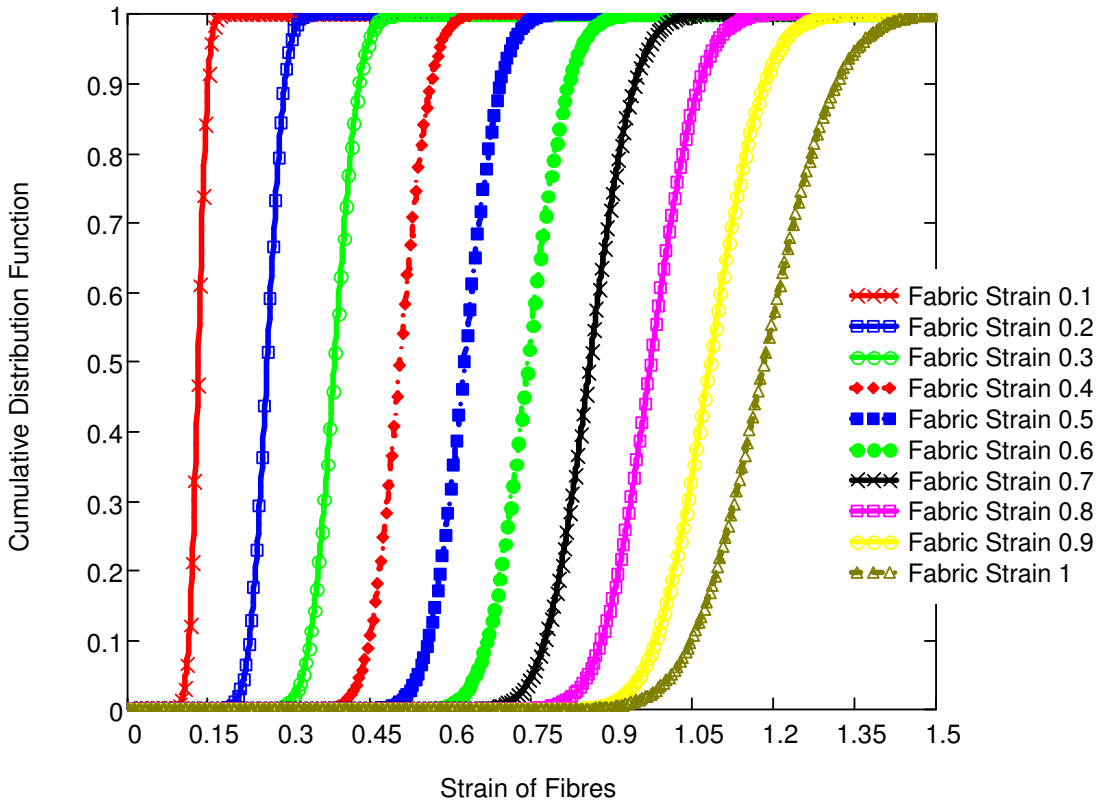

(b)

Figure 9.15. (a) Probability distribution function (b) and cumulative distribution function (b) for each interval of fabric strain (reference model)

9.3.2 Effect of mesh size (model MESH-I)

In this model the mesh size was reduced to 0.02 mm instead of 0.05 mm to study the effect of this variation on the distributions. At the same time, the shift tolerance (mentioned in Chapter 7) was changed by the same value as they are related to each other. A closer view to one of the bond points showing the fined mesh structure is presented in Figure 9.16.

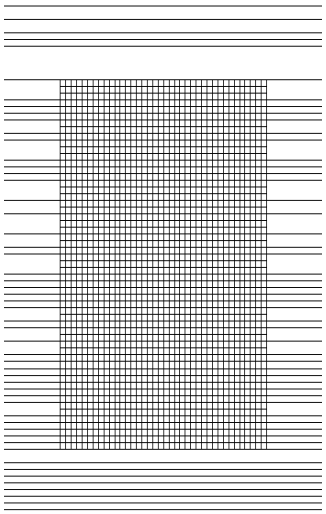

Figure 9.16. Mesh of bond points in model MESH-I

The respective statistical results are shown in Figure 9.17 until the fabric strain of 0.4. As seen, the same behaviour was observed as for the reference model. This behaviour proves that increasing the mesh of bond points does not change the distribution of fibre strains.

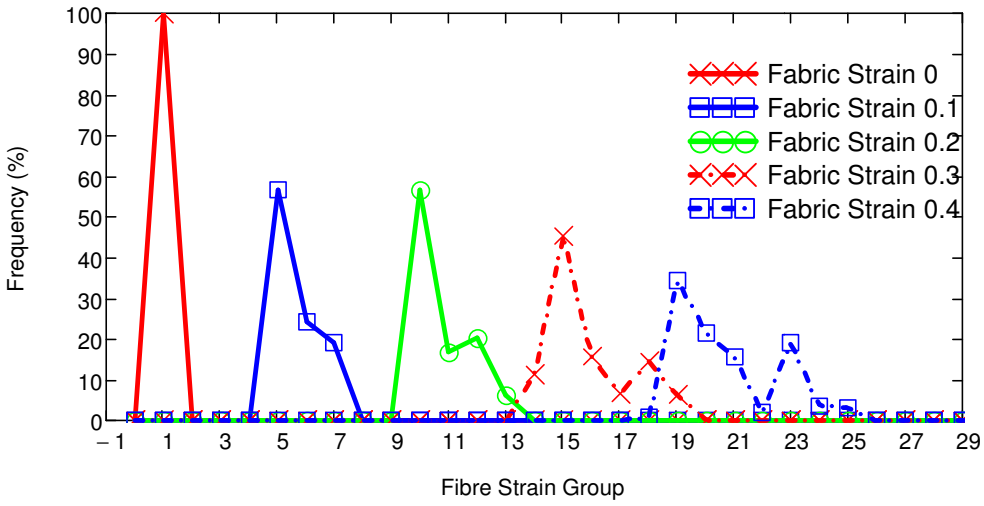

Figure 9.17. Distribution of strains for fibres for various values of fabric strain (model MESH-I)

9.3.3 Effect of Fibre Length (Model FL-I)

In this model, the continuous fibres were replaced with fibres with a length of 10 mm. The obtained distribution for fibre strains is shown in Figure 9.18. Compared to the Figure 9.6 for the reference model, it can be observed that the fibre strains in this model had a more random distribution. As the length of each fibre was limited, they were not connected to all the bond points situated along a specific horizontal direction. As a result, some bond points had number of fibres different from that of others. This random behaviour is shown at a fabric strain of 0.4 (Figure 9.19). Another observation is that at fabric strain exceeding 0.6, some of the fibres started having less strain than others as shown in Figure 9.18(c). This behaviour can be explained by observing the deformation pattern at fabric strain of 1, shown in Figure 9.20. Apparently, the fibres on the right-hand side of the model are stretched much more than the others. This shows the right hand-side of the model is less stiff than the left-hand side. In order to explain this behaviour, another model was generated by modifying the random numbers so that more fibres were located on the right hand side of the model. The deformation result is shown in Figure 9.21. As expected, this time, the fibres on the left-hand side of the model were extended much more compared to the rest of the model. Thus, it can be concluded that the horizontal location of fibres can have an effect on the deformation behaviour and strain distribution of fibres especially when the fibres are shorter.

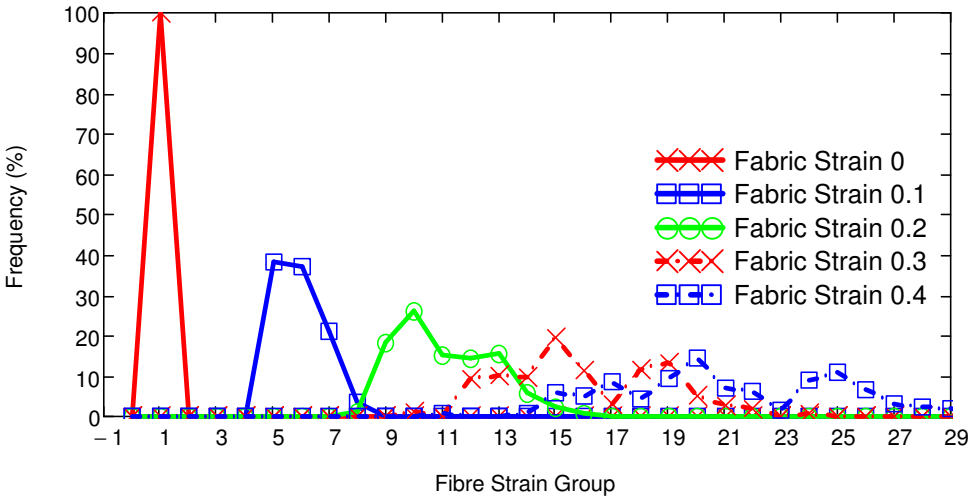
Frequency (%)
Fibre Strain Group
Fabric Strain 0
Fabric Strain 0.1
Fabric Strain 0.2
Fabric Strain 0.3
Fabric Strain 0.4

(a)

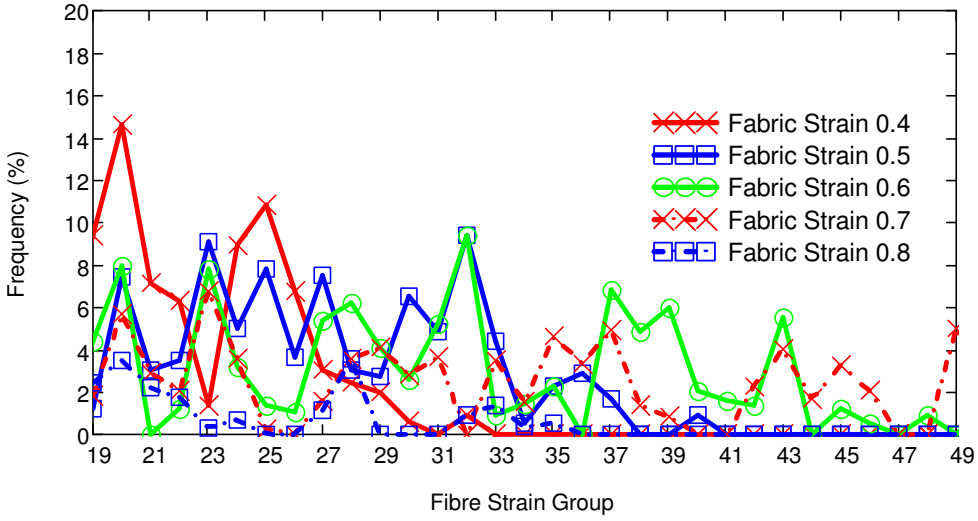
Frequency (%)
Fibre Strain Group
Fabric Strain 0.4
Fabric Strain 0.5
Fabric Strain 0.6
Fabric Strain 0.7
Fabric Strain 0.8

(b)

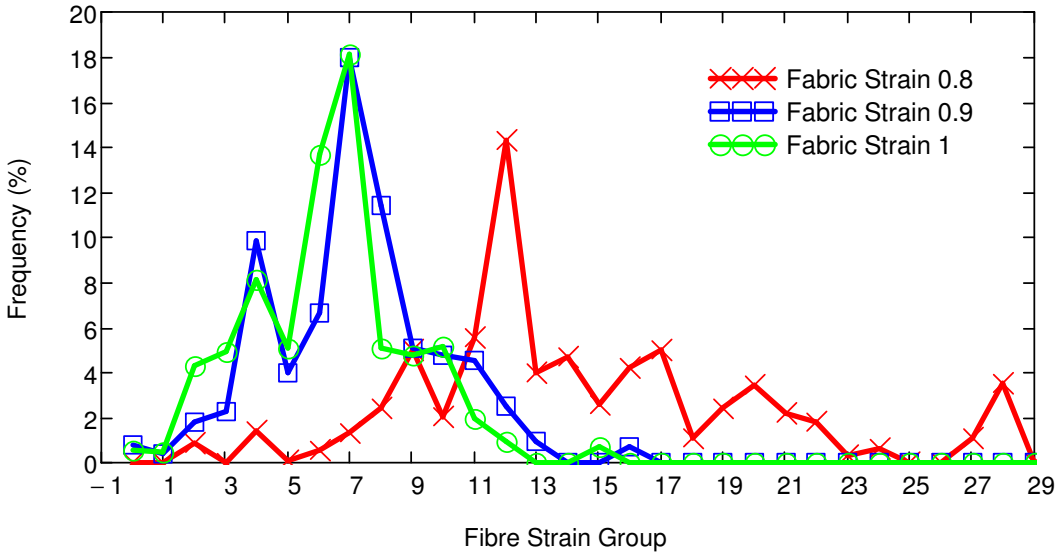

(c)

Figure 9.18. Strain distribution of fibres for various values of fabric strain (model FL-I): (a) 0-0.4; (b) 0.4-0.8, (c) 0.8-1

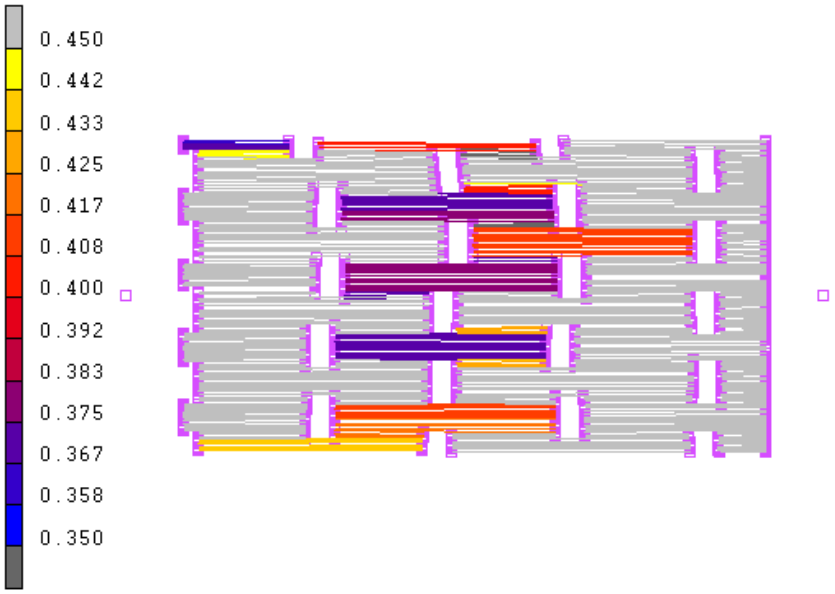

Figure 9.19. Strain distribution of fibres in the model at fabric strain of 0.4 (model FL-I)

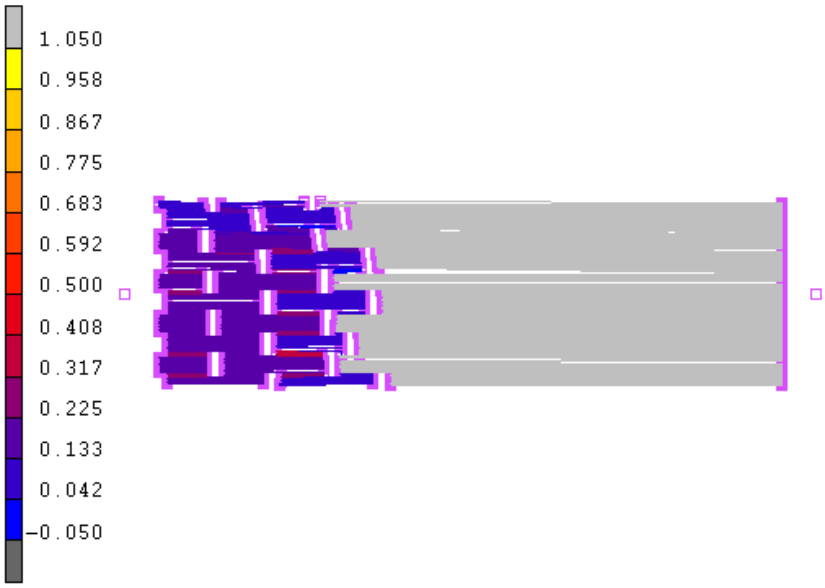

Figure 9.20. Distribution of strains for fibres in model at fabric strain of 1 (model FL-I)

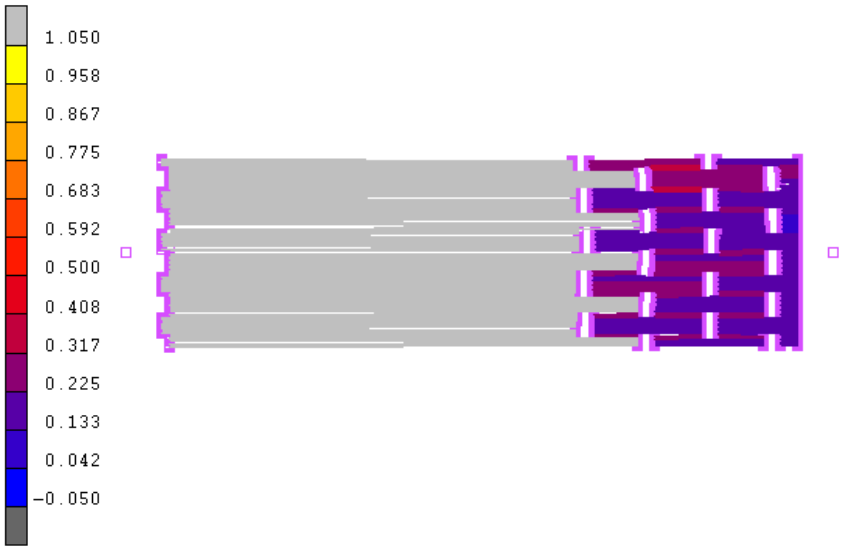

Figure 9.21. Distribution of strains for fibres in model at fabric strain of 1 (model FL-I but most fibres are located on right-hand side)

9.3.4 Effect of Fabric Density (Model FD-I)

The fabric density was reduced to 10 g/m^2 in the next model by the respective reduction in the number of fibres. As it can be seen from the obtained results, no

major change in the distribution was observed in this case (Figure 9.22). This confirms that even modelling the fabric with 10 g/m^2 of density is enough for the fibres to demonstrate similar deformation behaviour compared to the denser fabric models.

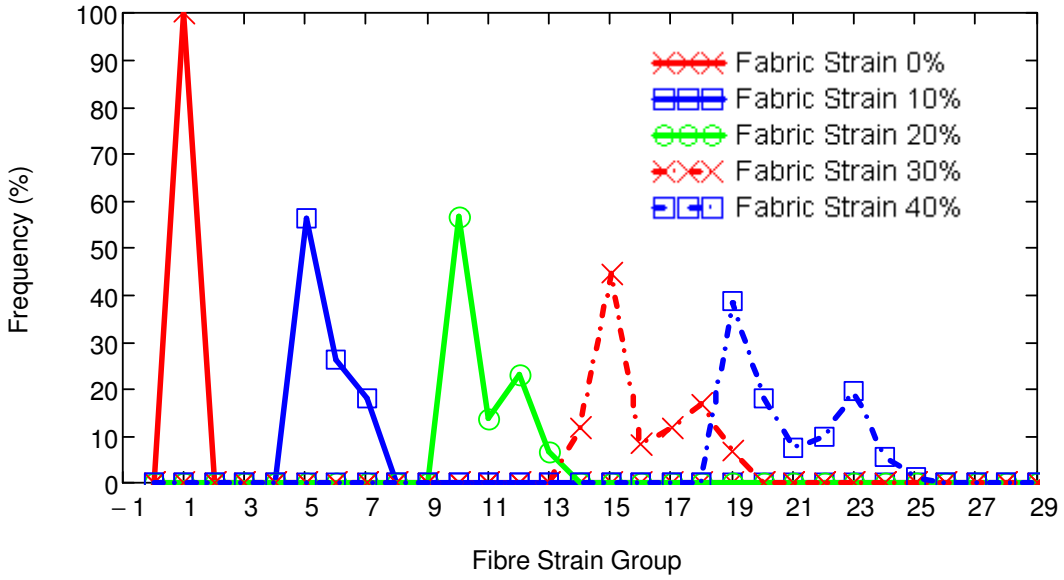

Figure 9.22. Distribution of strains for fibres in model at fabric strain (model FD-I)

9.3.5 Effect of Width of Bond Points (Model BPW-I)

In this study, the width of bond-points was increased to 1.5 mm and the width gap was reduced by the same amount. Statistical results are shown in Figure 9.23. It can be seen that more fibres had higher strain levels than the fabric strain compared to the reference model. For example in Figure 9.23, at fabric strain of 0.1, there were more fibres in group 7 when compared to the results obtained for the reference model. This behaviour was observed also for the other values of fabric strain.

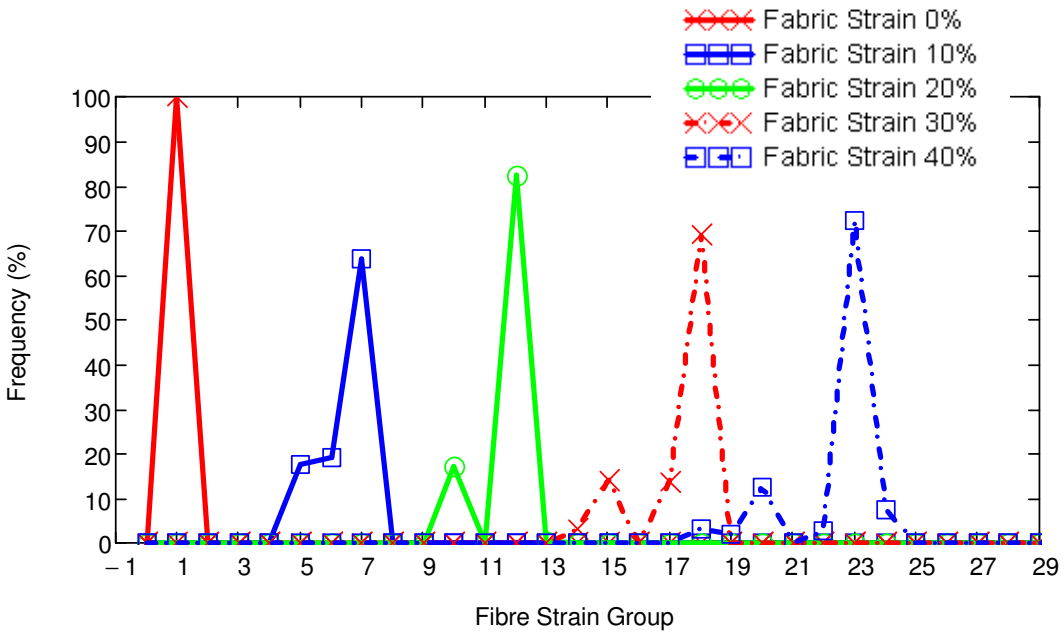

Figure 9.23. Distribution of strains for fibres in model at fabric strain of (model BPW-I)

The reason of this behaviour can be explained by the analysis of the deformation behaviour shown in Figure 9.24. As seen, there are much more short fibres than the reference model because bond points occupy more space in vertical direction. This confirms the importance of arrangement of bond points on the strain distribution and stiffness of the whole fabric. There are some studies indicating that when the area of bond points increase, the stiffness of the fabric increases as well (Bhat *et al.* 2003, Mi & Batra). Although the present model agrees with that previous study, it was shown that the arrangement of bond points plays a significant role for the strain distribution in the fabric.

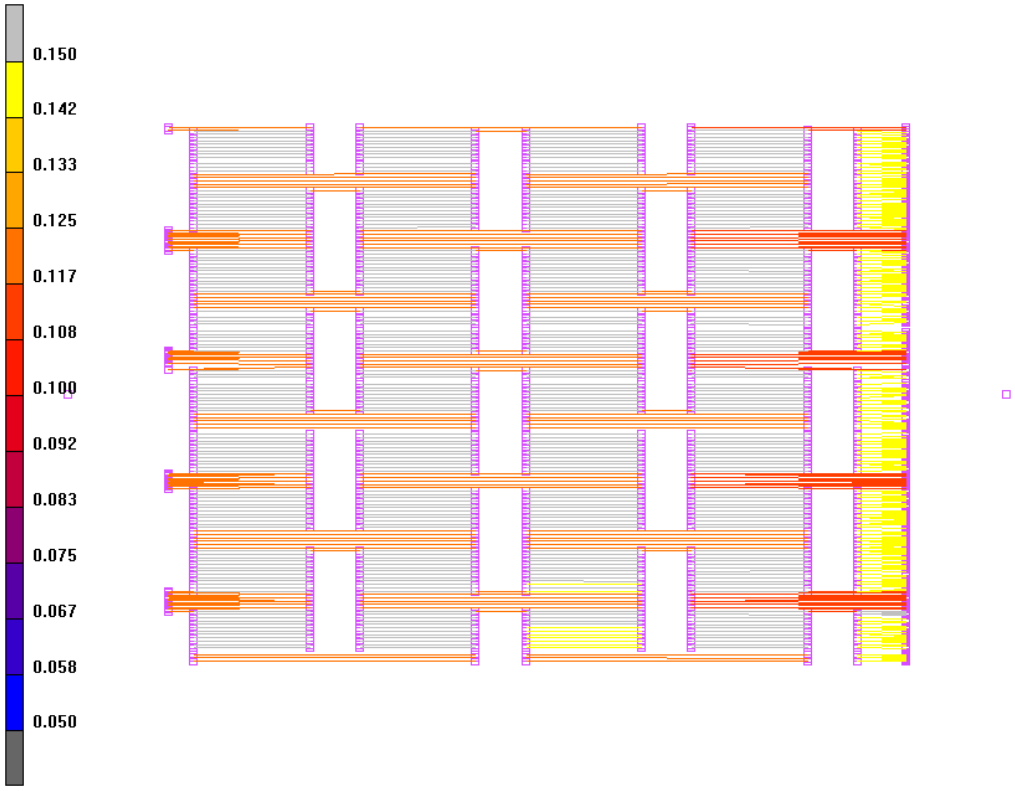

Figure 9.24 Distribution of strains for fibres in model at fabric strain of 0.1 (model BPW-I)

9.3.6 Effect of Length of the Bond Points (Model BPL-I)

In this model, the length of bond points was increased to 1.022 mm and the width gap was reduced by the same amount. The obtained statistical results are shown in Figure 9.25. As bond points occupy more space, they caused more strain in the fibres similar to the case of model BPW-I; however, the effect was lower. A change in bond point width causes more long fibres to become short fibres, which affects strongly the statistical results. In the current situation, the number of short and long fibres did not change. But the fibres become shorter with a certain ratio as width of bond points is increased. Thus, the effect may be less in this case compared to the change in BP width. However, as stated previously, the arrangement of bond points has a very strong effect and the effect of change of bond point dimensions is

significantly dependent on the arrangement of them which was also discussed in Hou (2010).

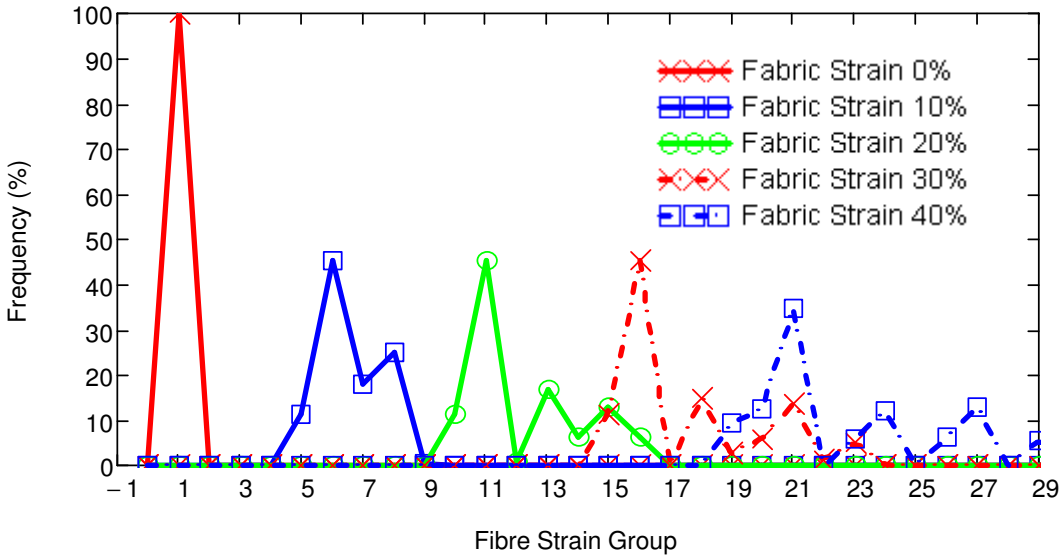

Figure 9.25. Distribution of strains for fibres for various values of fabric strain (model BPL-I)

9.3.7 Effect of Stiffness of Fibres (Model FM-I)

In this model, the Young's modulus of fibres is assigned the value equal to 1/10th of that in the reference model in order to observe the differences. The respective statistical results are shown in Figure 9.26. As expected, the figure is nearly the same as the figure obtained for the reference model. It can be concluded that the fibre stiffness does not affect the results. However, this statement is true as long as stiffness of bond points is much larger than that of fibres to be assumed as rigid.

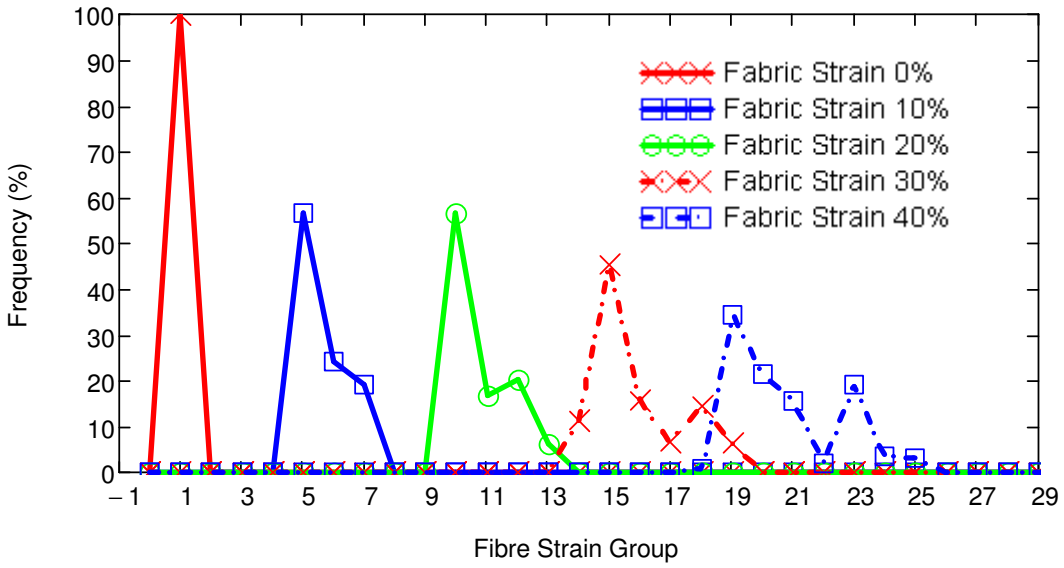

Figure 9.26. Distribution of strains for fibres for various values of fabric strain (model FM-I).

9.3.8 Effect of Stiffness of Bond Points (Models BPM-I, BPM-II)

At this stage of analysis, initially, the Young's Modulus of bond points was kept at the same level as for fibres (model BPM-I). It was seen that the behaviour of fibres did not change indicating that the bond points were still too stiff because of their geometrical shape. The cross-sectional area of each fibre is 3.1 x 10^{-4} mm^2, whereas that of the bond points is 2.2 x 10^{-2} mm^2. After this analysis, Young's modulus of bond points was further reduced to $1/10^{th}$ of that of the fibres (model BPM-II). The statistical distribution is shown in Figure 9.27. When compared with the respective data for the reference model (Figure 9.6), it can be observed that strains of fibres decrease for the same levels of fabric strain. As the bond points are not rigid anymore, they stretch with the fibres; thus decreasing the strain on the fibres. In the deformation behaviour shown in Figure 9.28, it is apparent that bond points were stretched along tensile direction and contracted along vertical direction because of the Poisson's effect. This caused the short fibres to rotate during stretching.

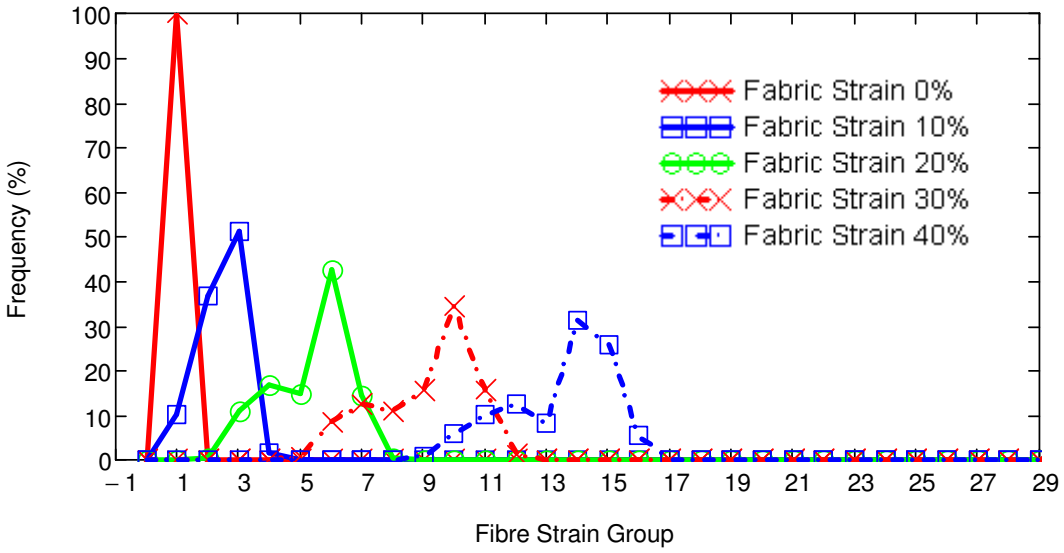

Figure 9.27. Distribution of strains for fibres for various values of fabric strain (model BPM-II)

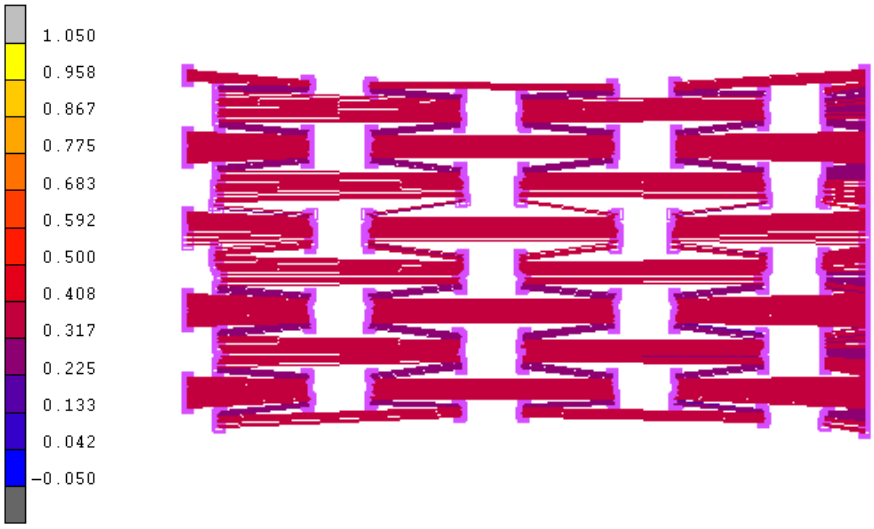

Figure 9.28. Distribution of strains for fibres at fabric strain of 0.4 (model BPM-II)

9.3.9 Account for Plasticity for Fibre Material (FM-II)

The entire stress-strain curve from the tensile test with the highest loading rate was implemented for the fibres to analyze their effect on the stress-strain behaviour; the obtained statistical results are shown in Figure 9.29. It can be seen that until a fabric strain 0.3, the behaviour is very similar to that of the reference model. In the first

stages of loading, the plasticity effects were not present so this similarity was expected. After reaching fabric strain of 0.3, with the effect of plasticity, more random distribution of strains were obtained when compared with the reference model. The deformed fabric with the distribution of strains at a fabric strain of 0.7 is given in Figure 9.30. As it can be seen, some fibres extended too much and as the tensile load continues, those fibres extend more and more, leaving the rest of the fibres with far lower strain. This is the result of accounting for plasticity. When a fibre is stretched in plastic region, its instantaneous module decreases and it stretches more. In order to understand this behaviour, analyses were performed again with simple truss models. Shown in Figure 9.31, two models were generated, each with three elements connected end-to-end. The rightmost element in each model had a high elastic modulus. The other two, equal-length elements were modelled, in one model, with a fully elastic material behaviour (Figure 9.31a), and in the other model, with an elasto-plastic behaviour (Figure 9.31b). According to the results in Figure 9.32, in the model with elastic elements, both elements extended by the same amount whereas in the model with elasto-plastic material behaviour, the one on the right extended much more than the other although they had the same material property and equal length. This may be due to the numerical calculations. During iterative calculation procedure, the stiffness of one of those fibres could be calculated marginally lower than the other. As the instantaneous module decreases by extension, the gap between the stiffness values of those fibres increases. Thus, the same behaviour of fibre elements can be observed in the global behaviour of the nonwoven model, FM-II.

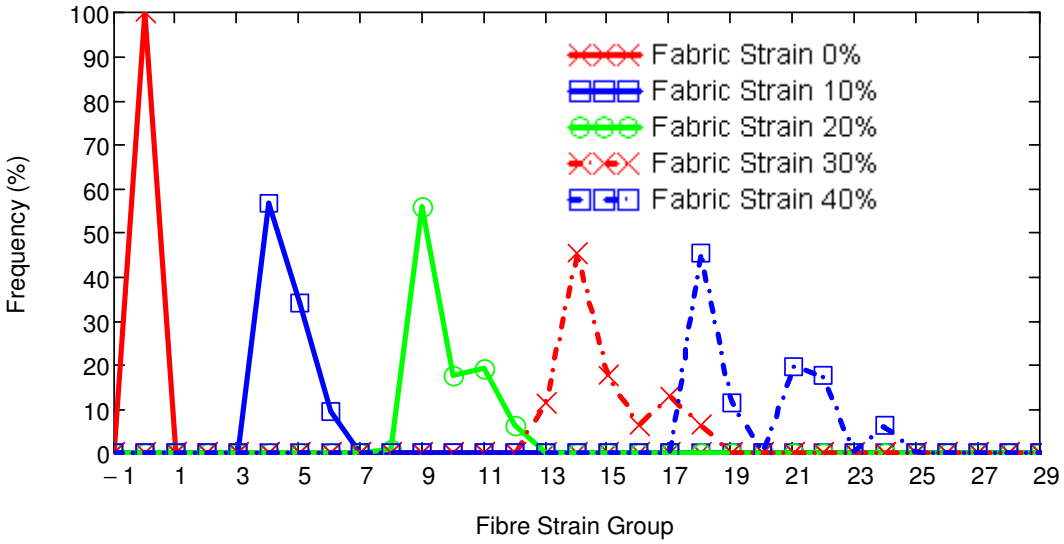

(a)

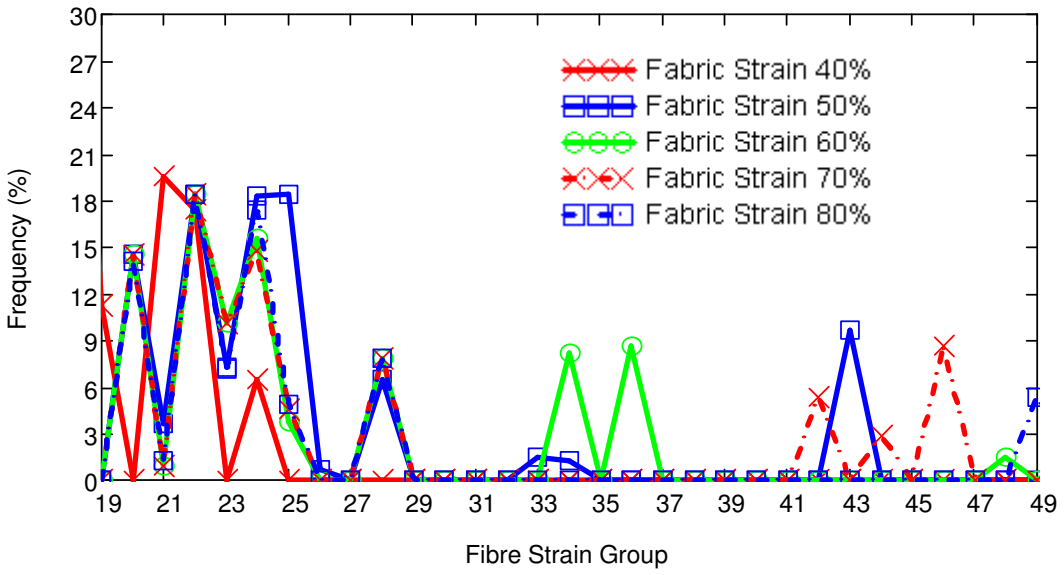

(b)

Figure 9.29. Distribution of strains for fibres for various values of fabric strain (model FM-II): (a) 0-0.4; (b) 0.4-0.8

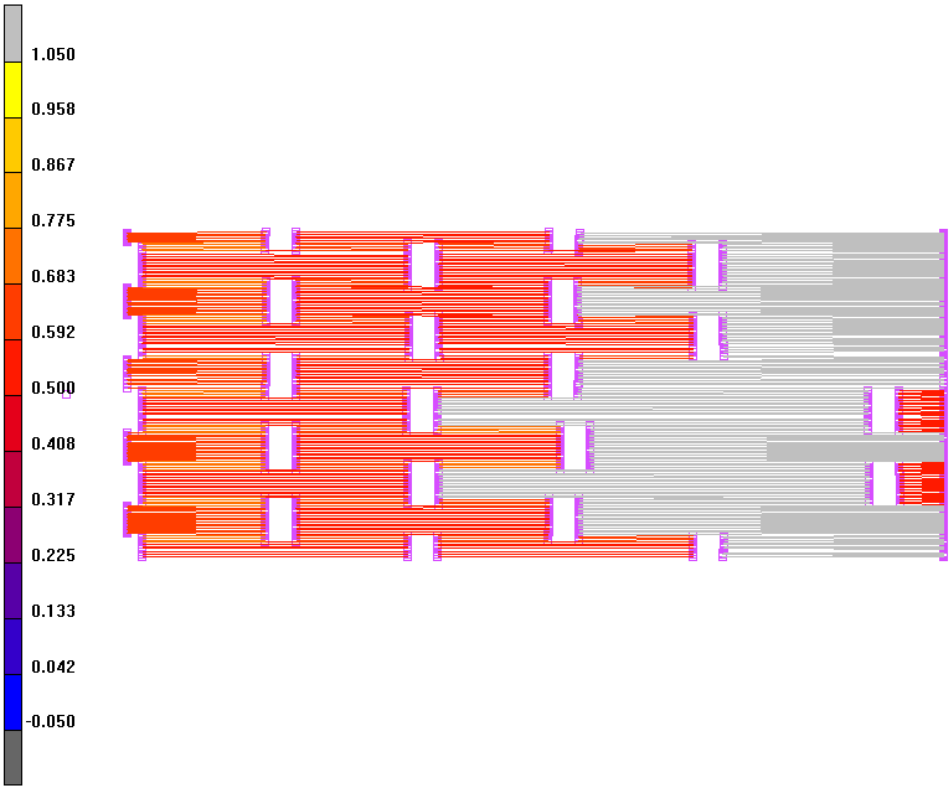

Figure 9.30. Strain distribution of fibres at the fabric strain of 0.7 (model FM-II)

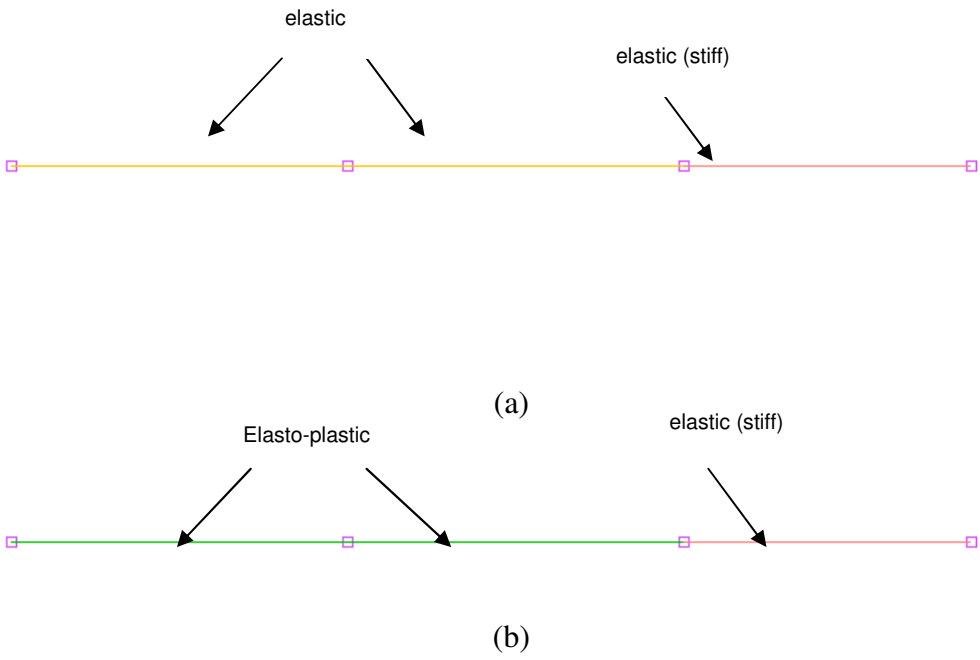

Figure 9.31. Simple truss models with material: (a) elastic; (b) elasto-plastic

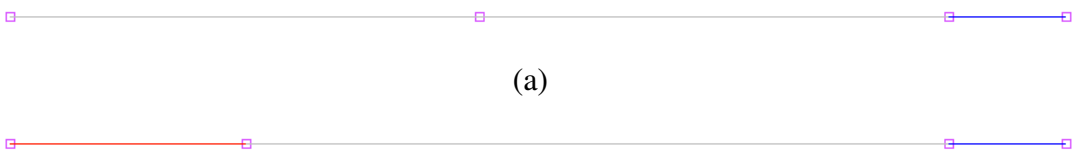

(a)

(b)

Figure 9.32. Simple truss models analysis deformation results for simple truss models with material: (a) elastic; (b) elasto-plastic

9.3.10 Effect of Tensile Rate (Models FV-I_TSR-I, II, III)

One of the important considerations is the effect of the test speed on the distribution of strains. In order to observe this effect, creep properties were assigned to the fibres. Bond points were still kept as rigid and the elastic behaviour was implemented linearly. Simulations were performed with decreasing the test rate by a factor of 10 (TSR-I), 100 (TSR-II) and 1000 (TSR-III). The distribution results for the model TSR-III are shown in Figure 9.33. According to the results, no significant variation was observed when compared with the reference model. There is a very slight decrease in the strain level which can be attributed to using adaptive time stepping in this model instead of fixed time step during analysis because of implementing the creep model (Marc Analysis Research Corporation, 2007). The deformation behaviour at fabric strain of 1 is shown in Figure 9.34. As it can be seen, the behaviour is very similar to the reference model and the bond points still keep the vertical orientation. A similar behaviour was observed with the other tensile rates as well. It can be concluded that the tensile rate does not have a significant effect on the strain distribution. However, modelling of creep affects the stresses in a great manner. Thus, in the next section, the distribution of stresses was studied for these models in which the creep properties were assigned to the model.

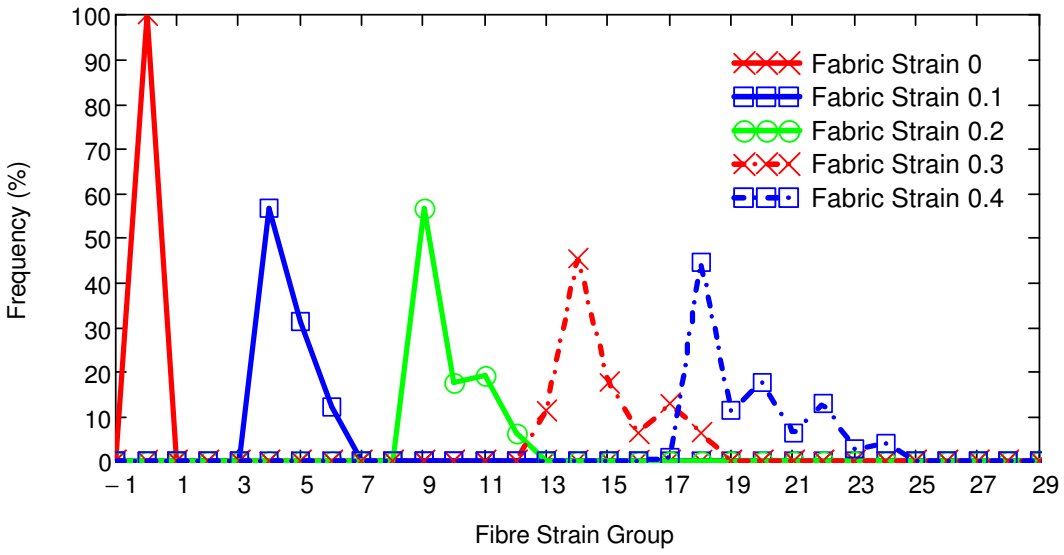

(a)

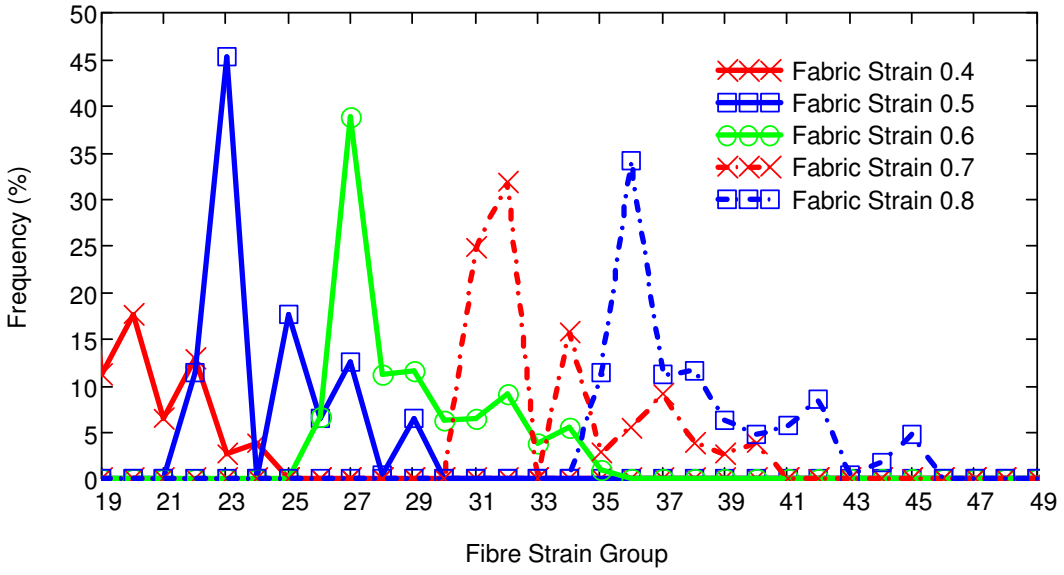

(b)

Figure 9.33. Distribution of strains for fibres for various values of fabric strain (model FV-I_TSR-III): (a) 0-0.4; (b) 0.4-0.8

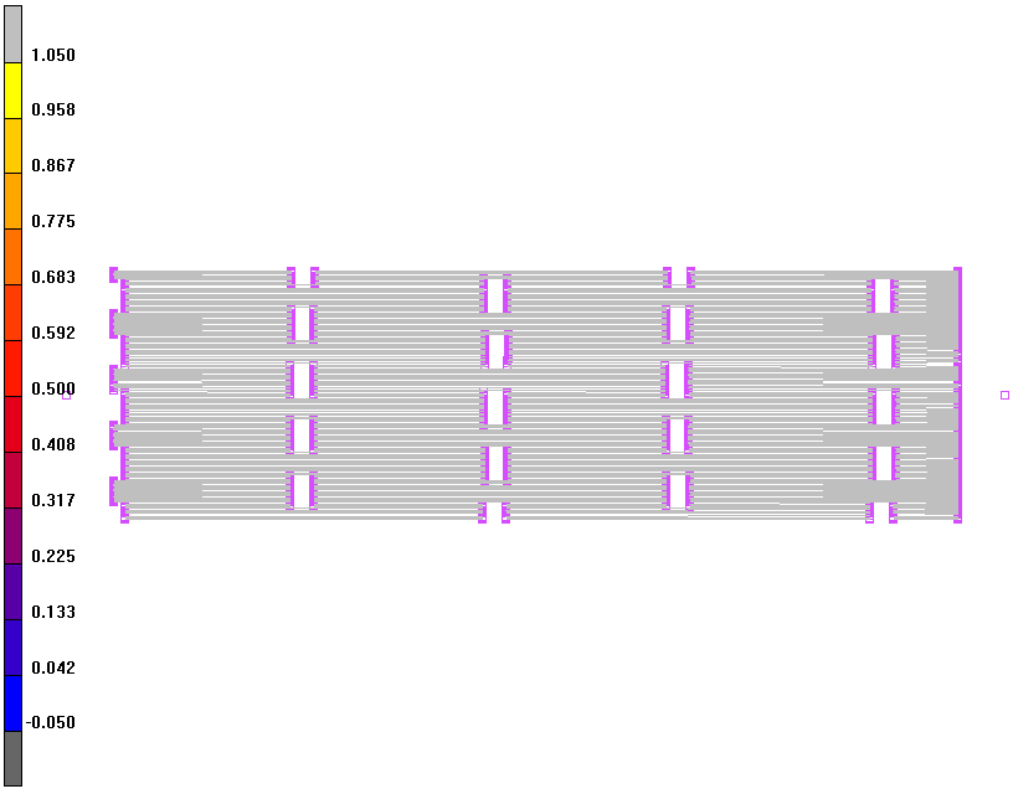

Figure 9.34. Distribution of strains for fibres at the fabric strain of 1 (model FV-I_TSR-III)

9.3.11 Effect of Creep on the Stress Distribution of Fibres

In linear elastic models, the stress distribution is the same as the strain distribution as a linear constitutive relation exists between stress and strain tensors. In the materials showing creep behaviour, the values of stresses can change significantly depending on the loading rate. As shown in Chapter 5, fibres of nonwovens show this behaviour under tensile loading with a low speed. The creep behaviour also depends on the instantaneous stresses on the fibres. In this section, the stress distribution of fibres was examined for the models in which creep behaviour was assigned to the fibre materials (model FV-I).

Distribution of stresses for fibres for various values of fabric strains for the reference model is presented in Figure 9.35. In this figure, fibre stress group represents 60 equal intervals until the maximum stress value obtained in the simulation. The stress values in the models FV-I were expected to be lower than the models with linear

elastic fibres especially for the loading with a low tensile strain rate. If the stress groups were kept constant, there would be many fibres in the same group for models FV. This would give misleading information regarding the stress distribution of fibres. In order to prevent this situation and to be able to compare the distribution of stresses with different models, stress groups were assigned as such.

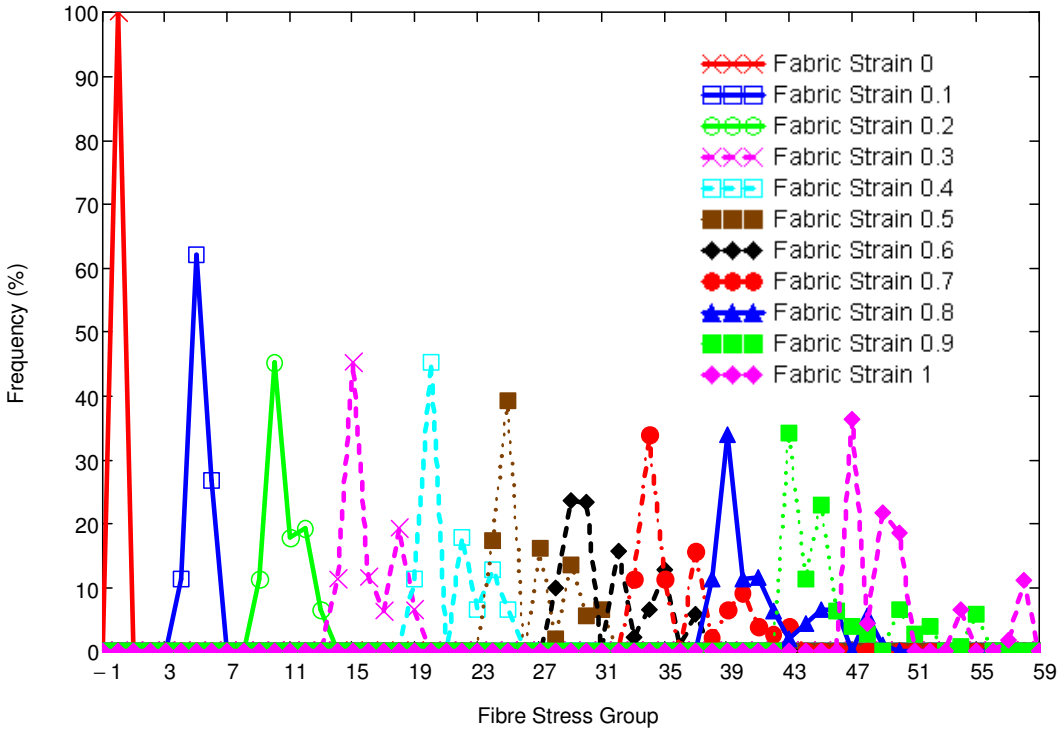

Figure 9.35. Distribution of stresses for fibres for various values of fabric strain (reference model)

The distribution of stresses for the model FV-I, TSR-III is shown in Figure 9.36. The maximum stress was obtained as 24 MPa as a result of the effect of creep behaviour in the fibres. Apparently, most of the fibres were in the same strain group after a fabric strain of 0.3. This reveals an interesting effect of implementing the creep behaviour. Fibres having more stress tend to have more creep because of stress and time dependency of creep strain rate (i.e., their stiffness decreases much more compared to the fibres having less stress). Thus, the load is transferred to the fibres which are stiffer (or have low stress). This results in more homogenous distribution

of stresses in the structure. It can be concluded that the creep behaviour of fibres causes a more homogenous distribution of stresses in the fibres of nonwovens.

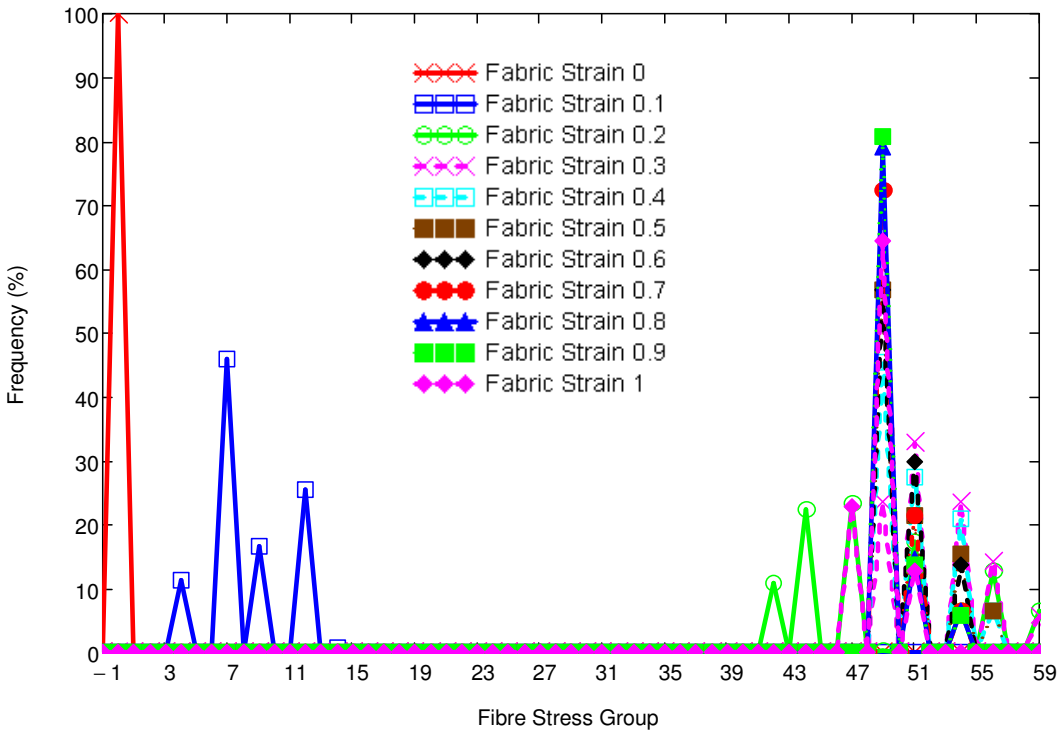

Figure 9.36. Distribution of stresses for fibres for various values of fabric strain (FV-I, TSR-III)

The distribution of stresses for the model FV-I, TSR-I is shown in Figure 9.36. The maximum stress was obtained as 370 MPa in this case. The distributions are close to the reference model. This implies that the test speed was not slow enough for creep behaviour to be effective in the distribution of stresses for this type of loading.

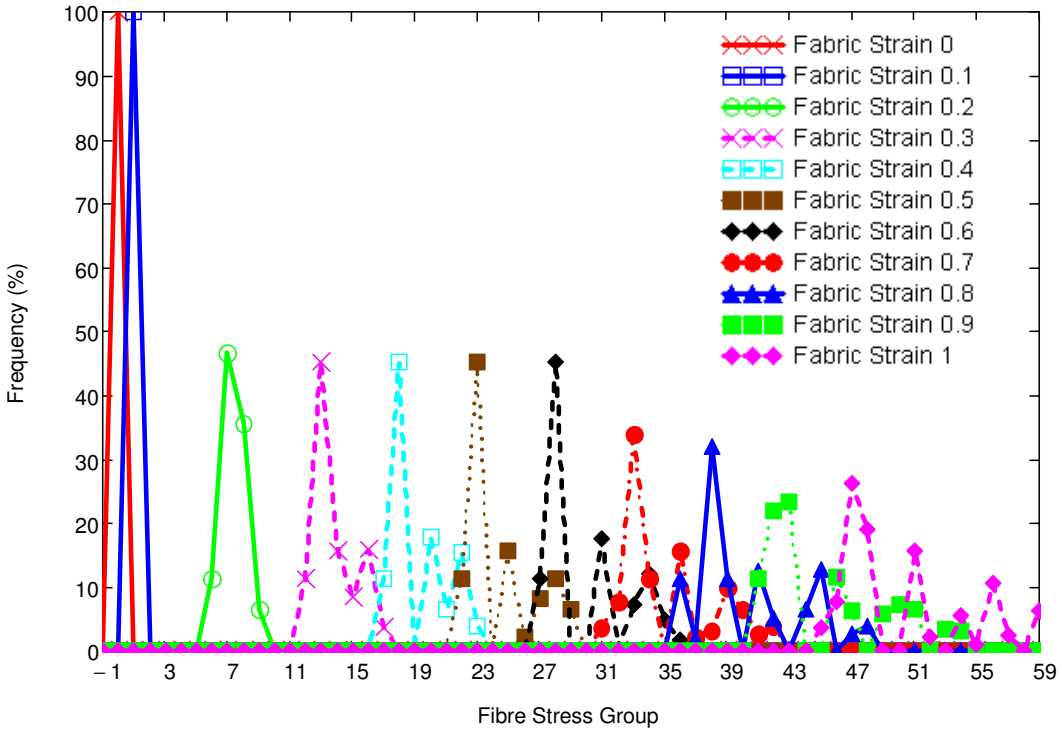

Figure 9.37. Distribution of stresses for fibres for various values of fabric strain (FV-I, TSR-I)

9.3.12 Effect of Random Orientation Distribution (ODF-I)

After studying the effect of individual parameters on the strain distribution for the regular model, the next objective was to observe the effect of random distribution of fibres. As shown in Figure 9.38, more random distribution was observed for fibre strains for all fabric strains, compared to the regular model. This was an expected result as fewer fibres were oriented along the loading direction. Some of the fibres had lower strain as they should rotate towards the loading direction. At fabric strain of 0.1, approximately 4% of fibres were still in the strain group of 0 indicating that they had no or very low strain. In addition, 1.7% of fibres were in the strain group, -1, which means there were some fibres under compression. Shown in Figure 9.39, those were the fibres oriented towards the cross direction. In a detailed view in Figure 9.40, it can be observed that some of the fibres which were oriented perpendicular to the stretching direction were exposed to low or compression strain. The maximum strain levels were observed in the short fibres oriented towards

machine direction which was expected due to the results of the reference model. These fibres are expected to fail in the first place.

Another point to mention is that there was a lateral contraction of the fabric, which was not seen in the regular model. This can be observed clearly at high values of fabric strain (Figure 9.41). Similar behaviour was also observed during the tests. Thus, we can conclude that the fibres oriented other than the loading direction is responsible for the lateral contraction.

Another interesting behaviour can be observed in Figure 9.38c. As, shown at fabric strains, 0.8, 0.9, and 1, significant fraction of fibres were in group 58 in contrast to the reference model. The randomness caused some fibres to stretch to extreme levels. Most of these fibres lie at the longitudinal sides of the fabric (Figure 9.41). An instant when the fibres started to fail during a tensile test is shown in Figure 9.42. It is possible to observe some free fibres on the sides indicating that they ruptured or pulled back from the bond points. This may indicate that the fibres at the sides fail earlier than the others. Having few fibres connecting the bond points which were located close to the fabric sides could be the reason for this behaviour. The failure of fibres in the inner parts of the fabric cannot be observed clearly. Thus, this finding should be confirmed with further studies.

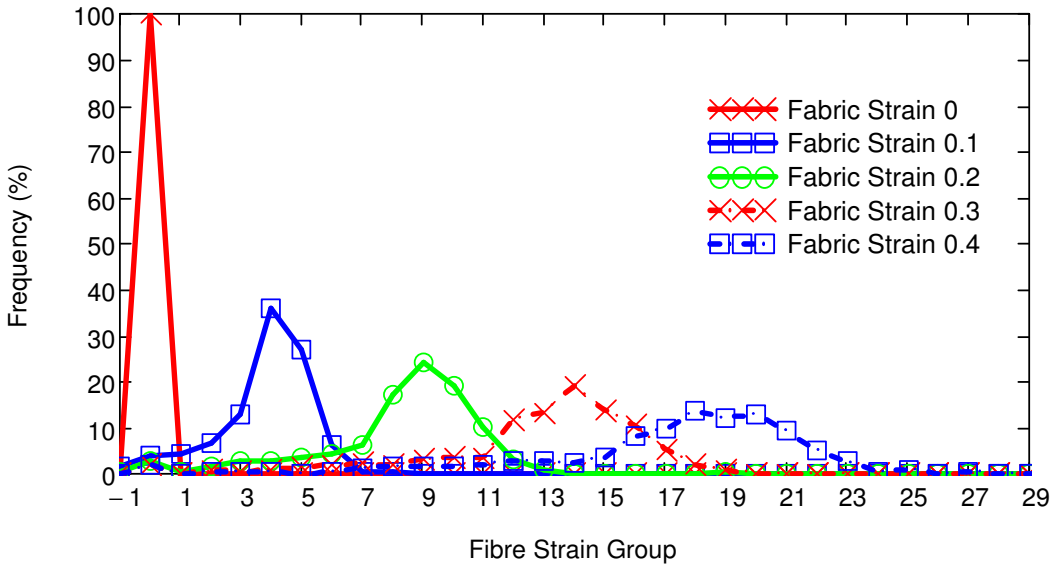

(a)

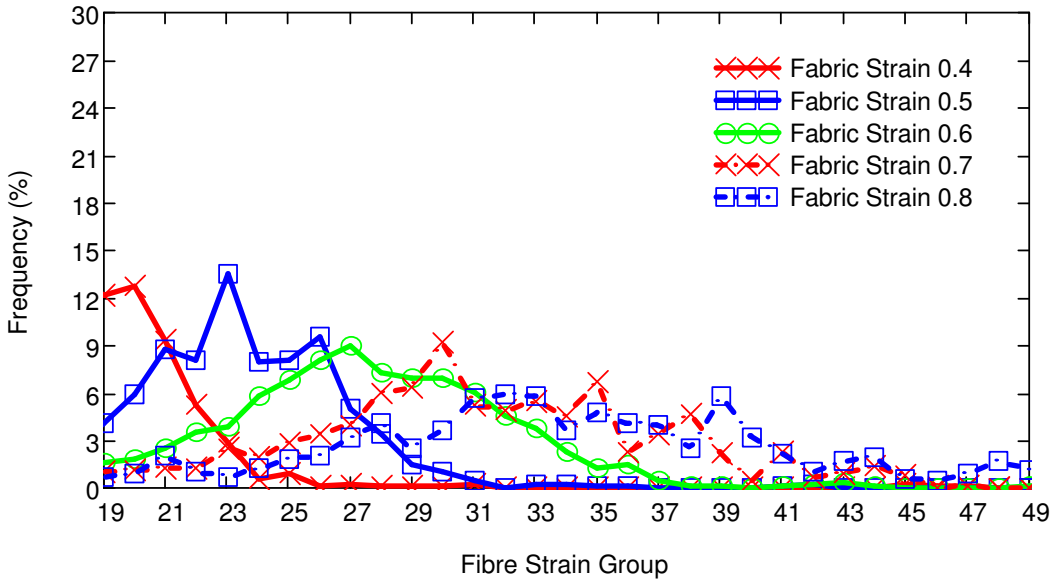

(b)

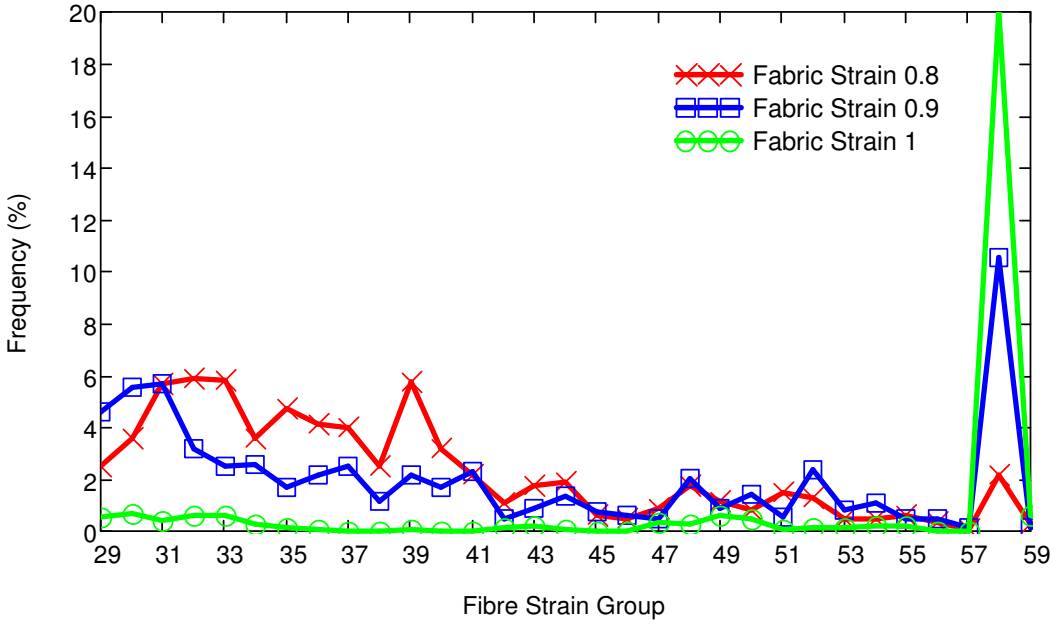

(c)

Figure 9.38. Distribution of strains for fibres for various values of fabric strain (model ODF-I): (a) 0-0.4; (b) 0.4-0.8; (c) 0.8-1

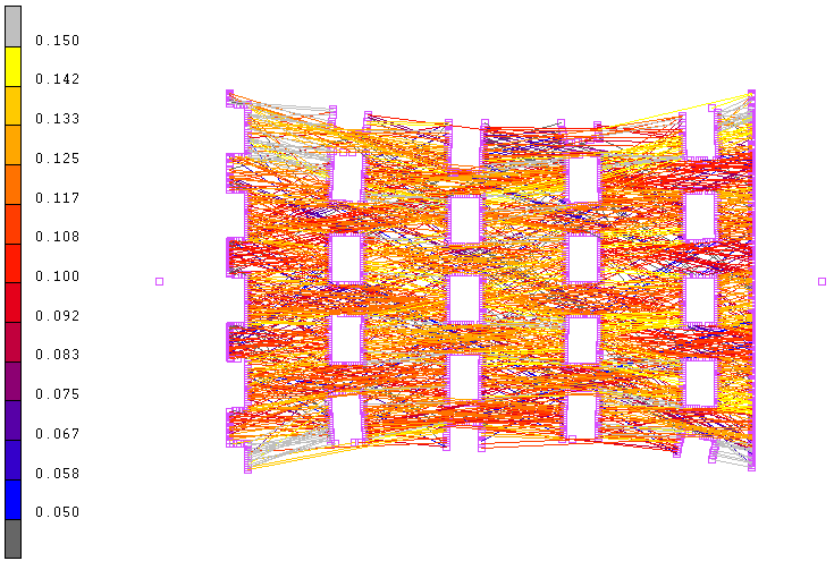

Figure 9.39. Distribution of strains for fibres at the fabric strain of 0.1 (model ODF-I)

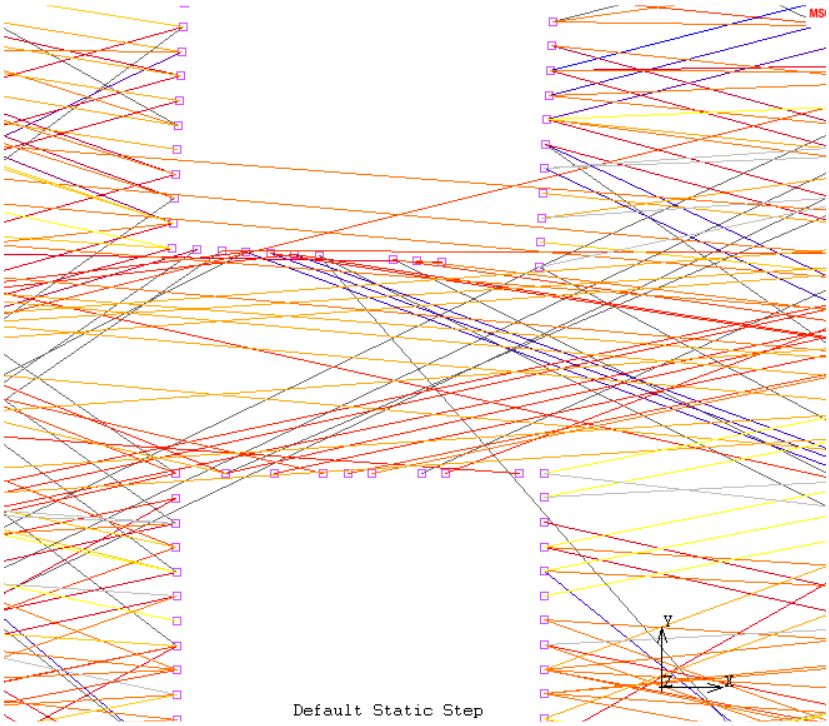

Figure 9.40. Detailed view of strain distribution at fabric strain of 0.1 (model ODF-I, see legend in Figure 9.36)

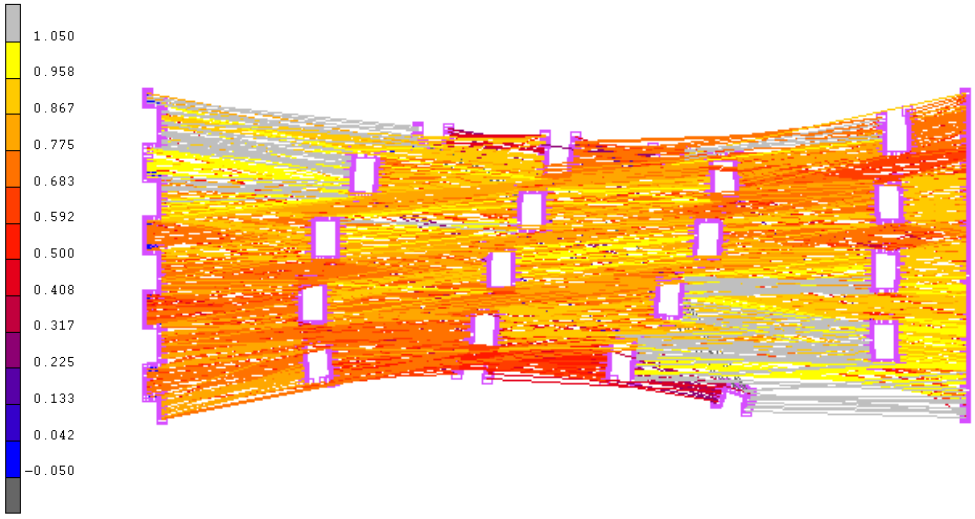

Figure 9.41. Strain distribution at fabric strain of 0.7 (model ODF-I)

Figure 9.42. Failure of fibres at sides of fabric sample in tensile test

The normal and cumulative distributions for model ODF-I are shown in Figure 9.43 and Figure 9.44, respectively. The effect of randomness can be seen clearly from these figures. The curves are much smoother when compared to the curves obtained for the reference model. This shows that the standard deviation values are much higher in the randomly distributed model as expected.

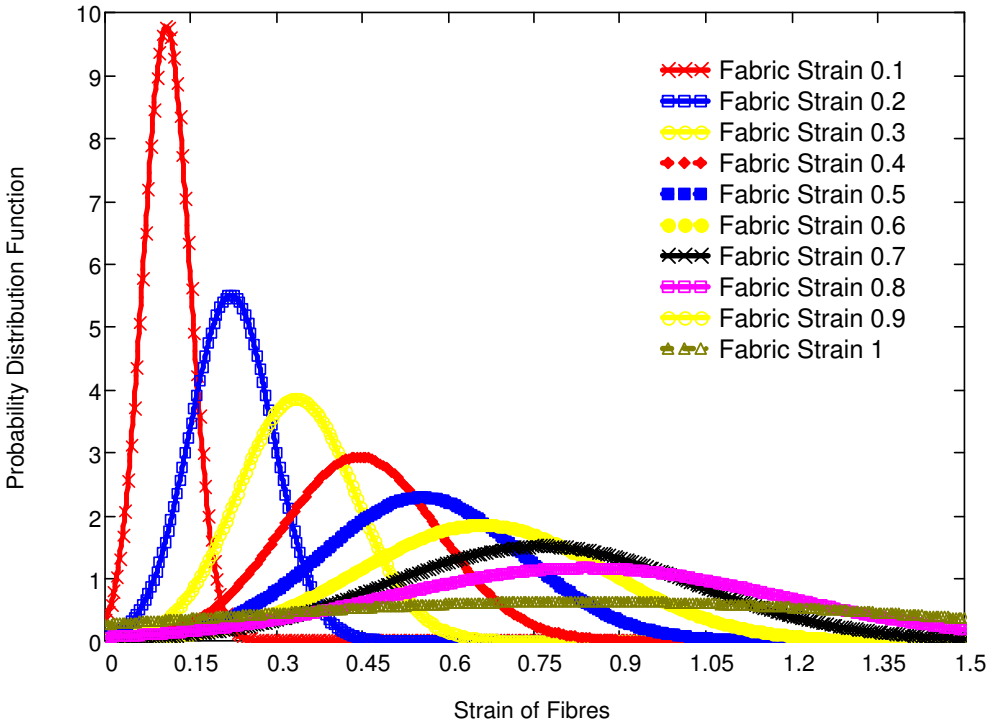

Figure 9.43. Probability distribution function for strain of fibres (model ODF-I).

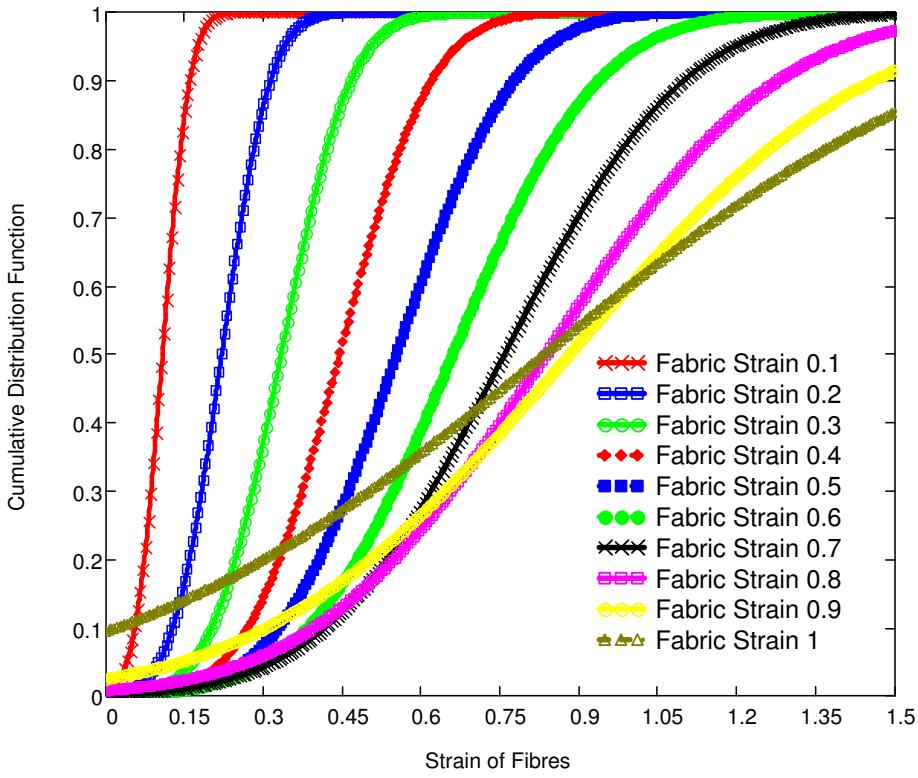

Figure 9.44. Cumulative distribution function for strain of fibres (model ODF-I).

9.4 Conclusions

In this chapter the distribution of strains for fibres inside several nonwoven types was analyzed for conditions of a tensile test using a parametric finite element model. The underlying mechanisms causing high strains in some of the fibres were explained. The effect of model parameters on the distribution of strains was investigated by performing analyses with various types of nonwoven models. Some further studies such as arrangement of bond points and the damage behaviour of fibres can reveal interesting conclusions regarding the distribution of strains and stresses in nonwoven structure.

CHAPTER 10

GENERAL CONCLUSIONS

10.1 Summary

Numerical modelling of materials is an indispensible tool for the designers to understand the mechanical behaviour of materials before the final product is manufactured. In the case of nonwoven materials, designers are faced with a more challenging study because of the complex deformation behaviour of such materials. In this study, two parametric finite element models were introduced for the structural analysis of thermally bonded nonwoven materials. The study started with the investigation of the microstructure and production methods of nonwoven materials. Then, the mechanical behaviour of these materials was analyzed by conducting a deep literature survey of previous studies about those materials. It was followed by some introduction about the scientific principles issued in the study. The studies that had been conducted until now gave some ideas for the methodology of the parametric finite element modelling. They also showed that the behaviour of these materials depended significantly on the rate of loading. The accuracy of numerical models was highly dependent on the accurate determination of material properties. Thus, this study began with understanding the rate-dependent behaviour of the basic element in the nonwoven structure - fibres. In Chapter 4, a methodology was introduced for determination of tensile behaviour of fibres according to various true-strain-rate states. It was shown that the rate-dependent behaviour of these materials is significant only during the initial stage of loading. This effect was determined in the subsequent chapter by conducting creep tests with various stress levels. A novel technique to implement the creep behaviour in the finite element model was introduced in the same chapter. After that, a finite element model was constructed parametrically employing the material behaviour obtained in the preceding chapters. Based on the analysis of the results obtained with the suggested approach, another,

more realistic modelling technique was introduced in Chapter 7. The new results showed that this new model was capable of representing the mechanical behaviour of nonwoven fabrics in a more realistic way compared to the previous one. It was also demonstrated that a nonhomogenous distribution of strains exist in the fibres under uniform loading. By using the developed method, two additional studies were conducted. In chapter 8, the effects of manufacturing, model parameters and loading conditions on the tensile behaviour of nonwovens were determined. In Chapter 9, the distributions of strains in the fibres and the factors governing these distributions were examined by conducting several analyses with various types of nonwovens.

10.2 Key Findings and Outcomes

The research performed in this study revealed many outcomes and key findings; they can be summarized as follows;

1. A methodology for the determination of the true-strain-rate-dependent tensile behaviour of fibres was introduced. Following findings were observed due to the results of this study:

a) For the polypropylene fibres, the use of the data obtained with constant engineering-strain-rate and constant-true-strain-rate tests would result in similar mechanical behaviours.

b) The rate dependent behaviour of polypropylene fibres is significant during the initial stage of tensile tests which leaded up for the determination of creep behaviour.

c) There is a high scatter in the tensile data between the fibres in the nonwoven structure.

d) The crimp on the fibres affects accurate determination of gage length during tensile tests.

2. In order to determine the viscous/creep properties of materials, a new methodology was proposed in Chapter 5, considering the initial stage of creep. The methodology is effective for implementing the creep data obtained from the tests into

the finite element model. Following key findings are obtained due to the results of this chapter:

a) The creep properties of fibres are dependent on both time and the stress level on them.

b) The properties show a great scatter due to the manufacturing operations experienced during nonwoven production.

c) Viscous effect is very severe during the initial stage of loading.

d) The creep behaviour should not be extrapolated towards plastic region. Preventing the extrapolation option for stress values can result in promising results to represent the creep behaviour in plastic region. However, a different material model should be implemented in plastic region which incorporates plasticity and creep.

3. The findings from the parametric model generated with the regular distribution of fibres are;

a) Fibre curl is an important factor governing the deformation behaviour of the studied nonwoven.

b) There is a continuous damage of bond points in the structure during deformation even at a very low strain levels.

c) A more comprehensive modelling technique is required which can handle orientation distribution and the length of fibres more accurately.

4. The parametric model developed in Chapter 7 is the main outcome of this study. The technique provides designers with capabilities to determine parameters in order to achieve the required structural behaviour before manufacturing the real product, which saves time and cost in the end. According to author's knowledge, it is the first study in the literature that handles the effect of length of fibres. The studies, presented in Chapter 8 and Chapter 9, revealed some examples of the utilization of the parametric model. It was also shown that fibre curl can be introduced into the model by distributing the material properties randomly. The model has the capability

to be extended with many further studies such as the effect of bending load, fatigue, damage etc.

5. According to the parametric studies performed with the developed model presented in chapter 8,

a) The density of fabric has a considerable effect in the deformation behaviour. The response to loading behaviour is linearly proportional to the fabric density.

b) Increasing the width of bond points causes the material to give stiffer results. However, its effect decreases as the gap between the bond points diminishes. Increasing the length of bond points causes also stiffer results in deformation behaviour but the effect is less significant compared to the increase in width of bond points. This showed that the arrangement of bond points play a significant role in the deformation.

c) Fibre length, which has been ignored in many studies, is a very crucial factor in the deformation behaviour of nonwoven materials. Its effect is also governed by the fabric dimensions. At a length, which is very large compared to fabric size, further increase in length causes a negligible change in the stiffness.

d) The dimensions of fabric sample along the machine direction affects the deformation behaviour in a great deal whereas the dimension along the cross direction affects slightly.

e) The significant creep behaviour of fibres results in different deformation results of nonwoven with various tensile strain rates.

f) The deformation behaviour of nonwoven is highly orthotropic and shows very stiffer results in machine direction compared to cross direction as confirmed by many studies.

6. In Chapter 9, the distribution of strains in the fibres reveals the mechanism of load transfer in the fibrous network of nonwovens. Factors affecting the distribution and the location of critical fibres were presented. The results of this section can be beneficial for designers to locate the critical locations for the structural integrity of

nonwovens. The results revealed many findings about the character of strain distributions. Following general points are highlighted based on this study:

a) The difference between the fabric strain and the average strain of fibres increases with increasing fibre strain, which can cause early rupture of fibres.

b) Arrangement of bond points significantly affects the strain distribution.

c) Fibre length is an important factor on the distribution of strains. As the length of fibres become shorter, the distribution of strains become more random

d) Creep properties of fibres do not contribute to the strain distribution in a great manner. However, they can cause a more homogenous distribution of stresses in the nonwoven structure depending on the loading rate.

e) The probability density and cumulative distribution functions show that the randomness (standard deviation) of fibres increases with growing fabric strain.

f) In order to achieve a more regular distribution of strains and stresses in the fibres,

- The fibres should be orientated as equal as possible,
- Bond points should be as small as possible
- Fibres should be as long as possible
- Fabric strain should be as low as possible
- Viscous behaviour of fibres and the yield point should be as large as possible.

10.3 Future Studies

Due to the results and outcomes of the research, following suggestions are presented for the future studies:

1. In order to develop such numerical models, the efforts should be spent towards the beginning of the manufacturing process of nonwoven materials. In this way, additional parameters such as calendaring temperature or pressure can be taken into account.

2. Modelling of bond points was always a big concern in many studies. Including the present study, many studies handled bond points as continuous structures. A CT image of a typical bond point is shown in Figure 10.1. Apparently, the bond point has some irregularities and voids because of the partially melted fibres in those regions. Based on the temperature and pressure applied during manufacturing, more realistic models for the bond points can be achieved as well.

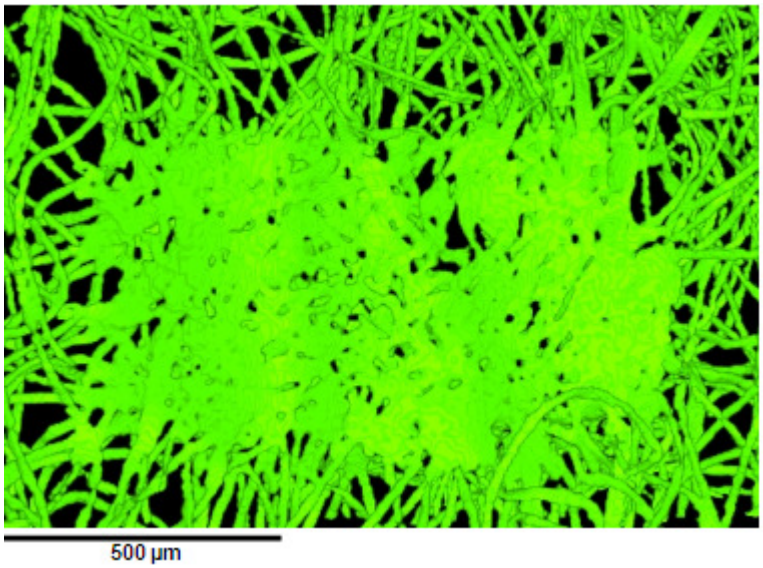

Figure 10.1. CT image of a bond point.

3. The behaviour of fibres can be expanded towards the plastic region and a viscoplastic model can be introduced for more realistic behaviour of fibres in plastic region

4. Due to the excessive deformation of fibres and bond points, implementation of damage behaviour is very important in this research which was also shown at the end of chapter 6 and chapter 7. The damage can be caused by fracture of fibres along bond point borders and/or the pullout of fibres from the bond points. By this way, some damage criteria can be introduced into the model.

5. It was shown in chapter 7 that with a fictitious curl distribution, the deformation behaviour of nonwoven materials can be affected significantly. Especially for nonwovens with staple fibres, this effect is very significant. An image analysis tool

can be developed in order to determine this distribution through the nonwoven structure.

APPENDIX A

DETERMINATION OF ORIENTATION DISTRIBUTION

As discussed in the thesis, the orientation distribution of fibres is one of the major issues regarding the material behaviour of nonwovens. Determination of the orientation distribution function (ODF) requires the micro structural image of nonwovens showing the fibres and sophisticated image analysis algorithms. The methodology of the determination of ODF is presented in Figure A.1. Initially, some fabric samples were prepared and the samples were scanned by a computed tomography (CT) machine. Then the 3D view of the fibrous structure was analyzed by the image analysis software developed by Demirci *et al.* (2009).

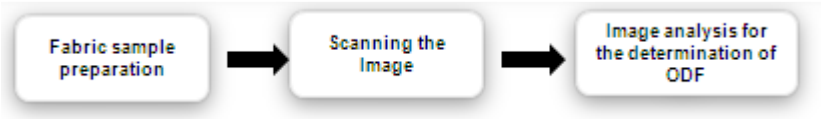

Figure A.1 Methodology of orientation distribution determination.

A.1 Fabric Sample Preparation and Installation

In order to determine orientation distribution, small fabric samples were prepared and installed in an x-ray computed tomography device to be scanned. To do this, firstly, a small part of fabric is cut from a nonwoven roll. Its size should be as small as possible for CT machine to catch detailed images. However, it should be as large as possible for the scan results to be more representative of the entire fabric. In addition, it is known that orientation distribution results could not be obtained accurately enough in the vicinity of bond points. Thus, it was decided to focus on the region where the bond points' contribution is minimal (Figure A.2). The fabric is then attached to a carton with a double-sided sticker to have an upright position during scanning. Then the sample is placed in front of the probe of the scanner of CT (Figure A.3).

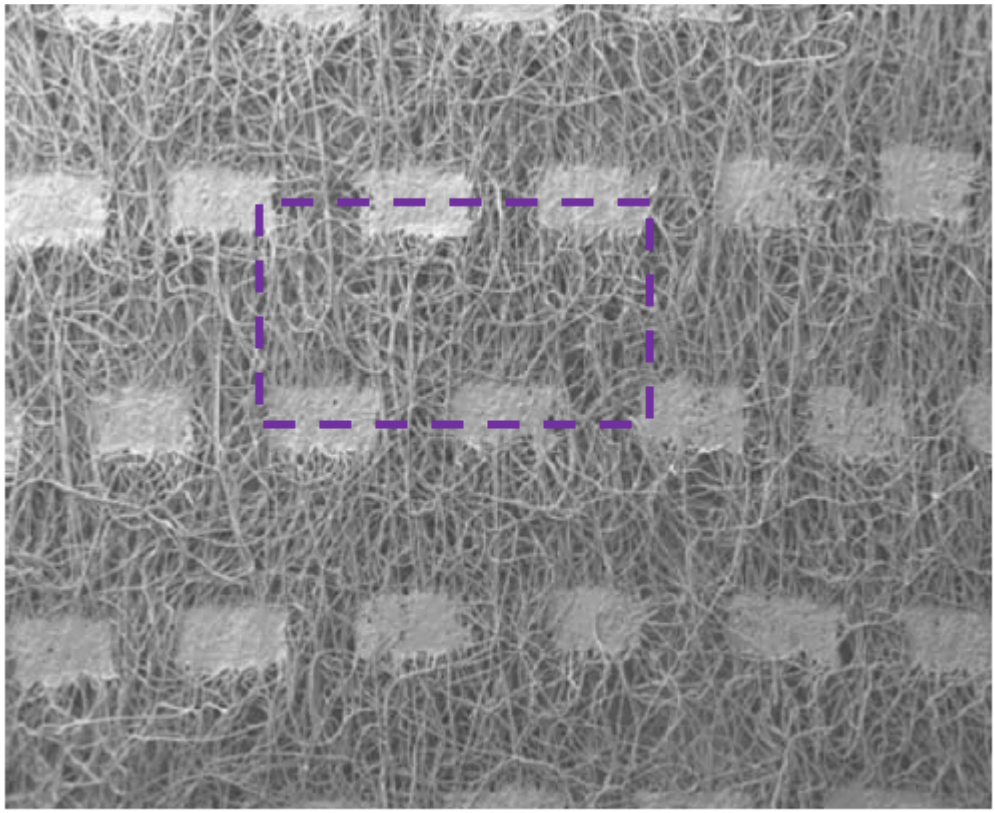

Figure A.2. Scanned region from the fabric

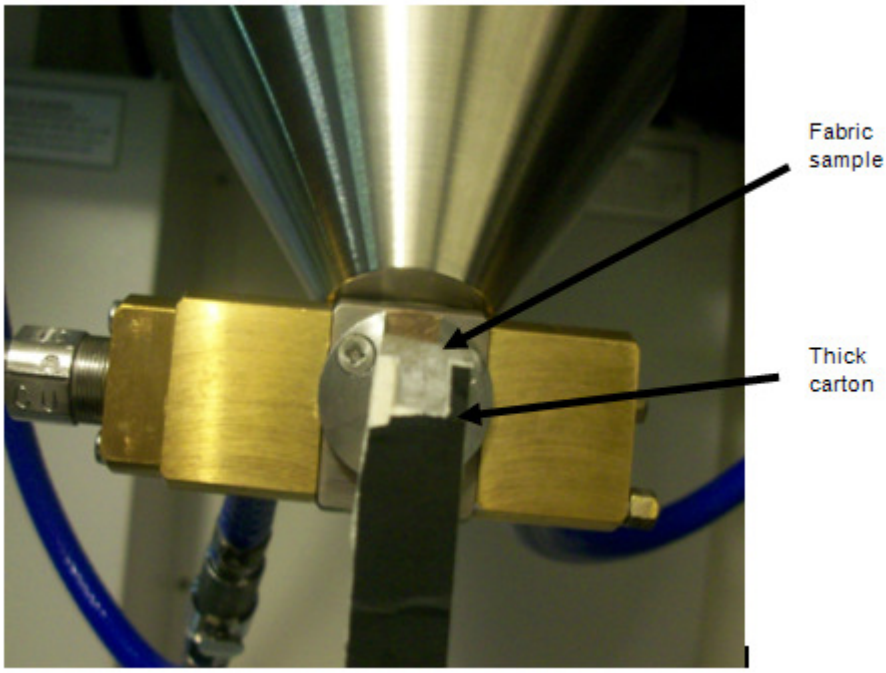

(a)

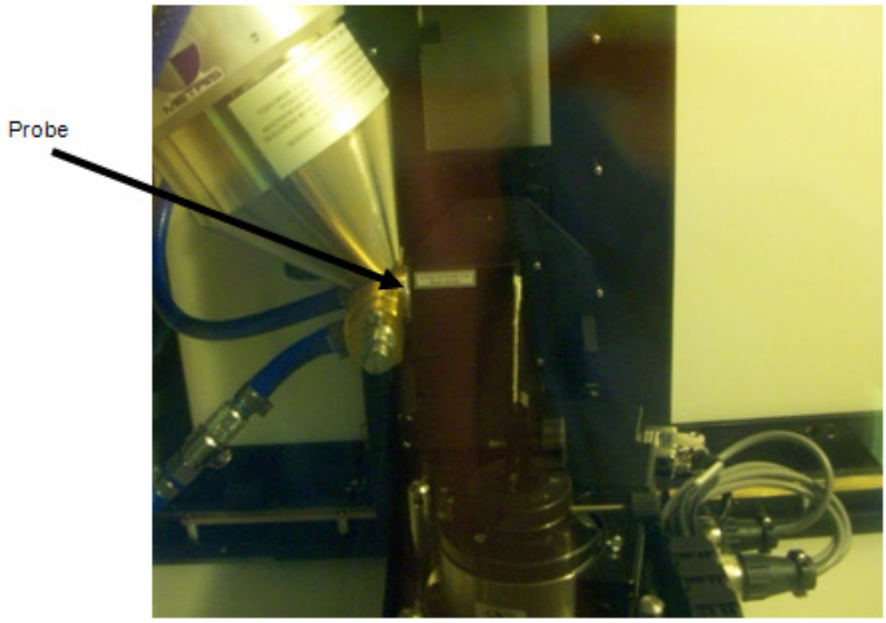

(b)

Figure A.3. Positioning fabric samples in CT device: (a) front view; (b) side view

A.2 Scanning the Image

After some trials, the scanning parameters for the CT machine for this type of material were determined. The test was repeated for three times with the samples from different fabric locations. One of the obtained 3D images of fabric is shown in Figure A.4. After the application of some image processing operations and changing the perspective, an image that shows the fibres in a closer view is obtained (Figure A.5).

A.3 Determination of ODF

The orientation distribution function for fibres in the fabric was obtained with the help of the image analysis software developed by Demirci *et al.* (2009); the results are shown in Figure A.6. In the figure, the fibre angles are given from the horizontal axis, coinciding with the cross direction.

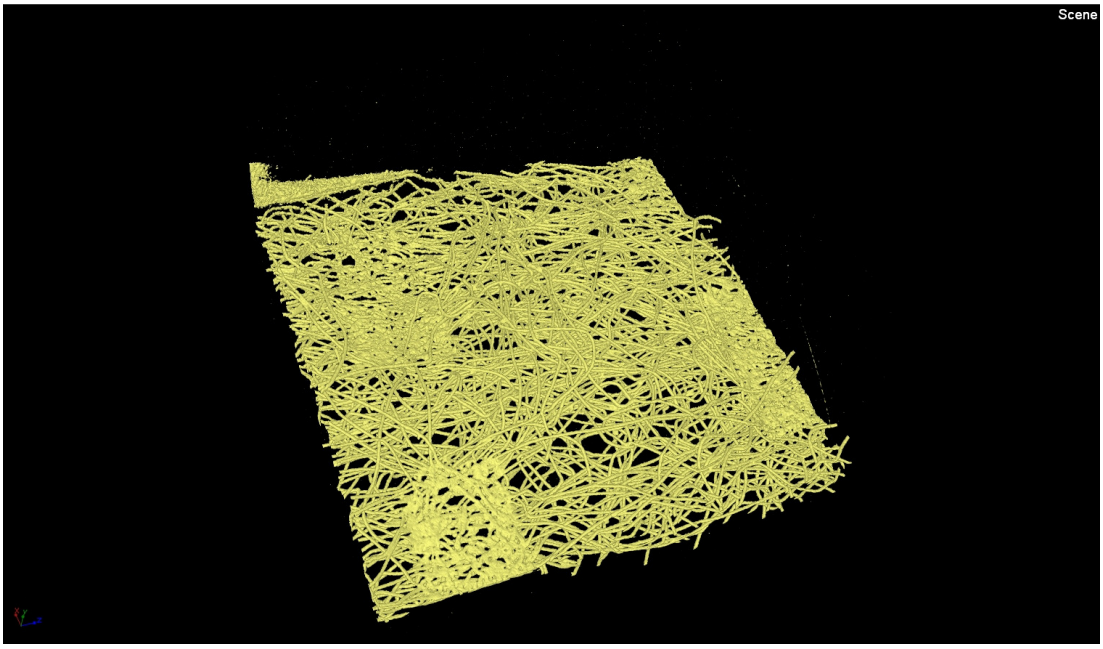

Figure A.4. 3D image of scanned fabric

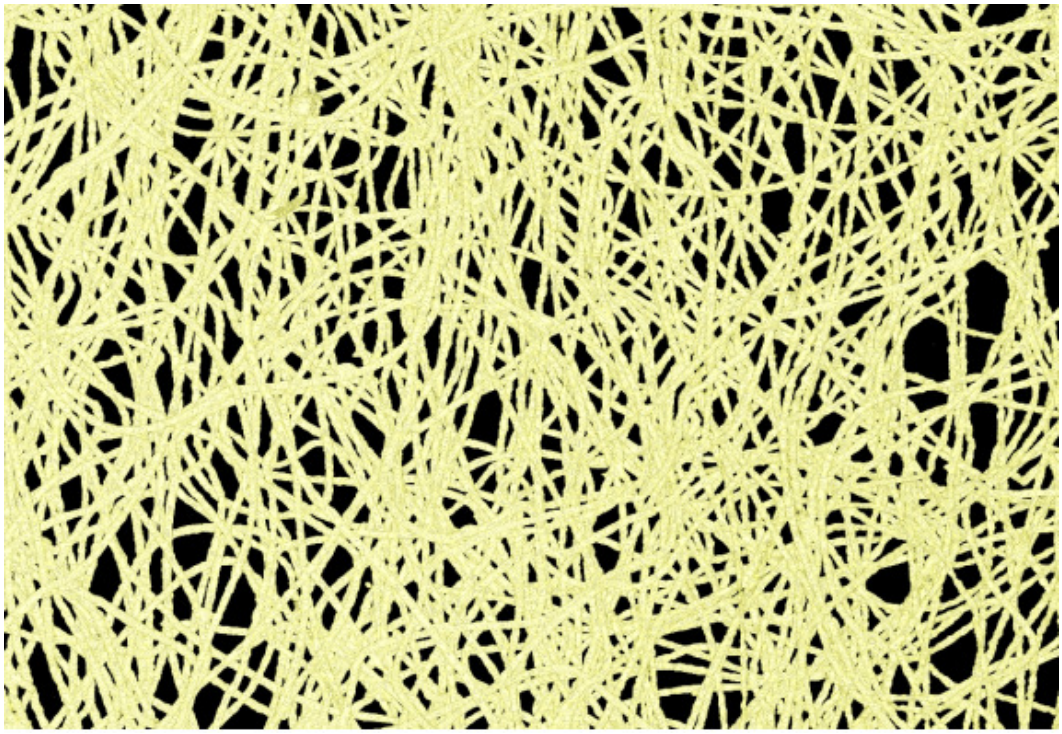

Figure A.5. CT Image showing fibbers

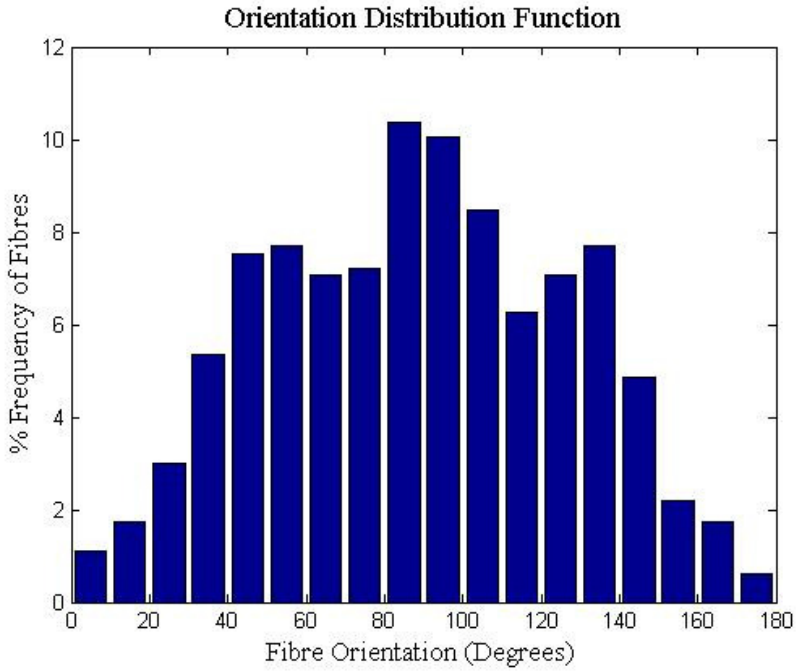

Figure A.6. Orientation distribution function of the modelled fabric

APPENDIX B

SIMULATION OF TENSILE BEHAVIOUR OF HIGH-DENSITY NONWOVENS

B.1 Introduction

The parametric model presented in the thesis was developed for the simulation of low-density thermally bonded nonwovens. However, apart from computational requirements, there is no limitation for the model to represent the behaviour of high-density nonwovens as well. Thus, an additional study is performed to see the efficiency of the model for simulating the tensile behaviour of high-density nonwovens. In order to do this, a high-density nonwoven model was generated (Figure B.1). The model simulated in this section is "Model A" in Demirci (2010) which is a type of thermally-bonded nonwoven with a density of 50 g/m^2. The stress-strain curves of fibres and the properties of bond points were also adapted from the mentioned study. The model was generated with a model coefficient (*MC)* of 5 in order to save time for generating the solid model. The model consists of 43904 shell elements for the bond points and 8907 truss elements for the fibres.

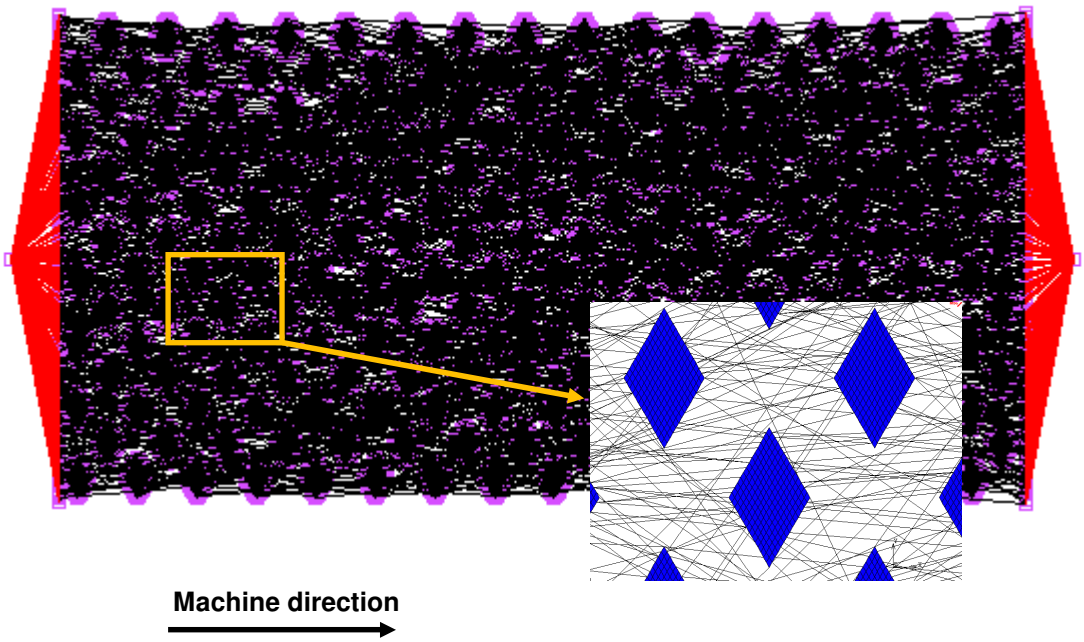

Figure B.1. Model generated to represent nonwoven model A in Demirci (2010)

B.2 Results and Discussions

Force vs. strain results of the simulations with the developed model and test are shown in Figure B.2. Apparently, a better match was observed between the model and test results compared to the case of simulations of a low-density nonwoven presented in Chapters 6 and 7. The reason can be the continuous fibres in the high-density nonwoven having less curled structure in the real material. The computed tomography (CT) image of a representative region is shown in Figure B.3. As it can be seen, the fibres are almost straight, which means that a high percentage of fibres started to carry load as soon as load is applied. Another reason could be the fibres having a bi-component structure in this model. It is known that the bond points in nonwovens having a bi-component fibre structure do not lose their structural integrity easily as compared with the nonwovens having mono-component fibre structure (Albrecht, 2003). Thus, the structure of this material was more close to that in simulation as damage in the bond points was not modelled. The analysis still diverges, which is the main problem of using truss elements connected to shell elements to represent the fibres as discussed in Chapter 7. Thus, a better convergence was observed in the study by Demirci (2010) in which not only the bond points, but also the fibrous network was modelled as shell elements.

The distributions of von Mises stresses in the current study and in Demirci (2010) are shown in Figures B.4 - B.5. The distributions are given for different extensions of the fabric as the simulation in the present study did not converge after 37% of fabric strain. Similar deformation behaviour was observed in both models. As it can be seen, there is a lateral contraction of fabric under the tensile load in both models. This was shown in Chapter 9 that this behaviour is due to the fibres, having an angle with the machine direction.

In the result with the present model, there were some high-stressed regions at the corners of the model, near the rigid links. This is due to the deformation of fibres as a result of high lateral contraction at those regions. They deform not only axially, but also laterally. The fibres at the application of boundary conditions are shorter than the other fibres located elsewhere in the structure. This can be another reason for

those fibres to carry higher stresses than the others. This behaviour was not observed in Demirci (2010). This may be the result of modelling the fibrous network with continuous shell elements. The stresses in the structure are distributed better in shell elements than in truss elements. However, it is thought that the present study is more realistic as individual fibres cannot transfer the load to the other fibres.

The distribution of stresses in the bond points are shown in Figure B.6. The bond points with high stresses are located randomly in the model in contrast to that in Demirci (2010), in which high stresses were observed in the bond points near the centre of the model. It is due to the random distribution of fibres inside the nonwoven structure. The distribution of von Mises stresses in a single bond point is shown in Figure B.6b. As it can be seen, high stresses were observed at certain locations in the bond points; these are the locations where fibres are connected to bond points. This is an expected result as the load transfer through bond points is by means of fibres.

It was observed that using the value of modelling coefficient (*MC*) as 5 was appropriate to represent the deformation behaviour of this type of nonwoven. Still, a model with an MC value of 1 was also simulated to study whether the tensile stiffness and/or deformation behaviour was affected or not. This model consists of 44505 truss elements and the same number of shell elements as the previous model. The obtained force *vs*. strain curve is given in Figure B.7. As it can be seen, the simulations with *MC*=1 and *MC*=5 showed similar stiffness. However, the divergence of the analysis was observed much earlier in the model with *MC*=1. The distribution of von Mises stress is shown in Figure B8 for the last converged step. Here, again, a similar behaviour was observed when compared with the distribution presented in Figure B.6. This confirms that the behaviour of this high-density nonwoven can be simulated with *MC*=5, significantly diminishing the computational effort.

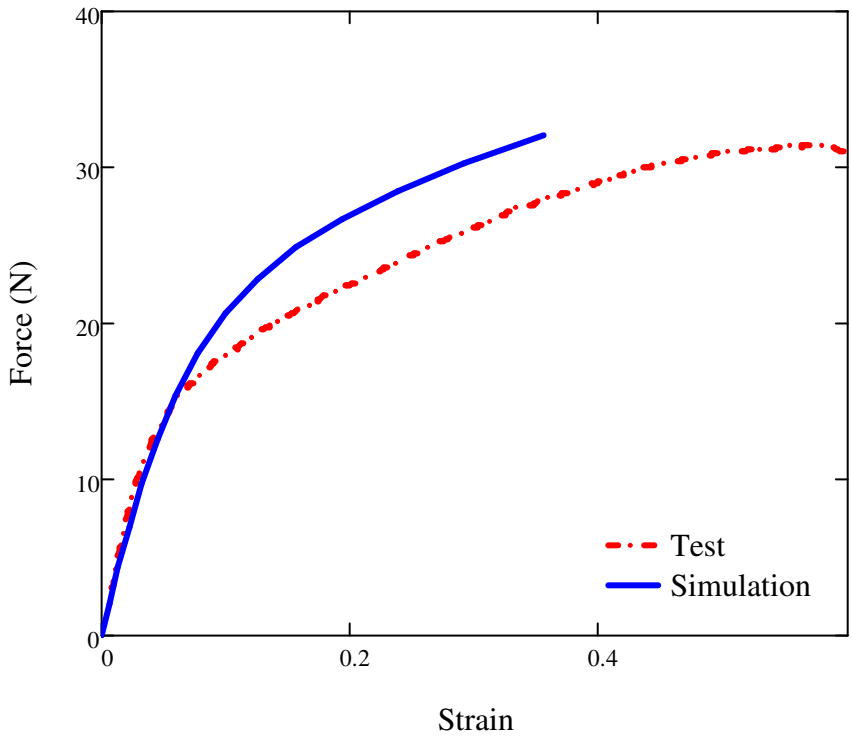

Figure B.2. Force *vs*. strain plots of simulation and test

Figure B.3. Computed tomography (CT) image of nonwoven model A in Demirci (2010)

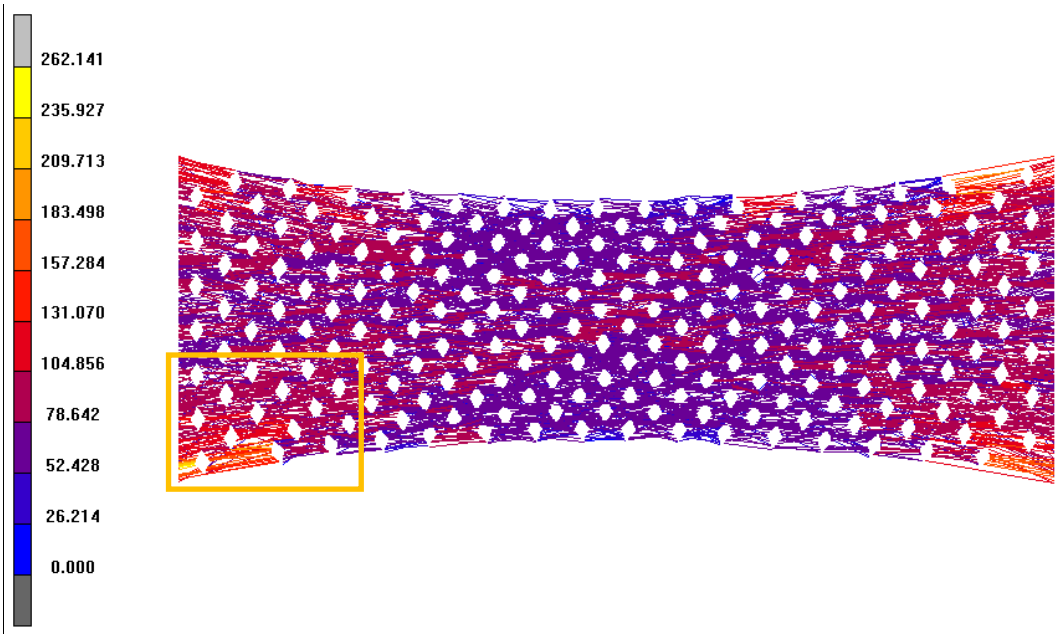

(a)

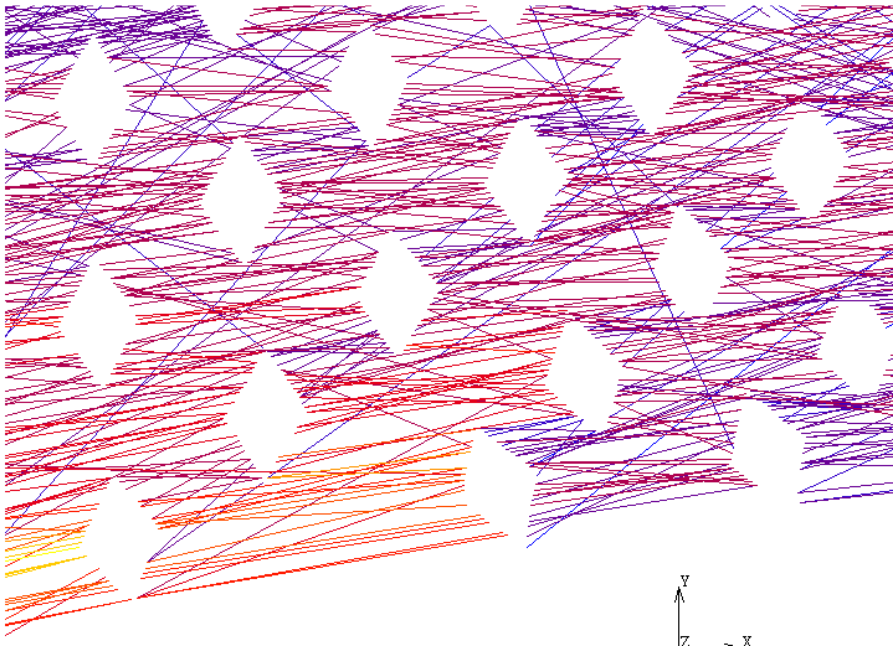

(b)

Figure B.4. Distribution of von Mises stress in nonwoven structure at fabric strain of 37%: (a) General view; (b) region close to one of model's corners

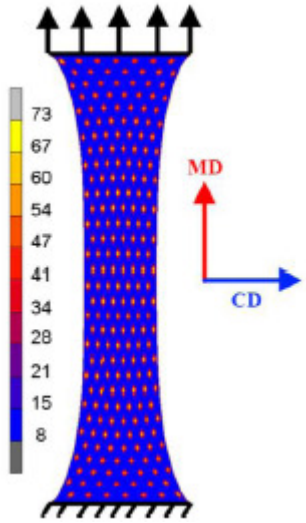

Figure B.5. Distribution of von Mises stress in nonwoven structure at 60% fabric extension of Model A in Demirci (2010)

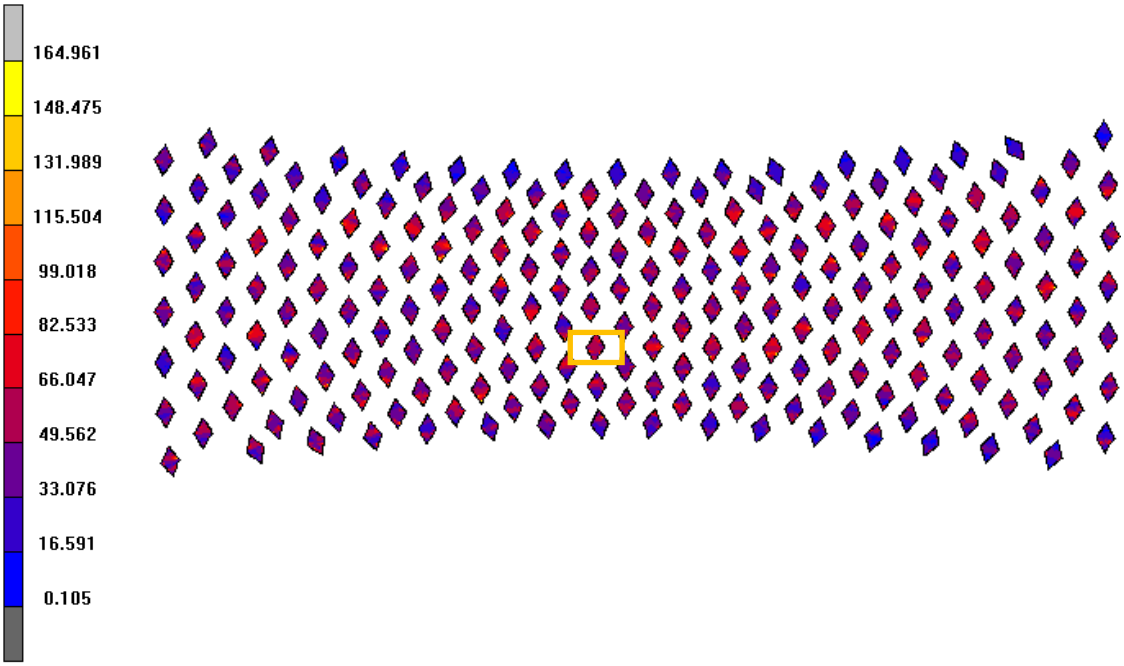

(a)

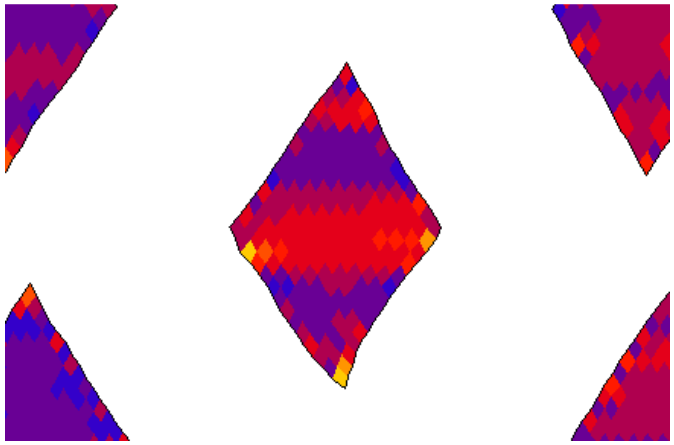

(b)

Figure B.6. Distribution of von Mises stresses in bond points in present model: (a) General view; (b) region close to a single bond point

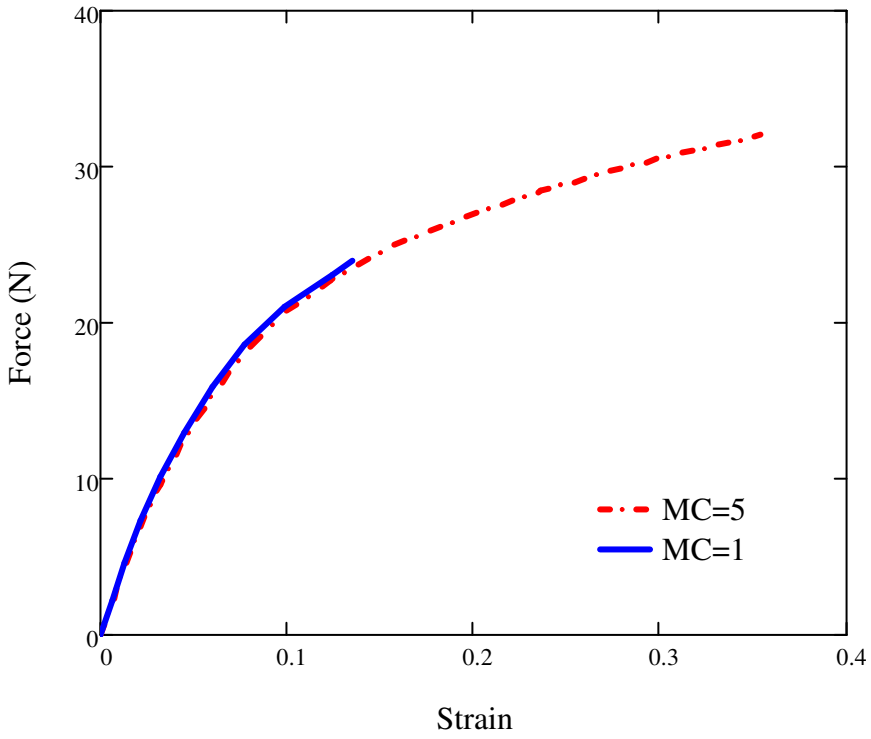

Figure B.7. Force *vs*. strain curves for various *MC* values

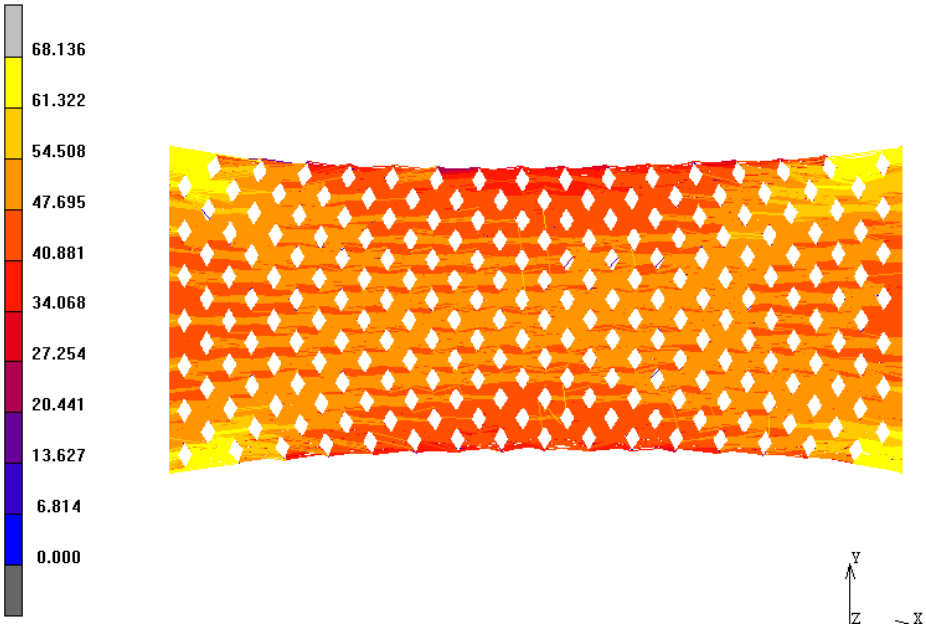

Figure B.8. Distribution of von Mises stresses at last converged step (*MC*=1)

REFERENCES

ANSYS, I., 2008. Release 11 Documentation for ANSYS.

Adanur, S. , Liao, T., 1999. Computerized Failure Analysis of Nonwoven Fabrics Based on Fiber Failure Criterion. *Textile Research Journal*, 69(11), 816-824.

Albrecht, W., 2003. *Nonwoven Fabrics* 1 ed. W. Albrecht, H. Fucsh, & W. Kittelmann, Weinheim: WILEY-VCH.

Ambroziak, A., Kłosowski, P., 2007. Determining the Viscoplastic Parameters of Toughened Plastics. *Task Quarterly*, 12(1), 1001-1009.

Arriaga, A., Lazkano, J., Pagaldal, R., Zaldua, A., Hernandez, R., Atxurra, R., Chrysostomou, A., 2007. Finite-element Analysis of Quasi-static Characterisation Tests in Thermoplastic Materials: Experimental and Numerical Analysis Results Correlation with ANSYS. *Polymer Testing*, 26(3), 284-305.

Ashcroft, I.A., Khokar, Z.R., Silberschmidt, V.V., 2012. Modelling the Effect of Microstructural Randomness on the Mechanical Response of Composite Laminates Through the Application of Stochastic Cohesive Zone Elements. *Computational Materials Science,* 52(1), 95-100.

Backer, S., Petterson, D.R., 1960. Some Principles of Nonwoven Fabrics. *Textile Research Journal*, 30(9), 704-711.

Bais-Singh, S., Goswami, B.C., 1995. Theoretical Determination of the Mechanical Response of Spun-bonded Nonwovens. *Journal of Textile Institute*, 86(2), 271-288.

Bechter, D., Kurz, G., Maag, E., Schütz, J., 1991. Über die thermische Verfestigung von Vliesstoffen 1. Mittlg: Der Einfluß der Kalanderbedingungen auf die Festigkeit von Polypropylenvliesstoffen, *Text Praxis Internat*, 11, 1236–1240.

Bhat, G.S., Malkan, S.R., 2000. Extruded Continuous Filament Nonwovens: Advances in Scientific Aspects. *Journal of Applied Polymer Science*, 83, 572-585

Bhat, G.S., Jangala, P.K., Spruiell, J.E., 2004. Thermal Bonding of Polypropylene Nonwovens: Effect of Bonding Variables on the Structure and Properties of the Fabrics. *Journal of Applied Polymer Science*, 92(6), 3593-3600.

Bhunavesh, Y.C., Gupta, V.B., 1995. Interaction between Viscoelastic and Structural Relaxation in Drawn Polypropylene Yarn. *Polymer*, 36(19), 3669-3674

Bodner, S.R., Partom, Y., 1975. Constitutive Equations for Elastic-viscoplastic Strain Hardening Materials. *Journal of Applied Mechanics*, 42, 385-389.

Brinson, H.F., Brinson, L.C., 2008. *Polymer Engineering Science and Viscoelasticity*, *An Introduction*, New York, USA: Springer Science +Business Media.

Cawsey, A., 1998. *Line Intersection*. Date accessed: 18/05/2010, Available at: http://www.macs.hw.ac.uk/~alison/ds98/node114.html.

Chidambaram, A., Davis, H., Batra, S. K., 2000. Strength Loss in Thermally Bonded Polypropylene Fibers, *International Nonwovens Journal* 2000, 9(3) 27-35

Colak, O.U., Dusunceli, N., 2006. Modeling Viscoelastic and Viscoplastic Behavior of High Density Polyethylene (HDPE). *Journal of Engineering Materials*, 128, 572-578.

Demirci, E., Memis, A., Pourdeyhimi, B., Silberschmidt, V.V., 2009. Computation of the Anisotropic Mechanical Properties of Thermally Bonded Bicomponent Fibre Nonwovens for Elastic-Plastic Response. *Proceedings of the Fiber Society Conference*, (1), 1-15.

Demirci, E., 2010. Mechanical Behaviour of Thermally Bonded Bicomponent Fibre Nonwovens: Experimental Analysis and Numerical Modelling. PhD thesis, Loughborough University, UK.

Dijkstra, P.T.S., Gaymans, R.J., Van Dijk, D.J., Huetink, J., 2003. Elasticity at Large Deformations and High Strain Rates in Injection Molded Polypropylene. *Polymer Engineering & Science*, 43(9), 1613-1623.

Dropik, M.J., Johnson, D.H., Roth, D.E., 2002. Developing an ANSYS Creep Model for Polypropylene from Experimental Data. *International ANSYS Conference*, Penn State-Erie, Erie, PA, USA

Drozdov, A.D., Christiansen, J.D., 2002. The Nonlinear Viscoelastic Behavior of Polypropylene. Aalborg : Denmark

Drozdov, A.D., Yuan Q., 2003. The Viscoelastic and Viscoplastic Behavior of Low-density Polyethylene. *Journal of Solids and Structures,* 40(10), 2321-2342

Duffo, F., Monasse, B., Haudin, J., 1995. Rheology in Polypropylene in Solid State. *Journal of Materials*, 30(3), 701-711.

EDANA, 2007. EDANA - Home Page., Date accessed: 18/05/2010 Available at: http://www.edana.org/Content/Default.asp.

Fathi, J., Ashrafi, S., Movla, H., Sobhaian, S., 2012. A novel method to determine Poisson's ratio by beta-ray absorption experiment*, Applied Radiation and Isotopes*, 70, 823-826.

Felhos, D., Xu, D., Schlarb, A.K., Varadi, K., Goda, T., 2008. Viscoelastic Characterization of an EPDM rubber and Finite element simulation of its Dry Rolling Friction. *Polymer*, 2(3), 157-164.

Fibervisions®, 2009, *Polypropylene Short-cut Fibers for Nonwovens and Paper Products*, Technical Data Sheet.

Fish, J., Belytschko, T., 2007. *A First Course in Finite Elements*, Chichester, England: John Wiley & Sons.

Ghassemieh, E., Acar, M., Versteeg, H., 2002. Microstructural Analysis of Non-woven Fabrics Using Scanning Electron Microscopy and Image Processing . Part 1 : Development and Verification of the Methods. *Journal of Materials: Design and Applications*, 216, 199-207.

Gomez-del Rio, T., Rodriguez, J., 2010. Compression Yielding of Polypropylenes above Glass Transition Temperature. *European Polymer Journal*, 46(6), 1244-1250

Gong, R.H., Dong, Z., Porat, I., 2003. Novel Technology for 3D Nonwovens, *Textile Research Journal*, 73(2), 120-123.

Hamza, A.A., Fouda, I.M., El-Farahaty, K.A., 1986. Interferometric Determination of Optical Properties of Bicomponent Fibers. *International Journal of Polymeric Materials*, 11(3), 169-184.

Hearle, J.W., Stevenson, P.J., 1963. Nonwoven Fabric Studies, part III: The Anisotropy of Nonwoven Fabrics. *Textile Research Journal*, 33, 877-888.

Hou, X., Acar, M., Silberschmidt, V.V., 2009. 2D Finite Element Analysis of Thermally Bonded Nonwoven Materials: Continuous and Discontinuous Models. *Computational Materials Science*, 46, 700-707.

Hou, X., 2010. Experimental and Numerical Analysis of Deformation of Low-density Thermally Bonded Nonwovens. PhD thesis, Loughborough University, UK.

Hutten, I. M., 2007. *Handbook of Nonwoven Filter Media*, Butterworth- Heinemann Publications, UK

INSTRON®, 2012. *Model 5948 MicroTester for Small-Scale Low-Force Testing up to 2 kN*. Date accessed: 07/06/2012, Available at: http://www.instron.co.uk/wa/product/MicroTester-System-for-Low-Force-Static.aspx?ref=http://www.google.co.uk/url

Kim, H.S., Pourdeyhimi, B., 2001. Computational Modeling of Mechanical Performance In Thermally Point Bonded Nonwovens. *Journal of Textile and Apparel*, Technology and Management, 1(4), 1-7.

Kim, H.S., Pourdeyhimi, B., Desai, P., Abhiraman, A.S., 2001. Anisotropy in the Mechanical Properties of Thermally Spot-Bonded Nonwovens: Experimental Observations. *Textile Research Journal*, 71(11), 965-976.

Kim, H.S., Pourdeyhimi, B., Abhiraman, A.S., Desai, P., 2002. Effect of Bonding Temperature on Load-Deformation Structural Changes in Point-Bonded Nonwoven Fabrics. *Textile Research Journal*, 72(7), 645-653.

Klosowski, P., Komar, W., Woznica, K., 2009. Finite Element Description of Nonlinear Viscoelastic Behaviour of Technical Fabric. *Construction and Building Materials*, 23, 1133-1140.

Krucinska, I., Stypka, T., 1991. Direct Measurement of the Axial Poisson's Ratio of Single Carbon Fibres, *Composites Science and Technology*, 41(19), 1-12.

Lee, B., 1993. Simulation of Large Strain Plastic Deformation and Texture Evolution in High Density Polyethylene. *Polymer*, 34(17), 3555-3575.

Limem, S., Warner, S.B., 2007. Adhesive Point-Bonded Fabrics. *Textile Research Journal*, 75(1), 63-72.

Lin, G., 2001. ANSYS.net tips and tricks., Date accessed: 27/05/2010, Available at: http://ansys.net/?mycat=tnt_guoyu2.

Lin, H.J., Tsai, C.C., Shie, J.S., 1995. Failure Analysis of Woven-Fabric Composites With Moulded-in Holes. *Composite Science and Technology,* 55, 231-239.

Lubliner, J., 2006. *Plasticity Theory,* Revised ed., Pearson Education, Inc.

Mallick, P.K., Zhou Y, 2003, Yield and Fatigue Behavior of Polypropylene and Polyamide Nanocomposites*, Journal of Materials Science*, 38(15), 3183-3190

Marc Analysis Research Coorporation, 2007. *MARC Volume A: Theory and User Information*.

Maze, B., Pourdeyhimi, B., 2005. Nonwoven Structure Modeling & Simulation. presentation given in Nonwovens Cooperative Research Center, North Carolina, USA

Meyers, M.A., Chawla, K.K., 1999. *Mechanical Behavior of Materials*, NJ: Prentice Hall; US edition.

Mezeix, L., Bouvet, C., Huez, J., Poquillon, D., 2009. Mechanical Behavior of Entangled Fibers and Entangled Cross-Linked Fibers During Compression. *Journal of Materials Science*, 44, 3652-3661.

Mi, Z.X., Batra, S.K., Computational Model for the Mechanical Behavior of Thermally Point-Bonded Nonwovens: Part I: Theoretical Background. *unpublished data*.

Mi, Z.X., Batra, S.K., Computational Model for the Mechanical Behavior of Thermally Point-bonded Nonwovens: Part II: Comparison with Experimental Results. *unpublished data*.

Michielsen, S., Pourdeyhimi, B., Desai, P., Carolina, N., 2005. Review of Thermally Point-Bonded Nonwovens : Materials , Processes , and Properties. *Journal of Applied Polymer Science*, 99, 2489-2496.

Mishakov, G.Y., Slutsker, G.Y., Stalevich, A.M., 2006. Modeling the Viscoelasticity of Nonwoven Material with Consideration of the Irreversible Strain Component. *Fibre Chemistry*, 38(1), 50-54.

Montefusco F., 2005. The Use of Nonwovens in Air Filtration, *Filtration & Separation,* 42(2), 30-31.

Mueller, D.H., Kochmann, M., 2004. Numerical Modeling of Thermobonded Nonwovens. *International Nonwovens Journal,* 13(1), 56-62.

Nikolov, S., Doghri, I., 2000. A Micro/Macro Constitutive Model for The Small-Deformation Behavior of Polyethylene. *Polymer*, 41(5), 1883-1891.

Ostoja-Starzewski, M., Stahl, D.C., 2000. Random Fiber Networks and Special Elastic Orthotropy of Paper. *Journal of Elasticity*, 60, 131-149.

Potluri, P., Manan, A., 2007. Mechanics of Non-orthogonally Interlaced Textile Composites, *Composites: Part A,* 38(4), 1216-1226.

Pourdeyhimi, B., Ramanathan, R., Dent, R., 1996. Measuring Fiber Orientation in Nonwovens Part I: Simulation. *Textile Research Journal*, 66, 713-722.

Pourdeyhimi, B., Kim, H.S., 2002. Measuring Fiber Orientation in Nonwovens: The Hough Transform. *Textile Research Journal,* 72(9), 803-809.

Pourdeyhimi, B., 2004. Directions in Nonwoven Technologies, presentation given in Nonwovens Cooperative Research Center, North Carolina, USA

Purdy, A.T., 1983. *Developments in nonwoven-fabrics.* Textile Progress, 12(4), 1-86.

Rawal, A., 2007. A Modified Micromechanical Model for the Prediction of Tensile Behavior of Nonwoven Structures. *Journal of Industrial Textiles*, 36(2), 133-149.

Russell, S.J., 2007. *Handbook of Nonwovens*, Cambridge, England: Woodhead Publishing Ltd.

Simo, J.C., 1987. On a Fully Three-Dimensional Finite-Strain Viscoelastic Damage Model: Formulation and Computational Aspects. *Computer Methods in Applied Mechanics and Engineering,* 60(2), 153-173.

Tekkaya, E., 1999. Introduction to Finite Element Analysis, Lecture Notes, Mechanical Engineering Department, Middle East Technical University, Ankara, Turkey.

The National Academy Press, 1995. *Polymers*, Available at: http://www.nap.edu/openbook.php?record_id=9947&page=15.

Truelove, P., Nordgren, G., 1981. Evolution of European Nonwoven Industry 1970-1985. In *INDEX '81 Conference Papers*. EDANA Brussels.

Van Dommelen, J., Parks, D, Boyce, M, Brekelmans, W., Baaijens, F., 2003. Micromechanical Modeling of Intraspherulitic Deformation of Semicrystalline Polymers. *Polymer*, 44(19), 6089-6101.

Wang, X., Michielsen, S., 2001. Morphology Gradients in Thermally Point-Bonded Polypropylene Nonwovens. *Textile Research Journal*, 71(6), 475-480.

Zhao, R.R., Wadsworth, LC, Sun, C & Zhang, D., 2003. Properties of Pp / Pet Bicomponent Melt Blown Microfiber Nonwovens after Heat-Treatment. *Polymer International*, 137, 133-137.

Zheng, H., 2003. The Impact of Input Energy, Fiber Properties, and Forming wires on the Performance of Hydroentangled Fabrics. PhD Thesis, NC State University, NC, USA.

Zrida, M., Laurent, H., Rio, G., Pimbert, S., Grolleau, V., Masmoudi, N., Bradai, C., 2009. Experimental and Numerical Study of Polypropylene Behavior Using a Hyper-Visco-Hysteresis Constitutive Law. *Computational Materials Science*, 45(2), 516-527.